The Complexity of Arc Magmatism: A Geochemical Investigation of Crustal Processes Beneath a Highly Productive Volcanic Center, Kamchatka, Russia

Theresa M. Kayzar

A dissertation
submitted in partial fulfillment of the
requirements for the degree of

Doctor of Philosophy

University of Washington
2012

Reading Committee:
Bruce K. Nelson, Chair
Olivier Bachmann, Co-Chair
George W. Bergantz

Program Authorized to Offer Degree:
Department of Earth and Space Sciences

University of Washington

Abstract

The Complexity of Arc Magmatism: A Geochemical Investigation of Crustal Processes Beneath a Highly Productive Volcanic Center, Kamchatka, Russia

Theresa M. Kayzar

Chair of Supervisory Committee:
Dr. Bruce K. Nelson
Department of Earth and Space Sciences

Understanding crustal modification of magmas in volcanic arcs is a fundamental problem of igneous petrology and geochemistry. This dissertation examines the role of crustal processes including crustal assimilation, magma mixing, magma differentiation, and volatile transport in generating erupted magmas from four volcanic systems in the Kamchatka Volcanic arc: Bezymianny, Klyuchevskoy, Shiveluch, and Karymsky. High-precision Pb isotope data from the Central Kamchatka Depression (CKD) record lower crustal assimilation and magma mixing of less radiogenic crust and melt into the magmas of Bezymianny volcano. Unradiogenic Pb isotope compositions in CKD magmas suggest that lower crustal assimilation occurs to a larger extent beneath the CKD than in other segments of the Kamchatka arc. Klyuchevskoy compositional variations support this argument and also show that the degree of assimilation beneath an individual volcanic center may vary on a decadal timescale.

Documented lower crustal assimilation by magmas beneath the CKD modifies uranium-series isotope disequilibrium compositions of CKD magmas. U-series isotopes are the only radioactive isotope system with half-lives useful for understanding the timing of volcanic processes. Constraining the affect of crustal processes that alter U-series compositions is essential to interpret isotope signatures. Chapter 2 of this dissertation shows that lower crustal assimilation and fractional crystallization of high-pressure clinopyroxene modifies U-excess to form Th-excess compositions. Global documentation of Th-excess reveals a correlation of Th-excess

disequilibria with hot lower crustal geologic settings. Th-excess may therefore be an important chemical tracer of lower crustal assimilation.

Shallow magma storage and degassing is investigated using (^{210}Pb)/(^{226}Ra) compositions at periodically erupting volcanoes with well-constrained degassing and eruptive histories. Current models that predict (^{210}Pb)/(^{226}Ra) as a function of gas loss do not accurately predict the observed compositions of erupted products in Kamchatka. This paradox has important implications for the timescales of magma storage and degassing in the crust.

Chapter 4 of this work is a detailed isotopic study of environmental uranium contamination from an abandoned open-pit mine. Uranium isotope data fingerprint alteration of the mine source and transport of uranium from the mine to sediment in Red Rock Creek on National Forest Service recreational land.

TABLE OF CONTENTS

LIST OF FIGURES

Figure Number Page

LIST OF FIGURES

LIST OF TABLES

ACKNOWLEDGEMENTS

I would like to thank my primary advisors: Dr. Bruce Nelson and Dr. Olivier Bachmann for their guidance, support and for challenging me throughout my graduate work. I am grateful to Bruce Nelson for encouraging my exploration of environmental management, K-12 education and outreach, and environmental contamination research, and for openly sharing his experiences and approaches to academia – I am privileged to have a primary advisor whom I am proud to model my career after. I thank Olivier Bachmann for his constant excitement and interest in my research. He is refreshing to work with because of his positive attitude and dedication to solving geological problems. I also thank my committee members: George Bergantz -for magmatic research discussions, and Kari Cooper for her scientific expertise and training, and for inspiring my interest in uranium-series isotopes. This work would not have been possible without contributed ideas, samples, and support from my collaborators at other institutions (Mark K. Reagan, Maxim Portnyagin, Pavel E. Izbekov, Ross Williams, and Amy Gaffney).

This doctoral research was primarily funded by a National Science Foundation Graduate Research Fellowship, as well as student grants from the University of Washington Earth and Space Sciences Department, Chevron Corporation, and ExxonMobil Corporation. Field travel to Kamchatka, Russia was supported through the University of Alaska-Fairbanks (National Science Foundation Partnerships in International Research and Education Grant to study explosive volcanism in Kamchatka: PIRE-Kamchatka OISE-0530278). I warmly thank all principle investigators (Pavel Izbekov, John Eichelberger, Jeffrey Freymeuller, and Mike West) and student researchers of the PIRE-Kamchatka project (specifically: Vasily Shcherbakov, Taryn Lopez, Jill Shipman, Helena Buurman, Gwyneth Hughes, Wendy Stovall, Stephen J. Turner, Owen Neill, Ronni Grapenthin, and Ashley Shuler).

Research in Kamchatka, Russia was successful because of extensive collaboration with my international colleagues at: The Institute of Volcanology and Seismology in Petropavlosk-Kamchatksky, Russia (Evgeny Gordeev, Sergey Ushakov, Marina Belousova, Alexander Belousov, Sergey Serovetnikov, and Slava Pilipenko); Moscow State University, Moscow, Russia (Vera Ponomareva and Vasily Shcherbakov); and the Leibniz Institute of Marine Sciences (IFM-GEOMAR), Kiel, Germany (Maxim Portnyagin). I hope that the results, data, and associated publications from this dissertation are an example of the significant contributions to geochemistry that result from international research and collaboration without borders.

For environmental work, I am grateful for working with Ross Williams, Amy Gaffney, Brad Esser, Victoria Genetti and Rachel Lindvall at Lawrence Livermore National Laboratory. This work was performed under the auspices of the U.S. Department of Energy by Lawrence Livermore National Laboratory under Contract DE-AC52-07NA27344; post number LLNL-JRNL-511840.

Finally, I thank my friends and mentors at the University of Washington who kept me smiling through this process (Aaron Wech, Sanjoy Som, Weston Thelen, Philipp Ruprecht, Rachel Headley, Robert Weekly, Daniel Morgan, Charles Plummer, Thomas Tobin, Maisie Nichols, Nathan Peters, Sarah Bergman, Megan Smith, and Dr. Joanne Bourgeois).

DEDICATION

This PhD dissertation is dedicated to Candice Rupprecht and Meredith Hunt – the strongest, most dedicated, and most philanthropic women that I have ever known. To my parents, George and Katharina, for raising me in a world that inspires creativity. Also to my fellow ESS graduate students for the company and laughter along the road.

INTRODUCTION

The destruction and creation of the Earth's crust via magmatic processing in subduction zone settings (magmatic arcs) has been a subject of geologic research since the establishment of plate tectonics. Geochemical and petrologic tools such as radiogenic isotopes, major and trace element compositions, and phase assemblages distinguish processes that operate within the intricate melt factory of volcanic arc environments. However, quantitatively assessing any individual processes (e.g. magma mixing) that affects magma on its journey from the mantle through the crust to the surface is arduous due to the complex nature of subduction zones.

Fortunately, components in subduction zones often have distinct isotopic chemical fingerprints. A growing crystal chemically fractionates a magma affecting its composition at the micro-scale, while ageing of continental crust leads to radioactive decay of elements affecting compositions at the macro-scale. Isotope compositions, therefore, are natural tracers of Earth processes. This dissertation uses isotope fractionation and the resulting diversity of isotope compositions to examine the role of magma source heterogeneity, crustal assimilation, fractional crystallization of melts, and magma mixing in creating the variable magma compositions erupted in the Kamchatka Volcanic Arc. The Kamchatka arc is one of the most productive volcanic arcs on Earth with over 100 volcanic centers (Fedotov 1991; Melekestsev *et al.,* 1991; Churikova *et al.,* 2001). This arc provides a natural laboratory within which individual volcanic centers may be densely sampled and studied temporally. Volcanic centers can also be compared and contrasted to other volcanic systems with the goal of examining broader arc-scale processes. The first three chapters of this dissertation focus on separate scales of arc magmatism in Kamchatka.

The origin and preservation of compositional variation in magmas is investigated both temporally and spatially in Chapter 1 using high-precision Pb isotope compositions from magmas erupted within the Central Kamchatka Depression. Klyuchevskoy and Bezymianny volcanoes in the Central Kamchatka Depression erupt compositionally distinct magmas despite being only 9 kilometers apart on the Earth's surface. Major and trace element chemistry as well as petrologic characteristics of the two systems were interpreted to suggest that the volcanoes are cogenetic and that Bezymianny magmas evolve through closed-system fractional crystallization from Klyuchevskoy magmas (Ozerov *et al.* 1997). Pb isotope data presented in this chapter from

Bezymianny eruptive products as well as crustal and magmatic inclusions, argues that the variation between these two volcanic centers results from more extensive lower crustal assimilation and fractional crystallization as well as magma mixing at Bezymianny relative to Klyuchevskoy. Pb isotope compositions document interaction with a young, mafic crust – a crustal composition that is cryptic and not easily identified with other geochemical tracers (Reagan *et al.* 2003). In addition, detailed time-series sampling reveals that the degree of assimilation may vary over decadal timescales representing rapid shifts in subsurface magmatic conditions. Rapid changes in the processes that control magma generation as well as the preservation of compositionally distinct magma sources on small spatial scales are fundamental issues of current geochemical research (Brunelli and Seyler, 2010; Madureira *et al.,* 2011).

Chapter 2 of this dissertation examines the generation of U-series disequilibria in volcanic arcs. Nuclides in the U-series decay chain are fractionated from one another by various subduction zone processes and have half-lives that are comparable to the timescales of magmatic processes in arc settings. Therefore, U-series isotope compositions can be used to assess the timing and processing of melts in an arc. Early applications of U-series to arc settings suggested that magma moves on a highway from the mantle to the surface and that primary signals generated in the mantle wedge (such as fluid fluxed melting) are preserved until eruption (Reagan *et al.* 1994; Turner *et al.* 2000; Turner *et al.* 2001; Sigmarsson *et al.* 2002). Recent studies, however, have suggested that crustal processes may modify or cause U-series disequilibria making it difficult to infer the timing of melting and deep mantle processes from U-series isotope compositions (Volpe and Hammond 1991; Volpe 1992; Bourdon *et al.*, 2000; Reagan *et al.*, 2003; Berlo *et al.*, 2004; Garrison *et al.*, 2006; Jicha *et al.*, 2007; Walker *et al.*, 2007; Finney *et al.*, 2008; Handley *et al.*, 2008; Jicha *et al.*, 2009; Price *et al.*, 2010; Reubi *et al.*, 2011; Singer *et al.*, 2011). Because U-series is currently the only radioactive isotope system with half-lives that are useful for understanding the timing of volcanic processes, it is essential that magmatic processes affecting magmas during transport through the crust be investigated as potential mechanisms for fractionating U-series nuclides.

The origin of Th-excess disequilibria ($(^{238}U)/(^{230}Th) < 1$, which is measured in eruptive products from the Central Kamchatka Depression, is specifically examined to test whether Th-excess is a

primary signal formed deep during mantle melting, or if it is formed through crustal assimilation. Crustal influence on U-series disequilibria is often examined in complex systems with many variables to constrain: sediment input to arcs, multiple magma sources and mixing, or very thick crust (Sigmarsson *et al.* 2002; Garrison *et al.* 2006). Thick crustal settings provide a higher probability to identify a crustal signature, which is useful, but is an extreme end-member situation that is not directly applicable to arc settings worldwide. This research demonstrates that a detailed study of individual volcanic centers with multiple eruptions on decadal to 10^2 year timescales in a geologic setting where the number of complex crustal processes can be reduced provides more insight into the role of the crust in fractionating U-series nuclides. Results show that U-excess generated by fluid addition during mantle melting may be overprinted by Th-excess that results from lower crustal assimilation in the presence of high-pressure clinopyroxene. Identifying that assimilation may explain U-series compositions in a very thin (< 35 km) volcanic arc, like the Kamchatka Volcanic arc, demands that crustal processes not be ignored in other geologic settings where the crust is equivalent in thickness or thicker.

The timescales and mechanisms by which volatiles are transported in magmatic systems are essential to understanding gas overpressure, which may trigger explosive eruptions. Research has shown the dynamics of volatile motion in magma chambers and conduits to be complex, ranging from individual bubble transfer to connected channels of gas (Kazahaya *et al.* 1994; Barclay *et al.* 1995; Stevenson and Blake 1998; Wallace 2001; Sparks 2003; Blower *et al.* 2003; Reagan *et al.* 2006). The U-series decay chain nuclides ^{226}Ra-^{222}Rn-^{210}Pb can be used to quantify gas motion because the intermediate nuclide, ^{222}Rn, is a noble gas that diffuses quickly into volatile phases (see review by Berlo and Turner (2011) and references therein). Gauthier and Condomines (1999) were the first to create a quantitative gas transport model using ^{226}Ra-^{222}Rn-^{210}Pb decay to examine gas loss at Merapi and Stromboli volcanoes. This model has since been applied to examine disequilibria in the form of ^{210}Pb deficits (gas loss) as well as ^{210}Pb excesses (gas accumulation) (Gauthier *et al.* 2000, Berlo *et al.* 2004, 2006, Turner *et al.* 2004, Reagan *et al.* 2006, Cunningham *et al.* 2009). However, the model does not incorporate any physical parameters for gas transport. Chapter 3 tests whether this model accurately predicts the amount of (^{210}Pb)/(^{226}Ra) disequilibria resulting from passive degassing at Bezymianny, Shiveluch, and Karymsky volcanoes. These volcanic centers are ideal because their eruptive activity is defined

by sequences of eruptions and the time periods between eruptive events are well documented (Izbekov *et al.* 2004).

Data collected here shows that (^{210}Pb)/(^{226}Ra) disequilibrium is not generated during continuous eruptive events despite visual observation of gas loss. However, disequilibrium is measured in magmas when the periodicity of eruptions is described by recurrence intervals longer than a few months. A measured trend towards ^{210}Pb deficits in volcanic bombs at Bezymianny (15% in 2007) and Shiveluch (8% in 2007) suggests periodic explosive eruptions are caused by the loss of gas and formation of a shallow degassed plug of magma sealing a system with continued deep degassing. Data presented from Kamchatka identifies a "degassed magma paradox" in which ^{210}Pb deficits that are lower than predicted with existing gas transfer models. This observation implies that residence times of magma in magmatic systems must be longer than the duration between eruptions.

Chapter 4 of this dissertation diverges from magmatic research, and uses isotope fingerprinting in an environmental context to understand the movement of uranium in a surface stream environment on Earth's surface. The transport of uranium through the environment is an issue of concern for many regulatory agencies because uranium is a heavy metal that is both chemically toxic and a radioactive material (ATSDR 1999; Coryell and Stearns 2006; Vahakangas *et al.* 1992). The Juniper Uranium Mine is an abandoned open mine pit from which one branch of Red Rock Creek emanates in the Stanislaus National Forest of California. Mining in the Sierra Nevada range of California has increased the amount of toxic metals available for transport through the natural environment (Conaway *et al.* 2004; Goldhaber *et al.* 2009).

Uranium transport is affected by many variables in natural surface water environments (organic content, pH, grain size of sediment, etc.) (Cowart and Osmond 1977; Dosseto *et al.* 2006; Hostetler and Garrels 1962; Moliner-Martinez *et al.* 2004; Rodriguez *et al.* 2008; Ryu *et al.* 2009; Vandenhove *et al.* 2009) that can be difficult to isolate in large river systems (Camacho *et al.* 2010; Chabaux *et al.* 2001; Moliner-Martinez *et al.* 2004; Ryu *et al.* 2009). Red Rock Creek provides an ideal study area with a limited number of factors influencing uranium transport as well as geologic bedrock control. Sediment and water samples from Red Rock Creek studied

here, show that uranium has been weathered from abandoned mine tailings and adsorbed onto sediment in the creek. Isotopic compositions of sediment imply that contamination is present even when concentrations of uranium in the waters and sediment have been highly diluted.

Chapters 1 and 4 of this dissertation are currently under review for international publication in the *Journal of Petrology* and *Applied Geochemistry* respectively. Chapters 2 and 3 are under co-author review and will be submitted for publication to *Geochimica et Cosmochimica Acta* and *Geology* in May 2012. Results from these studies have been presented at multiple international meetings listed in the vitae at the end of this dissertation.

CHAPTER 1

High-Precision Pb Isotope Ratios from Time-Series Samples at Bezymianny and Klyuchevskoy Volcanoes Record Lower Crustal Assimilation and Magma Mixing in the Central Kamchatka Depression

Co-authors:
Bruce K. Nelson, Olivier Bachmann, Ann M. Bauer, Pavel E. Izbekov

ABSTRACT

The Klyuchevskoy Group of volcanoes in the Kamchatka arc erupts magmas with a wide range of compositional diversity (high-Mg basalts to dacites). Generation of this diversity on very small spatial scales (<10's of kilometers) has been interpreted to result primarily from fractional crystallization (Ozerov *et al.,* 1997). New high-precision Pb isotope data from juvenile (1956-present) erupted products and hosted inclusions from Bezymianny volcano reveal that Bezymianny and Klyuchevskoy volcanoes, separated by only 9 km, undergo varying degrees of crustal processing and are not required to be cogenetic magmas. Pb isotope compositions of Klyuchevskoy magmas (basalts) are more radiogenic than Bezymianny magmas (andesites) ($^{208}Pb/^{204}Pb$ = 37.850-37.903, $^{207}Pb/^{204}Pb$ = 15.468-15.480, and $^{206}Pb/^{204}Pb$ = 18.249-18.278 at Bezymianny; $^{208}Pb/^{204}Pb$ = 37.907-37.949, $^{207}Pb/^{204}Pb$ = 15.478-15.487, and $^{206}Pb/^{204}Pb$ = 18.289-18.305 at Klyuchevskoy). These data suggest that the previous interpretation that Bezymianny andesites evolve from Klyuchevskoy-like magmas through closed-system fractional crystallization must be re-evaluated. A lower crustal xenolith (with a crystallization pressure of 5.2 ± 0.6 kilobars based on 2-pyroxene geobarometry) as well as magmatic inclusions from recent Bezymianny eruptive units record Pb-isotope compositions that are less radiogenic than their host magmas. The data are consistent with magma mixing (with magma from the nearby Tolbachik volcano) and with deep crustal assimilation generating the less radiogenic compositions measured at Bezymianny. Pb isotope compositions for the Central Kamchatka Depression (CKD) are less radiogenic than other segments of the arc (Karymsky – Eastern Volcanic Zone; Shiveluch – Northern Central Kamchatka Depression) which we interpret as resulting from increased lower crustal assimilation beneath the CKD relative to the rest of the arc. Pb isotope compositions vary on decadal timescales at Klyuchevskoy, demonstrating that the magnitude of assimilation at one volcanic center can change rapidly. Pb-isotope data coupled with major and trace element data reflect the importance of crustal processes on influencing magma compositions even in very thin juvenile volcanic arcs such as Kamchatka.

INTRODUCTION

The generation of compositional diversity in igneous rocks on small spatial scales within a volcanic arc, or within single volcanoes is a complex problem of petrology and geochemistry because compositional variation can result from fractional crystallization, assimilation, mixing, or source heterogeneity – mechanisms that chemically may not be possible to decouple in crustal settings. However, the Kamchatka arc is a unique arc end-member within which the origin of compositional variation in magmatic suites may be investigated due to the ability to place limits on the geochemical components in this region. Volcanoes in the Central Kamchatka Depression erupt primitive magmas with MORB-like isotopic signatures (Kepezhinskas *et al.,* 1997), the crust is thin (~35km), and there is little to no subducted sediment involved in the generation of magmas (Kersting & Arculus, 1995). In addition, the Klyuchevskoy Group of volcanoes in the Central Kamchatka Depression is home to twelve different volcanic centers within ~100 km of one another that erupt a wide range of compositions.

Two volcanoes within the Klyuchevskoy Group, Bezymianny and Klyuchevskoy, are separated by only 9km and erupt compositions from high-magnesium basalts to dacites. These two systems erupt frequently and permit the investigation of compositional variation on both short temporal and spatial scales in the Central Kamchatka Depression. Klyuchevskoy volcano has been well-studied (Khrenov *et al.,* 1991; Kersting & Arculus 1994; Khubanaya *et al.,* 1994; Ariskin *et al.,* 1995; Ozerov *et al.,* 1997; Khubanaya *et al.,* 1998; Pineau *et al.,* 1999; Dorendorf *et al.,* 2000, Ozerov *et al.,* 2000; Volynets *et al.,* 2000; Dosseto *et al.,* 2003; Mironov *et al.,* 2001; Portnyagin *et al.,* 2007a; Portnyagin *et al.,* 2007b; Turner *et al.,* 2007; Auer *et al.,* 2009; Mironov & Portnyagin 2011). However, Bezymianny volcano, which erupts the most evolved melts in the Klyuchevskoy Group, has been investigated in much less geochemical detail. It has been suggested that Klyuchevskoy and Bezymianny are genetically related (Ozerov *et al.,* 1997) and available isotopic data for the two systems overlap in composition (Kersting & Arculus, 1995; Pineau *et al.,* 1999; Dorendorf *et al.,* 2000; Churikova *et al.,* 2001; Bindeman *et al.,* 2004; Münker *et al.,* 2004).

Most studies of volcanism in Kamchatka tend to be arc-length in scale (Hochstaedter *et al.,* 1996; Kepezhinskas *et al.,* 1997; Churikova *et al.,* 2001; Ishikawa *et al.,* 2001; Tolstykh *et al.,*

2003; Bindeman *et al.,* 2004; Portnyagin *et al.,* 2005) or focused on one volcano e.g. Klyuchevskoy (cited above). However, there are few studies with detailed sampling of modern eruptions that compare one magmatic system to another in the Klyuchevskoy Group with the goal of understanding compositional variation (Ozerov *et al.,* 1997; Dosseto *et al.,* 2003; Turner *et al.,* 2007). We present new data from dense sampling of Bezymianny volcano including modern eruptive products, extrusive domes, and inclusions brought to the surface in juvenile erupted magmas. We use high-precision Pb-isotope data to investigate hypotheses regarding the source of magmatism in the CKD, the extent of crustal involvement or modification of magmas, and the degree of geochemical contamination to the melting source. We couple isotopic compositions with detailed major element and trace element characterization of Bezymianny and use geochemical modeling to investigate the hypothesis that Bezymianny and Klyuchevskoy share the same parental magma. We present evidence for the preservation of small spatial scale compositional variations between adjacent Bezymianny and Klyuchevskoy magmatic systems.

BACKGROUND AND GEOLOGIC SETTING

The Kamchatka Volcanic Arc is the result of the convergence of 80-90Ma oceanic crust with accreted Mesozoic and Tertiary mafic volcanic terranes that compose the Kamchatka Peninsula (Watson & Fujita, 1985; Gorbatov *et al.,* 1997; Konstantinovskaia 2001). The northwest corner of the Pacific plate subducts beneath Kamchatka at 8-9cm/yr (Minster & Jordan, 1978; Gorbatov *et al.,* 1997). The volcanic arc is comprised of three active segments: the Eastern Volcanic Front (EVF), the Central Kamchatka Depression (CKD) and the Northern Volcanic Front (NVF) (**Figure 1**). With over 25 active volcanic centers, the Kamchatka Volcanic Arc is the most productive arc on the Earth (Fedotov 1991; Melekestsev *et al.,* 1991; Churikova *et al.,* 2001).

The Klyuchevskoy Group of volcanoes resides within the CKD, which is a large graben resulting from intra-arc rifting that is approximately 350km in length by 5-100km in width (Kepezhinskas *et al.,* 1997). Twelve volcanic centers comprise the volcanism in the CKD, of which Bezymianny and Klyuchevskoy are the most active. The composition of the crust beneath the CKD is uncertain but is proposed to consist of Cenozoic volcanic deposits to depths of 8km, below which mafic crust at greenschist and/or amphibolite metamorphic facies extend to depths of

~30km (Fedotov 1991; Dorendorf *et al.,* 2000). The amphibolitic Ganal Massif beneath Eastern Kamchatka farther to the south, a likely analogue for the lower crust in Kamchatka, developed approximately 66Ma, while accretion of the terrane is thought to have occurred ~24Ma (Bindeman *et al.,* 2002). The total thickness of crust beneath the CKD is 30-40km with a 10-12km thick crust-mantle transition interpreted as deep ponding of basaltic magmas generated in the mantle wedge (Balesta 1991; Lees 2007).

CKD magmatism is a product of partial melting of a depleted mantle source that has been metasomatized by hydrous slab-derived fluids with possible additional contributions from altered oceanic crust associated with the emperor seamount chain (Portnyagin *et al.,* 2007b). Trace element variations and REE patterns of CKD magmas indicate fluid-fluxed arc melting in the wedge (enriched LILE and LREE, and depleted HREE and HFSE) (Kepezhinskas *et al.,* 1997; Dorendorf *et al.,* 2000; Portnyagin *et al.,* 2005). Although decompression melting is hypothesized to take place beneath the extinct Sredinny Range to the west of the CKD as well as to the north of the CKD where the corner of the Pacific plate intersects the Aleutian Arc (Yogodzinski *et al.,* 2001; Portnyagin *et al.,* 2005; Portnyagin *et al.,* 2007; Volynets *et al.,* 2010), there is no conclusive evidence for decompression melting below the CKD. If decompression melting does contribute to CKD magmas, it is coupled with fluid-fluxed melting in the wedge (Churikova *et al.,* 2001).

Isotope systematics, coupled with major element trends of the CKD, constrain the amount of sediment and crustal assimilation that is incorporated into primitive melts of the mantle wedge. A strong MORB-like signature in Nd and Pb isotopes is observed in products from Bezymianny and Klyuchevskoy (Kersting & Arculus 1995; Kepezhinskas *et al.,* 1997; Dorendorf *et al.,* 2000; Churikova *et al.,* 2001; our data). Pb-isotope compositions of sediments from the ODP 145 drill core from the Pacific Ocean off the coast of Kamchatka limit models for the amount of sediment input to the arc to less than 1% (Kersting & Arculus, 1995). In addition, the primitive nature of melts (Mg# 71 at Klyuchevskoy) suggests limited crustal assimilation (Pineau *et al.,* 1999; Dorendorf *et al.,* 2000; Ishikawa *et al.,* 2001). Oxygen isotope data, however, suggest that large amounts of assimilation may occur beneath the CKD but the required assimilant is altered lithospheric mantle that would not modify Mg values (Auer *et al.,* 2009).

Klyuchevskoy and Bezymianny Volcanic Systems

Klyuchevskoy volcano is the most voluminous arc volcano in the world and erupts ~ 55 x 10^6 t/yr of high-Mg basalt and high-Al basaltic andesite (Melekestsev *et al.,* 1991). Activity prior to 1932 was focused primarily in the central vent region of the volcano. However, after 1932, numerous flank eruptions occurred (Ozerov *et al.,* 1997). Eruptions last from weeks to years and range in style including vulcanian, stombolian, lava fountaining and lava flows. Sub-plinian events occur at Klyuchevskoy, but are very rare with the last observed event in October 1994 (Ozerov 2000).

Bezymianny is the only volcano in the Klyuchevskoy Group that erupts dominantly andesite. Following a catastrophic lateral blast eruption in 1956, Bezymianny has been active for the past 55 years making it one of the most active volcanoes in Kamchatka (Plechov *et al.,* 2008). Since the late 1970's, typical activity at Bezymianny consists of dome growth and collapse resulting in block and ash flows, lahars, and sub-plinian eruptions with frequencies on the order of one to two eruptions per year (Belousov *et al.,* 1996; Belousov *et al.,* 2002). Occasionally, eruptions are followed by short lava flows in the main crater of the volcano.

Klyuchevskoy and Bezymianny share common O, Sr, Pb, and Nd isotopic characteristics, which are interpreted as demonstrating that the two systems originate from a common Klyuchevskoy-type parental magma (Ozerov *et al.,* 1997; Bindeman *et al.,* 2004; Auer *et al.,* 2009). The source of the parental magma is a large melt body imaged geophysically near the Moho (Lees 2007). The current interpretation is that Bezymianny magmas further evolve in an intermediate magma chamber at shallower depth (Ozerov *et al.,* 1997; Fedotov *et al.,* 2010).

SAMPLE DESCRIPTIONS AND PETROGRAPHY

We collected a time-series suite of erupted volcanic products from Bezymianny and Klyuchevskoy volcanoes (**Table 1**). Bezymianny samples include five samples from extrusive domes that surround the modern edifice of the volcano as well as 13 juvenile samples from

modern eruptions spanning an age from the 1956 directed-blast eruption to the June 1, 2010 pyroclastic flow eruption. Most juvenile samples from Bezymianny are from bombs with obvious cooling textures (breadcrusted outer surfaces or slumping over larger dense blocks), which were emplaced in pyroclastic flows. Three of the modern eruptions at Bezymianny (December 2006, October 2007, and August 2008) contain large inclusions (enclaves and xenoliths) within the sampled juvenile material. Twelve inclusions from these eruptive units are incorporated into this study. Klyuchevskoy samples include five historic lavas erupted over the time period of 1945-2007. We focused primarily on the less sampled Bezymianny volcano, and we rely on the wealth of published data from Klyuchevskoy for compositional comparisons and interpretations.

The petrography of Klyuchevskoy lavas has been described in detail (Kersting & Arculus, 1994; Ariskin *et al.,* 1995; Ozerov *et al.,* 1997; Mironov *et al.,* 2001; Khubanaya *et al.,* 1994; Khubanaya *et al.,* 1998; Auer *et al.,* 2009). Kersting & Arculus (1995) define a complete crystallization sequence from high-magnesian basalts to high-alumina basalts based on mineral compositions and textures. The high-alumina basalts that result from this crystallization sequence have phenocrysts of plagioclase (An_{85-54}), olivine (Fo_{80-85}), augite, and orthopyroxene with groundmass plagioclase, olivine, pigeonite, and magnetite. Plagioclase and pyroxene phenocrysts have very complex zoning recording multiple recharges of new magma (Kersting & Arculus, 1994). One xenolith with cumulate texture has been described from Klyuchevskoy deposits as an olivine two-pyroxene gabbro from a 1937 lava flow (K-256, Kersting & Arculus, 1994).

The textures and mineralogy of Bezymianny modern eruptive products (1956-2007) have been described in detail by our collaborators at Moscow State University and the University of Alaska, Fairbanks (Plechov *et al.,* 2008; Shipman *et al.*, 2010; Shcherbakov *et al.,* 2011). Juvenile vesicular andesite from Bezymianny is dominated by plagioclase and 2-pyroxene phenocrysts. A typical mineral assemblage is plagioclase (70-90% of phenocrysts), orthopyroxene, clinopyroxene, Fe-Ti oxides and trace apatite and/or amphibole. Orthopyroxene is the dominant pyroxene phase. The sample groundmass is typically clear glass or glassy with abundant microlites of plagioclase and pyroxene. Plagioclase phenocrysts range in An content from 45-78 wt.% and are highly zoned and sieved (**Figure 2A and B**). Zoning patterns in

plagioclase have been interpreted as magma heating caused by frequent mafic recharge (Shcherbakov *et al.,* 2011). Bezymianny extrusive domes contain less glass than the juvenile products and have abundant large (up to 2-4mm) amphibole phenocrysts in addition to the phases described above (**Figure 2C and D**).

Observed inclusions in Bezymianny juvenile samples have a wide range of textures but contain mineral assemblages similar to those of the host rocks. Most inclusions have glassy magmatic textures (phenocrysts of plagioclase and pyroxene in a groundmass with Fe-Ti oxides, plagioclase, pyroxene, trace apatite and hornblende). One inclusion, 01BZT09**, differs dramatically in texture from the typical magmatic inclusions. 01BZT09**, from the October 2007 eruption of Bezymianny, is highly crystalline and has a texture that is granular and suggests subsolidus recrystallization. Rather than the large plagioclase phenocrysts with complex zoning typical of other Bezymianny samples (**Figure 2A, B, E**), this inclusion has small euhedral plagioclase grains that share grain boundaries (**Figure 2F and G**). The plagioclase display simple twinning and do not display oscillatory zoning. Large pyroxene grains have poikilitic texture enclosing the smaller euhedral plagioclase. These oikocrysts do not consist of just one pyroxene grain, but are themselves made of many possibly recrystallized clinopyroxene and orthopyroxene grains that share grain boundaries (**Figure 2F and G**). The inclusion has an overall minor foliation (aligned pyroxene chains) as well as abundant Fe-Ti oxides (**Figure 2H**). We interpret this sample as a metamorphosed piece of the lower mafic crust beneath the Klyuchevskoy Group of volcanoes.

ANALYTICAL METHODS

Major and Trace Element Analyses

Major and trace element analyses were completed at Washington State University (WSU). Protocols and precision for major element analyses by XRF and trace element analyses by ICP-MS are outlined in Johnson *et al.,* (1999) and in technical notes at the WSU Geoanalytical Laboratory website (www.sees.wsu.edu/Geolab/note.html). XRF precision is typically <1% error

for major and minor elements. Long-term precision for ICP-MS is <5% for REEs and <10% for all other trace elements.

Pb-isotope Chemistry

Approximately 100 mg splits of sample powders were digested in a 10:1 concentrated HF:HNO_3 solution on a hotplate at 125°C. After digestion, samples were dried and re-dissolved in 6M HCl to convert to Cl^- form and verify complete dissolution. Samples were dried and brought up in 1M HBr for ion exchange chromatographic separation of Pb. Pb was purified from the sample matrix using a 300µl resin bed of BioRad AG-1-X8 100-200 mesh anion exchange resin. The resin is cleaned with 6M HCl and DI H_2O. Samples are loaded in 1M HBr and Pb is eluted with 6M HCl. The columns are then cleaned and the separation process is repeated for complete Pb purification. All reagents were purified by sub-boiling distillation in teflon.

Pb-isotope MC-ICP-MS Analysis

Pb isotope compositions were analyzed by dry plasma multi-collector ICP-MS (inductively coupled plasma mass spectrometry) using a Nu Plasma-HR at the University of Washington. Prior to analysis, purified sample solutions were doped with a standard Tl solution to monitor instrumental mass bias. Instrument mass bias and drift was corrected for using standard-sample-sample-standard bracketing with certified Pb solution standard NBS-981. Replicate analyses of a laboratory internal rock standard, UW-BCR, record 2σ analytical precisions of 150 ppm, 225 ppm, and 250 ppm for $^{206}Pb/^{204}Pb$, $^{207}Pb/^{204}Pb$, and $^{208}Pb/^{204}Pb$ respectively. Duplicates of 13 different samples were analyzed. The data for these duplicate analyses are presented as averages included in **Table 3**. Detailed analytical procedures are described in Harkins *et al.,* (2008).

Microprobe Analysis

Electron microprobe (EMP) analyses were completed at the University of Washington using a JOEL 733 SuperProbe equipped with four WDS and one EDS spectrometers. Plagioclase, pyroxene, Fe-Ti oxide, apatite and glass compositions were measured for samples 06BZT05,

06BZT02b, and 02BZT08 from the 1956 cryptodome, a 2006 breadcrust bomb with clean glass, and a breadcrust bomb from 2007 with highly microlitic glass. These samples were chosen to represent the spectrum of types of deposits and textures seen at Bezymianny. In addition to these analyses, plagioclase and pyroxene analyses were measured for an extrusive dome sample from Bezymianny (06BZT08) and for two inclusions: 1) 02BZT09a – an inclusion with typical magmatic textures in host 02BZT09b and 2) 01BZT09** - a lower crustal inclusion.

RESULTS

Major and Trace Element Chemistry

Bezymianny modern products range in composition from basaltic andesites to andesites with SiO_2 between 56.6 and 60.2 wt.% (**Table 2**). The extrusive domes at Bezymianny are slightly more evolved andesites with SiO_2 between 56.6 and 62.8 wt.%. In general, the deposits at Bezymianny become slightly more mafic with time (Izbekov *et al.,* 2010). This transition is reflected in shifts to lower SiO_2 from the domes to modern products as well as in MgO abundances, which increase in the younger samples (**Figure 3**). Alkali contents ($Na_2O + K_2O$) at Bezymianny are 4.53-4.97 wt.% for modern juvenile samples and 4.87-5.48 wt.% for the more evolved extrusive domes. Measured Klyuchevskoy lavas have SiO_2 between 53.8 and 54.6 wt.%, MgO between 8.3 and 8.5 wt. %, and alkalis (Na_2O+K_2O) between 4.1 and 4.7 wt.%. Klyuchevskoy lavas have higher CaO and TiO_2 and lower Al_2O_3 abundances than modern Bezymianny juvenile deposits.

The extrusive domes on the edifice of Bezymianny display the most evolved compositions at Bezymianny and within the CKD. These samples are also texturally evolved and contain large phenocrysts (amphibole up to 2mm) in a mostly crystalline groundmass compared to the modern eruptive products where most phenocrysts are smaller and amphibole occurs only in a glassy and/or microcrystalline groundmass and not as phenocrysts (**Figure 2**). While these extrusive domes represent a different eruptive period of Bezymianny prior to the modern edifice and post-1956 activity, they still lie along an evolutionary trend with the historical eruptive products of Bezymianny that have become progressively more mafic over time (**Figure 3**).

Trace element concentrations at Bezymianny and Klyuchevskoy record typical arc magmatic characteristics with enrichments in LILE and fluid mobile trace elements and depletions in HFSE. Incompatible trace element abundances are slightly higher in the more evolved magmas from Bezymianny than those from Klyuchevskoy. In addition, V and Ti are lower at Bezymianny than Klyuchevskoy consistent with fractionation of Fe-Ti oxides.

Bezymianny Mineral Chemistry

Plagioclase phenocrysts at Bezymianny volcano range in An content between ~ 40 and 83 wt.% (**Figure 4**). This range of An contents is measured in the older extrusive dome (Lohkmaty), the 1956 cryptodome, as well as in modern juvenile eruptive products at Bezymianny (samples 06BZT08 (Lohkmaty), 06BZT05 (cryptodome), 02BZT08, 06IPE17, and 06BZT02b). Plagioclase phenocrysts are strongly zoned and display a range of textures including euhedral grains, grains with sieved cores, and grains with rings or zones of sieved texture.

Pyroxene phenocrysts at Bezymianny are dominated by orthopyroxene for the older extrusive dome (Lohkmaty), the 1956 cryptodome, and the modern juvenile eruptive products at Bezymianny (same samples as listed above for plagioclase). Clinopyroxene is present in these samples, but is much less abundant than orthopyroxene. Orthopyroxene compositions range from ~21-25 wt.% MgO and 16-23 wt.% FeO with CaO abundances less than 5 wt. % (**Figure 5A and B**).

Glass compositions measured at Bezymianny vary depending on whether the glass is clean glass or highly microlitic. Clean glass from 06BZT02b has an average SiO_2 content of 71.0 ± 0.8 wt.%.

Bezymianny Inclusion Major Element and Mineral Chemistry

The inclusions from juvenile Bezymianny erupted products have diverse major element compositions. Most magmatic textured inclusions are either slightly more mafic (basaltic

andesites) than modern Bezymianny magmas (overall SiO_2 between 53.6 and 57.4 wt.%) or overlap in composition with their host magmas (**Figure 3)**. On the crystal scale, pyroxene compositions measured in the magmatic inclusion, 02BZT09b, are similar to the compositions of pyroxenes from other Bezymianny erupted products and the host magma (02BZT09a) (**Figure 5**). Two inclusions from the October 2007 pyroclastic flow of Bezymianny are obvious outliers that do not match either Bezymianny or Klyuchevskoy compositions (01BZT09* and 01BZT09**). These inclusions are basaltic (SiO_2 ~51 wt.%, MgO ~ 9 wt.%), have lower alkali contents ($Na_2O + K_2O$) and higher CaO, MnO, and FeO abundances. N-MORB normalized rare earth element patterns of these samples are flat and less than 1.0, unlike other Bezymianny products (**Figure 6**). Pyroxene and plagioclase compositions from 01BZT09** differ from other inclusions and Bezymianny magmas as well. Pyroxenes from this sample have a restricted range in composition relative to other samples. Orthopyroxenes are less Fe-rich (~16-19 wt. % FeO) and have between ~23 and 26 wt.% MgO. Clinopyroxene is much more abundant in this sample and forms a tight cluster in compositional space with ~ 21 wt.% CaO, 15 wt.% MgO, and 8 wt.% FeO (**Figure 5A and B**). 01BZT09** has lower An contents between ~ 40 and 62 wt.% An (**Figure 4**). These compositional observations on the whole rock and crystal scale are consistent with the textural interpretation above that this inclusion is a lower crustal xenolith.

Mineral Thermo-barometry

Temperatures and pressures of crystallization were calculated using two-pyroxene thermometry and barometry for our inferred lower crustal sample 01BZT09**. This sample, described above, is highly crystalline and granular with unzoned plagioclase and a granoblastic texture. We interpret this as a subsolidus recrystallization texture of an originally mafic igneous rock. The orthopyroxene and clinopyroxene grains from this sample have very restricted compositional ranges (**Figure 5A and B**), which suggests that both orthopyroxenes and clinopyroxenes reached equilibrium and can be used for P-T determinations.

We used the two-pyroxene thermometer and barometer of Putirka (2008) (Equations 39 and 37) to calculate pressures and temperatures of pyroxene crystallization for 19 contiguous pairs of clinopyroxene and orthopyroxene. In addition to physical proximity, this method requires a test

for equilibrium Fe-Mg partitioning between clinopyroxene and orthopyroxene pairs. Equilibrium partitioning between pyroxene grains may be affected by many factors such as Fe^{3+} partitioning (Putirka, pers. comm.). Experiments suggest that equilibrium Fe-Mg exchange should produce $K_D(Fe\text{-}Mg)^{cpx\text{-}opx} = 1.09 \pm 0.14$ (Putirka, 2008). Our pyroxene pairs have $K_D(Fe\text{-}Mg)^{cpx\text{-}opx} = 0.82 \pm 0.07$, which is within two standard deviations of the experimental equilibrium value. The homogeneity of the pyroxene compositions in this sample combined with Fe-Mg partitioning within experimental equilibrium values justifies the use of this method to calculate pressures and temperatures of formation. Using the Putirka (2008) model, we calculate an average temperature and pressure of crystallization for 01BZT09** of 929 ± 26 °C and 5.2 ± 0.6 kilobars (depth greater than 15km).

Pb Isotope Compositions

All samples from Kamchatka have $^{207}Pb/^{204}Pb$ and $^{206}Pb/^{204}Pb$ isotope compositions that plot just above the Northern Hemisphere Reference Line (NHRL; Hart, 1984) and have MORB-like signatures (**Table 3, Figure 7**). Previous authors have identified the primitive MORB-like nature of Pb-isotopes in Kamchatka (Kersting & Arculus, 1995; Kepezhinskas *et al.,* 1997; Turner *et al.,* 1998; Churikova *et al.,* 2001). We also record unradiogenic Pb compositions for Bezymianny and Klyuchevskoy ($^{208}Pb/^{204}Pb = 37.850\text{-}37.903$, $^{207}Pb/^{204}Pb = 15.468\text{-}15.480$, and $^{206}Pb/^{204}Pb = 18.249\text{-}18.278$ at Bezymianny; $^{208}Pb/^{204}Pb = 37.907\text{-}37.949$, $^{207}Pb/^{204}Pb = 15.478\text{-}15.487$, and $^{206}Pb/^{204}Pb = 18.289\text{-}18.305$ at Klyuchevskoy). These compositions overlap only the unradiogenic extreme of MORB compositions (N-MORB and Pacific MORB).

Our high-precision MC-ICP-MS Pb-isotopic data are the first to reveal that each of the volcanic centers that we analyzed (Bezymianny, Klyuchevskoy, Shiveluch, and Karymsky) is compositionally distinct in Pb-isotopic space (**Figure 7**). We measured Pb-isotope compositions for Shiveluch volcano in the Northern CKD and Karymsky volcano in the Eastern Volcanic Front for comparison to the Klyuchevskoy Group (**Table 3**). Sample descriptions for Karymsky and Shiveluch volcano are reported in **Table 1** of **Appendix A**. Pb-isotope compositions for Bezymianny and Klyuchevskoy are lower than compositions recorded at Shiveluch and Karymsky volcanoes.

Compositional distinctions between Bezymianny and Klyuchevskoy show variation on very small spatial scales (~9km). The isotopic contrast between Klyuchevskoy and Bezymianny melt compositions is larger than conservative analytical error (~200 ppm) for all measured samples. In addition, the andesitic Bezymianny is more radiogenic than its basaltic neighbor, Klyuchevskoy.

DISCUSSION

Subduction Zone Components and Melt Generation Beneath Bezymianny

Because Klyuchevskoy and Bezymianny volcano are postulated to share the same source, we would expect the chemical signal of subduction zone components to be the same for both volcanoes. Bezymianny magmas have trace element patterns similar to those observed in Klyuchevskoy lavas in this study (**Figure 8).** The magmas have enrichments in LILE and LREE and depletions in HFSE that are characteristic of fluid transfer from the subducting slab (e.g., Brenan *et al.,* 1994; Ayers *et al.,* 1997) and support previous conclusions that melting in the CKD is caused primarily by fluid fluxed melting (Kepezhinskas *et al.,* 1997; Dorendorf *et al.,* 2000; Churikova *et al.,* 2001; Portnyagin *et al.,* 2005; Turner *et al.,* 2007). Notable differences between the two volcanoes are that Bezymianny magmas have higher concentrations of Rb, Ba, Th, U, Pb, and La and lower concentrations of Ti and the HREE. The enrichment in incompatible elements may be a function of the more evolved nature of Bezymianny magmas (lower Ti reflecting the crystallization of Fe-Ti oxides and hornblende).

La/Yb and Th/Yb can be used to distinguish mantle source enrichment by subduction zone components such as fluid and sediment (Pearce *et al.,* 1984). Bezymianny and Klyuchevskoy compositions are distinct from one another in La/Yb and Th/Yb space (**Figure 9**) with Bezymianny having a stronger subduction zone component signal. The same signal is also seen in Ce/Yb vs. Th/Yb, where Ce is also a fluid mobile element. However, both systems have compositions on the lower end of arc systems worldwide (most continental margins produce magmas with La/Yb ranging ~8-20) supporting previous observations (described above) that the Kamchatka arc has a depleted MORB-source mantle composition.

Bezymianny has steeper REE patterns than Klyuchevskoy (**Figure 10**). Steepening in REE patterns can be caused by varying degrees of melting or melting in the presence of a phase that partitions light from heavy REEs such as garnet. Sr/Y and Dy/Yb ratios at Bezymianny fall within the range of values of Klyuchevskoy (**Figure 11**), so it is unlikely that varying degrees of garnet present during melting explain the REE variations between the two systems. This is highlighted if the Dy/Yb values observed here are compared to those that may be generated from fluid-fluxed mantle melting.

We calculate Dy/Yb using a simple batch melting model of a fluid-fluxed garnet peridotite mantle to test for the amount of garnet that may be present in the melting region beneath the CKD. The effect of garnet on Dy/Yb chemical variation is opposite to that of fractionation by pyroxene and amphibole making Dy/Yb ratios a more accurate tracer of garnet than other trace element ratios such as Sr/Y. Dy/Yb ratios calculated with our model require a garnet free melting source. Dy/Yb measured at Bezymianny ranges from 1.7-1.9 (**Figure 11**), which are below the lowest Dy/Yb values produced with 1% garnet in a mantle source (greater than 2 for melt fractions less than 10%) (**Figure 12**). Dy/Yb values for Klyuchevskoy lavas measured here are slightly higher than Bezymianny (1.9-2) but would still require a garnet free melting region given this simplified batch model (**Figure 12**). Churikova *et al.,* (2001) report flat REE patterns on N-MORB normalized diagrams, low La/Yb (1.83-10.28) and HREE only 6-15 times chondritic values for an arc-wide Kamchatka study that also support the hypothesis that garnet is probably not a prominent residual component in the mantle source of the Kamchatka arc.

Are Bezymianny and Klyuchevskoy Cogenetic?

The magmas at Bezymianny are hypothesized to have evolved through fractional crystallization from the same parental magmas as Klyuchevskoy volcano (Ozerov *et al.,* 1997). In general, major and trace element data presented here do not refute this concept. However, Pb isotopic data from these volcanoes require that mixing and assimilation also occur during the generation of Bezymianny magmas in order to account for isotopic variation between the two volcanic systems.

Major and Trace Element Variations

The major element trends between Bezymianny and Klyuchevskoy are consistent with Klyuchevskoy magmas undergoing fractional crystallization to produce Bezymianny erupted products assuming fractional crystallization of the observed phases erupted at both volcanoes: olivine, plagioclase, pyroxene, Fe-Ti oxides, and minor hornblende (Bezymianny only). Bezymianny products are more evolved than Klyuchevskoy magmas with lower MgO, FeO, CaO, TiO_2, and higher Na_2O, and K_2O (**Figure 3**). The spread in Klyuchevskoy compositions for TiO_2, Al_2O_3, MgO, Na_2O, and K_2O is much larger than at Bezymianny volcano. If linear trends are fit to the Klyuchevskoy literature data and to the Bezymianny data from this study, we observe kinks between the trends of the two volcanoes in these same elements representing onset or loss of mineral phases (dashed lines, **Figure 3**).

Similar to major element trends, trace element systematics at Bezymianny also could imply that Klyuchevskoy magmas fractionally crystallize to form Bezymianny magmas. Zr/Y ratios show enrichment from ~3-5 at Klyuchevskoy to ~ 4.5-7.5 at Bezymianny (**Figure 13**). Bezymianny magmas are not evolved enough to saturate zircon, and our data correspond to Zr remaining an incompatible element during the crystallization of other phases (plagioclase, clinopyroxene, orthopyroxene, Fe-Ti oxides, hornblende, and apatite). The two samples that cannot be explained by fractional crystallization are inclusions from Bezymianny, which have lower Zr/Y values than all of the Klyuchevskoy data. These inclusions are the same samples that are outliers in major element space (01BZT09* and 01BZT09**) and demonstrate a sampled magma composition at Bezymianny that is not connected to Klyuchevskoy through crystallization.

Ratios of incompatible trace elements to more compatible trace elements such as Rb/La, Cs/Yb, and Zr/Sr all increase from Klyuchevskoy to Bezymianny as magmas increase in SiO_2 content (not shown). As discussed previously, Dy/Yb remains fairly constant between Klyuchevskoy and Bezymianny, which precludes amphibole from being a dominant phase during fractional crystallization (Davidson *et al.,* 2007).

Rare Earth Element Modeling for Bezymianny Magmas

We modeled fractional crystallization of Klyuchevskoy lavas using multiple fractionating assemblages to compare with observed Bezymianny REE patterns. The two initial Klyuchevskoy compositions used for modeling were our 2007 Klyuchevskoy lava (KL-Krest-07) and a high-alumina basalt end member from Ariskin *et al.,* (1995) (sample K-31, 1951 lava from Bylinkinoi). These end-members were chosen because Bezymianny andesites have been proposed to originate from the high-alumina basalts at Klyuchevskoy (Ozerov *et al.,* 1997). We modeled four different mineral assemblages representing a range of possible crystallization paths and residues beneath Bezymianny (**Figure 14** describes assemblages in detail). None of these simplified models of pure crystal fractionation reproduce the crossing pattern observed between Bezymianny and Klyuchevskoy REEs. Only by choosing the most extreme partition coefficients reported in the literature can we reproduce the crossing patterns from Klyuchevskoy to Bezymianny. Because of the range of possible outcomes in trace element modeling, these models cannot disprove the cogenetic nature of Bezymianny and Klyuchevskoy magmas. They do, however, show that the formation of crossing REE patterns between the two volcanoes via pure fractional crystallization is unlikely.

Tolstykh *et al.,* (2003) proposed that light REE enrichment and heavy REE depletion develops during the evolution of Klyuchevskoy magmas to Bezymianny magmas as a result of "extensive amphibole fractionation". Crystallization of 18% amphibole, 40% clinopyroxene, 20% plagioclase, 15% orthopyroxene, and 7% magnetite using the same initial compositions and partition coefficients as above still produces REE patterns that do not have heavy REE depletions. To reproduce the observed mid to heavy REE depletions in Bezymianny magmas from Klyuchevskoy, would require 50-80% fractional crystallization of an assemblage that is 60% or greater amphibole. Not only is this highly unlikely given the constant Dy/Yb ratios at Klyuchevskoy and Bezymianny, but it would also require the melts to have unusual major element compositions far from the andesitic composition of Bezymianny. Therefore, REE trends may suggest that there is an additional source of magma aside from Klyuchevskoy-like magmas or that assimilation is involved in the generation of Bezymianny magmas.

Isotopic Heterogeneity

1. Distinct Pb-isotope Signatures at Bezymianny and Klyuchevskoy

In support of the REE evidence that Bezymianny and Klyuchevskoy may evolve from different parental magmas, we resolve distinct Pb-isotope compositions for Bezymianny and Klyuchevskoy volcanoes respectively (**Figure 7**). The older extrusive domes on the southern edifice of Bezymianny have slightly more radiogenic Pb than the modern eruptions of Bezymianny, and plot closer to Klyuchevskoy compositions (**Figure 7**), implying that at an earlier stage the two volcanic systems may have had a more similar source. However, even the more radiogenic extrusive domes do not overlap Klyuchevskoy compositions.

Bezymianny, a more evolved volcanic center (andesites and dacites) has less radiogenic Pb isotopes than Klyuchevskoy, the more primitive volcanic center (basalt). If Bezymianny is indeed the product of the evolution of Klyuchevskoy magmas in an upper crustal magma chamber (Ozerov *et al.,* 1997), then the Pb isotopic composition of Bezymianny products should be the same as Klyuchevskoy for closed system fractionation. If Bezymianny is related to Klyuchevskoy by fractionation associated with upper crustal assimilation, then any Pb isotope shift would likely be to more, not less, radiogenic composition. Differentiated upper crust typically develops more radiogenic Pb isotope compositions with time; however, the absence of substantial intracrustal differentiation and the young age of the crust in Kamchatka (Cenozoic; Fedotov 1991; Dorendorf *et al.,* 2000) mitigate against any such contrast in composition.

To place better constraints on the subsurface composition of the crust at Bezymianny volcano we use data from the large suite of magmatic inclusions from the December 2006, October 2007, August 2008, December 2009, and June 2010 eruptions. Based on their mineralogy, texture, and major element composition we interpret these inclusions to have two distinct origins: 1) magmatic and 2) lower crustal. Most of the sampled inclusions have Pb isotope compositions that match those of the modern juvenile eruptions at Bezymianny and are likely cogenetic with their host eruptive units (**Figure 15A**). However, four inclusions have lower $^{207}Pb/^{204}Pb$ and $^{206}Pb/^{204}Pb$ than modern Bezymianny magmas (01BZT09**, 01BZT09***, 02BZT09b, and

10IPE1B from the October 2007, August 2008, and June 2010 eruptions). 01BZT09** is a lower crustal xenolith, while we interpret the other inclusions as magmas beneath Bezymianny.

We evaluate four hypotheses to explain the chemical and isotopic contrast between Bezymianny and Klyuchevskoy: 1) Sampling only five lava samples at Klyuchevskoy produced a biased data set and that Klyuchevskoy compositions actually encompass a much broader range of Pb isotope values that would overlap Bezymianny modern juvenile products and inclusion compositions, 2) Klyuchevskoy magmas may assimilate more radiogenic material on their path through the crust to shift them to higher $^{207}Pb/^{204}Pb$ and $^{206}Pb/^{204}Pb$ than is measured at Bezymianny, 3) There may be sediment contamination in the source of Klyuchevskoy that is absent in the Bezymianny source that produces more radiogenic Pb isotope signatures at Klyuchevskoy and 4) There may be multiple magma sources or crustal contaminants beneath Bezymianny and Klyuchevskoy that are represented by the lower $^{207}Pb/^{204}Pb$ and $^{206}Pb/^{204}Pb$ of the Bezymianny inclusions.

Hypothesis 1: Biased sampling of Klyuchevskoy compositions.

Our fieldwork focused on detailed sampling of the less studied Bezymianny volcano; therefore, we present high-precision isotope data for only 5 lavas of Klyuchevskoy volcano. If these data are not representative of the entire range of Klyuchevskoy compositions, we could incorrectly interpret the isotopic data as evidence for distinct CKD magma sources. We compare our new data with published Pb isotope data summarized by Portnyagin *et al.,* (2007b) for Klyuchevskoy volcano (**Figure 15B**). In addition, we compare high-precision double-spike Pb isotope data for 25 Klyuchevskoy tephras that span a range of ages from ca. 200 to 9000 BP. These tephras were collected and analyzed by our collaborators at IFM-GEOMAR as part of the large German-Russian KALMAR (Kurile-Kamchatka Aleutian Marginal Sea-Island Arc Systems) project (Portnyagin *et al.,* 2011; Portnyagin & Ponomareva 2012). Only a few samples from the large Klyuchevskoy database overlap Bezymianny compositions and none of these are high-precision isotopic analyses. In addition, these data overlap only the range of the extrusive domes at Bezymianny and not the more recent eruptive products. Tephra Pb isotope data from KALMAR is high-precision, covers a greater range of values than our data, and represents over 6000 years of eruptive activity at Klyuchevskoy. These data all have more radiogenic Pb compared to 1956-

recent Bezymianny products, but some of the tephras overlap the older Bezymianny extrusive domes (pers. comm. Maxim Portnyagin). Our data for Klyuchevskoy fall entirely within the range of and along the same trend as the KALMAR high-precision data for Klyuchevskoy. Therefore, we interpret the contrast in Pb-isotopes between Klyuchevskoy and Bezymianny to be a real compositional variation rather than one that results from sampling bias.

Hypothesis 2: Klyuchevskoy Magmas Assimilate Material with a Radiogenic Pb-isotope Signature

If Bezymianny and Klyuchevskoy share magmas in a deep chamber, then Klyuchevskoy must acquire more radiogenic Pb isotope compositions at shallow levels. Typically more radiogenic crust is concentrated in the upper portions of the crust as a function of differentiation and age of continental/island arc crust (Hofmann, 1997). Due to the juvenile nature of the Kamchatka arc, however, there is no evidence for the presence of a more radiogenic upper crust. In addition, assimilation of the upper crust within the Klyuchevskoy magmatic plumbing system is unlikely from geochemical, geophysical, and thermal modeling perspectives, and certainly less likely than for the more differentiated Bezymianny magmas.

Geochemical constraints that make upper crustal assimilation unlikely at Klyuchevskoy are the high Mg# of Klyuchevskoy magmas, low SiO_2 contents, and MORB-like Nd and Sr isotopic compositions (Kersting & Arculus, 1995; Dorendorf *et al.,* 2000; Portnyagin *et al.,* 2007). MORB-like Nd isotopes coupled with slightly radiogenic Sr isotopes is not consistent with assimilation of old crustal terrane and suggest that if assimilation does occur, magmas must assimilate juvenile crust with isotopic compositions similar to MORB (Kersting & Arculus, 1995).

Geophysical compilations that attempt to reconstruct the volcanic structure of Klyuchevskoy suggest that magma moves from the base of the crust and/or mantle to the surface through a narrow vertical conduit that lacks crustal magma chambers (Anosov *et al.,* 1978; Ozerov *et al.,* 1997; Ozerov *et al.,* 2007; Lees *et al.,* 2007). However, based on the earthquake catalog and geodetic measurements, Fedotov *et al.,* (2010) argue for a shallow magma body at approximately

3km beneath Klyuchevskoy. This depth would place a shallow magma chamber into what Fedotov *et al.,* (2010) consider "sedimentary" layers composed of young volcanic material that would not have a significant Pb-isotope contrast from current eruptive products in the CKD.

Assimilation of crustal material is both thermally inhibited (Dufek & Bergantz, 2005) and causes crystallization and evolution of magmas (Reiners *et al.,* 1995) that we do not see reflected in Klyuchevskoy lavas. Assimilation of the mafic roots of arc volcanic systems via melting of amphibolite at grain boundaries can shift incompatible element compositions without altering SiO_2 contents to more evolved magmas (Dungan & Davidson, 2004); however, we have no evidence or model to suggest that the mafic root or lower crust of the CKD is more radiogenic in Pb-isotope composition than the melts passing through it. In addition, we have no evidence for extensive amphibole fractionation beneath the CKD (**Figure 11**). Frequent eruptions of Klyuchevskoy and its status as the most voluminous arc volcano in the world suggest that magmas move quickly through the system and likely do not have time to undergo much upper crustal assimilation. Finally, the hypothesis that a common parental Klyuchevskoy-Bezymianny magma now has a contrasting Pb isotopic composition due to assimilation of radiogenic crust in Klyuchevskoy rather than assimilation of unradiogenic crust in Bezymianny, is not consistent with the geophysical contrasts between the two volcanoes. Bezymianny has geophysical evidence for shallow crustal magma chambers (Fedotov *et al.,* 2010), less frequent eruptive behavior, and a more evolved melt composition.

Hypothesis 3: Sediment Contamination Alters Magmatic Pb-isotope Composition

Previous models based on isotope systematics coupled with major element trends at Klyuchevskoy and within the CKD have placed tight constraints on the amount of sediment that can be added to the mantle source via subduction (Kersting & Arculus, 1995; Kepezhinskas *et al.,* 1997; Dorendorf *et al.,* 2000; Churikova *et al.,* 2001). If Pb-isotope compositions of sediments from the ODP 145 drill core from the northwest Pacific Ocean just east of Kamchatka are characteristic of sediment subducted beneath the arc, Kersting & Arculus (1995) show that the amount of sediment input to the Kamchatka mantle source must be less than 1% in order to preserve the primary MORB isotopic compositions in erupted products. Tsvetkov *et al.,* (1989)

came to a similar conclusion based on Be isotopes, and Dorendorf *et al.,* (2000) use Sr and O isotopes to show that fluids come from the altered oceanic crust and not sediments on the subducted slab beneath the Kamchatka arc. While in general, sediment addition to the source can be limited to small amounts, we can refine this model specifically for Bezymianny and Klyuchevskoy with our new high-precision Pb isotope data.

For the models, we used an average ODP 145 drill core sediment composition (Kersting & Arculus, 1995) of $^{207}Pb/^{204}Pb = 15.6$, $^{206}Pb/^{204}Pb = 18.6$, and [Pb] = 11.5 ppm. Mixing calculations with the lowest range of N-MORB Pb-isotopes (Hofmann, 1988; Sun & McDonough, 1989) allow 0% of sediment to be added to the mantle wedge because $^{207}Pb/^{204}Pb$ and $^{206}Pb/^{204}Pb$ values at Bezymianny and Klyuchevskoy are less radiogenic than N-MORB. If an average Pacific MORB (P-MORB) mantle composition is used, the same conclusion is drawn (no sediment allowed). The only scenario by which sediment may be added to the mantle wedge is if the wedge is assumed to have the least radiogenic P-MORB values reported. We assumed a P-MORB composition that is two standard deviations below the mean for P-MORB (Arevalo *et al.,* 2010) so as to represent a "low" P-MORB value that is not the lowest outlier measured. With this composition of the mantle wedge, 0.2% and 0.4% sediment at Bezymianny and Klyuchevskoy, respectively, can be accommodated if the sediment is added to a fluid-fluxed solid mantle with a Pb concentration of 0.16ppm (**Figure 16A**). If sediment is added to a fluid-fluxed mantle melt of this depleted source (melt Pb concentration of 3ppm) rather than a solid mantle source, then 4% and 7% sediment may be added to Bezymianny and Klyuchevskoy sources respectively (**Figure 16B**). We argue that because this calculation relies on the choice of an extreme P-MORB end-member, that this represents a maximum amount of sediment addition allowable.

Ce/Pb ratios are approximately the same for Klyuchevskoy (5.15 to 5.52) and Bezymianny (4.38 to 5.07) (**Figure 17**). These values are within the range of typical arc basalts (1-10: Miller *et al.,* 1994; Noll *et al.,* 1996; Plank, 2005), and are low compared to MORB values (Hofmann, 1988). The lower Ce/Pb ratios of arc basalts reflect addition of a slab fluid, which preferentially partitions Pb with respect to Ce (Brenan *et al.,* 1994; Miller *et al.,* 1994), or partial melt of the subducting slab or sediment (Tatsumi, 2000; Kelemen *et al.,* 2003). If sediment contamination

was affecting the Pb-isotope compositions at Bezymianny and Klyuchevskoy, it should impart a high $^{207}Pb/^{204}Pb$ and $^{206}Pb/^{204}Pb$ signal coupled with a low Ce/Pb ratio. However, Klyuchevskoy has equal or higher Ce/Pb relative to Bezymianny. These observations extend to the published dataset for Klyuchevskoy eruptive products as well (**Figure 17**). Coupling Ce/Pb evidence with our modeling, which quantifies the maximum amount of sediment that has been added to Bezymianny and Klyuchevskoy sources, suggests that it is unlikely the measured Pb-isotope variations between Bezymianny and Klyuchevskoy are a result of variable sediment contamination of the mantle source region.

Hypothesis 4: Multiple Magma Sources or Contaminants Beneath Bezymianny Volcano

Because four inclusions found in Bezymianny eruptive products have relatively unradiogenic Pb compositions, we propose that these samples represent sources beneath the CKD that alter magmas similar to those at Klyuchevskoy to produce Bezymianny magmas. Two of these inclusions have magmatic textures with crystal assemblages similar to their hosts and may therefore be magmas that mix with Bezymianny magmas. Another inclusion is the lower crustal xenolith sample, which may represent crust that Bezymianny magmas assimilate during residence in the crust.

Hypothesis 4, Part 1: Magma Mixing at Bezymianny

We use the inclusion, 02BZT09b, which has magmatic textures, as a hypothetical magma to mix with Klyuchevskoy magmas (KL-Krest-07) to produce the lower Pb isotope signature at Bezymianny. Bezymianny compositions are produced by 40-60% mixing of this alternate source into Klyuchevskoy-like magmas (**Figure 15C)**.

The compositions of magmas from Tolbachik and Kamen volcanoes (**Figure 15C)** represent other possible magmas beneath Bezymianny. The Pb isotope composition of Tolbachik magmas from both the primary edifice of Tolbachik and the 1975 great fissure eruption of Tolbachik are low relative to Bezymianny and overlap with the compositions of the inclusions from Bezymianny. The edifice of Tolbachik volcano lies 20km southwest of Bezymianny volcano.

Between the two volcanoes is a linear trend of extrusive volcanic cones and domes (**Figure 18**). This may be a linear structure in the crust along which Tolbachik's mafic magmas can rise and interact with the plumbing system of Bezymianny volcano. In addition, Bezymianny trace element trends show a shift in the mid 1970's (Izbekov *et al.,* 2010; Turner *et al., submitted*) that could correlate with the timing of Tolbachik's great fissure eruption and may explain some of the mafic input at Bezymianny volcano. Churikova *et al.,* (2011) suggest that Kamen and Bezymianny share similar sources; however, published Pb isotope data from Kamen reflect Klyuchevskoy-like compositions rather than the less radiogenic compositions of Bezymianny (**Figure 15C**). Data are not available to model mixing a Kamen-like magma composition with Bezymianny magma.

Zr/Sr and Th/Yb define two parallel fractionation paths distinct in Pb-space (**Figure 19**). Zr/Sr and Th/Yb both increase with magmatic differentiation and positively correlate with $^{206}Pb/^{204}Pb$. Therefore, magmas beneath Bezymianny and Klyuchevskoy may evolve in a similar fashion towards higher incompatible element concentrations and more radiogenic Pb from different initial compositions. This observation supports the conclusion that the Bezymianny magma system includes melt with an initial Pb isotope composition that cannot be sourced from Klyuchevskoy. The Pb isotope compositions record source variation on a spatial scale less than 10km (the distance between Bezymianny and Klyuchevskoy volcanoes). An influx of a less differentiated magma to the Bezymianny magma system would also explain why most of the inclusions at Bezymianny are more mafic in composition than modern eruptive products (**Figure 3**).

Hypothesis 4, Part 2: Lower Crustal Assimilation

The chemical composition of two inclusions suggests that in addition to evidence for an alternative magma source at Bezymianny, there is evidence for assimilation as well. The REE patterns of 01BZT09** and 01BZT09*** are flat and depleted relative to all other samples of Bezymianny and N-MORB (**Figure 6**). This suggests that these two inclusions may be samples of magmatic residues left in the lower crust. One of these inclusions (01BZT09**) (**Figure 2**) is the lower crustal inclusion for which we calculate a crystallization temperature of ~929°C and a

pressure of ~5.2 kbar. Because this sample of the lower crust has a Pb-isotope signature lower than that of Bezymianny, assimilation of this material would cause Bezymianny magma compositions to shift away from Klyuchevskoy compositions. Therefore, there is evidence that some degree of the variable Pb-isotope composition between Bezymianny and Klyuchevskoy comes from assimilation of the lower crust beneath Bezymianny.

The Pb-isotope compositions of the magmatic inclusions and lower crustal inclusion are both less radiogenic than Bezymianny and are not distinguishable from one another in Pb isotopes. Therefore, quantifying how much of the variation in Pb-isotope composition between Bezymianny magmas and Klyuchevskoy magmas is a function of magma mixing versus assimilation is not possible. These inclusions, however, suggest that both of these processes take place beneath Bezymianny volcano.

Crustal assimilation and fractional crystallization at a depth of ~ 15 to 20 km beneath Bezymianny is consistent with other studies of the Klyuchevskoy Group of volcanoes. Ozerov *et al.,* (1997) describe a deep magma chamber beneath Bezymianny at the same depths that we calculate for our lower crustal inclusion (15-20km). Ozerov *et al.,* (1997) also found evidence for minor assimilation at Bezymianny recorded in Sr isotope compositions. Our model differs from the previous model, which suggests that only fractional crystallization is required to evolve Klyuchevskoy magmas to Bezymianny compositions (Ozerov *et al.,* 1997). High-precision Pb isotopes show that Bezymianny and Klyuchevskoy magmas do not compose a continuous genetic sequence produced from a single source. Bezymianny magma compositions require contribution from the lower crust and mafic magmas.

2. Unique Composition of the CKD

Given the Pb isotopic evidence for lower crustal assimilation at Bezymianny, we explore a hypothesis that Klyuchevskoy Group magmas are relatively unradiogenic compared to the rest of the Kamchatka Arc due to assimilation of a less radiogenic lower crust beneath the CKD. Bezymianny and Klyuchevskoy magmas have less radiogenic Pb isotope compositions than both Karymsky volcano to the south (Eastern Volcanic Front) and Shiveluch volcano to the north

(Northern CKD) (**Figure 7**). Our data differ from Churikova *et al.,* (2001) who report that Shiveluch Pb isotope compositions are comparable to the CKD.

Despite little data characterization of the lower crust of Kamchatka, amphibolite massif outcrops south of the CKD preserve evidence suggesting that the island arcs that were accreted to form western Kamchatka are young (< ~ 66Ma; Bindeman *et al.,* 2002). Unlike older continental arcs, the young lower crust beneath Kamchatka mitigates against much contrast in Pb-isotope compositions with the underlying mantle. Assuming a range of U/Pb ratios for the lower crust (μ = 2.1 to 10), the $^{206}Pb/^{204}Pb$ ratio of the lower crust only varies between 0.16 and 0.56% over 66 million years. The $^{206}Pb/^{204}Pb$ isotope composition of the lower crustal inclusion described above deviates from Klyuchevskoy-like basalts by approximately 0.6% and from Shiveluch magmas by ~1%. Although the lower crust does not contrast greatly with juvenile magmas in Pb isotope composition, the differences are resolvable with high-precision Pb isotope data and lower crustal assimilation beneath the entire CKD may explain the unradiogenic composition of the CKD relative to Shiveluch and Karymsky volcanoes.

Magma residence in the lower crust of the CKD is supported by geophysical evidence. Geophysical data do not resolve a sharp Moho beneath the CKD. Rather, there is an approximately 12-14 km thick region of slow seismic velocities between depths of 23 and 37 km beneath the Klyuchevskoy group of volcanoes (Balesta 1991; Lees *et al.,* 2007). This observation has been interpreted to represent a region with considerable proportions of partial melting and either magma storage in the lower crust or magma underplating the crust (Balesta, 1991; Churikova *et al.,* 2001; Lees *et al.,* 2007). We hypothesize that this blurred Moho region represents an area where rising magmas pond and where regional baseline assimilation of the lower crust beneath the CKD occurs. Granulitic facies with unradiogenic Pb isotope compositions similar to the crustal inclusion sampled by Bezymianny magma may extend from depths > 15km down to this region of partial melt. Therefore, a lower Pb isotope composition is imparted to magmas generated beneath the CKD during regional assimilation of this lower crust. The unradiogenic Pb composition imparted through lower crustal assimilation is not observable along the remainder of the arc outside of the CKD.

Other tracers (Sr and O isotopes) present two opposing models for the magnitude and type of assimilation in the CKD. Sr isotopic compositions suggest limited crustal assimilation by magmas beneath the CKD. $^{87}Sr/^{86}Sr$ values of amphibolites from Kamchatka are high (Bindeman *et al.*, 2004) so minor assimilation may explain the more radiogenic Sr isotope composition that is seen beneath Kamchatka (Kersting & Arculus, 1994; Kepezhinskas *et al.,* 1997; Dorendorf *et al.,* 2000). Assimilation of amphibolite would have to be limited to not shift the $^{87}Sr/^{86}Sr$ to values that are more radiogenic than those observed at Klyuchevskoy (Auer *et al.,* 2009). Given the uncertainty in the composition of the crust (may vary from amphibolites measured by Bindeman *et al.,* 2004), low Sr isotope values of juvenile magmas may still permit assimilation of mafic crustal roots. Oxygen isotope data, unlike Sr, suggest that large amounts of assimilation may occur beneath the CKD; however, the assimilant required is fluid altered lithospheric mantle that does not displace Mg values (Auer *et al.,* 2009). Oxygen and Pb isotope compositions would be decoupled during this type of fluid alteration so this form of assimilation, while a possible explanation for oxygen isotope variation, does not explain the lower Pb isotope compositions of the CKD.

It is possible that other mechanisms may generate the unradiogenic Pb compositions in the CKD as well. Small scale (<10's of kilometers) mantle heterogeneity has been documented (Brunelli and Seyler, 2010, Madureira *et al.,* 2011) so variation in the Pb isotopic signature of the CKD may solely reflect a heterogeneous mantle source that varies in composition on a small spatial scale (hundred of kilometers). The presence of the subducting Emperor seamount chain may contribute a different source of melting that affects the Pb isotope composition within the CKD and is not chemically traceable in the remainder of the Kamchatka arc. Meiji seamount (85Ma) off the coast of Kamchatka is less radiogenic in both $^{207}Pb/^{204}Pb$ and $^{206}Pb/^{204}Pb$ than Bezymianny and Klyuchevskoy magmas (Regelous *et al.,* 2003).

3. Pb-isotope Variation Over Short Timescales

In addition to isotopic contrast between Bezymianny and Klyuchevskoy volcanoes we also document changes in Pb-isotope composition over short time periods (decades) and longer time periods (difference between extrusive dome emplacement and the modern edifice of

Bezymianny). Older Klyuchevskoy lavas (1939-1946) are less radiogenic than lavas from 2007 (**Figure 20A**) and record compositional change in the very recent history of the volcano. On a longer timescale, the extrusive domes on the southern flank of Bezymianny's edifice are more radiogenic than modern eruptions (1956-present) (**Figure 20B**). The extrusive domes at Bezymianny have not been precisely dated but are estimated to be upper Pleistocene and Holocene in age (Almeev 2005; Bogoyavlenskaya *et al.,* 1991). The Pb isotope compositions of Bezymianny and Klyuchevskoy appear to be diverging with time.

These shifts in isotopic composition suggest that either the sources of melt beneath the CKD change rapidly (~ decades) or that the intensity of deep magmatic processes such as assimilation vary over short time periods. Variations in the amount of crustal assimilation have been suggested to correspond to the non-steady-state eruptive history of Klyuchevskoy volcano during the Holocene (Portnyagin *et al.,* 2011). Our decadal scale data suggest that these variations occur at timescales much shorter as well. Here, we show that the less radiogenic Pb-isotope compositions at Bezymianny relative to Klyuchevskoy are a function of magma mixing and/or assimilation of the lower crust. The shift observed in Pb-isotope compositions between Bezymianny extrusive domes and 1956-present day juvenile deposits shows that, only a few million years ago, magmas extruded at Bezymianny were distinctively more radiogenic (**Figure 20B**). Assuming that the shift to lower $^{207}Pb/^{204}Pb$ and $^{206}Pb/^{204}Pb$ compositions is a function of assimilation and mixing requires that either: 1) the degree of assimilation beneath a volcanic center can vary within a few million years or 2) the introduction of a new magma source beneath a volcanic center can vary within a few million years. Shifts on these timescales at Bezymianny are reasonable; however, they are required to be much more rapid at Klyuchevskoy. Klyuchevskoy lavas vary in Pb-isotopic composition over a 60-70 year time frame. Using the same reasoning as above, this requires changes in the magma source or the degree of assimilation on the order of decades.

CONCLUSIONS

Our detailed geochemical and isotopic study of Bezymianny magmas shows that the generation of Bezymianny magmas is best modeled with assimilation of the lower crust beneath the CKD as

well as mixing with mafic magmas that are not cogenetic with Klyuchevskoy volcano. The unradiogenic Pb isotope signature of Bezymianny relative to Klyuchevskoy volcano requires that Bezymianny magmas cannot be produced only by crystal fractionation of Klyuchevskoy-like magmas as was previously hypothesized (Ozerov *et al.,* 1997). Initial melts from the mantle source region beneath both Bezymianny and Klyuchevskoy may be similar in composition when they underplate the crust; however, magmas that are erupted at Bezymianny have assimilated more lower crustal material than those erupted at Klyuchevskoy (**Figure 21**). High-precision Pb isotope data are able to document the interaction of magmas with the lower crust, which is not resolvable using only major or trace element compositions.

Less radiogenic Pb isotope compositions measured for the CKD relative to magmas erupted in northern and southern Kamchatka suggest that lower crustal assimilation-fractional-crystallization (AFC) processes are more dominant beneath the CKD than in other regions of the Kamchatka arc. This geochemical observation is supported by the presence of a geophysically imaged thick blurred Moho suggesting large amounts of mafic underplating below the crust in the CKD. In addition, variation in Pb isotope compositions beneath single volcanic centers in the CKD suggests that the degree of assimilation can change over decadal timescales and on spatial scales less than 10 km.

In continental arc settings, lower crustal AFC processes are documented by unambiguous geochemical excursions such as clear amphibole signatures (Dy/Yb variation), deep garnet signatures (adakitic or high Sr/Y), or measurable isotopic shifts from assimilation of old crust (Gao *et al.,* 2004). However, Kamchatka represents a class of arcs within which lower crustal AFC processes are not obvious. In young, thin, arcs with juvenile MORB-like isotopic compositions, lower crustal AFC is often cryptic (Reagan *et al.,* 2003) or may go unobserved altogether. High-precision Pb isotope data from the Kamchatka arc suggest that even in arc settings such as these, deep assimilation and magma mixing play an important role in the generation of erupted magmas.

FIGURES

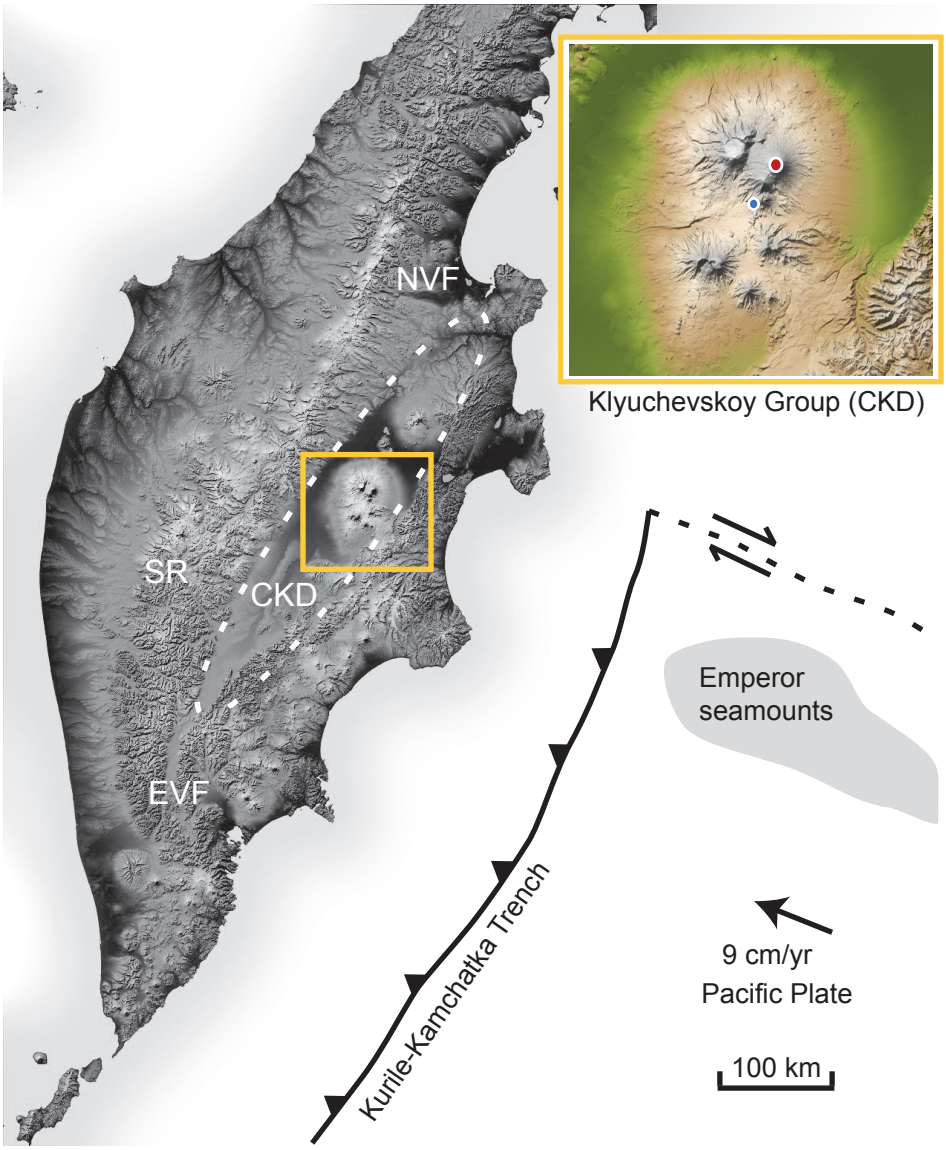

Figure 1. Tectonic map of the Kamchatka Peninsula showing the location of the Klyuchevskoy Group of volcanoes within the Central Kamchatka Depression – CKD. Other volcanic segments in Kamchatka are labeled (Eastern Volcanic Front – EVF, Northern Volcanic Front – NVF, and the extinct Sredinny Range – SR. Inset – Klyuchevskoy Group of volcanoes. Colored circles in the inset denote volcanoes in this study (Red – Klyuchevskoy, Blue – Bezymianny).

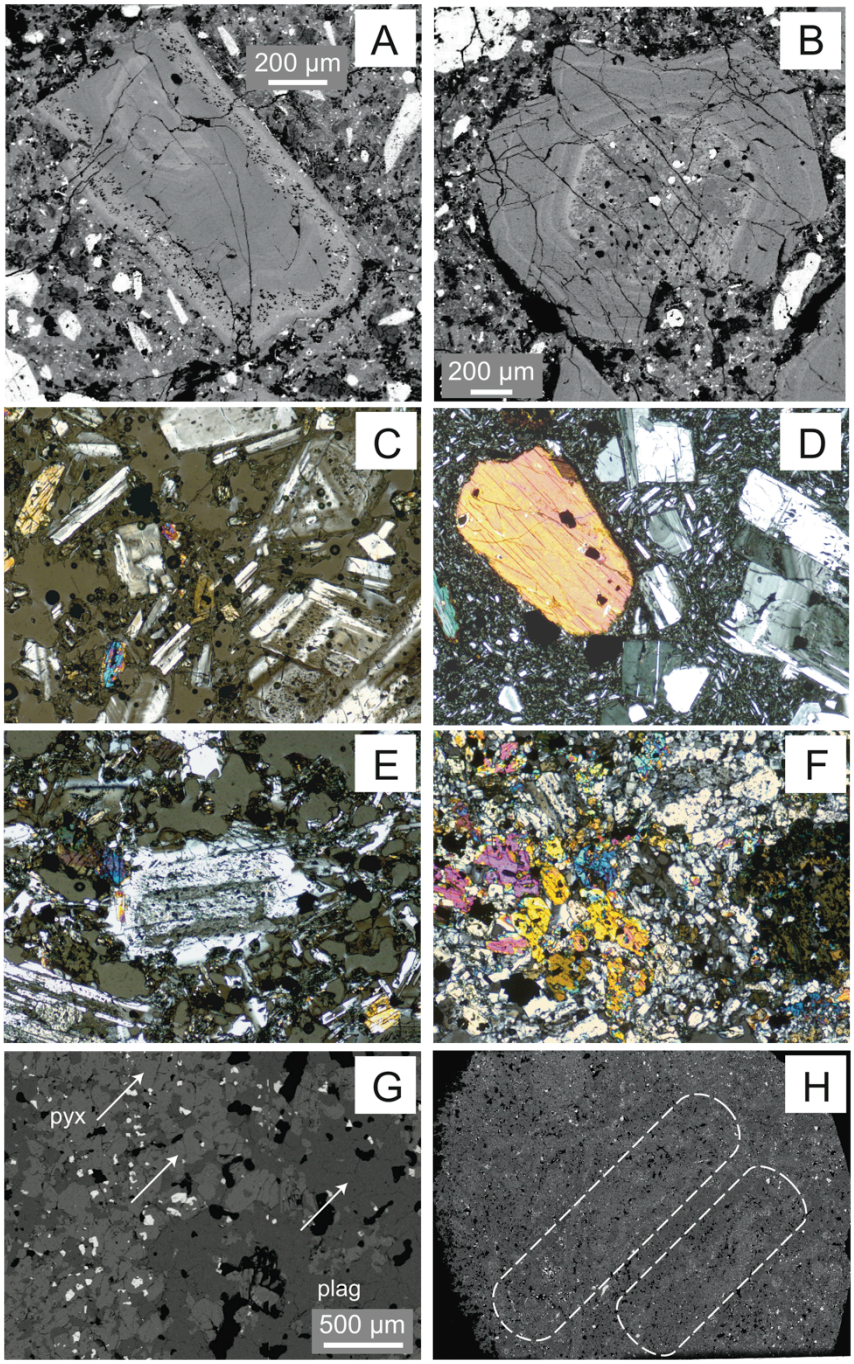

Figure 2. Textures of Bezymianny erupted products. A – zoned plagioclase with sieved ring; B – zoned plagioclase with sieved core; C – modern juvenile sample with plagioclase, 2-pyroxene and Fe-Ti oxide phenocrysts; D – extrusive dome with large amphibole phenocryst; E – common texture of magmatic inclusions: glassy matrix with plagioclase, pyroxene, and Fe-Ti oxides; F – unique recrystallized inclusion with large pyroxene oikocrysts and small euhedral plagioclase; G – BSE image showing texture of recrystallized inclusion with shared grain boundaries (arrows) in plagioclase and pyroxene; H – BSE image showing pyroxene chains (light grey) in the recrystallized inclusion.

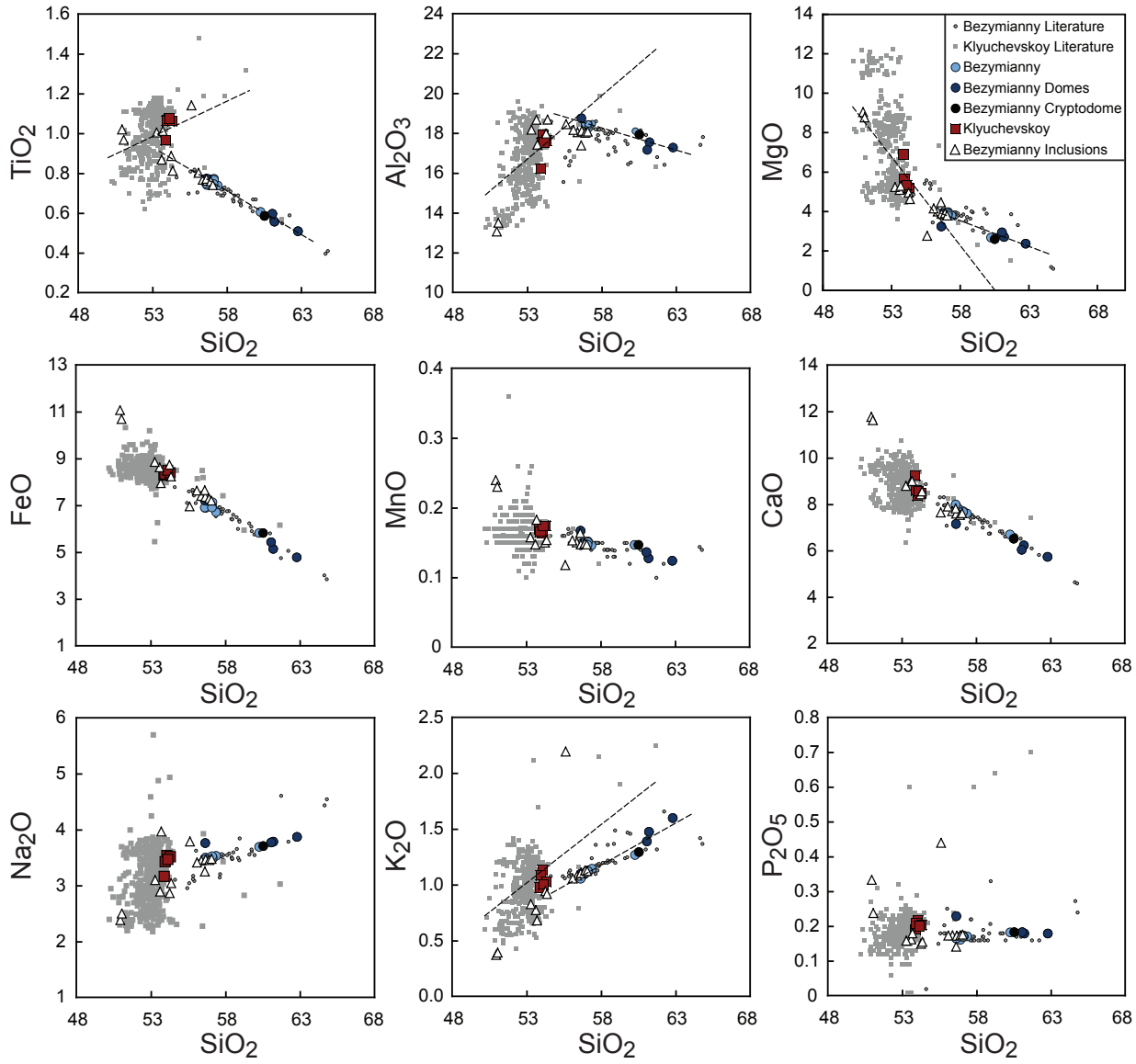

Figure 3. Harker diagrams with Bezymianny and Klyuchevskoy erupted product compositions. Dashed lines represent linear regressions through Bezymianny and Klyuchevskoy data. Literature data shown for Bezymianny and Klyuchevskoy is from Portnyagin *et al.* (2007b).

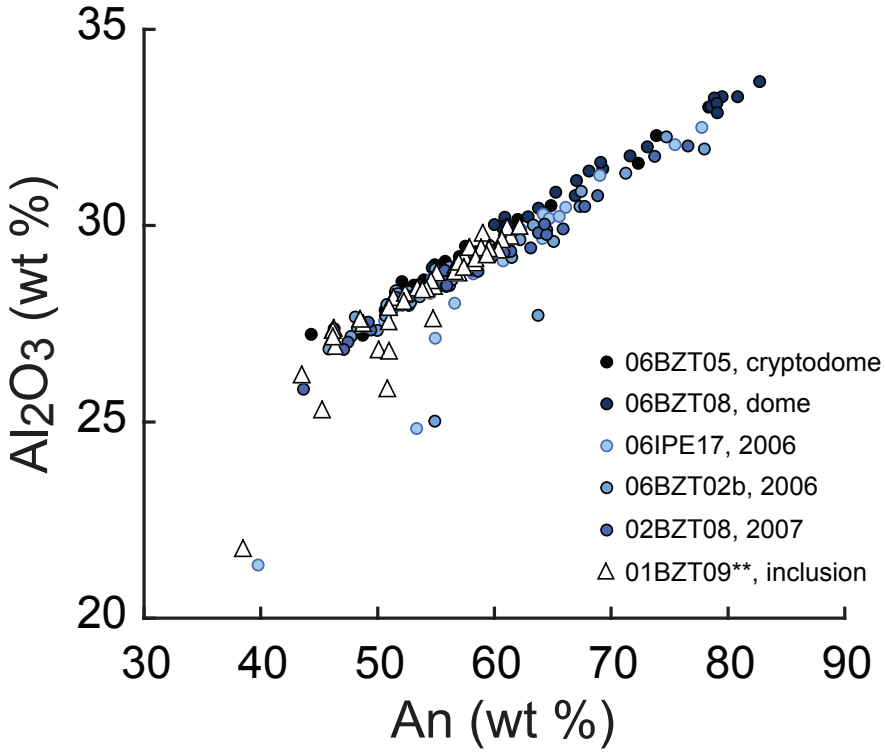

Figure 4. Plagioclase compositions from Bezymianny erupted products. Samples from extrusive domes, the 1956 cryptodome, and modern eruptions from 2006 and 2007 contain plagioclase phenocrysts from ~An_{45}-An_{80} that overlap in composition. Plagioclase grains from the lower crustal inclusion (01BZT09**) are less anorthite rich and record lower Al_2O_3 contents (white triangles).

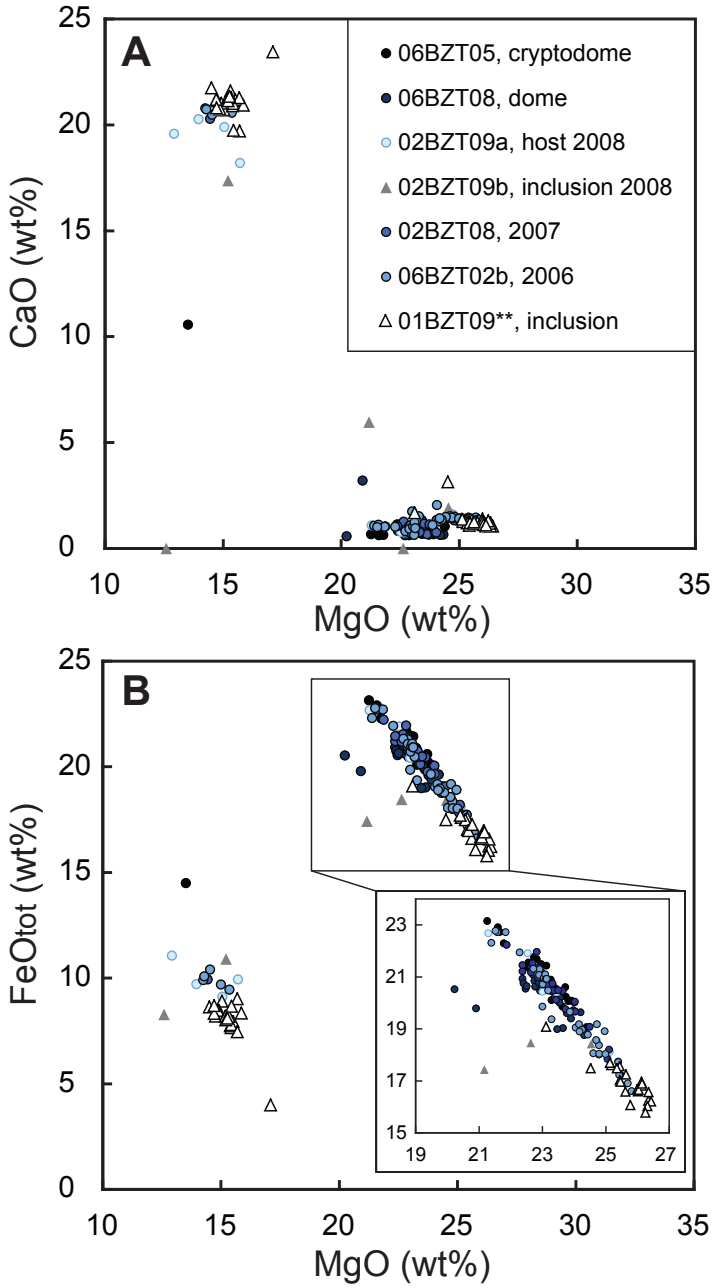

Figure 5. Clinopyroxene and orthopyroxene compositions from Bezymianny erupted products. A - the majority of pyroxene compositions from extrusive domes, 1956, 2006, 2007, as well as inclusions are orthopyroxenes with similar compositions (20-25 wt.% MgO). B – inset shows zoom around the range in Bezymianny orthopyroxene compositions. Compositions of pyroxenes from the lower crustal inclusion (01BZT09**) differ from typical Bezymianny pyroxene compositions (white triangles in A and B). Clinopyroxene and orthopyroxene from 01BZT09** form two tight clusters in compositional space in contrast to the broader range recorded in other Bezymianny juvenile products.

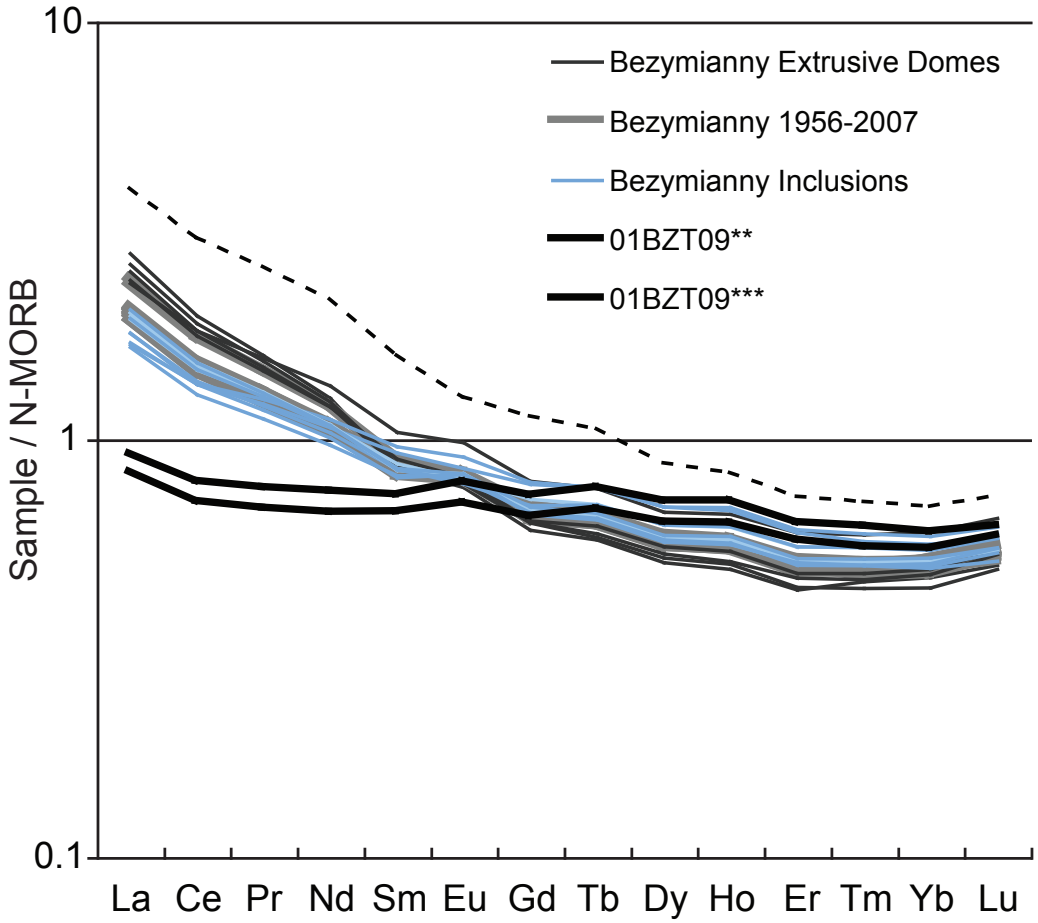

Figure 6. REE patterns for Bezymianny erupted products normalized to N-MORB (Hofmann 1988). Bezymianny domes, juvenile samples from 1956-2007, and magmatic inclusions all have enriched LREE and depleted HREE relative to N-MORB. Two inclusions, 01BZT09** and 01BZT09*** found in bombs from the October 2007 eruption have flat depleted REE patterns relative to N-MORB. 01BZT09** is the sample inferred to be a lower crustal inclusion. The dotted line represents the composition of a mega-plagioclase basalt that outcrops in the CKD near all volcanic centers.

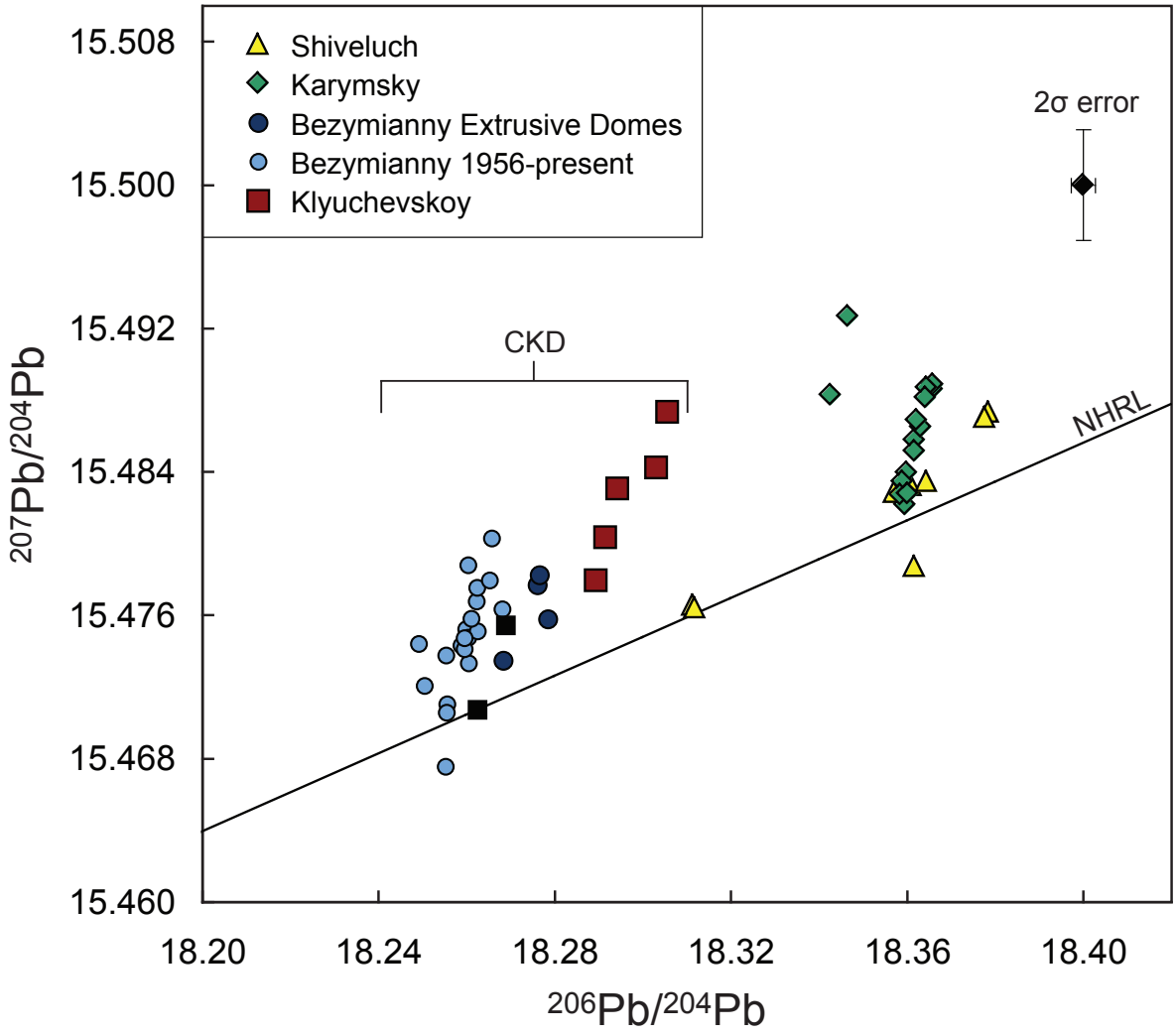

Figure 7. Pb isotope compositions from Kamchatka using high-precision MC-ICP-MS. Two-sigma analytical error of 150ppm ($^{206}Pb/^{204}Pb$) and 225ppm ($^{207}Pb/^{204}Pb$) resolves isotopic differences between Bezymianny, Klyuchevskoy, Shiveluch, and Karymsky volcanic centers. Pb isotope compositions in the Central Kamchatka Depression (CKD) are less radiogenic than those from the Eastern Volcanic Front (Karymsky) and Northern CKD (Shiveluch). Black squares are data from a mega-plagioclase basalt that outcrops beneath the CKD volcanic centers. NHRL from Hart (1984).

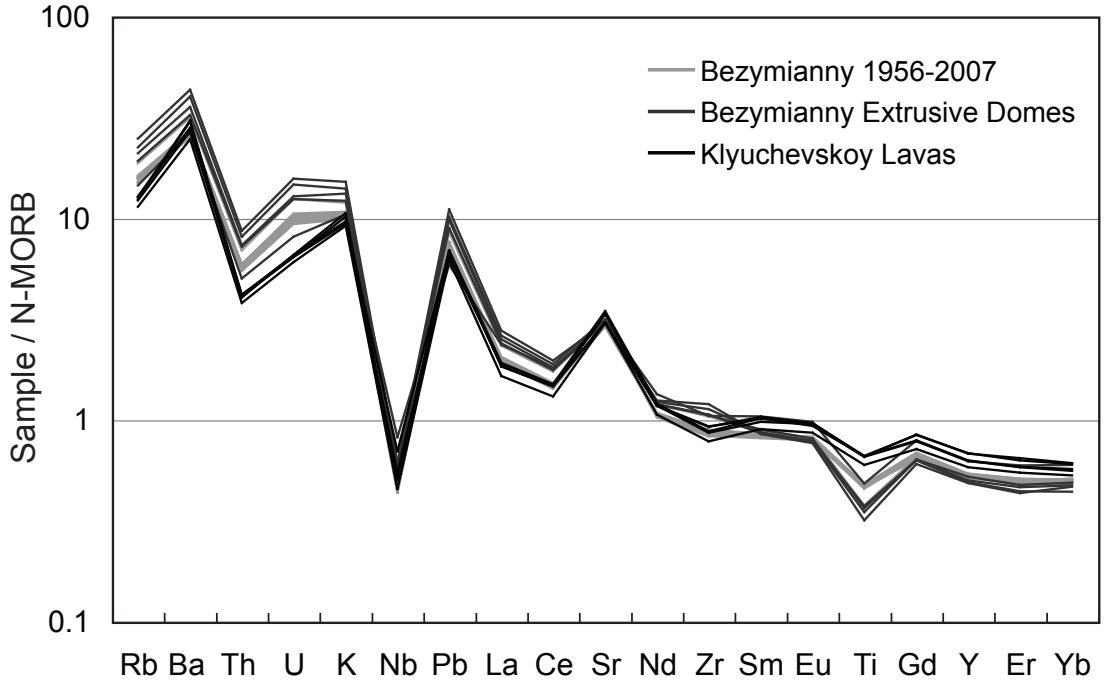

Figure 8. Bezymianny and Klyuchevskoy trace element compositions. Bezymianny has N-MORB normalized trace element trends similar to Klyuchevskoy lavas. Both systems show enrichments in LILE and LREE and depletions in HFSE and HREE characteristic of fluid-fluxed subduction zones. Bezymianny samples have higher concentrations of Rb, Ba, Th, U, Pb and La and lower Ti and HREE. N-MORB compositions from Hofmann (1988).

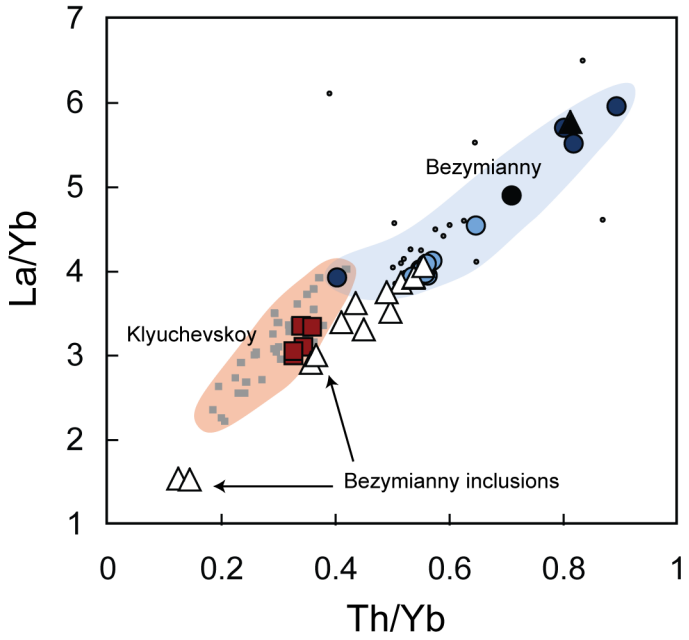

Figure 9. La/Yb vs. Th/Yb for Bezymianny and Klyuchevskoy. Bezymianny displays more of a subduction zone component than Klyuchevskoy (higher La/Yb and Th/Yb). Inclusions from Bezymianny overlap both Bezymianny and Klyuchevskoy fields. Symbols same as Figure 3.

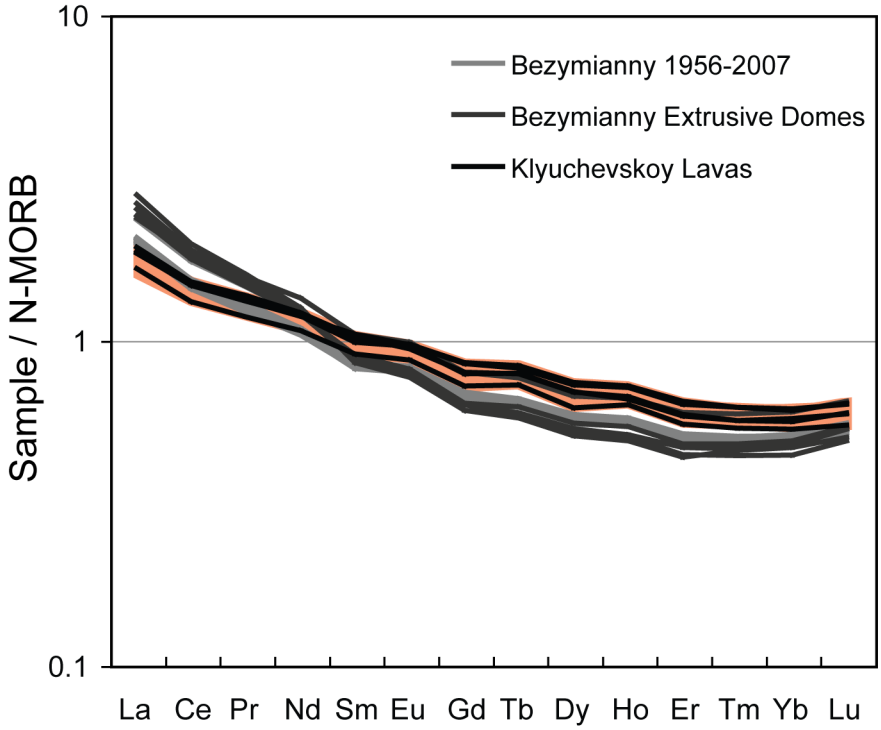

Figure 10. Rare earth element patterns for Bezymianny and Klyuchevskoy. Bezymianny erupted products and extrusive domes have enriched light REEs and depleted mid-to-heavy REEs relative to Klyuchevskoy lavas. The orange shaded region denotes the field of Klyuchevskoy lavas.

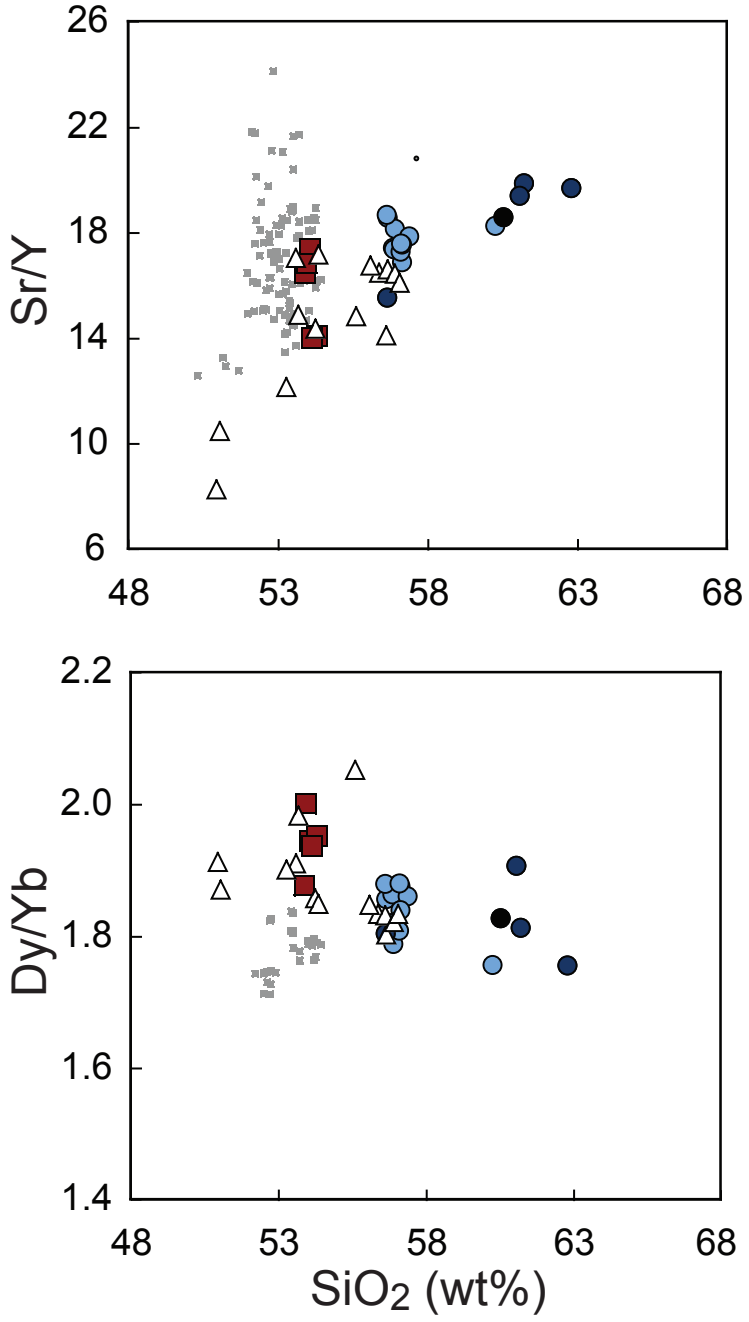

Figure 11. Sr/Y and Dy/Yb ratios from Bezymianny and Klyuchevskoy. Both ratios are similar between the two volcanic centers. Dy/Yb < 2 for both Bezymianny and Klyuchevskoy suggests minor garnet involvement (see Figure 12). Symbols same as Figure 3.

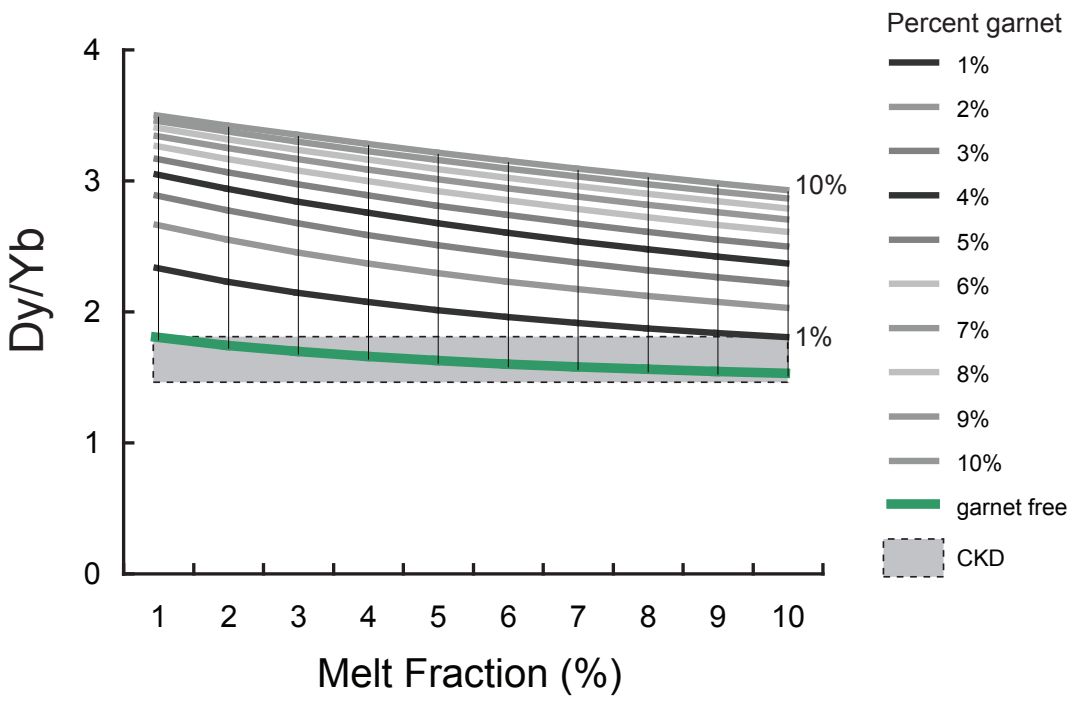

Figure 12. Modeled Dy/Yb during batch melting of a fluid-fluxed garnet-bearing peridotite mantle. Composition of the starting mantle: Dy = 0.531 ppm, Yb = 0.401 ppm (depleted mantle of Salters & Stracke (2004)). Assumed that REEs are not significantly altered by fluid addition. Starting modal mineralogy is 66.7% olivine, 22.2% orthopyroxene, 11.1% clinopyroxene, and no garnet. Garnet is increased to 10% with the proportions of other minerals remaining constant. Modal mineralogy and partition coefficients are taken from Johnson (1998) and references therein. Field of Bezymianny and Klyuchevskoy compositions measured here shown as "CKD" shaded region. Dy/Yb for the CKD samples suggests less than 1% garnet or a garnet-free mantle melting region based on this simple batch model.

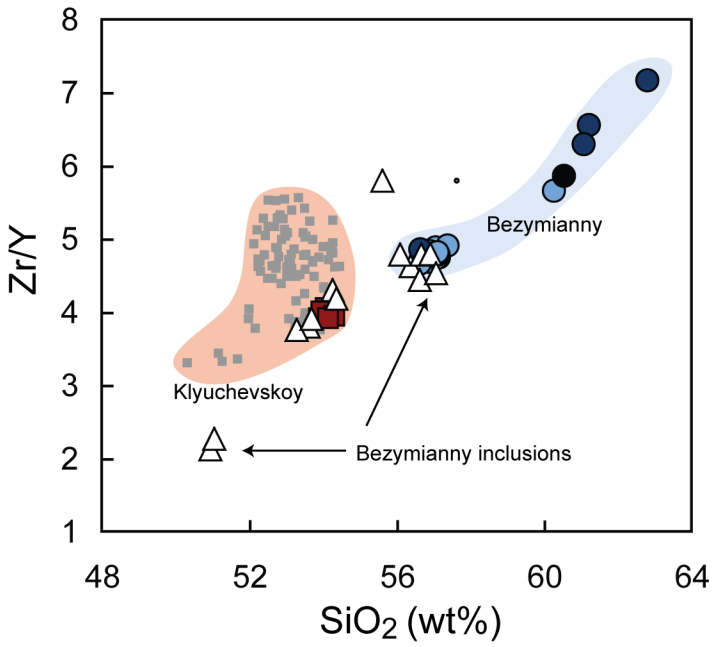

Figure 13. Zr/Y incompatible versus compatible trace element variation between Bezymianny and Klyuchevskoy. Bezymianny Zr/Y values are higher than Klyuchevskoy and are consistent with Zr remaining incompatible during fractionation of magmas in the CKD. Two Bezymianny inclusions have Zr/Y compositions much lower than Klyuchevskoy magmas representing a separate magma composition sampled during Bezymianny eruptions.

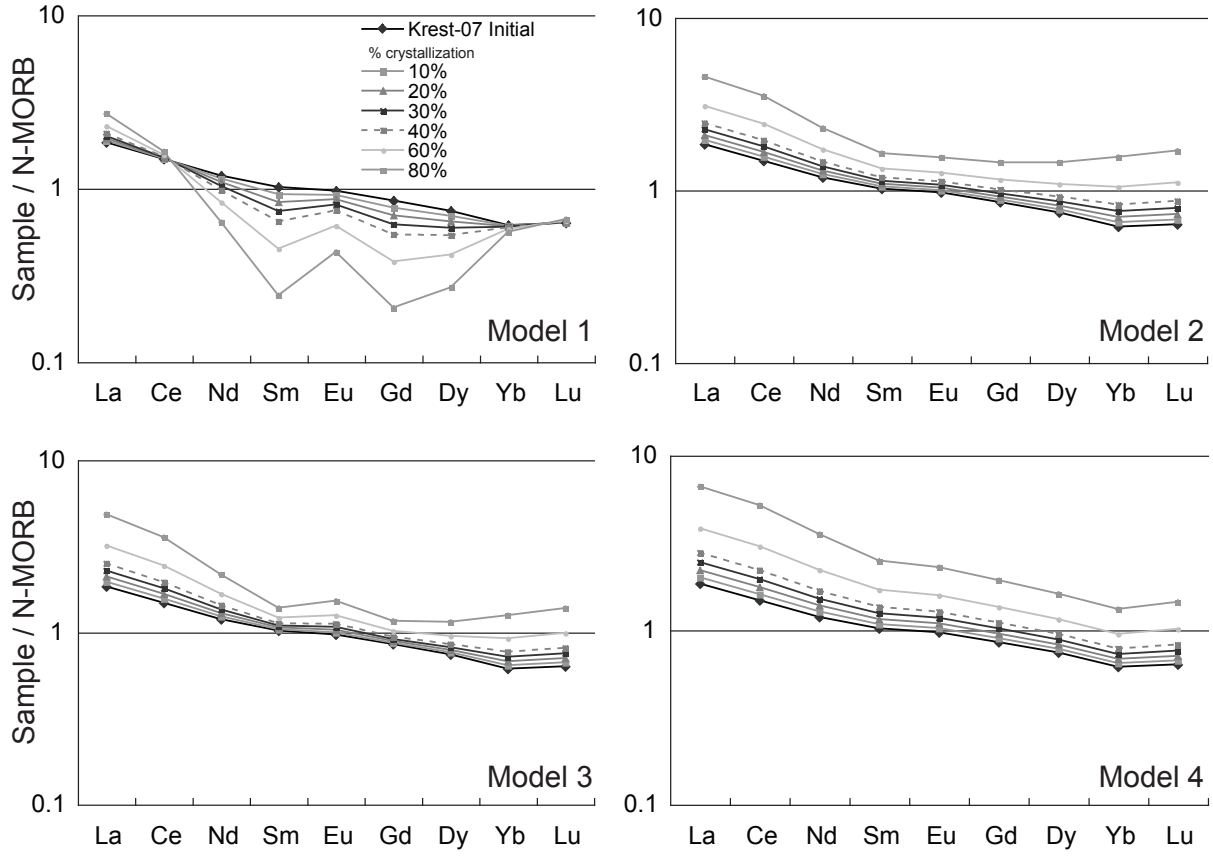

Figure 14. REE models showing pure crystal fractionation of a Klyuchevskoy parental magma. Model 1 - phase assemblage observed in modern Bezymianny products (Shipman *et al. in preparation*): 67% plagioclase, 5% clinopyroxene, 15% orthopyroxene, 7% magnetite, 3% amphibole and 3% apatite; Model 2 - this same assemblage with 1% apatite; Model 3 - an assemblage with increased clinopyroxene and less plagioclase: 39% plagioclase, 35% clinopyroxene, 15% orthopyroxene, 7% magnetite, 3% amphibole, 1% apatite; Model 4 - an assemblage with 73% clinopyroxene, 10% plagioclase, 10% orthopyroxene, 7% magnetite and no apatite. The concentrations of pyroxenes and apatite were varied between models because these minerals have partition coefficients that enrich LREE and deplete HREE with fractional crystallization. Partition coefficients are from the compilation by Rollinson (1993) for basaltic andesites and Fujimaki (1986) (apatite). Model curves for 10%-80% fractional crystallization are shown. None of these models produce the depletions in mid to heavy REEs observed in Bezymianny erupted products.

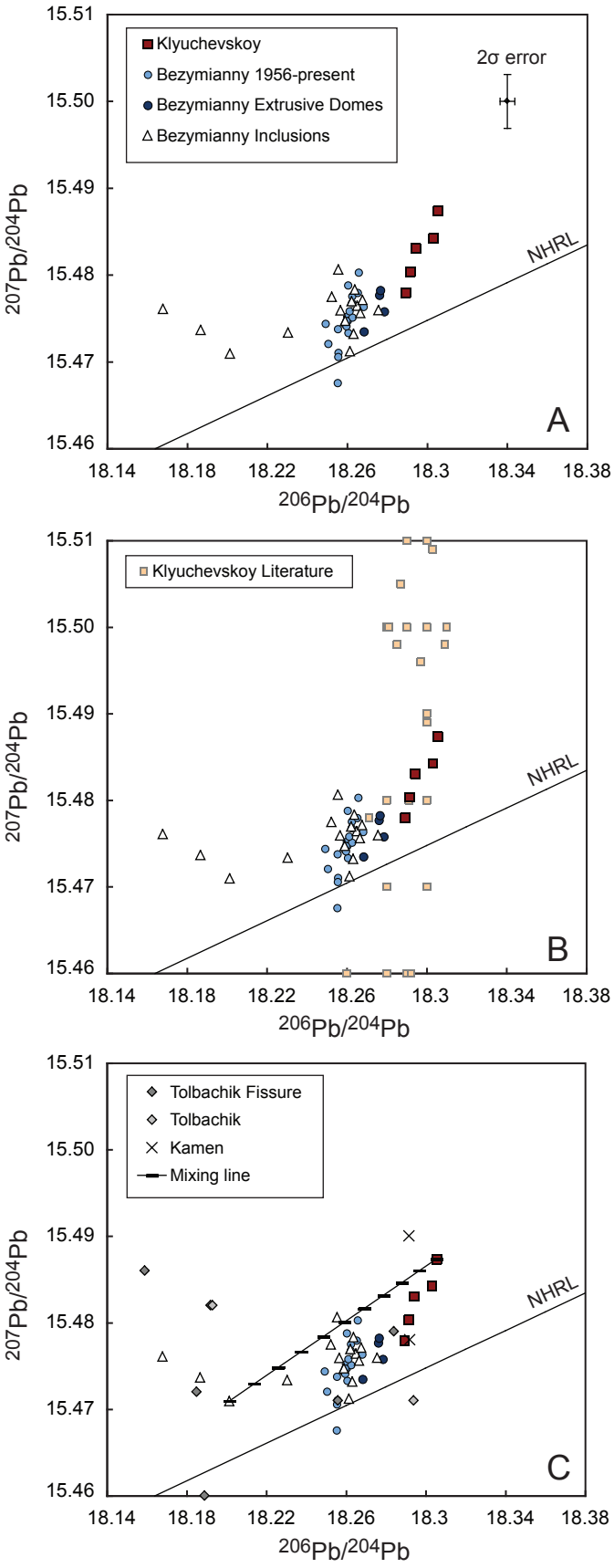

Figure 15. Pb isotope compositions at Bezymianny and Klyuchevskoy. Bezymianny and Klyuchevskoy have distinct compositions with Bezymianny products being less radiogenic. A – Bezymianny magmatic and lower crustal inclusions (triangles) shown with Bezymianny and Klyuchevskoy data. Most inclusions have similar compositions to Bezymianny juvenile products; however, four inclusions are less radiogenic (samples 01BZT08**, 01BZT09***, 02BZT09b, and 10IPE1B). B – Klyuchevskoy literature data relative to Klyuchevskoy lavas from this study and Bezymianny compositions. All Klyuchevskoy products are more radiogenic than modern Bezymianny erupted products. Klyuchevskoy literature data have order of magnitude larger errors (not shown) from TIMS analysis. C – Pb isotope compositions of other CKD volcanic centers (Kamen and Tolbachik) near Bezymianny. Published Pb isotope compositions for Tolbachik volcano are less radiogenic than Bezymianny modern erupted products and plot near the compositions of the Bezymianny inclusions. Compositions for Kamen volcano are similar to Klyuchevskoy and more radiogenic than Bezymianny. Mixing curve is shown between a Klyuchevskoy lava and a magmatic inclusion. The composition of Bezymianny can be explained by ~ 40-60% mixing of crust represented by the inclusions composition with a Klyuchevskoy lava (tick marks represent 10% mixing intervals). Literature data from compilation of Portnyagin *et al.* (2007b) and Churikova *et al.* (2001).

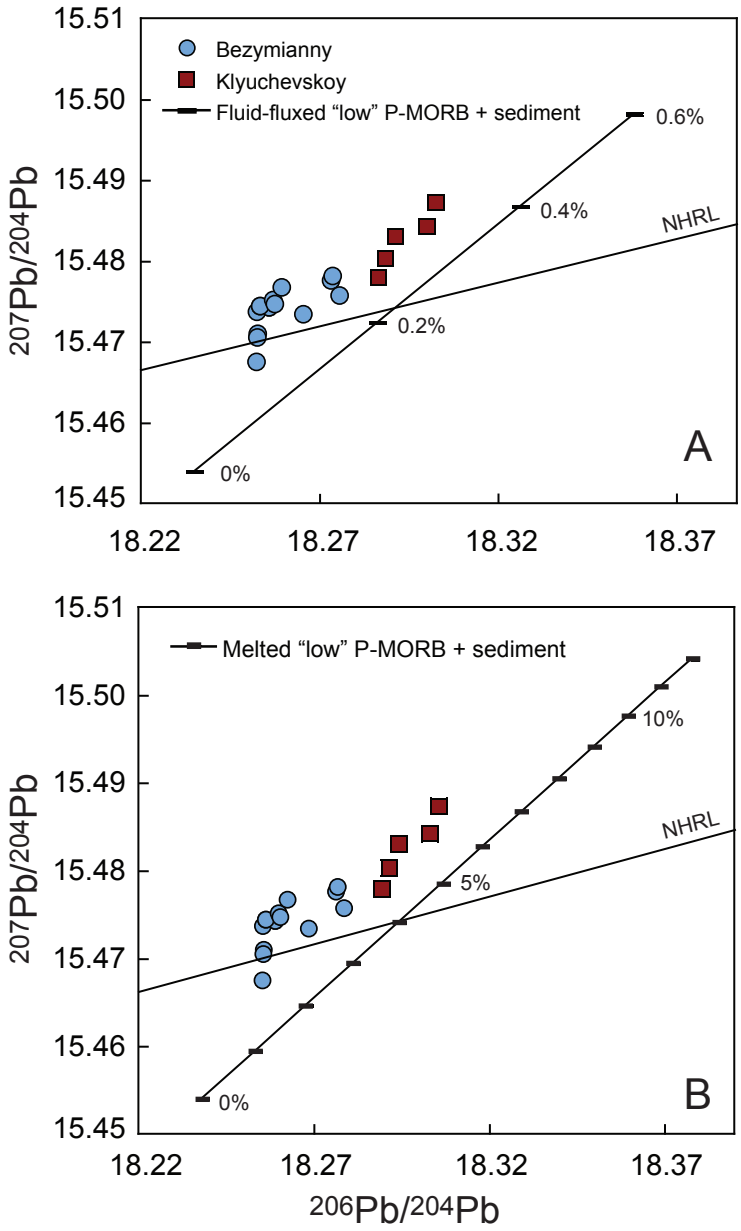

Figure 16. Sediment mixing models for the Central Kamchatka Depression. A – Mixing curve shows addition of sediment to a fluid-fluxed solid mantle. Tick marks represent 0.2% intervals of mixing. Sediment composition is an average for sediments off the coast of Kamchatka (ODP Leg 145, Kersting and Arculus 1995). The initial composition of the mantle is a value two standard deviations less radiogenic than the mean for Pacific MORB (Arevalo *et al.* 2010) – referred to here as a "low" P-MORB. Concentration of Pb in the mantle is 0.16ppm. Bezymianny and Klyuchevskoy compositions can be generated with 0.2-0.4% sediment added to a mantle source. B – Mixing curve showing the addition of sediment (described for A) to a fluid-fluxed mantle melt. Concentration of Pb is 3ppm in the melt from the mantle. Tick marks denote 1% intervals of sediment mixing. This model allows for more sediment addition (4-7%).

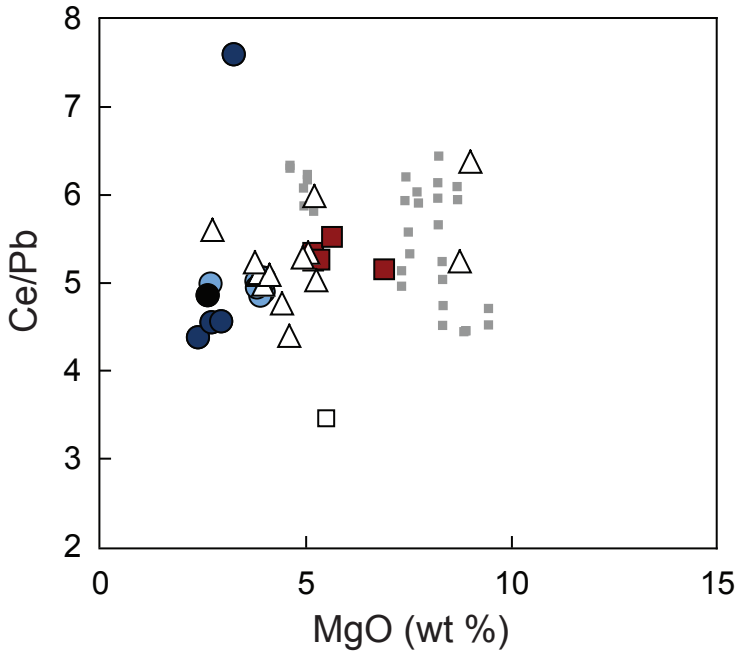

Figure 17. Ce/Pb compositions for Bezymianny and Klyuchevskoy. Ce/Pb ratios for both volcanic centers fall within the same range ~ 4-6. Published data for Klyuchevskoy shows the same range as our measurements. Symbols are the same as Figure 3.

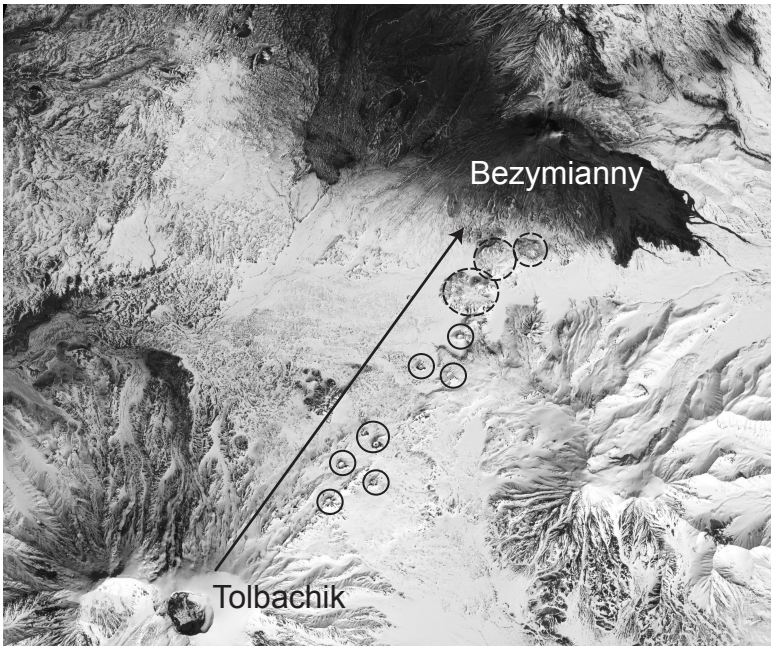

Figure 18. Satellite image of Bezymianny and Tolbachik volcanic centers. There is a linear feature of vents (cones and domes) between Tolbachik and Bezymianny volcanoes (rough strike of feature shown with arrow). Extrusive domes associated with Bezymianny outlined in dashed circles, other cones and domes are outlined in solid circles. Image modified from NASA Earth Observatory.

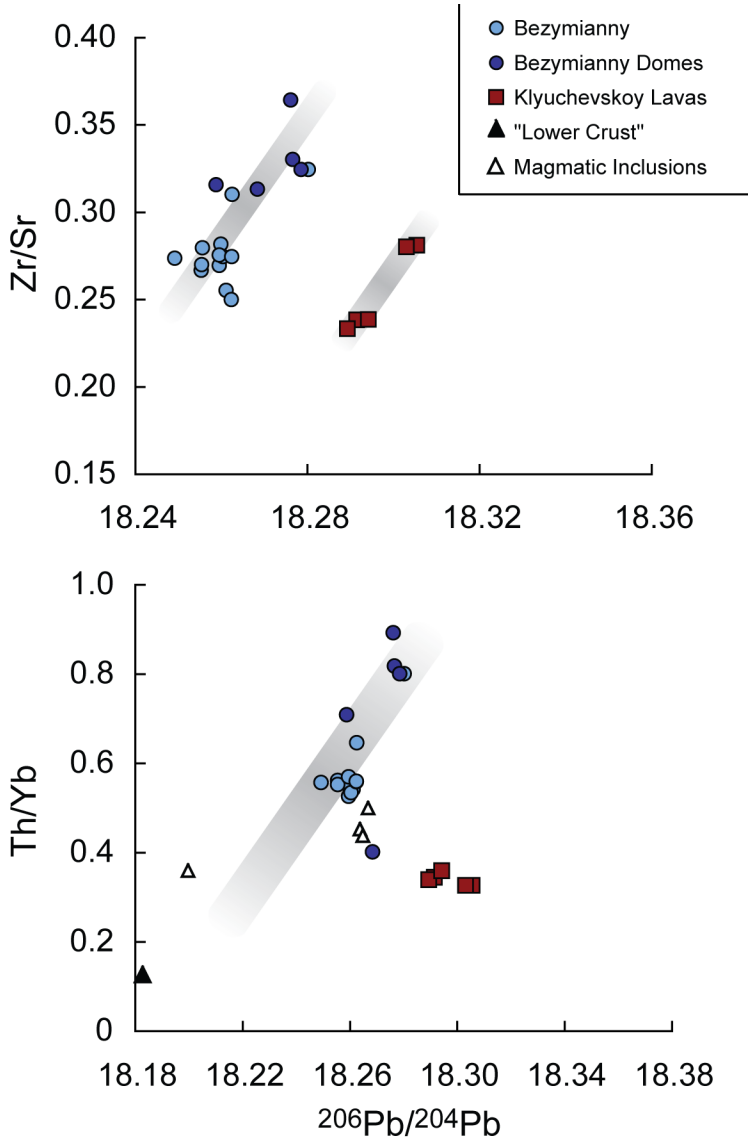

Figure 19. Parallel fractionation patterns of Bezymianny and Klyuchevskoy erupted products. Both Zr/Sr and Th/Yb positively correlate with $^{206}Pb/^{204}Pb$ at each volcanic center. Patterns suggest that the magmas of these neighboring volcanoes may evolve in a similar way to higher incompatible element concentrations and more radiogenic Pb within the crust beneath the CKD.

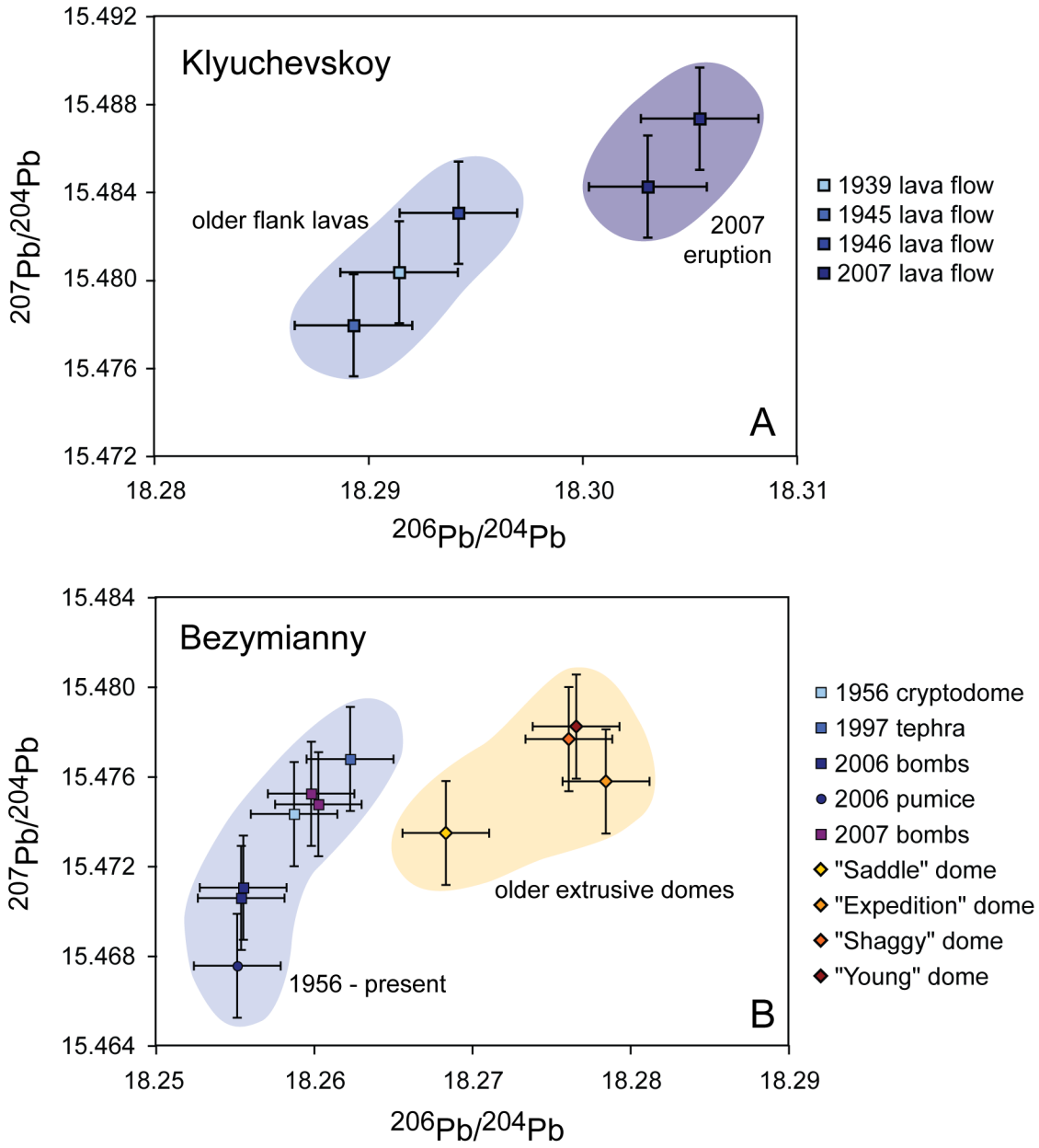

Figure 20. Temporal Pb isotope variation at Bezymianny and Klyuchevskoy volcanoes. A – Klyuchevskoy Pb isotope variation. Five different eruptive units from Klyuchevskoy are shown. The youngest lavas (2007) are more radiogenic than older flank lavas of Klyuchevskoy. B – Bezymianny Pb isotope variation. The older extrusive domes at Bezymianny are more radiogenic than the 1956-2007 modern juvenile eruptive units.

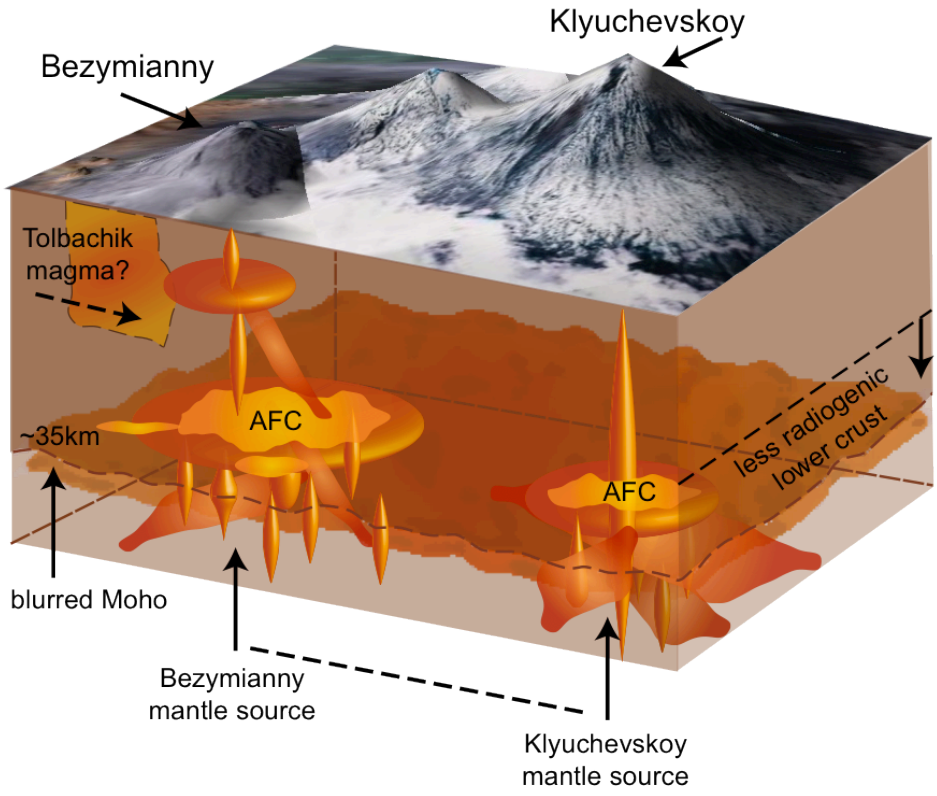

Figure 21. New conceptual model for magma generation beneath Bezymianny and Klyuchevskoy volcanoes. Magmas generated in the mantle source regions beneath Bezymianny and Klyuchevskoy have similar compositions. The entire lower crust of the CKD is underplated with mafic magmas from the mantle at a depth of ~35km (blurred Moho arrow). All CKD magmas interact with the lower crust to some degree – this lower crust has a less radiogenic Pb isotope composition relative to mantle-derived magmas. Bezymianny magmas and Klyuchevskoy magmas take paths through the crust that are not connected to one another. Klyuchevskoy magmas experience some lower-crustal assimilation and fractional crystallization (AFC), but in general are transported through a well-developed vertical conduit system. Bezymianny magmas, however, undergo more extensive AFC processing in the lower crust (shown here with a larger region of deep AFC) and are stored at various depths in the upper crust. Bezymianny magmas also mix with more mafic melts unrelated to Klyuchevskoy that may be sourced from Tolbachik volcano's subsurface plumbing system.

TABLES

Table 1. Sample Descriptions

Bezymianny Volcano

Bezymianny Modern Eruptions 1956-present

Sample Name	Date of Eruption	Material Collected
06BZT05	1956	crystalline 1956 cryptodome with cooling jointing
05BZT08	1956	crystalline 1956 cryptodome with cooling jointing
06BZT11	1997	tephra deposit on eastern ridge of blast zone
06BZT02a	2006	outer rim of juvenile breadcrust bomb, in May 2006 pyroclastic flow
06BZT02b	2006	inner portion of juvenile breadcrust bomb, in May 2006 pyroclastic flow
06BZT03	2006	juvenile pumice from May 2006 eruption taken from crater rim
06IPE16	2006	juvenile bomb from May 2006 eruption taken from fan deposits within crater
06IPE17	2006	juvenile bomb from May 2006 eruption, large sample from crater, warm when collected
02BZTK07	2006	juvenile breadcrust bomb, in December 2006 pyroclastic flow
01BZTK07	2007	juvenile breadcrust bomb, in May 2007 pyroclastic flow
02BZT08	2007	juvenile breadcrust bomb, in October 2007 pyroclastic flow
03BZT08	2007	juvenile breadcrust bomb, in October 2007 pyroclastic flow
04BZT08	2007	juvenile breadcrust bomb, in October 2007 pyroclastic flow

Bezymianny Exrusive Domes[a]

Sample Name	Date of Eruption	Material Collected
06BZT05[b]	1956	crystalline 1956 cryptodome with cooling jointing
06BZT04	unknown, <3000 ya	crystalline "youngest" dome, highest on Bezymianny edifice
06BZT08	unknown, 3000-5000 ya	Lohkmaty dome, crystalline hornblende-pyroxene andesite
08BZT08	unknown, Holocene	Expedition dome, crystalline
06CBZT08	uknown, upper Pleistocene	Plotina dome, crystalline
MPBZT06	unknown	megaplag lava unit that outcrops near Tolbachik and on the south side of Bezymianny

Bezymianny Inclusions and Host Juvenile Eruptive Products

Sample Name	Date of Eruption	Material Collected
03BZT09	2007	juvenile breadcrust bomb, in October 2007 pyroclastic flow
03BZT09a	2007	dense, almost aphyric, metamorphosed inclusion, in October 2007 breadcrust bomb
03BZT09b (host)	2007	rounded inclusion, zoned in vesicularity, in October 2007 breadcrust bomb
03BZT09c	2007	crystalline ol-sp-pyx inclusion with ~2mm reaction rim in October 2007 breadcrust bomb
03BZT09d	2007	unzoned inclusion with mineralogy similar to host in October 2007 breadcrust bomb
04BZT09 (host)	2007	juvenile breadcrust bomb, in October 2007 pyroclastic flow
04BZT09d	2007	unzoned inclusion with mineralogy similar to host in October 2007 breadcrust bomb
01BZT09*	2007	dense inclusion in 02BZT08 breadcrust bomb from October 2007
01BZT09**	2007	dense inclusion in 02BZT08 breadcrust bomb from October 2007
01BZT09***	2007	inclusion in 02BZT08 breadcrust bomb from October 2007
02BZT09a (host)	2008	juvenile breadcrust bomb, in August 2008 pyroclastic flow
02BZT09b	2008	inclusion in breadcrust bomb from August 2008
10IPE1A (host)	2010	juvenile breadcrust bomb from June 2010 eruption
10IPE1A (inclusion)	2010	inclusion in breadcrust bomb from June 2010
10IPE1B (host)	2010	juvenile breadcrust bomb from June 2010 eruption
10IPE1B (inclusion)	2010	inclusion in breadcrust bomb from June 2010

Klyuchevskoy Volcano

Klyuchevskoy Lavas

Sample Name	Date of Eruption	Material Collected
KL-1939	1939	lava from 1939 flank eruption
KL-1945Y	1945	lava from 1945 flank eruption
KL-1946A	1946	lava from 1946 flank eruption
KL-Krest-07	2007	lava from 2007 main vent eruption
KL-Apah-232-07	2007	lava from 2007 main vent eruption

[a] Extrusive domes at Bezymianny have not been dated. These ages are based on maps by Bogoyavlenskaya (1991) and Almeev (2009).
[b] This sample is the same as the one listed under the juvenile Bezymianny products, but is noted here as a dome sample.

Table 2. Major and trace element abundances in Bezymianny and Klyuchevskoy samples

	Bezymianny Modern Eruptions 1956-Present						
Sample Name	06BZT02b	06IPE17	02BZT08	06BZT03	06IPE16	06BZT02a	04BZT08
Eruption Year	2006	2006	2007.5	2006	2006	2006	2007.5
Brief Description	juvenile PF	juvenile PF	juvenile PF	juvenile PF	juvenile PF	juvenile PF	juvenile PF
SiO_2	56.64	57.04	57.12	56.82	56.88	56.85	57.07
TiO_2	0.74	0.76	0.77	0.77	0.76	0.76	0.77
Al_2O_3	18.82	18.34	18.24	18.43	18.38	18.47	18.36
FeO*	6.90	7.03	7.15	7.13	7.14	7.04	6.98
MnO	0.15	0.15	0.15	0.15	0.15	0.15	0.15
MgO	3.82	3.88	3.97	3.98	3.90	3.90	3.94
CaO	7.95	7.64	7.65	7.80	7.69	7.78	7.69
Na_2O	3.51	3.50	3.49	3.46	3.48	3.50	3.48
K_2O	1.07	1.13	1.13	1.09	1.10	1.10	1.12
P_2O_5	0.16	0.17	0.17	0.17	0.16	0.17	0.17
Total	99.76	99.64	99.86	99.81	99.64	99.73	99.73
ICP-MS							
La	7.48	7.73	7.96	7.65	7.67	7.78	7.84
Ce	17.34	17.94	18.21	17.77	17.75	17.97	18.00
Pr	2.53	2.62	2.65	2.60	2.60	2.64	2.66
Nd	11.67	11.98	12.11	11.88	11.91	11.97	12.08
Sm	3.05	3.17	3.20	3.16	3.15	3.20	3.20
Eu	1.06	1.07	1.10	1.06	1.06	1.11	1.08
Gd	3.31	3.24	3.50	3.39	3.26	3.31	3.38
Tb	0.55	0.57	0.58	0.57	0.56	0.57	0.57
Dy	3.52	3.64	3.71	3.57	3.47	3.60	3.60
Ho	0.74	0.76	0.77	0.75	0.73	0.76	0.75
Er	2.04	2.08	2.13	2.11	2.04	2.09	2.09
Tm	0.30	0.30	0.31	0.30	0.30	0.30	0.31
Yb	1.90	1.94	1.98	1.96	1.94	1.93	1.99
Lu	0.30	0.31	0.32	0.31	0.31	0.32	0.31
Ba	354	371	371	357	365	364	370
Th	1.03	1.08	1.08	1.03	1.09	1.07	1.06
Nb	1.55	2.02	1.73	1.64	1.85	1.68	1.63
Y	18.44	19.01	19.49	18.95	18.59	19.23	19.14
Hf	2.40	2.54	2.53	2.44	2.43	2.44	2.48
Ta	0.13	0.15	0.15	0.13	0.14	0.13	0.13
U	0.67	0.72	0.72	0.68	0.70	0.70	0.71
Pb	3.50	3.57	3.72	3.51	3.50	3.59	3.62
Rb	18.96	20.22	20.14	19.23	19.89	19.63	19.94
Cs	0.68	0.73	0.76	0.68	0.73	0.71	0.73
Sr	343	333	329	331	338	334	331
Sc	20.25	20.02	22.20	20.02	19.49	19.77	20.98
Zr	87.54	93.11	92.81	89.13	90.10	90.37	91.00
XRF							
Ni	10	18	13	12	17	13	12
Cr	17	33	19	19	31	22	22
V	194	194	198	201	198	198	197
Ga	17	17	16	17	17	17	16
Cu	40	34	41	41	39	42	39
Zn	74	77	78	78	78	76	78

Table 2. Continued

Sample Name	06BZT11	02BZTK07	03BZT08	05BZT08	01BZTK07
Eruption Year	1997	2006.5	2007.5	1956	2007
Brief Description	juvenile PF	juvenile PF	juvenile PF	juvenile PF	juvenile PF
SiO_2	56.60	57.36	57.12	60.24	57.08
TiO_2	0.75	0.74	0.77	0.61	0.75
Al_2O_3	18.80	18.50	18.49	18.12	18.47
FeO*	6.92	6.72	6.95	5.83	6.92
MnO	0.15	0.15	0.15	0.15	0.15
MgO	3.88	3.79	3.89	2.68	3.80
CaO	8.00	7.61	7.70	6.71	7.69
Na_2O	3.47	3.54	3.50	3.70	3.53
K_2O	1.06	1.15	1.12	1.27	1.13
P_2O_5	0.17	0.17	0.17	0.18	0.17
Total	99.81	99.73	99.86	99.49	99.69
ICP-MS					
La	7.49	8.02	7.93	9.12	7.94
Ce	17.22	18.43	18.18	20.92	18.18
Pr	2.52	2.70	2.69	3.01	2.66
Nd	11.55	12.02	12.14	13.32	11.82
Sm	3.08	3.18	3.18	3.29	3.22
Eu	1.10	1.08	1.08	1.09	1.10
Gd	3.26	3.39	3.37	3.33	3.38
Tb	0.55	0.57	0.58	0.56	0.57
Dy	3.48	3.62	3.67	3.52	3.65
Ho	0.73	0.76	0.76	0.73	0.76
Er	2.04	2.09	2.09	2.06	2.11
Tm	0.29	0.31	0.31	0.30	0.31
Yb	1.85	1.94	1.99	2.01	1.94
Lu	0.31	0.31	0.32	0.33	0.32
Ba	352	377	372	440	374
Th	1.03	1.11	1.11	1.30	1.09
Nb	1.53	1.71	1.70	1.96	1.69
Y	18.53	18.86	19.17	19.14	19.34
Hf	2.35	2.52	2.54	2.86	2.53
Ta	0.13	0.14	0.14	0.16	0.14
U	0.67	0.75	0.74	0.89	0.71
Pb	3.49	3.67	3.75	4.19	3.68
Rb	18.99	20.33	20.16	23.67	20.63
Cs	0.70	0.76	0.72	0.89	0.76
Sr	346	337	337	350	340
Sc	22.42	20.09	20.76	13.74	22.03
Zr	86.59	92.90	92.15	108.56	93.48
XRF					
Ni	10	11	11	3	10
Cr	18	18	19	18	19
V	197	186	198	123	191
Ga	17	17	17	17	18
Cu	43	48	35	20	40
Zn	77	76	77	78	76

Table 2. Continued

	Bezymianny Inclusions and Hosts Juvenile Eruptive Products						
Sample Name	01BZT09*	01BZT09**	01BZT09***	02BZT09a	02BZT09b	03BZT09	03BZT09a
Eruption Year	2007.5	2007.5	2007.5	2008	2008	2006	2006
Brief Description	inclusion	inclusion	inclusion	juvenile host	inclusion	juvenile host	inclusion
SiO_2	53.61	50.95	51.06	56.39	53.28	56.67	53.69
TiO_2	0.87	1.02	0.97	0.77	1.00	0.76	1.01
Al_2O_3	18.66	13.06	13.49	18.05	18.17	18.11	17.42
FeO*	8.62	11.06	10.68	7.40	8.85	7.36	7.95
MnO	0.15	0.24	0.23	0.15	0.16	0.15	0.18
MgO	5.07	9.02	8.75	3.98	5.22	3.86	5.27
CaO	8.99	11.76	11.62	7.70	8.79	7.59	8.99
Na_2O	2.89	2.38	2.50	3.44	3.10	3.47	3.96
K_2O	0.77	0.37	0.39	1.08	0.83	1.11	0.68
P_2O_5	0.16	0.33	0.24	0.17	0.16	0.17	0.18
Total	99.80	100.20	99.94	99.13	99.55	99.24	99.34
ICP-MS							
La	6.48	3.58	3.24	7.70	6.65	7.86	6.56
Ce	15.38	9.47	8.48	17.91	16.24	18.19	16.29
Pr	2.33	1.58	1.41	2.63	2.52	2.66	2.59
Nd	10.84	8.36	7.44	12.13	11.95	12.12	12.47
Sm	3.07	2.76	2.50	3.18	3.49	3.20	3.60
Eu	1.09	1.05	0.94	1.08	1.14	1.09	1.21
Gd	3.38	3.72	3.30	3.44	3.96	3.43	4.01
Tb	0.58	0.68	0.60	0.58	0.68	0.58	0.68
Dy	3.66	4.46	3.98	3.67	4.35	3.62	4.34
Ho	0.76	0.95	0.84	0.77	0.92	0.75	0.91
Er	2.07	2.61	2.37	2.13	2.52	2.10	2.48
Tm	0.31	0.38	0.34	0.32	0.37	0.32	0.35
Yb	1.92	2.34	2.13	2.00	2.29	2.01	2.19
Lu	0.30	0.36	0.35	0.32	0.36	0.32	0.34
Ba	320	147	155	358	286	367	364
Th	0.79	0.29	0.31	1.03	0.82	1.08	0.81
Nb	1.32	1.16	1.11	1.63	1.58	1.66	1.82
Y	19.30	23.62	20.96	19.69	23.16	19.39	22.66
Hf	2.04	1.52	1.42	2.48	2.41	2.52	2.39
Ta	0.10	0.09	0.08	0.13	0.12	0.14	0.14
U	0.50	0.20	0.20	0.69	0.53	0.71	0.48
Pb	2.88	1.49	1.62	3.60	2.72	3.58	3.25
Rb	14.52	5.85	5.94	19.88	14.85	19.98	12.88
Cs	0.54	0.18	0.19	0.72	0.53	0.73	0.73
Sr	329	195	219	324	281	322	337
Sc	29.13	45.11	42.53	23.04	33.10	22.04	30.58
Zr	73.38	50.19	47.51	91.16	86.93	92.75	88.49
XRF							
Ni	21	52	49	14	22	14	25
Cr	18	213	220	18	16	17	67
V	252	358	327	201	280	193	241
Ga	17	16	13	17	16	18	18
Cu	255	91	127	45	128	41	42
Zn	85	111	101	75	74	74	139

Table 2. Continued

Sample Name	03BZT09b	03BZT09d	04BZT09	04BZT09d	MPZBZT06	10IPE1A	10IPE1A*
Eruption Year	2006	2006	2007.5	2007.5	not known	2010	2010
Brief Description	inclusion	inclusion	juvenile host	inclusion	mega plag basalt	juvenile host	inclusion
SiO_2	56.63	54.26	56.92	54.36	55.62	56.85	57.07
TiO_2	0.77	0.89	0.76	0.81	1.14	0.80	0.74
Al_2O_3	17.38	17.97	18.01	18.67	18.45	18.45	18.08
FeO*	7.65	8.73	7.28	8.23	6.95	8.27	7.20
MnO	0.16	0.15	0.15	0.15	0.12	0.15	0.15
MgO	4.44	4.94	3.89	4.61	2.74	4.18	3.78
CaO	7.81	8.43	7.54	8.55	7.65	8.10	7.61
Na_2O	3.25	2.86	3.45	3.04	3.79	2.89	3.47
K_2O	1.10	0.94	1.13	0.92	2.19	1.04	1.12
P_2O_5	0.14	0.15	0.17	0.15	0.44	0.17	0.18
Total	99.33	99.32	99.30	99.51	99.09	100.89	99.39
ICP-MS							
La	7.56	6.99	7.84	7.00	15.48	-	7.59
Ce	17.59	16.53	18.31	16.26	36.35	-	17.64
Pr	2.65	2.50	2.69	2.44	5.35	-	2.63
Nd	12.03	11.61	12.10	11.29	24.16	-	12.02
Sm	3.28	3.19	3.17	3.04	5.95	-	3.20
Eu	1.07	1.05	1.11	1.10	1.68	-	1.10
Gd	3.65	3.53	3.43	3.35	5.76	-	3.50
Tb	0.62	0.62	0.57	0.57	0.93	-	0.59
Dy	3.94	3.93	3.63	3.58	5.51	-	3.72
Ho	0.83	0.83	0.76	0.75	1.11	-	0.79
Er	2.29	2.29	2.14	2.10	3.02	-	2.15
Tm	0.34	0.34	0.31	0.31	0.44	-	0.32
Yb	2.15	2.12	2.00	1.94	2.69	-	2.03
Lu	0.35	0.34	0.32	0.32	0.43	-	0.32
Ba	356	320	373	360	702	-	350
Th	1.07	0.95	1.08	0.85	2.18	-	1.00
Nb	1.66	1.55	1.65	1.41	3.77	-	1.60
Y	21.31	20.70	19.66	19.11	28.89	-	19.89
Hf	2.56	2.45	2.51	2.22	4.49	-	2.44
Ta	0.14	0.13	0.14	0.11	0.27	-	0.13
U	0.70	0.62	0.72	0.56	1.31	-	0.66
Pb	3.70	3.13	3.59	3.71	6.50	-	3.38
Rb	20.07	17.10	20.62	17.50	46.03	-	19.02
Cs	0.72	0.63	0.72	0.65	1.27	-	0.69
Sr	300	297	323	328	428	-	320
Sc	27.17	29.44	22.24	25.63	19.47	-	23.89
Zr	94.61	88.94	94.13	79.91	167.34	-	90.07
XRF							
Ni	17	20	13	15	17	21	12
Cr	32	16	19	12	37	19	17
V	208	253	190	228	226	202	191
Ga	16	17	17	18	20	-	16
Cu	100	307	41	277	190	45	36
Zn	80	77	76	78	73	82	73

Table 2. Continued

			Bezymianny Extrusive Domes			
Sample Name	10IPE1B	10IPE1B*	06BZT08	06BZT04	06CBZT08	08BZT08
Eruption Year	2010	2010	Lokmaty	"youngest"	P dome	Expedition
Brief Description	juveile host	inclusion	dome	dome	dome	dome
SiO_2	57.38	56.10	62.78	61.19	56.62	61.05
TiO_2	0.75	0.80	0.51	0.56	0.77	0.60
Al_2O_3	18.21	18.16	17.29	17.56	18.76	17.18
FeO*	7.84	7.63	4.79	5.15	7.21	5.45
MnO	0.15	0.15	0.12	0.13	0.17	0.14
MgO	3.85	4.13	2.37	2.71	3.24	2.94
CaO	7.71	7.90	5.75	6.24	7.16	6.06
Na_2O	2.97	3.41	3.88	3.79	3.77	3.78
K_2O	1.10	1.06	1.60	1.48	1.10	1.39
P_2O_5	0.17	0.17	0.18	0.18	0.23	0.18
Total	100.12	99.51	99.27	98.99	99.03	98.75
ICP-MS						
La	-	7.97	10.85	10.22	9.20	9.82
Ce	-	18.34	23.73	22.73	21.85	21.87
Pr	-	2.68	3.30	3.20	3.24	3.08
Nd	-	12.08	14.02	13.76	15.02	13.42
Sm	-	3.17	3.20	3.27	3.91	3.23
Eu	-	1.07	1.02	1.05	1.31	1.05
Gd	-	3.40	3.08	3.22	4.03	3.20
Tb	-	0.57	0.51	0.53	0.68	0.52
Dy	-	3.63	3.20	3.36	4.23	3.28
Ho	-	0.76	0.66	0.68	0.89	0.67
Er	-	2.08	1.81	1.93	2.48	1.84
Tm	-	0.31	0.28	0.29	0.37	0.27
Yb	-	1.96	1.82	1.85	2.34	1.72
Lu	-	0.32	0.29	0.31	0.38	0.29
Ba	-	372	602	556	369	496
Th	-	1.09	1.63	1.52	0.94	1.38
Nb	-	1.70	2.14	2.14	2.88	2.15
Y	-	19.44	17.48	17.99	22.41	17.61
Hf	-	2.53	3.20	3.07	2.95	3.01
Ta	-	0.14	0.19	0.18	0.23	0.18
U	-	0.71	1.12	1.05	0.58	0.91
Pb	-	3.61	5.42	4.99	2.87	4.79
Rb	-	20.13	31.41	28.45	18.36	26.50
Cs	-	0.74	1.12	1.03	0.57	0.94
Sr	-	325	344	358	349	342
Sc	-	21.79	11.73	13.06	14.35	15.29
Zr	-	92.96	125.49	118.18	109.15	111.03
XRF						
Ni	21	14	6	11	7	13
Cr	15	16	28	41	14	62
V	189	211	98	113	153	119
Ga	-	16	17	16	18	18
Cu	36	47	10	6	22	11
Zn	79	77	69	71	87	76

Table 2. Continued

		Klyuchevskoy Lavas				
Sample Name	06BZT05	KL-1939	KL-1945Y	KL-1946A	KL-Krest 07	KL-Aoah 232-07
Eruption Year	1956	1949	1945	1946	2007	2007
Brief Description	cryptodome	lava	lava	lava	lava	lava
SiO_2	60.51	53.83	54.14	54.30	54.59	54.28
TiO_2	0.59	0.97	1.07	1.07	1.07	1.08
Al_2O_3	17.95	16.21	17.96	17.64	17.73	17.60
FeO*	5.83	8.29	8.36	8.40	8.45	8.53
MnO	0.15	0.17	0.16	0.17	0.18	0.17
MgO	2.60	6.89	5.18	5.67	5.21	5.35
CaO	6.53	9.23	8.39	8.67	8.54	8.60
Na_2O	3.71	3.17	3.55	3.46	3.54	3.48
K_2O	1.29	0.98	1.14	1.09	1.04	1.01
P_2O_5	0.18	0.19	0.22	0.21	0.20	0.20
Total	99.35	99.92	100.15	100.67	100.54	100.30
ICP-MS						
La	9.36	6.43	7.49	7.29	7.17	7.22
Ce	21.25	15.71	18.11	17.63	17.72	17.61
Pr	3.02	2.44	2.84	2.72	2.76	2.73
Nd	13.38	11.93	13.53	13.25	13.25	13.17
Sm	3.37	3.40	3.83	3.69	3.82	3.90
Eu	1.08	1.16	1.25	1.27	1.29	1.29
Gd	3.24	3.66	4.04	4.00	4.31	4.28
Tb	0.55	0.64	0.70	0.70	0.74	0.72
Dy	3.49	3.89	4.35	4.37	4.67	4.58
Ho	0.72	0.85	0.90	0.88	0.97	0.96
Er	1.98	2.28	2.44	2.42	2.68	2.62
Tm	0.30	0.33	0.35	0.35	0.38	0.38
Yb	1.91	2.07	2.24	2.18	2.39	2.37
Lu	0.32	0.32	0.35	0.35	0.37	0.38
Ba	450	342	391	375	424	420
Th	1.35	0.71	0.76	0.78	0.78	0.77
Nb	2.07	1.60	1.77	1.77	2.46	1.93
Y	18.79	20.92	22.62	22.46	24.51	24.60
Hf	2.91	2.29	2.54	2.45	2.63	2.66
Ta	0.16	0.11	0.13	0.13	0.15	0.14
U	0.89	0.43	0.47	0.46	0.47	0.46
Pb	4.37	3.05	3.39	3.20	3.38	3.35
Rb	24.28	14.42	16.23	15.46	16.07	15.74
Cs	0.91	0.47	0.53	0.48	0.49	0.48
Sr	350	344	394	378	345	345
Sc	12.50	30.80	25.13	28.99	27.85	28.51
Zr	110.41	82.06	91.84	90.18	97.06	96.58
XRF						
Ni	6	54	30	33	39	27
Cr	19	215	42	73	84	65
V	120	261	263	268	256	260
Ga	17	16	18	19	18	19
Cu	18	74	95	97	76	71
Zn	79	82	86	86	93	90

Table 3. High-precision MC-ICP-MS Pb-isotope Compositions

Bezymianny Volcano

Bezymianny Extrusive Domes

Sample Name	Eruption Date	$^{208}Pb/^{204}Pb$	$^{207}Pb/^{204}Pb$	$^{206}Pb/^{204}Pb$	n[a]	Description
06BZT04	< 3 ka	37.90284	15.47823	18.27658		"Young" dome
06BZT08	3-5 ka	37.89930	15.47767	18.27612		Lokmaty dome
08BZT08[b]	Holocene	37.90277	15.47825	18.27805	3	Expedition dome
06CBZT08	Pleistocene	37.87009	15.47348	18.26834		Cedlo dome
MP1BZT09	unknown	37.86538	15.47073	18.26244		mega plag lava
MP2BZT09	unknown	37.88058	15.47544	18.26889		mega plag lava

Bezymianny Modern Eruptions 1956 - present

Sample Name	Eruption Date	$^{208}Pb/^{204}Pb$	$^{207}Pb/^{204}Pb$	$^{206}Pb/^{204}Pb$	n[a]	Description
06BZT05	1956	37.88938	15.47432	18.25875		cryptodome
05BZT08	1956	37.88642	15.47511	18.26249		cryptodome
06BZT11	1997	37.88885	15.47678	18.26229		pumice, tephra
06IPE16	2006 (May)	37.87762	15.47377	18.25531		juvenile breadcrust bomb
06IPE17	2006 (May)	37.87465	15.47104	18.25553		juvenile breadcrust bomb
06BZT02a	2006 (May)	37.87243	15.47058	18.25540		juvenile breadcrust bomb
06BZT02b[b]	2006 (May)	37.87901	15.47394	18.25574	2	inner, breadcrust bomb
06BZT03	2006 (May)	37.84996	15.46756	18.25516		pumice
06BZT03	2006 (May)	37.88377	15.47473	18.25946		pumice
02BZTK07	2006 (Dec)	37.88243	15.47411	18.25950		juvenile breadcrust bomb
05BZT09[b]	2006/2007	37.88169	15.47423	18.26125	2	juvenile breadcrust bomb
01BZTK07	2007 (May)	37.89225	15.47754	18.26237		juvenile breadcrust bomb
02BZT08	2007 (Oct)	37.88111	15.47523	18.25983		juvenile breadcrust bomb
03BZT08	2007 (Oct)	37.87697	15.47440	18.24911		juvenile breadcrust bomb
04BZT08	2007 (Oct)	37.88150	15.47476	18.26029		juvenile breadcrust bomb
03BZT09	2007 (Oct)	37.88823	15.47459	18.26494		juvenile breadcrust bomb
04BZT09	2007 (Oct)	37.89608	15.48029	18.26573		juvenile breadcrust bomb
11BZT09	2007 (Oct)	37.88808	15.47735	18.26224		juvenile breadcrust bomb
06BZT09	2008 (Aug)	37.89004	15.47688	18.26913		juvenile bomb
10IPE5A	2009 (Dec)	37.88876	15.47880	18.26031		juvenile breadcrust bomb
10IPE7A	2009 (Dec)	37.89281	15.47913	18.26102		juvenile breadcrust bomb
10IPE8	2010 (Jan/Feb)	37.89210	15.48010	18.25938		lava flow
10IPE1A	2010 (June)	37.88564	15.47633	18.26810		juvenile bomb
10IPE2A	2010 (June)	37.89219	15.47796	18.26525		juvenile bomb
10IPE9	2010 (June)	37.89326	15.47945	18.25655		lava flow

Bezymianny Inclusions

Sample Name	Eruption Date	$^{208}Pb/^{204}Pb$	$^{207}Pb/^{204}Pb$	$^{206}Pb/^{204}Pb$	n[a]	Description
01BZT09*	2007 (Oct)	37.88124	15.47469	18.25901		inclusion in 02BZT08
01BZT09**[b]	2007 (Oct)	37.82761	15.47301	18.18345	3	inclusion in 02BZT08
01BZT09***	2007 (Oct)	37.85427	15.47332	18.23050		inclusion in 02BZT08
03BZT09a	2007 (Oct)	37.89293	15.47592	18.27573		inclusion in 03BZT09
03BZT09b	2007 (Oct)	37.88989	15.47558	18.26665		inclusion in 03BZT09
03BZT09d	2007 (Oct)	37.89204	15.47828	18.26386		inclusion in 03BZT09
04BZT09d	2007 (Oct)	37.89176	15.47641	18.26504		inclusion in 04BZT09
11BZT09a	2007 (Oct)	37.87336	15.47119	18.26149		inclusion in 11BZT09
05BZT09a[b]	2006/2007	37.88935	15.47737	18.26311	2	inclusion in 05BZT09
05BZT09b[b]	2006/2007	37.89281	15.47708	18.26820	2	inclusion in 05BZT09
02BZT09b[b]	2008 (Aug)	37.81487	15.47209	18.19986	3	inclusion in juvenile breadcrust bomb
06BZT09a	2008 (Aug)	37.88308	15.47318	18.26324		inclusion in 06BZT09
10IPE5B	2009 (Dec)	37.88559	15.47589	18.25669		inclusion in 10IPE5A
10IPE7B	2009 (Dec)	37.89684	15.48060	18.25564		inclusion in 10IPE7A
10IPE1B[b]	2010 (June)	37.80047	15.47680	18.16601	3	inclusion in 10IPE1A
10IPE2B	2010 (June)	37.88035	15.47745	18.25241		inclusion in 10IPE2A

[a] number of duplicates used to produce average value reported
[b] denotes that the value reported results from the averaging of multiple duplicate analyses

Table 3 (cont.). High-precision MC-ICP-MS Pb-isotope Compositions

Klyuchevskoy Volcano

Klyuchevskoy Lavas

Sample Name	Eruption Date	$^{208}Pb/^{204}Pb$	$^{207}Pb/^{204}Pb$	$^{206}Pb/^{204}Pb$	n[a]	Description
KL 1939	1939	37.91472	15.48036	18.29144		lava flow, flank
KL 1945Y	1945	37.90677	15.47795	18.28931		lava flow, flank
KL 1946A	1946	37.91812	15.48306	18.29421		lava flow, flank
KL Krest07	2007	37.94911	15.48734	18.30548		lava flow, summit
KL-Apah 232-07	2007	37.94361	15.48425	18.30305		lava flow, summit

Shiveluch Volcano

Shiveluch Modern Eruptions 1964-2007

Sample Name	Eruption Date	$^{208}Pb/^{204}Pb$	$^{207}Pb/^{204}Pb$	$^{206}Pb/^{204}Pb$	n[a]	Description
SHIV 1964	1964	37.91172	15.48323	18.36096		juvenile clast in pyroclastic flow
SHIV 1980[b]	1980	37.93437	15.48716	18.37811	2	juvenile clast in pyroclastic flow
SHIV 1993	1993	37.91000	15.48345	18.36440		juvenile clast in pyroclastic flow
SHIV2001 PFDMB	2001	37.90122	15.47872	18.36174		dome block in pyroclastic flow
SHIV2001 DMB[b]	2001	37.87491	15.47646	18.31161	2	dome
SHIV7 2007	2007	37.90791	15.48285	18.35718		juvenile clast in pyroclastic flow

Karymsky Volcano

Karymsky Modern Eruptions 1971-2007

Sample Name	Eruption Date	$^{208}Pb/^{204}Pb$	$^{207}Pb/^{204}Pb$	$^{206}Pb/^{204}Pb$	n[a]	Description
KTK0308	1964	37.98805	15.48394	18.35986		lava flow
K1971 PFMB	1971	37.99438	15.48687	18.36221		juvenile bomb in pyroclastic flow
KTK0408	1971	37.99282	15.48515	18.36168		lava flow toe
97IPE4[b]	1996 (Apr-Aug)	37.99797	15.48753	18.36343	3	lava flow
98IPE28	1996 (Sep-Oct)	37.98322	15.48279	18.35998		lava flow
98IPE22d[b]	1996	37.97992	15.48247	18.35983	2	juvenile bomb, Academy Nauk
98IPE26	1998 (June-July)	37.99374	15.48650	18.36313		lava flow
K2003	2003	37.98475	15.48345	18.35894		lava flow
K2004	2004	37.98337	15.48273	18.35851		lava flow
K2007[b]	2007	37.99225	15.49047	18.34455	2	ash, collected while falling
KTK0508	2008 (April)	38.00061	15.48860	18.36569		juvenile bomb
KTK0908	2008 (July 25)	38.00192	15.48886	18.36590		juvenile bomb

[a] number of duplicates used to produce average value reported
[b] denotes that the value reported results from the averaging of multiple duplicate analyses

APPENDIX A

Table 1. Shiveluch and Karymsky Sample Descriptions

Shiveluch Volcano

Shiveluch Juvenile Eruptive Products

Sample Name	Date of Eruption	Material Collected
SHIV 1980	1980	juvenile clast in 1980 pyroclastic flow
SHIV 1993	1993	juvenile clast in 1993 pyroclastic flow
SHIV 2001 DMB	2001	dome block from 2001 dome
SHIV 2001 PFDMB	2001	juvenile clast in large pyroclastic flow from 2001
SHIV 2007	2007	juvenile clast in pyroclastic flow from 2007

Karymsky Volcano

Karymsky Juvenile Eruptive Products

Sample Name	Date of Eruption	Material Collected
KTK0308	1964	lava flow on edifice
K1971 PFMB	1971	juvenile bomb in pyroclastic flow
KTK0408	1971	lava flow toe in crater on edifice
98IPE22d	1996	juvenile bomb from the Academy Nauk vent
97IPE4	1996 (Apr-Aug)	lava flow on edifice
98IPE28	1996 (Sep-Oct)	lava flow on edifice
98IPE26	1998 (June -July)	lava flow on edifice
K2003	2003	lava flow on edifice
K2004	2004	lava flow on edifice
K2007	2007	ash, collected near IVS research station while falling
KTK0508	2008 (April)	juvenile bomb from explosive event
KTK0908	2008 (July 25)	juvenile bomb from explosive event

REFERENCES:

Almeev R.R. (2005) Geochemistry of Bezymianny volcano: Evidence for mantle source and insights on fractionating parameters of the parental magmas, *Ph.D Dissertation, Moscow State University*, 238 pp. (In Russian)

Anosov, G.I., Bikkenina, S.K., & Popov, A.A. (1978) *Glubinnoe seismicheskoe zondirovanie Kamchatki* (Deep Seismic Sounding of Kamchatka), Moscow: *Nauka*, 129 pp. (In Russian)

Arevalo, R. Jr. & McDonough, W.F., (2010). Chemical variations and regional diversity observed in MORB. *Chemical Geology* **271**, 70-85.

Ariskin, A.A., Barmina, G.S., Ozerov, A. Yu., & Nielsen, R.L. (1995). Genesis of high-alumina basalts from Klyuchevskoi volcano. *Petrology* **3**, 449-472.

Auer, S., Bindeman, I., Wallace, P., Ponomareva, V., & Portnyagin, M. (2009). The origin of hydrous, high-δ18O voluminous volcanism: diverse oxygen isotope values and high magmatic water contents within the volcanic record of Klyuchevskoy volcano, Kamchatka, Russia. *Contributions to Mineralogy and Petrology* **157**, 209-230.

Ayers, J.C., Dittmer, S.K., & Layne, G.D. (1997). Partitioning of elements between peridotite and H_2O at 2.0-3.0 GPa and 900-1100oC, and application to models of subduction zone processes. *Earth and Planetary Science Letters* **150***,* 381-398.

Balesta, S.T. (1991). Earth crust structure and magma chambers of the areas of present Kamchatka volcanism. In: Fedotov, S.A., Masurenkov, Y.P., and Balesta, S.T. eds., *Active volcanoes of Kamchatka, Moscow, Nauka* pp. 36-45

Belousov, A.B., Belousova, M.G., & Zhdanova, E.Yu. (1996). Northern group of Kamchatkan volcanoes: Activity in 1990-1992. *Journal of Volcanology and Seismology* **18**, 161-170.

Belousov, A., Voight, B., Belousova, M., & Petukhin, A. (2002). Pyroclastic surges and flows from the 8-10 May 1997 explosive eruption of Bezymianny volcano, Kamchatka, Russia. *Bulletin of Volcanology* **64**, 455-471.

Bindeman, I., Vinogradov, V.I., Valley, J.W., Wooden, J.L., & Natal'in, B.A. (2002). Archean protolith and accretion of crust in Kamchatka: SHRIMP dating of zircons from Sredinny and Ganal Massifs. *The Journal of Geology* **110**, 271-289.

Bindeman, I.N., Ponomareva, V., Bailey, J.C., & Valley, J.W. (2004). Volcanic arc of Kamchatka: a province with high-δ18O magma sources and large-scale $^{18}O/^{16}O$ depletion of the upper crust. *Geochemica et Cosmochimica Acta* **68** (4), 841-865.

Bogoyavlenskaya, G. Ye., Braitseva, O. A., Melekestsev, I.V., Maksimov, A. P., & Ivanov, B.V. (1991). Bezymianny volcano. In: Fedotov, S.A., and Masurenkob, Y.P. (eds.) *Active volcanoes of Kamchatka, Moscow: Nauka*, 168-197.

Brenan, J.M., Shaw, H.F., Phinney, D.L., & Ryerson, F.J. (1994). Rutile-aqueous fluid partitioning of Nb, Ta, Hf, Zr, U and Th: implications for high field strength element depletions in island-arc basalts. *Earth and Planetary Science Letters* **128**, 327-339.

Brunelli, D., & Seyler, M. (2010). Asthenospheric percolation of alkaline melts beneath the St. Paul region (Central Atlantic Ocean). *Earth and Planetary Science Letters* **289**, 393–405.

Churikova, T., Dorendorf, F., & Wörner, G. (2001). Sources and fluids in the mantle wedge below Kamchatka, evidence from across-arc geochemical variation. *Journal of Petrology* **42** (8), 1567-1593.

Churikova, T.G., Gordeychik, B.N., Wörner, G., & Ivanov, B.V. (2011). Variable fluids and mantle sources documented in the geochemistry of Kamen volcano and the Klyuchevskaya volcanic group. *Japan Kamchatka Aleutian Subduction Processes Meeting Abstracts*

Davidson, J., Turner, S., Handley, H., Macpherson, C., & Dosseto, A. (2007). Amphibole "sponge" in arc crust? *Geology* **35**, 787-790.

Dorendorf, F., Weichert, U., & Wörner, G. (2000). Hydrated sub-arc mantle: a source for the Klyuchevskoy volcano, Kamchatka/Russia. *Earth and Planetary Science Letters* **175**, 69-86.

Dosseto, A., Bourdon, B., Joron, J. & Dupre, B. (2003). U-Th-Pa-Ra study of the Kamchatka arc: New constraints on the genesis of arc lavas. *Geochimica et Cosmochimica Acta* **67**, 2857-2877.

Dufek, J. & Bergantz, G.W. (2005). Lower crustal magma genesis and preservation: a stochastic framework for the evaluation of basalt-crust interaction. *Journal of Petrology* **142**, 113-132.

Dungan, M.A., & Davidson, J. (2004). Partial assimilative recycling of the mafic plutonic roots of arc volcanoes: An example from the Chilean Andes. *Geology* **32**, 773-776.

Fedotov, S.A., Masurenkov, Y.P., & Balesta, S.T. eds. (1991). *Active volcanoes of Kamchatka, Moscow, Nauka*, pp

Fedotov, S.A., Zharinov, N.A., & Gontovaya, L.I. (2010). The magmatic system of the Klyuchevskaya Group of volcanoes inferred from data on its eruptions, earthquakes, deformation, and deep structure. *Journal of Volcanology and Seismology* **4**, 1-33.

Gao, S., Rudnick, R.L., Yuan, H., Liu, X., Liu, Y., Xy, W., Ling, W., Ayers, J., Wang, X., & Wang, Q. (2004). Recycling lower continental crust in the North China Craton. *Nature* **432**, 892-897.

Gorbatov, A., Kostoglodov, V., Suarez, G., & Gordeev, E. (1997). Seismicity and structure of the Kamchatka subduction zone. *Journal of Geophysical Research* **102**, 17883-17898.

Harkins, S.A., Appold, M.S., Nelson, B.K., Brewer, A.M., & Groves, I.M. (2008). Lead isotope constraints on the origin of nonsulfide zinc and sulfide zinc-lead deposits in the Flinders Ranges, South Australia. *Economic Geology* **103**, 353-364

Hart, S.R. (1984). A large-scale anomaly in the Southern Hemisphere mantle. *Nature* **309**, 753-757.

Hochstaedter, A.G., Kepezhinskas, P., & Defant, M. (1996). Insights into the volcanic arc mantle wedge from magnesian lavas from the Kamchatka arc. *Journal of Geophysical Research* **101** (B1), 697-712.

Hofmann, A.W., (1988). Chemical differentiation of the Earth: the relationship between mantle, continental crust, and oceanic crust. *Earth and Planetary Science Letters* **90**, 297-314.

Hofmann, A.W., (1997). Mantle geochemistry: the message from oceanic volcanism. *Nature* **385**, 219-229.

Ishikawa, T., Tera, F., & Nakazawa, T. (2001). Boron isotope and trace element systematics of the three volcanic zones in the Kamchatka arc. *Geochemica et Cosmochimica Acta* **65** (24), 4523-4537.

Izbekov, P.E., Neill, O.K., Shipman, J.S., Turner, S.J., Shcherbakov, V.D., & Plechov, P. (2010). Silicic enclaves in products of 2009-2010 eruptions of Bezymianny volcano, Kamchatka: Implications for magmatic processes. *AGU Fall Meeting Supplemental Abstract*.

Johnson, D.M., Hooper, P.R. & Conrey, R.M. (1999). XRF analysis of rocks and minerals for major and trace elements on a single low dilution Li-tetraborate fused bead. *Advances in X-Ray Analysis* **41**, 843–867.

Johnson, K.T.M. (1998). Experimental determination of partition coefficients for rare earth and high-field-strength elements between clinopyroxene, garnet, and basaltic melt at high pressures. *Contributions to Mineralogy and Petrology* **133**, 60-68.

Kelemen, P. B., Yogodzinski, G. M. & Scholl, D. W. (2003). Along strike variation in the Aleutian island arc: genesis of high-Mg# andesite and implications for continental crust. *In: Eiler, J. (ed.) Inside the Subduction Factory*. *Geophysical Monograph, American Geophysical Union* **138**, 223–276.

Kepezhinskas, P., McDermott, F., Defant, M.J., Hochstaedter, A., Drummond, M.S., Hawkesworth, C.J., Koloskov, A., Maury, R.C., & Bellon, H. (1997). Trace element and Sr-Nd-Pb isotopic constraints on a three-component model of Kamchatka Arc petrogenesis. *Geochimica et Cosmochimica Acta* **61** (3), 577-600.

Kersting, A.B., & Arculus, R.J. (1994). Klyuchevskoy volcano, Kamchatka, Russia: The role of high-flux recharged, tapped, and fractionated magma chamber(s) in the genesis of high-Al_2O_3 from high-MgO basalt. *Journal of Petrology* **35**, 1-41.

Kersting, A.B., & Arculus, R.J. (1995). Pb isotope composition of Klyuchevskoy volcano, Kamchatka and North Pacific sediments: Implications for magma genesis and crustal recycling in the Kamchatkan arc. *Earth and Planetary Science Letters* **136**, 133-148.

Khrenov, A.P., Dvigalo, V.N., Kirsanov, I.T., Fedotov, S.A., Gorel'chik, V.I., & Zharinov, N.A., (1991). Klyuchevskoy Volcano. In: Fedotov, S.A., and Masurenkob, Y.P. (eds.) *Active volcanoes of Kamchatka, Moscow: Nauka*, 106-153 (in Russian and English).

Khubanaya, S.A., Bogoyavlenskiy, S.O., Novogorodtseva, T.A., & Okrugina, A.I. (1994). The mineralogy of the Klyuchevskoi magnesian basalts depicting the fractionation in the magma chamber. *Volkanologiya I Seismologiya* **3**, 315-338 (in Russian).

Khubanaya, S.A., & Sobolev, A.V. (1998). Primary melts of calc-alkaline magnesian basalts from the Klyuchevskoi volcano, Kamchatka. *Doklady Earth Sciences* **360**, 537-539.

Konstantinovskaia, E.A. (2001). Arc-continent collision and subduction reversal in the Cenozoic evolution of the Northwest pacific: an example from Kamchatka (NE Russia). *Tectonophysics*, **333**, 75-94.

Lees, J.M. (2007). Seismic tomography of magmatic systems. *Journal of Volcanology and Geothermal Research* **167**, 37-56.

Lees, J.M., VanDecar, J., Gordeev, E., Ozerov, A., Brandon, M., Park, J., & Levin, V. (2007). Three dimensional images of the Kamchatka-Pacific plate cusp. *In: Kamchatka Geophysical Monograph Series, American Geophysical Union,* **172**, 65-75.

Madureira, P., Mata, J., Mattielli, N., Queiroz, G., & Silva, P. (2011). Mantle source heterogeneity, magma generation and magmatic evolution at Terceira Island (Azores archipelago): Constraints from elemental and isotopic (Sr, Nd, Hf, and Pb) data. *Lithos* **126**, 402-418.

Melekestsev, I.V., Khrenov, A.P., & Kozhernyaka, N.N. (1991). Tectonic position and general description of volcanoes of Northern group and Sredinny Range. In: Fedotov, S.A., and Masurenkob, Y.P. (eds.) *Active volcanoes of Kamchatka, Moscow: Nauka*, 74-81.

Miller, D.M., Goldstein, S.L., & Langmuir, C.H. (1994). Cerium/lead and lead isotope ratios in arc magmas and the enrichment of lead in the continents. *Nature* **368**, 514-519.

Minster, J.B., & Jordan, T.H. (1978). Present-day plate motions. *Journal of Geophysical Research* **83**, 5331-5354.

Mironov, N.L., Portnyagin, M.V., Pletchov, P.Yu., & Khubunaya, S.A. (2001). Kamchatka: Evidence from melt inclusions in minerals of high-alumina basalts. *Petrology* **9** (1), 46-62.

Mironov, N.L. & Portnyagin, M.V., (2011). H_2O and CO_2 in parental magmas of Kliuchevskoi volcano inferred from study of melt and fluid inclusions in olivine. *Russian Geology and Geophysics* **52**, 1353-1367.

Münker, C., Wörner, G., Yogodzinski, G., & Churikova, T., (2004). Behaviour of high field strength elements in subduction zones: constraints from Kamchatka-Aleutian arc lavas. *Earth and Planetary Science Letters* **224**, 275-293.

Noll, P. D., Newsom, H. E., Leeman, W. P. & Ryan, J. G. (1996). The role of hydrothermal fluids in the production of subduction zone magmas: evidence from siderophile and chalcophile trace elements and boron. *Geochimica et Cosmochimica Acta* **60**, 587–611.

Ozerov, A.Yu., Ariskin, A.A., Kyle, P., Bogoyavlenskaya, G.E., & Karpenko, S.F. (1997). Petrological-geochemical model for genetic relationships between basaltic and andesitic magmatism of Klyuchevskoi and Bezymyannyi volcanoes, Kamchatka. *Petrology* **5**, 550-569.

Ozerov, A.Yu. (2000). The evolution of high-alumina basalts of the Klyuchevskoy volcano, Kamchatka, Russia, based on microprobe analyses of mineral inclusions. *Journal of Volcanology and Geothermal Research* **95**, 65-79.

Ozerov, A.Yu., Firstov, P.P., & Gavrilov, V.A. (2007). Periodicities in the dynamics of eruptions of Klyuchevskoi volcano, Kamchatka. *In: Kamchatka Geophysical Monograph Series, American Geophysical Union* **172**, 283-291.

Pearce, J.A., Harris, N.B.W., & Tindle, A.G. (1984). Trace-element discrimination diagrams for the tectonic interpretation of granitic-rocks. *Journal of Petrology* **25**, 956-983.

Pineau, F., Semet, M.P., Grassineau, N., Okrugin, V.M., & Javoy, M. (1999). The genesis of the stable isotope (O, H) record in arc magmas: the Kamchatka's case. *Chemical Geology* **135**, 93-124.

Plank, T., (2005). Constraints from thorium/lanthanum on sediment recycling at subduction zones and the evolution of the continents. *Journal of Petrology* **46**, 921-944.

Plechov, P.Yu., Tsai, A.E., Shcherbakov, V.D., & Dirksen, O.V. (2008). Opacitization conditions of hornblende in Bezymyannyi volcano andesites (March 30, 1956 eruption). *Petrology* **16**, 19-35.

Portnyagin, M., Hoernle, K., Avdeiko, G., Hauff, F., Werner, R., Bindeman, I., Uspensky, V., & Garbe-Schoenberg, D. (2005). Transition from arc to oceanic magmatism at the Kamchatka-Aleutian junction. *Geology* **33**, 25-28.

Portnyagin, M., Hoernle, K., Plechov, P., Mironov, N., & Khubunaya, S. (2007). Constraints on mantle melting and composition and nature of slab components in volcanic arcs from volatiles

(H_2O, S, Cl, F) and trace elements in melt inclusions from the Kamchatka Arc. *Earth and Planetary Science Letters* **255**, 53-69.

Portnyagin, M., Bindeman, I., Hoernle, K., & Hauff, F. (2007). Geochemistry of primitive lavas of the Central Kamchatka Depression: magma generation at the edge of the Pacific Plate. *In: Kamchatka Geophysical Monograph Series, American Geophysical Union* **172**, 199-239.

Portnyagin, M., Mironov, N., Ponomareva, V., Bindeman, I., Hauff, F., Sobolev, A., Kayzar, T., Garbe-Schonberg, D., & Hoernle, K (2011). Arc magmas from slab to eruption: The case of Kliuchevskoy volcano. *Goldschmidt Conference Abstracts* **75**, 1661.

Portnyagin, M.V., & Ponomareva, V.V. (2012). Kliuchevskoy volcano diary. *International Journal of Earth Sciences* **101**, 195.

Putirka, K.D. (2008). Thermometers and barometers for volcanic systems. *Reviews in Mineralogy and Petrology* **69**, 61-120.

Reagan, M.K., Sims, K.W.W., Erich, J., Thomas, R.B., Cheng, H., Edwards, R.L., Laybe, G., & Ball, L. (2003). Time-scales of differentiation from mafic parents to rhyolite in North American continental arcs. *Journal of Petrology* **44**, 1703-1726.

Regelous, M., Hofmann, A.W., Abouchami, W., & Galer, S.J.G. (2003). Geochemistry of lavas from the Emperor Seamounts, and the geochemical evolution of Hawaiian magmatism from 85 to 42 Ma. *Journal of Petrology* **44**, 113-140.

Reiners, P.W., Nelson, B.K., & Ghiorso, M.S., (1995). Assimilation of Felsic Crust by Basaltic Magma - Thermal Limits and Extents of Crustal Contamination of Mantle-Derived Magmas. *Geology*, **23** (6), 563-566.

Shcherbakov, V.D., Plechov, P. Yu., Izbekov, P.E., & Shipman, J.S. (2011). Plagioclase zoning as an indicator of magma processes at Bezymianny Volcano, Kamchatka. *Contributions to Mineralogy and Petrology* **162**, 83-99.

Shipman, J.S., Turner, S.J., Gavrilenko, M., & Izbekov, P.E. (2010). Rapid modal analysis and whole-rock geochemistry of the 1956-present eruptive products of Bezymianny volcano. *AGU Fall Meeting Supplemental Abstract.*

Sun, S.-s. & McDonough, W.F., (1989). Chemical and isotopic systematics of oceanic basalts: implications for mantle composition and processes. *In: Saunders, A.D. & Norry, M.J., (eds.), Magmatism in the Ocean Basins, Geological Society Special Publication No.* **42**, 313-345.

Tatsumi, Y. (2000). Slab melting: its role in continental crust formation and mantle evolution. *Geophysical Research Letters* **27**, 3941–3944.

Tolstykh, M.L., Naumov, V.B., Babansky, A.D., Bogoyavlenskaya, G.E., & Khubunaya, S.A. (2003). Chemical composition, volatile components, and trace elements in andesitic magmas of the Kurile-Kamchatka region. *Petrology* **5**, 407-425.

Tsvetkov A.A., Gladkov N.G., & Volynets O.N. (1989). Problem of sediment subduction and 10Be isotope in lavas of Kuril Islands and Kamchatka Peninsula. Translated from USSR Academy of Sciences 306, 1220–1225.

Turner, S., McDermott, F., Hawkesworth, C., & Kepezhinskas, P. (1998). A U-series study of lavas from Kamchatka and the Aleutians: constraints on source composition and melting processes. *Contributions to Mineralogy and Petrology* **133**, 217-234.

Turner, S., Sims, K.W.W., Reagan, M., & Cook, C. (2007). A ^{210}Pb-^{226}Ra-^{230}Th-^{238}U study of Klyuchevskoy and Bezymianny volcanoes, Kamchatka. *Geochimica et Cosmochimica Acta* **71**, 4771-4785.

Turner, S.J., Izbekov, P.I., & Langmuir, C. (submitted). The magma plumbing system of Bezymianny Volcano: Insights from trace element whole-rock geochemistry and amphibole compositions. *Submitted to Journal of Volcanology and Geothermal Research.*

Volynets, O.N., Babanskii, A.D., & Gol'tsman (2000). Variations in isotopic and trace-element composition of lavas from volcanoes of the Northern Group, Kamchatka, in relation to specific features of subduction. *Geochemistry International* **38**, 974-989.

Volynets, A., Churikova, T., Woerner, G., Gordeychik, B.N., & Layer, P. (2010). Mafic late Miocene-quaternary volcanic rocks in the Kamchatka back arc region: implications for subduction geometry and slab history at the Pacific-Aleutian junction. *Contributions to Mineralogy and Petrology* **159**, 659-687.

Watson, B.F., & Fujita, K. (1985). Tectonic evolution of Kamchatka and the sea of Okhotsk and implications for the Pacific Basin. *In: Tectonostratigraphic Terranes. (ed. D.G. Howell), AAPG*, 333-348.

Yogodzinski, G.M., Lees, J.M., Churikova, T.G., Dorendorf, F., Woerner, G., & Volynets, O.N. (2001). Geochemical evidence for the melting of subducting oceanic lithosphere at plate edges. *Nature* **409**, 500-503.

Washington State University (WSU) Geoanalytical Laboratory
http://www.sees.wsu.edu/Geolab/note.html

CHAPTER 2

Formation of Th-excess Isotopic Disequilibrium by Assimilation and Fractional Crystallization in Volcanic Arcs: (^{238}U)/(^{230}Th) from Volcanoes in the Central Kamchatka Depression

Co-authors
Bruce K. Nelson, Olivier Bachmann, Maxim Portnyagin

ABSTRACT

The Central Kamchatka Depression of the Kamchatka Volcanic Arc erupts magmas with 3 to 11% Th-excess disequilibria ((^{238}U)/(^{230}Th) from 0.97 to 0.89). Th-excess is not typically observed in fluid-fluxed arc settings, and is generally attributed to garnet fractionation. However, an inverse correlation of Th-excess with Dy/Yb at Klyuchevskoy volcano implies that pyroxene rather than garnet generates Th-excess in Kamchatka. We demonstrate that small degrees of Th-excess in the CKD result from deep crustal assimilation and fractional crystallization (AFC) of high-pressure clinopyroxene. Lower crustal AFC modeling suggests that 20-30% fractional crystallization of magmas during assimilation can reproduce the Th-excess measured at Bezymianny and Klyuchevskoy volcanoes indicating the importance of lower crustal assimilation even in thin (~ 35km) juvenile arcs. Th-excess models assume 5-10% U-excess in initial magmas before interaction with the lower crust and imply that crustal AFC processing may modify and overprint initial U-series disequilibria generated in the mantle wedge. Th-excess is observed in arc settings with either geophysical evidence for hot lower crust or petrologic evidence for crustal assimilation supporting our hypothesis that local crustal AFC rather than deep mantle melting conditions results in Th-excess.

1. INTRODUCTION

Disequilibrium in the short-lived U-series isotopic system occurs during partial melting, crystal fractionation, and volatile transport making the U-series decay chain a unique tool to examine the magnitude and timing of magmatic processes. Fractionation mechanisms within subduction zones are potentially very complex, with later processes modifying or overprinting the isotopic signatures of earlier processes. At volcanic arcs in particular, early interpretation of U-series disequilibria converged on a concept that (^{238}U)/(^{230}Th) and (^{226}Ra)/(^{230}Th) activity ratios greater than 1 coupled with indications of source modification by hydrous fluids (e.g., high Ba/Th, Sr/Th) result from melting generated during fluid-fluxing from the slab to the mantle wedge (see Turner *et al.*, (2003) and Peate and Hawkesworth (2005) for reviews). The preservation of (^{226}Ra)/(^{230}Th) disequilibria requires rapid melt transport from the mantle wedge to the surface

(^{226}Ra returns to equilibrium with ^{230}Th in ~8000 years). The implication of rapid transport coupled with the incompatibility of U-series elements suggest that U-series fractionation is not measurably affected by crustal processes. However, some well-studied arc systems, including the very productive Central Kamchatka Depression of the Kamchatka Volcanic Arc, have U-series data that conflict with this commonly accepted conceptual model.

Limited experimental data suggest preferential U transport over Th in subduction zone fluids; therefore, U-excess rather than Th-excess should characterize arcs (Brenan *et al.*, 1994; Keppler 1996). Yet, global arc data record Th-excess, (^{238}U)/(^{230}Th) < 1, in ~20% of fluid-fluxed subduction zone magmas (Peate and Hawkesworth 2005). Considerable research on the mechanism of Th-excess generation at mid-ocean ridge basalt systems attributes Th-excess to dynamic melting during near adiabatic decompression of the upper mantle (Condomines *et al.*, 1981; LaTourette and Burnett 1992; Spiegelman and Elliott 1993; Hauri *et al.*, 1994; Wood *et al.*, 1999; Lundstrom *et al.*, 2003 (review); Zhang and Zeng 2010). However, continental margins are not directly comparable to spreading ridges due to differences in physical dynamics, geochemical components, oxygen fugacity, and the presence of fluids from subducted slabs. Thus, the generation of Th-excess in hydrous arcs built on a thick overlying crustal column remains uncertain and perhaps quite different from the ocean ridge setting.

The most common interpretation of Th-excess in arcs postulates garnet as a residual phase present during mantle or crustal melting (Thomas *et al.*, 2002; Reagan *et al.*, 2003; Garrison *et al.*, 2006; Jicha *et al.*, 2009). U is more compatible than Th in garnet ($D_U/D_{Th} > 1$); therefore, deep crustal roots of garnet eclogite or garnet-bearing amphibolite as well as garnet peridotite in the melting region could retain high U/Th in the residue and conversely generate Th-excess in melt. Similar arguments have been made for residual high-pressure clinopyroxene and magnetite (Reagan *et al.*, 2003; Jicha *et al.*, 2007; Handley *et al.*, 2008). Other trace phases such as zircon, apatite, and allanite may also fractionate U-Th in arc settings. Therefore, it is ambiguous whether arc U-series disequilibria are deep geochemical signals that form in the mantle wedge or are the result of crustal processing (Volpe and Hammond 1991; Volpe 1992; Bourdon *et al.*, 2000; Reagan *et al.*, 2003; Berlo *et al.*, 2004; Garrison *et al.*, 2006; Jicha *et al.*, 2007; Walker *et al.*, 2007; Finney *et al.*, 2008; Handley *et al.*, 2008; Jicha *et al.*, 2009; Price *et al.*, 2010; Reubi *et al.*,

2011; Singer *et al.*, 2011).

We investigate the hypothesis that small degrees of Th-excess in the Central Kamchatka Depression (CKD) are the result of deep crustal assimilation and fractional crystallization. Published major and trace element data as well as Pb isotope data from the CKD suggest a role for deep crustal assimilation beneath Klyuchevskoy and Bezymianny volcanoes (Kayzar *et al.*, *submitted*; Portnyagin *et al.*, 2008; Portnyagin *et al.*, 2011). In addition, thermal and chemical models suggest that deep assimilation and fractional crystallization (AFC) occurs in many arc settings (Bowen 1928; Taylor 1980; DePaolo 1981; Rudnick *et al.*, 1986; Hildreth and Moorbath 1988; Stern and Kilian 1996; Spera and Bohrson 2001; Annen and Sparks 2002; Reagan *et al.*, 2003; Dufek and Bergantz 2005; Annen *et al.*, 2006; Bohrson and Spera 2007). If U is more compatible than Th in any phase fractionated during deep crustal melting and AFC processing, then Th-excess should be generated in melts extracted from these regions.

The CKD is an ideal setting within which to investigate Th-excess generation. First, the crustal thickness beneath the CKD is ~35km, which is not thick enough to stabilize garnet. Also, trace element compositions also imply a limited role, if any, for garnet in the residues of erupted magmas (Kayzar *et al.*, *submitted*). This suggests that the common interpretation of Th-excess formation in arcs (U compatibility in garnet) requires modification, and that Kamchatka represents a garnet free end-member where the generation of Th-excess may be investigated. Second, the Kamchatka arc mantle source is fluid-fluxed beneath the CKD, which is problematic for the generation of Th-excess concurrent with preferential transport of U by fluid transfer from the slab. Third, the sedimentary geochemical component that may contaminate U-series signals (Reagan *et al.*, 1994; Sigmarsson *et al.*, 2002) beneath the CKD is limited. Less than 1% sediment may be added during the generation of erupted magmas in order to preserve their very unradiogenic Pb-isotope compositions (Kersting and Arculus 1995; Kayzar *et al. submitted*). Finally, the erupted products in the CKD are basaltic and andesitic in composition and have, therefore, not evolved enough to saturate trace phases such as allanite and zircon. This reduces the quantitative complications that arise during interpretation of U-series disequilibria in the presence of trace zircon fractionation.

We present new U-series isotope data for time-series samples from Bezymianny and

Klyuchevskoy in the CKD and Shiveluch volcano in the northern CKD, and compare our data to a global database that we compiled of volcanic arcs that have Th-excess (**Appendix A**). We investigate Th-excess generation in the context of garnet fractionation, upper crustal fractional crystallization, dynamic melting in the mantle wedge, and lower crustal AFC processing.

2. BACKGROUND AND GEOLOGIC SETTING

The Central Kamchatka Depression is a large (~350 km long) graben-like structure in northern Kamchatka, Russia with multiple volcanic centers that includes two very active volcanoes: Klyuchevskoy and Bezymianny (Fedotov 1991; Kepezhinskas *et al.*, 1997; Fedotov *et al.*, 2010) (**Figure 1**). The geologic setting of Bezymianny and Klyuchevskoy volcanoes has been described in detail (Minster and Jordan 1978; Watson and Fujita 1985; Balesta 1991; Fedotov 1991; Melekestsev *et al.,* 1991; Kersting & Arculus 1995; Belousov *et al.,* 1996; Gorbatov *et al.,* 1997; Ozerov *et al.,* 1997; Kepezhinskas *et al.,* 1997; Dorendorf *et al.,* 2000; Konstantinovskaia 2001; Belousov *et al.,* 2002; Bindeman *et al.,* 2004, Lees 2007; Kayzar *et al. submitted*). Briefly, volcanism in the CKD is the result of subduction of the ~80-90Ma Pacific Plate which releases hydrous slab-derived fluids causing partial melting of a depleted mantle source (Watson and Fujita 1985; Gorbatov *et al.*, 1997; Portnyagin *et al.*, 2007). The crust beneath the CKD is relatively thin, ~35 km, with a 10-12km thick geophysically blurred Moho that is interpreted as deep basaltic magma ponding at the crust-mantle interface (Balesta 1991; Lees 2007). There is less than a 1% contribution of subducted sediment to magmas during generation beneath the CKD (Kersting and Arculus 1995; Kayzar *et al.*, *submitted*). Detailed major element, trace element and isotope data imply that magmas beneath Bezymianny and Klyuchevskoy have MORB-like isotopic compositions (Kersting & Arculus 1995; Kepezhinskas *et al.*, 1997; Dorendorf *et al.*, 2000; Churikova *et al.,* 2001; Kayzar *et al.*, submitted) and undergo varying degrees of assimilation and fractional crystallization in the lower crust, which shifts magmas to more unradiogenic Pb isotope compositions in erupted products (Kayzar *et al.*, *submitted*).

Bezymianny and Klyuchevskoy volcanoes display frequent eruptive activity (eruptions every year) that persists for extended periods of time. The current eruptive cycle at Bezymianny began with a lateral blast in 1956. Since that time, activity has been characterized by basaltic andesitic

to andesitic pyroclastic flows, lahars, block and ash flows and occasional small lava flows (Bogoyavlenskaya *et al.*, 1991; Belousov *et al.*, 1996; Ozerov *et al.*, 1997; Mironov 2001; Belousov *et al.*, 2002; Portnyagin *et al.*, 2007; Plechov *et al.*, 2008; Shcherbakov *et al.*, 2011; Kayzar *et al.*, *submitted*). Klyuchevskoy volcano has been active throughout the Holocene and historical periods erupting primarily high-alumina and high-magnesia basaltic tephra and lavas (Melekestsev *et al.*, 1991, Kersting and Arculus 1994, Ariskin *et al.*, 1995; Ozerov *et al.*, 1997; Portnyagin *et al.*, 2007; Auer *et al.*, 2009; Portnyagin and Ponomareva 2012).

Shiveluch volcano in the Northern Central Kamchatka Depression (NCKD) is compositionally distinct from the Klyuchevskoy Group to the south (Volynets *et al.*, 2000). Shiveluch magmas have higher MgO contents than Klyuchevskoy and Bezymianny at similar SiO_2 contents and also have higher Sr/Y ratios (Volynets *et al.*, 2000; Yogodzinski *et al.*, 2001; Portnyagin *et al.*, 2007). Shiveluch magmas have been interpreted to be similar to "adakitic" magmas (Yogodzinski *et al.*, 2001). Geophysical evidence and thermal modeling of the Pacific Plate suggest that a slab tear exists between the Klyuchevskoy Group and Shiveluch volcano and that high heat flow and mantle shearing occur along the tear (Davaille and Lees 2004). Slab shallowing beneath Shiveluch is consistent with this hypothesis (Gorbatov *et al.*, 1997; Park *et al.*, 2002). Shiveluch volcano erupted frequently throughout the Holocene and is also active historically producing many well-described eruptive units (Melekestsev *et al.*, 1991; Belousov 1995; Ponomareva *et al.*, 1998; Belousov *et al.*, 1999; Dirksen *et al.*, 2006; Gorbach and Portnyagin 2011).

3. METHODS

3.1 Sample Descriptions

Samples from Bezymianny and Shiveluch volcanoes were collected over the course of four summer field seasons in Kamchatka, Russia from 2006-2009 as part of a large NSF Partnerships in International Research and Education award (University of Alaska, Fairbanks). Field sampling was conducted in collaboration with colleagues with experience working on these volcanic centers from Moscow State University and the Institute of Volcanology and Seismology in Petropavlovsk-Kamchatsky, Russia. Fresh samples were collected from juvenile eruptive

products and the corresponding eruption ages and GPS locations for sampling are documented (**Table 1,** Kayzar *et al.*, *submitted*). Juvenile vesicular andesite from Bezymianny is dominated by plagioclase and 2-pyroxene phenocrysts and typical mineral assemblages contain plagioclase, orthopyroxene, clinopyroxene, Fe-Ti oxides and trace apatite and/or amphibole.

Samples from Klyuchevskoy volcano were sampled during field seasons funded by the KALMAR project through IFM-GEOMAR. Klyuchevskoy samples were taken from well-characterized and dated tephra deposits approximately 15 km northeast of the Klyuchevskoy summit (Portnyagin and Ponomareva 2012). Approximately 100 tephra samples from 9500 years BP to the present eruptive activity were collected during this project (Portnyagin *et al.*, 2008). We analyzed a small subset (10 samples) spanning ages from 212-4753 years BP for U-series isotope compositions.

3.2 Uranium-Series Chemical Separation

Laboratory separations of U and Th were done at the University of Washington. Clean, unaltered blocks of erupted products were chipped in a stainless steel mortar and pestle and then ground to powder in an agate mortar and pestle. Large whole rock powder splits > 5g/sample were dissolved in a Milestone® microwave digestion unit with 15mL HF and 20mL HNO_3 ultrapure acids at 210°C and 30 bars of pressure to ensure complete dissolution. Sample solutions were then evaporated with added HBO_3 and $HClO_4$ to remove fluorides formed during microwave dissolution. Following evaporation, samples were wetted and dried in concentrated HCl and brought up in 100-150mL 3M HCl + trace HBO_3 sample solutions. Procedures for chemical separation of U-series elements were modified slightly from those described in detail in Cooper and Donnelly (2009). Sample solutions were split into 3 aliquots for U and Th concentration measurements by isotope dilution (two separate aliquots), and U and Th isotope composition measurements (one aliquot). Aliquots for isotope dilution were spiked with ^{233}U and ^{229}Th isotopic tracers. The ^{233}U spike was made directly from a NIST CRM-112A uranium metal and calibrated by K.M. Cooper. The ^{229}Th spike used for chemistry was obtained from A. Pietruszka at San Diego State University as part of the high-purity Th-229 project and was diluted and calibrated at the University of Washington using an Ames Th solution standard.

Uranium and thorium were separated from sample standard solutions using Eichrom pre-filter and TRU resin followed by BioRad AG-1-X8 anion exchange resin. Spiked U and Th isotope dilution separations were done with an Eichrom TRU resin bed column volume of 0.5mL. Samples were loaded onto columns in 7M HNO_3, washed with 7M HNO_3, 1.5M HNO_3, and 3M HCl, and then eluted with 0.2M HCl (Th) and 0.1M HCl + 0.05M HF (U). Uranium and thorium isotope composition samples were chemically purified by the same procedure, but with a larger column volume of 1mL. Separations for isotope compositions were also purified a second time through a 0.5mL anion exchange column to remove products that bleed from the Eichrom resins into the sample collection during the TRU resin separation. Purified sample collections were dried and brought up in 2% HCl for MC-ICP-MS.

3.3 Uranium-Series Analysis by MC-ICP-MS

U and Th concentrations and isotope compositions were measured on a Nu Instruments MC-ICP-MS at the University of Washington. Analytical procedures were developed by K.M. Cooper and are described in detail in Cooper and Donnelly, (2009). Standards used during analysis were modified slightly from these procedures and are described further in **Appendix B**.
Briefly, samples are analyzed in a calibrate-standard-sample-sample-calibrate order. The NIST uranium standard, CRM-112A (20.5ppb solution) is used to calibrate instrumental mass bias and ion-counter to faraday gains. A Th Spex standard ICP-MS solution is used to correct for tailing of ^{232}Th into ^{230}Th. Tailing is corrected for by exponential fit to the ^{232}Th tail. Th solution standards IRMM-035, IRMM-036, and WUN-1 are measured as unknowns and isotopic compositions are compared to inter-laboratory values from Sims *et al.*, (2008) (**Appendix B**). A University of Washington in-house rock standard (UW-BCR-1, collected from the same locality as USGS BCR-2) was taken through the same chemical separation procedures as sample unknowns and analyzed as an unknown. Accuracy and reproducibility of standards analyzed as unknowns compared to certified values is generally better than 1% for U and Th concentrations and ~1% for (^{230}Th)/(^{232}Th) compositions. (^{234}U)/(^{238}U) ratios were monitored to check for alteration.

3.4 Additional Chemical Data

Major, trace element, and high-precision Pb isotope data for all samples are presented in Kayzar *et al.*, *submitted* and Portnyagin *et al.*, (2008) (data is available upon request from the authors).

We compiled a Th-excess global database with uranium and thorium isotopic compositions, as well as major and trace element data as part of this study in order directly compare CKD erupted products to volcanic systems in other well-studied arcs (**Appendix A**). This database is not complete in that it does not incorporate every U-series study in which Th-excess was recorded. However, it does represent a range of compositions and arcs where the cause of Th-excess generation has been interpreted. It is rare for published studies to incorporate both U-series disequilibria data and trace element data, which is the primary motivation for this compilation.

4. RESULTS

4.1 Uranium-Series Disequilibria

4.1.1 Central Kamchatka Depression: Bezymianny and Klyuchevskoy Volcanoes

Erupted products from Bezymianny and Klyuchevskoy volcanoes in the Central Kamchatka Depression generally display Th-excess: (^{238}U)/(^{230}Th) ratios are less than 1 and samples plot to the left of the U-Th equiline (**Figure 2**). Bezymianny modern juvenile eruptive products have 4-5% Th-excess: (^{238}U)/(^{230}Th) between 0.961 and 0.948 and (^{230}Th)/(^{232}Th) between 1.997 and 2.021 (**Table 2**). Older extrusive domes on the flank of Bezymianny display both Th-excess and U-excess. Lohkmaty dome is the only sample from Bezymianny with a U-excess, and the U-excess is small: (^{238}U)/(^{230}Th) = 1.040. The age of Lohkmaty dome is unknown but its chemical variation from the remainder of Bezymianny products implies that magma that formed this dome on the southern edifice of Bezymianny is not related to the historic activity of Bezymianny. The tephra units analyzed from Klyuchevskoy have variable Th-excess from ~ 1% to 11%. Ambiguity in previous U-series studies prevents us from making direct comparisons of these U-

series data to published data; therefore, we interpret these data as an independent data set (see **Appendix C** for discussion). Standard (UW-BCR-1) and sample measurements record $(^{234}U)/(^{238}U)$ within 4-5‰ of equilibrium (1.000).

The degree to which Klyuchevskoy samples record Th-excess varies with time. Recent eruptive units have less Th-excess (1-5%), while the largest Th-excesses measured (6-11%) are from tephra erupted between 3591 and 4076 years BP (**Table 2, Figure 3**). Tephra from Klyuchevskoy also record a larger range in $(^{230}Th)/(^{232}Th)$ than measured at Bezymianny. These Klyuchevskoy tephras represent ~ 5000 years of compositional variation relative to only 50 years at Bezymianny (**Figure 2**). Therefore, it may only be possible to document cyclic changes in uranium-series disequilibria over thousands of year timescales in the CKD whereas decadal eruptive timescales appear more homogeneous in the degree of disequilibria measured.

Bezymianny and Klyuchevskoy eruptive products record high $(^{230}Th)/(^{232}Th)$ ratios between 1.977 and 2.385 (**Table 2**). $(^{230}Th)/(^{232}Th)$ ratios above 1.5 are common in fluid-fluxed subduction zones that record U-excess (see review by Peate and Hawkesworth (2005)). However, in arcs that display Th-excess, $(^{230}Th)/(^{232}Th)$ ratios are usually less than 1.5 and are very rarely above 2. Bezymianny and Klyuchevskoy deposits therefore represent an end-member Th isotope composition of global eruptive products with Th-excess.

4.1.2 Northern Central Kamchatka Depression: Shiveluch Volcano

Unlike the CKD, eruptive products from Shiveluch volcano in the NCKD record U-excess (**Table 2, Figure 2**). Juvenile volcanic clasts from eruptions in 1993, 2001, and 2007 have between 4 and 9% U-excess: $(^{238}U)/(^{232}Th)$ from 1.600 to 1.659 and $(^{230}Th)/(^{232}Th)$ from 1.523 to 1.542. $(^{230}Th)/(^{232}Th)$ are lower in the NCKD than those measured for the CKD. Differences in $(^{238}U)/(^{230}Th)$ and Th isotope compositions between the CKD and the NCKD document along-strike variation of U-series disequilibria in the Kamchatka arc.

5. DISCUSSION

5.1 Fluid Addition in the Central Kamchatka Depression

Several lines of geochemical evidence suggest that the subduction zone beneath the CKD is fluid-fluxed. Erupted magmas from Bezymianny and Klyuchevskoy have enrichments in large ion lithophile elements (LILE) and light rare earth elements (LREE) as well as depletions in high field strength elements (HFSE) (**Figure 4A**, and Kayzar *et al.*, *submitted*) that reflect fluid transfer from the subducting Pacific Plate (Brenan *et al.*, 1994; Ayers *et al.*, 1997). Melt inclusions from Klyuchevskoy have up to 5 - 7.1 wt% H_2O (Mironov *et al.*, 2001; Auer *et al.*, 2009). In addition, these magmas have some of the highest (^{230}Th)/(^{232}Th) measured for arc magmas with Th-excess (**Figure 4B**). Fluid transfer of U to the mantle wedge followed by decay of ^{238}U to ^{230}Th over long periods of time (> 100,000 years) will produce high (^{230}Th)/(^{232}Th) (Turner *et al.*, 1998). (^{230}Th)/(^{232}Th) at Bezymianny and Klyuchevskoy positively correlates with Ba/Th, a trace element ratio that increases with fluid addition (**Figure 4B**). Therefore, we interpret high (^{230}Th)/(^{232}Th) in the CKD to reflect a long period of fluid fluxing from the slab to mantle wedge beneath the CKD.

Fluid transfer of U to the mantle wedge beneath Kamchatka is hypothesized to cause U-excess in magmas produced in the Kamchatka Arc (Turner *et al.*, 1998; Dosseto *et al.*, 2003; Turner *et al.*, 2007). Because magmas from Bezymianny and Klyuchevskoy have Th-excess despite showing chemical evidence for fluid-fluxing, we propose that crustal magmatic processing and differentiation overprint U-excess inherited from fluid transfer of U from slab to mantle beneath the CKD. Th may be more fluid mobile in arc environments than U (Kessel *et al.*, 2005); however, this is unlikely beneath the CKD. The amount of Th-excess measured in erupted products negatively correlates with Ba/Th (**Figure 5**) requiring Th-excess to be unrelated to fluid transfer at Bezymianny and Klyuchevskoy. In addition, preferential transport of Th by fluids, rather than transport of U followed by decay of ^{238}U, would fail to explain the high (^{230}Th)/(^{232}Th) described above. Furthermore, the widespread correlations of U-excess with fluid indicators (Ba/Th and Sr/Th) and the presence of U-excess in most global arc environments

support preferential transport of U in subduction zone fluids (Gill 1981; Allegre and Condomines 1982; Turner *et al.*, 1996; Elliott *et al.*, 1997; Hawkesworth *et al.*, 1997; Turner *et al.*, 2003).

5.2 Garnet and Th-excess Generation

Th-excess generation in arc settings is most commonly attributed to either crystallization of residual garnet in the lower crust, or melting in the presence of a garnet bearing mantle or subducted slab (Sigmarsson *et al.*, 1998, Bourdon *et al.*, 2000; Thomas *et al.*, 2002; Dosseto *et al.*, 2003; Reagan *et al.*, 2003; Berlo *et al.*, 2004; Dufek and Cooper 2005; Garrison *et al.*, 2006; Jicha *et al.*, 2009). Early work found that Th-excess was higher in arcs with thick crust, supporting the concept of residual garnet in the lower crust (Garrison *et al.*, 2006). However, more recent studies as well as our data for the CKD document Th-excess in arcs that are not thick enough (< 40 km) to stabilize garnet in their roots (Jicha *et al.*, 2007; Walker *et al.*, 2007, *this study*). We review the hypothesis that Th-excess is generated by equilibration with garnet using the global database, the compositions of the CKD and NCKD, and trace element signatures expected from garnet partitioning.

Heavy rare earth elements are more compatible than light rare earth elements during garnet-melt equilibration; therefore, high Dy/Yb ratios in a magma may signify melting with residual garnet or the fractional crystallization of garnet (Shimizu and Kushiro, 1975; Nicholls and Harris, 1980). Crystallization of other phases common in arc settings, such as amphibole and clinopyroxene, result in a lowering of Dy/Yb opposite to the effect of garnet (Nicholls and Harris, 1980; Davidson *et al.*, 2007). The Dy/Yb ratio is thus unique because the influence of garnet on Dy/Yb differs from that of other crystalline phases. High Sr/Y ratios have been used to investigate the role of garnet as well, particularly in adakite generation (Stern and Kilian 1996, Martin 1999; Macpherson *et al.*, 2006), but many magmatic processes, such as crystallization or melting of amphibole, pyroxene, and plagioclase may alter Sr/Y ratios making Sr/Y an ambiguous tracer of garnet in an arc setting (Garrison *et al.*, 2003; Moyen 2009).

To investigate the role of garnet in generating Th-excess, we compare $(^{238}U)/(^{230}Th)$ compositions to Dy/Yb from the Th-excess database (**Appendix A**). We filtered the Th-excess

database to include only basalt to andesite compositions in order to remove the effects of fractional crystallization of phases such as apatite and zircon on Dy/Yb variation in dacitic and rhyolitic magmas. We find no global arc correlation between the degree of Th-excess, (^{238}U)/(^{230}Th), and Dy/Yb (**Figure 6A**) suggesting that not all cases of Th-excess may be related to garnet, particularly in Kamchatka. Investigating the CKD volcanoes individually, we find that at Bezymianny volcano there is no correlation between (^{238}U)/(^{230}Th) and Dy/Yb, although chemical variation is restricted and sampling on the last 50 years of eruptive compositions at Bezymianny may not be a long enough time series to capture change in either chemical signal. Klyuchevskoy tephras erupted over a much longer time period do show a positive correlation (R^2=0.63) between (^{238}U)/(^{230}Th) and Dy/Yb (**Figure 6B**). The correlation suggests that Th-excess is negatively correlated with Dy/Yb at Klyuchevskoy, which is counter to the relationship expected if garnet partitioning generates Th-excess. If Th-excess is generated by garnet, then high (^{238}U)/(^{230}Th) should be associated with low Dy/Yb rather than high as seen in the tephras (**Figure 6B**). We compare our results from Kamchatka with the Cascades and the Northern Volcanic Zone of the Andes, two volcanic arcs from the global database where garnet has been interpreted to generate Th-excess. These arcs show contrasting correlations of Dy/Yb with (^{238}U)/(^{230}Th) (**Figure 6C**). In the Cascades, (^{238}U)/(^{230}Th) positively correlates with Dy/Yb which is consistent with the interpretation that garnet generates Th-excess beneath the Cascades (Reagan *et al.*, 2003). Conversely, in the Northern Volcanic Zone of the Andes, (^{238}U)/(^{230}Th) and Dy/Yb are negatively correlated as observed for Klyuchevskoy. The observation of contrasting trends between volcanic arcs suggests that Th-excess is likely not a consequence of a single process, but rather can be generated multiple different ways in the arc environment.

Additional evidence that falsifies the Th-excess by garnet hypothesis for the Kamchatka arc is the presence of U-excess at Shiveluch volcano (**Figure 2**). Volcanism at Shiveluch is associated with anomalously high temperatures and upwelling near the torn edge of the subducting Pacific plate, which may initiate slab melting. Therefore, Shiveluch volcanism is commonly related not to its volcanic neighbors to the south in the CKD but to the western Aleutians where there is more evidence for slab melting (Yogodzinski and Kelemen 1998; Volynets *et al.*, 2000; Yogodzinski *et al.*, 2001). Indeed, trace element evidence suggests that garnet may contribute to the distinctive chemical composition of Shiveluch magmas. Sr/Y and Dy/Yb ratios are higher at

Shiveluch than in the CKD (Sr/Y = 36-47 at Shiveluch and 15-20 in the CKD; Dy/Yb = 2 at Shiveluch and 1.6-1.9 in the CKD) (Kayzar *et al.*, *submitted*). Thus, if we hypothesize that garnet causes the Th-excess in Kamchatka magmas, we would expect Shiveluch to have an even higher Th-excess than the CKD, which is contrary to the U-excess that we measured. Because little evidence exists for a major role of garnet in CKD magma compositions (Kayzar *et al.*, *submitted*), and because Th-excess negatively correlates with Dy/Yb in Kamchatka and other arcs (Northern Volcanic Zone of the Andes shown here), we propose alternative mechanisms to explain Th-excess generation in volcanic arcs that do not require equilibration with garnet as a phase which preferentially fractionates uranium.

5.3 Th-excess by Fractional Crystallization in the Shallow Crust

As described above, Bezymianny and Klyuchevskoy volcanoes are thought to share similar though compositionally distinct sources. Klyuchevskoy has primitive compositions (51-56 wt%) while Bezymianny erupts more differentiated andesites (57-63 wt% SiO_2). Therefore, by examining the U-series signals in these two systems it is possible to distinguish a primary signal of mantle melting from one having undergone more extensive differentiation in the crust. If Th-excess resulted from fractional crystallization in the upper crust, andesitic magmas of Bezymianny should have higher Th-excess than basalts erupted from Klyuchevskoy. This is not observed; in fact, Klyuchevskoy tephras record the highest Th-excess and there is no correlation of Th-excess in the CKD or globally with SiO_2 or MgO content (**Figure 7**).

Uranium is more compatible than Th during zircon crystallization, and zircon fractionation has been suggested as the source of Th-excess particularly in rhyolite systems (Reagan *et al.*, 2003; Jicha *et al.*, 2007). However, the basaltic and andesitic magma compositions of Bezymianny and Klyuchevskoy are not evolved enough to be saturated in Zr and crystallize zircon so it is unlikely that this is the cause of Th-excess in the CKD. Other low-pressure phases (plagioclase, clinopyroxene, olivine, apatite) observed in erupted products at Bezymianny and Klyuchevskoy have $D_U/D_{Th} < 1$ (Blundy and Wood 2003). Uranium only becomes more compatible than Th in clinopyroxene at high-pressure (> 1.2 GPa) (Wood *et al.*, 1999; Landwehr *et al.*, 2001). Also, no correlation is observed between Th-excess and Sc, Cr, Ni, or Sr concentrations – elements that

are compatible in olivine, pyroxenes, and plagioclase. We find no evidence that supports upper crustal fractionation as a mechanism to produce Th-excess during magma differentiation.

Additionally, if magma differentiation from basalt to andesite led to Th-excess, most arc magmas should be characterized by Th-excess disequilibria as most magmas undergo some degree of differentiation. As discussed earlier, only ~ 20% of all global arc magmas (including dacitic and rhyolitic compositions) have Th-excess (Peate and Hawkesworth 2005) and would require unique chemical behavior during magma differentiation only in these arcs, which we infer to be highly unlikely.

5.4 Th-excess by Dynamic Melting with High-Pressure Clinopyroxene

Experimental studies of the partitioning of U and Th at conditions appropriate for magma generation at mid-ocean ridges, as well as data from MORB lavas have found that U is more compatible than Th in high-pressure (> 1.2 GPa) clinopyroxene (Wood *et al.*, 1999; Landwehr *et al.*, 2001), relaxing the requirement of garnet partitioning to generate Th-excess (Beattie 1993a; Beattie 1993b; LaTourette *et al.*, 1993). Dynamic melting in the presence of clinopyroxene is now postulated as a mechanism to form Th-excess in mid-ocean ridge basalt (Wood *et al.*, 1999; Landwehr *et al.*, 2001; Zhang and Zeng 2010). This debate has not been resolved for arc settings; however, many studies suggest that dynamic decompression melting produces Th-excess (Thomas *et al.*, 2002; George *et al.*, 2003; Reagan *et al.*, 2003). We test the hypothesis that dynamic melting of the mantle wedge beneath the CKD generates Th-excess at depths shallower than the stability field of garnet.

We calculate dynamic melting of a depleted mantle source beneath the CKD using analytical solutions of Zou and Zindler (2000) for U-series disequilibria in extracted melts. These solutions add transport and extraction of dynamically produced melts to earlier melting models which did not take incorporate the effects of melt extraction (McKenzie 1985; Williams and Gill 1989). In our calculations, we assume a melting rate of 0.0001 kg/m^{3}yr and vary the porosity of the melting region from 0.2% to 2%. Conservative bulk partition coefficients that minimize U/Th fractionation of $D_U = 0.0025$ and $D_{Th} = 0.0013$ are calculated assuming a mantle mineralogy that

is 67% olivine, 22% orthopyroxene, and 11% clinopyroxene (Johnson *et al.*, 1998; Landwehr *et al.*, 2001; Blundy and Wood 2003, see **Figure 8** for details). The dynamic melting model assumes that the mantle wedge is in U-series equilibrium prior to melting. Model results indicate that dynamic melting can result in 6 to 38% Th-excess depending on the porosity during melt extraction (**Figure 8**). As shown in other studies (Spiegelman and Elliott 1993; Lundstrom *et al.*, 1995; Kelemen *et al.*, 1997), lower porosities produce higher degrees of U-series disequilibria. Porosities of 1-2% produce the amount of Th-excess measured at Klyuchevskoy and Bezymianny (**Figure 8**).

These results must be interpreted cautiously because of critical model assumptions. First, the model assumes that the initial condition before melting is isotopic equilibrium, which is unlikely for the fluid-fluxed mantle wedge beneath the CKD. If fluid has been added to the mantle wedge resulting in U-excess (which we expect given high (^{230}Th)/(^{232}Th) and compositional evidence for fluid transfer), then only very low porosities (<1%) during melting could explain the measured Th-excess. In models of the Aleutian Arc, dynamic melting of a wedge initially in U-excess required porosities of 0.002 (0.2%) or less to produce Th-excess (George *et al.*, 2003). The porosity of the mantle through which melts may be extracted is limited by the bulk viscosity of the melt being transported (Sleep 1988) and typically requires larger porous channels with porosities >1% (Kelemen *et al.*, 1997). Therefore, Th-excesses in the CKD magmas formed by overprinting primary U-excess caused by fluid metasomatism would need to result from near fractional melting in a source region with low porosity (< 1%) prior to melt transfer in channels (Sobolev and Shimizu 1993; Aharonov *et al.*, 1995; Kelemen *et al.*, 1997).

While it is possible to generate Th-excess by dynamic melting under conditions where conduit porosities are larger than source porosities, it is difficult to reconcile why these conditions would be unique to the CKD and would not exist in every arc. Because only ~20% of arc magmas have Th-excess, and because Th-excess is present in CKD magmas but not at Shiveluch, we propose that Th-excess is a local phenomenon and not a source condition that would result from typical mantle melting conditions seen globally.

5.5 Th-excess by Lower Crustal Assimilation

Many recent studies of U-series disequilibria in arc settings have shown that chemical disequilibria between U and Th is affected by crustal processes such as crystallization and assimilation (Volpe and Hammond 1991; Volpe 1992; Bourdon *et al.*, 2000; Reagan *et al.*, 2003; Garrison *et al.*, 2006; Jicha *et al.*, 2007; Walker *et al.*, 2007; Finney *et al.*, 2008; Handley *et al.*, 2008; Jicha *et al.*, 2009; Price *et al.*, 2010; Reubi *et al.*, 2011; Singer *et al.*, 2011). Unradiogenic Pb isotope compositions in the CKD relative to other sections of the Kamchatka Arc, as well as geophysical evidence for magma ponding beneath the CKD, suggest that magmas from Bezymianny and Klyuchevskoy undergo more lower crustal assimilation and fractional crystallization (AFC) relative to magmas in the remainder of the arc (Lees 2007; Kayzar *et al.*, *submitted*). In addition, millennial cycles at Klyuchevskoy in major element, trace element, and O-Sr-Nd-Pb and U-series isotope compositions of erupted magmas imply varying degrees of crustal assimilation (Portnyagin *et al.*, 2011, **Figure 3**). We test whether Th-excess in the CKD may be a product of lower crustal AFC processing of magmas.

In some arcs, the generation of Th-excess via AFC has been proposed to result from crystallization of deep garnet-amphibolite residues crystallize (Garrison *et al.*, 2006; Singer *et al.*, 2011). However, as shown earlier, there is no correlation between Th-excess and garnet in the compositions of CKD magmas, and the crust beneath the CKD is relatively thin (<35km) so garnet would not be a stable phase. Dosseto *et al.*, (2003) rule out the possibility of Th-excess by AFC in Kamchatka because the crust is too thin to have residual garnet. The Austral Volcanic Zone of Chile is similar to the CKD in that it is also relatively thin and erupts magmas with Th-excess at Puyehue-Cordon Caulle (Jicha *et al.*, 2007). At Puyehue-Cordon Caulle, lower crustal melting and AFC in the presence of abundant residual magnetite (7-10 modal percent) is hypothesized to produce the measured 1-6% Th-excess (Jicha *et al.*, 2007). However, magmatic products and xenoliths from the CKD do not show evidence for the presence of large amounts (>10%) of magnetite, which would significantly affect SiO_2 compositions. At Klyuchevskoy, the inverse correlation of Th-excess with Dy/Yb (**Figure 6B**) may result from lower crustal pyroxene fractionation where high-pressure clinopyroxene is capable of preferentially sequestering U relative to Th in its crystal lattice (Wood *et al.*, 1999; Landwehr *et al.*, 2001).

Extensive amphibole fractionation is not inferred beneath the CKD from compositions of erupted magmas (Kersting and Arculus 1994; *Kayzar et al., submitted*). Therefore, we model deep AFC beneath the CKD without garnet or abundant magnetite.

5.5.1 Lower Crustal Bulk AFC Model Parameters

Our objective is to model general geochemical patterns and provide constraints on the range of Th-excess generated using plausible models. The poorly constrained nature of AFC model parameters in the CKD does not justify a more complex formulation than the essential AFC process calculated here using equations of DePaolo (1981). For lower crustal AFC beneath Bezymianny and Klyuchevskoy, we use a fractionating assemblage of 45% clinopyroxene, 17% orthopyroxene, 35% plagioclase, and 3% magnetite as calculated from MELTS (Ghiorso and Sack 1995) simulations of high-magnesium and high-alumina CKD basalts compositions crystallizing at pressures between 5 and 7 kilobars. We consider two initial magmas compositions: 1) a high-alumina basalt composition measured from Klyuchevskoy (Kersting and Arculus 1995; sample K-114) and 2) an average composition calculated from Klyuchevskoy tephras. $(^{238}U)/(^{232}Th)$ activity ratios are calculated based on concentrations of U and Th in these initial magmas. The composition of the assimilant is assumed to be that measured in a lower crustal inclusion erupted at Bezymianny in 2007 (Kayzar *et al.*, *submitted*). The lower crust is also assumed to be in isotopic equilibrium (i.e. $(^{238}U)/(^{230}Th) = 1$). Conservative bulk partition coefficients that minimize U-Th fractionation of $D_U = 0.0076$ and $D_{Th} = 0.0051$ were calculated for the fractionating assemblage above (Landwehr *et al.*, 2001; Blundy and Wood 2003; Jicha *et al.*, 2009). Published partition coefficients for U and Th in these phases vary by orders of magnitude. To encompass this uncertainty, we also model AFC using "liberal" partition coefficients that produce more U-Th fractionation of $D_U = 0.042$ and $D_{Th} = 0.022$. These partition coefficients are based on a 40% plagioclase, 20% clinopyroxene, 40% orthopyroxene assemblage from Handley *et al.*, (2008), which represents another possible lower crustal phase assemblage allowing our models to capture a wide range of lower crustal environments.

5.5.2 Lower Crustal Bulk AFC Model Interpretations

Based on AFC modeling, it is possible for a Th-excess geochemical signal from lower crustal AFC to overprint U-excess in magmas beneath Bezymianny and Klyuchevskoy (**Figure 9A-F)**. The degree to which Th-excess is formed is highly dependent on the partition coefficients used and the extent of initial U-excess, and is less dependent on initial magma composition. Using an initial high-alumina basalt magma with 10% U-excess we find that liberal partition coefficients begin to produce Th-excess after F values decrease to 0.85 (15% AFC) (**Figure 9A,** r = 0.9). If we use conservative partition coefficients, Th-excess is not reached until after F values drop to 0.5 (more than 50% AFC) (**Figure 9B**). Changing the initial magma composition to an average from Klyuchevskoy tephra starts the magma at a lower (^{230}Th)/(^{232}Th) value but does not affect the degree of Th-excess. Again, Th-excess is easily created using liberal partition coefficients (**Figure 9C**), but requires much more crystallization for conservative partitioning (**Figure 9D**).

In order to represent plausible variability in nature, we model AFC using the same high-alumina basalt calculations shown in **Figure 9A-B** but alter the presumed initial U-excess and the concentration of U and Th in the assimilant and initial magmas. We assume a 5% rather than 10% initial U-excess. At Shiveluch volcano in the NCKD, erupted magmas have between 4 and 9% U-excess, so reducing the initial U-excess modeled to 5% allows the model to capture the variability expected from fluid-fluxing along the arc. We adjust the concentration of U and Th in the assimilant and initial magmas by 5% to account for typical error on U and Th concentrations measured by ICP-MS. Adjusting these two parameters makes it much more likely that Th-excess will form as a result of lower crustal AFC. In the case of liberal partitioning, Th-excess is created after ~7% AFC (F = 0.93) and the data at Bezymianny are fit very well by AFC curves with F values of 0.7-0.85 (~15-30% AFC) (**Figure 9E**). Using conservative partitioning also accounts for Th-excess generation. In this case, Th-excess is reached at F = 0.93 (~7% crystallization) as well, and the degree of Th-excess measured in the CKD (between 3 and 10%) is generated after 20-25% crystallization (**Figure 9F**).

The range of Th-excess described above is based on an r-value (mass assimilated/mass crystallized) of 0.9 chosen to describe lower-crustal melting. Based on the higher temperature of

the lower crust at depths near 30km, sensible heat consumption to increase the temperature of the wallrock would be minimal and higher r-values (≤1) are expected (DePaolo 1981). The value for r decreases as AFC moves into the upper crust and cooler wallrock conditions. AFC models for r-values of 0.6 only produce Th-excess in the cases of liberal partitioning or for an initial magma with only 5% U-excess (**Figure 9A, E, F**). This supports the concept that lower crustal assimilation may be driving Th-excess and not shallow magma processes.

5.5.3 Trace Elements During Lower Crustal Bulk AFC

To further test U-series AFC model calculations we also model the behavior of Rb, Sr, and Pb during lower crustal AFC (**Figure 10A-F**). Unlike U-series disequilibria, variation in Rb, Sr, and Pb is more dependent on the concentrations of these elements in the initial magmas. A high-alumina basalt composition has been hypothesized to be the parental magma composition that evolves to form Bezymianny magmas (Ozerov *et al.*, 1997). Primary Klyuchevskoy magmas are more difficult to sample so again we use an average composition from the Klyuchevskoy tephras (representing variation through time). AFC models with high-alumina basalt parent magmas and r = 0.9 fit historical Bezymianny compositions well for Rb, Sr, and Pb compositions (**Figure 10 A, C, E**) with between 5 and 10% fractional crystallization. In order to fit older extrusive dome data, lower r-values are required (**Figure 10A, E**) suggesting that non-historic eruptions of Bezymianny may have undergone more *shallow* AFC (assuming the initial magma has not changed). This is consistent with the more evolved petrologic character of these domes (Kayzar *et al.*, *submitted*).

Using an average Klyuchevskoy tephra composition for an initial magma composition during AFC requires similar r-values between 0.9 and 0.6 and larger degrees of crystallization (25-50%) to fit Bezymianny data (**Figure 10B, D**). Pb data are not reproduced well by the model suggesting that averaging Pb concentrations from Klyuchevskoy tephra to assume an initial magma composition may not be appropriate to model Pb behavior. These trace element models, while dependent on initial magma compositions, do support the U-series observations that lower crustal AFC processing of magmas beneath Bezymianny and Klyuchevskoy can explain the compositions of erupted magmas.

5.5.4 Assimilating Lower Crustal Melt

If the lower crust melts prior to AFC and this melt is assimilated rather than simple bulk assimilation of the crust, then Th-excess may be enhanced or affected due to the incompatibility of U and Th during melting. To model the behavior of U and Th during lower crustal melting, we use simple batch melting of the same assemblage described for AFC models above. We model 10% and 1% batch melts of the lower crust to produce melt compositions assumed to be the assimilant for AFC rather than the whole rock composition of a lower crustal inclusion used above. Even though we are assimilating a melt, we are still modeling AFC r-values of 0.3-0.9 to represent a wide-range of thermal AFC conditions. Using these models, Th-excess also overprints magmas with initial U-excess and is again dependent on partitioning of U and Th (**Figure 11A-D**).

Using a high-alumina basalt magma, Th-excess occurs after 10-25% crystallization with 10% batch melting and after 5-10% crystallization with 1% batch melting (**Figure 11A, B**). The maximum Th-excess produced by the 10% batch melting after 50% crystallization is 15% with liberal partitioning (**Figure 11A**) and 2% with conservative partitioning (**Figure 11B**). Th-excess produced by AFC after 1% batch melting is of the same order of magnitude but has lower (^{230}Th)/(^{232}Th) compositions (**Figure 11A, B**). Adjusting the composition of the initial magma to the Klyuchevskoy tephra composition does not alter the degree of Th-excess generated by AFC (**Figure 11C, D**).

5.5.5 Lower Crustal AFC Summary

To summarize our lower-crustal AFC models, Th-excess beneath the CKD can be produced by AFC in the lower crust (r-values > 0.6) and this process can overprint U-excesses in magmas inherited from fluid transfer from the slab to the mantle wedge. The degree of Th-excess caused by AFC is strongly dependent on the choice of partition coefficients for U and Th. However, even conservative partitioning with minimized U/Th fractionation is capable of producing the Th-excess observed at Bezymianny and Klyuchevskoy (3-10%) with 20-30% fractional crystallization during AFC of a magma with an initial 5% U-excess. These models show that Th-

excess does not require garnet or high percentages of magnetite but rather can be produced with the mineral phases observed in typical lower crustal granulites (plagioclase, clinopyroxene, orthopyroxene). Therefore, crustal processes even in thin arcs < 35km, may alter the signature of primary U-series disequilibria generated in the mantle wedge and significant lower crustal AFC may lead to Th-excess.

5.6 Timing of Crustal Assimilation Beneath the CKD

If Th-excess beneath the CKD is a product of AFC processing, then the extent of lower crustal AFC may vary through time beneath Klyuchevskoy volcano because we observe variation in the magnitude of Th-excess with time (**Figure 3**). Detailed analysis of tephra from Klyuchevskoy shows that magma fractionation and possibly assimilation varied beneath Klyuchevskoy in cycles lasting approximately 3000 years during the Holocene (Portnyagin *et al.*, 2008). Portnyagin *et al.*, (2008) report that the least evolved magmas of Klyuchevskoy erupted approximately 3000 years BP and the most evolved erupted approximately 4000 years BP. Comparing this pattern to the U-series disequilibria measured in the same tephra, we find that Th-excess increased in magnitude at Klyuchevskoy between 4000 years BP and 3000 years BP. The coincidence in timing of these two observations may indicate that when less evolved magmas erupt at Klyuchevskoy they migrate relatively quickly through the crust and do not stall in the lower crust where AFC processes produce Th-excess. However, slightly more evolved melts (from 4076 years BP to 3591 years BP) erupt with the highest Th-excess suggesting they may have passed through a period of magma ponding in the lower crust. If these assumptions are correct, they predict that changes in the magnitude of AFC, and thus the generation of Th-excess can occur in an arc setting over timescales of thousands of years. We do not observe large variations in Th-excess at Bezymianny, which is expected based on observations at Klyuchevskoy because we are only sampling ~ 50 years of eruptive activity and consequently a very restricted range of compositions.

5.7 The Global Geography of Th-Excess

Based on data from the CKD and global data we hypothesize that Th-excess in arcs is a local geochemical phenomenon that results from assimilation and fractional crystallization of the lower crust in the presence of high-pressure clinopyroxene with or without garnet. Trace element chemistry of erupted magmas can determine whether or not garnet is involved in creating chemical disequilibria. We show here that garnet fractionation is not required beneath the CKD and by analogy also not in the lower crust of other arcs with relatively thin crust. AFC processes at the base of arc crust, under conditions of a plausible mineralogy and crystallization history, may imprint a Th-excess that can erase an original U-excess inherited from a fluid-fluxed mantle source.

If AFC is a cause of Th-excess, we would expect to find Th-excess beneath volcanic centers where either: 1) the lower crust is relatively fertile (and residues contain clinopyroxene and/or garnet) or 2) the lower crust is relatively hot. This is the case for many regions where Th-excess has been reported. In Kamchatka, high heat flow near the CKD is a consequence of a tear in the corner of the Pacific Plate between the Aleutians and Kamchatka (Davaille and Lees 2004). In the Cascade Arc, Th-excess is observed at Mt. Shasta, Mt. Lassen, Mt. St. Helens and Crater Lake and Medicine Lake volcanic centers (Reagan *et al.*, 2003; Berlo *et al.*, 2004; Jicha *et al.*, 2009), which are near the southern end of the arc where slow velocity zones in the lower crust have been interpreted to reflect near to super solidus conditions (Gao *et al.*, 2011). The structure of the Austral Volcanic Zone in Chile is not well known but is interpreted to be hot due to the subduction of a young plate (18-20 Ma) and a lack of seismicity (Forsyth 1975; Sigmarsson *et al.*, 1998). Petrologic and geochemical studies of the Andean Southern Volcanic Zone and Austral Volcanic Zone do not report hot lower crustal temperatures but do imply that AFC processing is significant in these thin crustal regions (Stern and Kilian 1996; Stern 2004; Dungan and Davidson 2004; Reubi *et al.*, 2011). Abnormally high crustal temperatures also accompany Th-excess in central Guatemala (Walker *et al.*, 2007 and references therein). Therefore, the association of Th-excess with regions of hot lower crust supports our hypothesis that Th-excess may result from lower crustal AFC in the presence of residual clinopyroxene and or/garnet.

Finally, in arc settings, Th-excess is generally observed in magmas erupted near continental margins/plate boundaries rather than in the centers of volcanic arcs (Newman *et al.*, 1984; George *et al.*, 2003; Davidson *et al.*, 2005; Garrison *et al.*, 2006; Walker *et al.*, 2007). Therefore, the dynamics of subduction zones near plate boundaries may also lead to enhanced interaction between rising magmas and the lower crustal.

CONCLUSIONS

The Central Kamchatka Depression (CKD) of the Kamchatka Volcanic Arc is a high magma-flux region at the northern corner of Pacific Plate subduction where magmas erupt with Th-excess disequilibria ($(^{238}U)/(^{230}Th) < 1$). Investigation of data from the CKD as well as published global Th-excess data suggest that Th-excess generation is a local phenomenon that can be created by multiple mechanisms and does not require garnet fractionation. Beneath the thin (< 35km), hot, Kamchatka arc, Th-excess may be formed by clinopyroxene fractionation during lower crustal assimilation and fractional crystallization. Lower crustal models of AFC show that moderate U-excess between 5 and 10% may be modified and subsequently overprinted by AFC resulting in Th-excess. Global data reveal that Th-excess appears commonly near the edge of plate margins. Therefore, the dynamics of heat flow in these regions may result in greater degrees of lower crustal AFC. U-series isotope studies can provide a sensitive geochemical tracer of lower crustal processes in thin, young arc crust that might otherwise be difficult to detect.

The magnitude of Th-excess depends highly upon the partitioning behavior of U and Th, which is uncertain and varies by orders of magnitude. Partitioning uncertainty demands more research to resolve an issue brought to light by Albarede and Bottinga (1972) who noted that, "inspection of the literature on partition coefficients for trace element partitioning between crystals and silicate liquids, reveals considerable disagreement among the results of various investigators". As a community, we will not be able to quantitatively describe crustal magmatic processes without a better understanding of the behavior of elements in crystals and liquids.

FIGURES

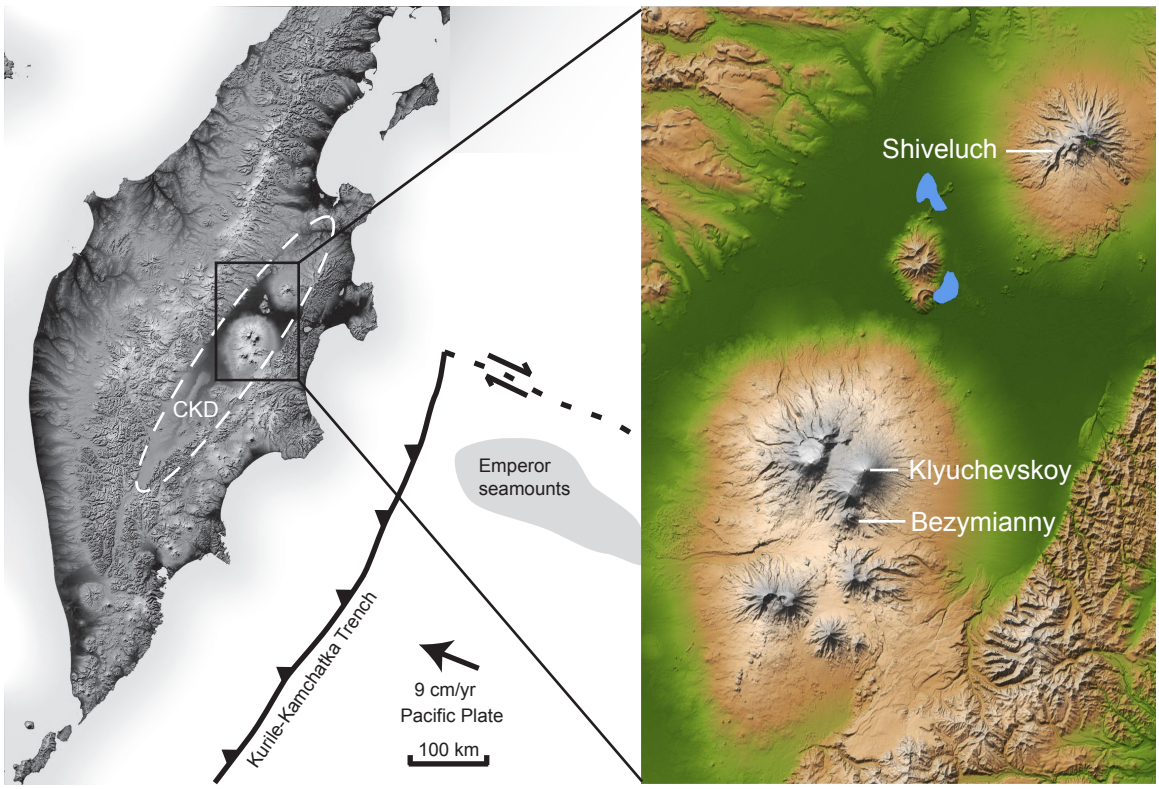

Figure 1. Map of the Kamchatka Peninsula and the Central Kamchatka Depression (CKD). Left: The Kamchatka peninsula with the CKD outlined in white dashed line. The Pacific Plate corner lies just northeast of the main volcanic cluster (Klyuchevskoy Group) of the CKD and is shown with the Kurile-Kamchatka trench on the southern plate edge and the Bering Fracture Zone on the north-eastern plate edge (dashed line with transform motion) (Image modified from NASA Earth Observatory). Right inset: Klyuchevskoy Group of volcanoes with Klyuchevskoy and Bezymianny volcano marked. To the north, separated from the Klyuchevskoy Group is Shiveluch volcano (Northern Central Kamchatka Depression, NCKD).

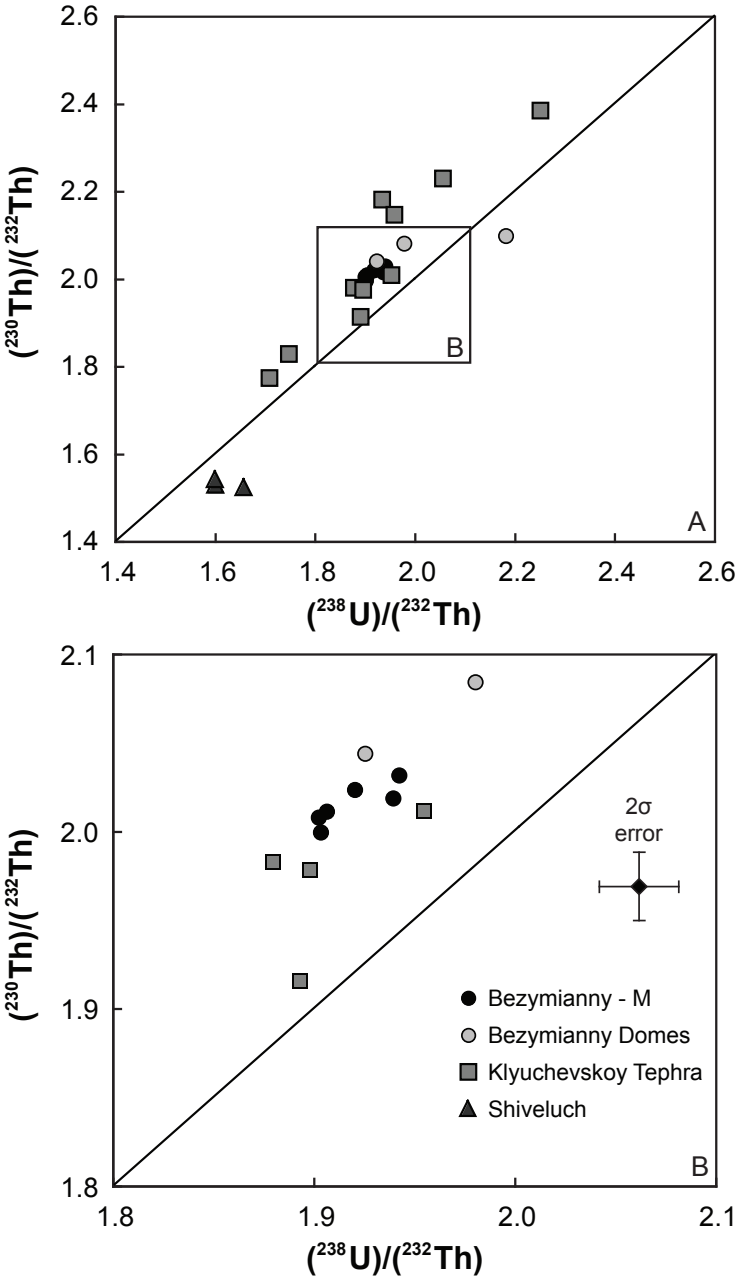

Figure 2. U-Th Equiline Diagram with Kamchatka U-series Isotope Compositions. A. Samples from Bezymianny (circles: black = modern eruptions and grey = extrusive domes) and Klyuchevskoy (squares) volcanoes plot mainly to the left of the U-Th equiline in the field of Th-excess. In general, the CKD samples have between 1 and 11% Th-excess. One sample from Lohkmaty dome at Bezymianny falls to the right of the equiline with U-excess. Shiveluch samples have between 4 and 9% U-excess (triangles). Errors are smaller than symbols. B. Inset from **A** showing compositions of Bezymianny modern eruptive products. Reference 2σ error bar size for data points is shown.

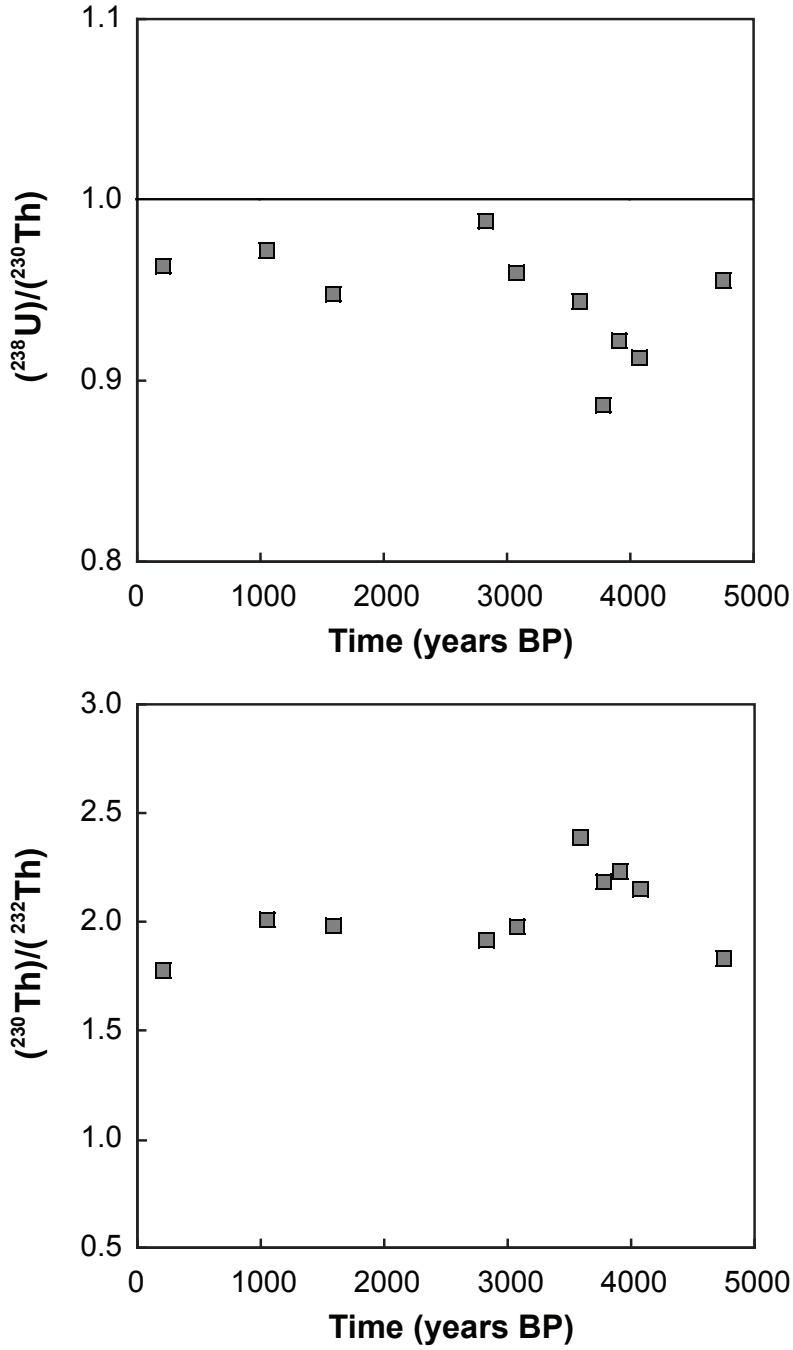

Figure 3. Klyuchevskoy Tephra U-series Compositional Variation. Top: (^{238}U)/(^{230}Th) variation with time measured in Klyuchevskoy tephra units. The largest Th-excess (^{238}U)/(^{230}Th) < 1 occurs between 3000 and 4000 years BP (before present). Bottom: (^{230}Th)/(^{232}Th) compositional variation with time. (^{230}Th)/(^{232}Th) is high in Klyuchevskoy tephras ($\geq$2.0 for most samples). Tephra layers have been age-dated by the KALMAR project using the help of ^{14}C dated regional marker tephras (Braitseva *et al.* 1997; Portnyagin and Ponomareva 2012).

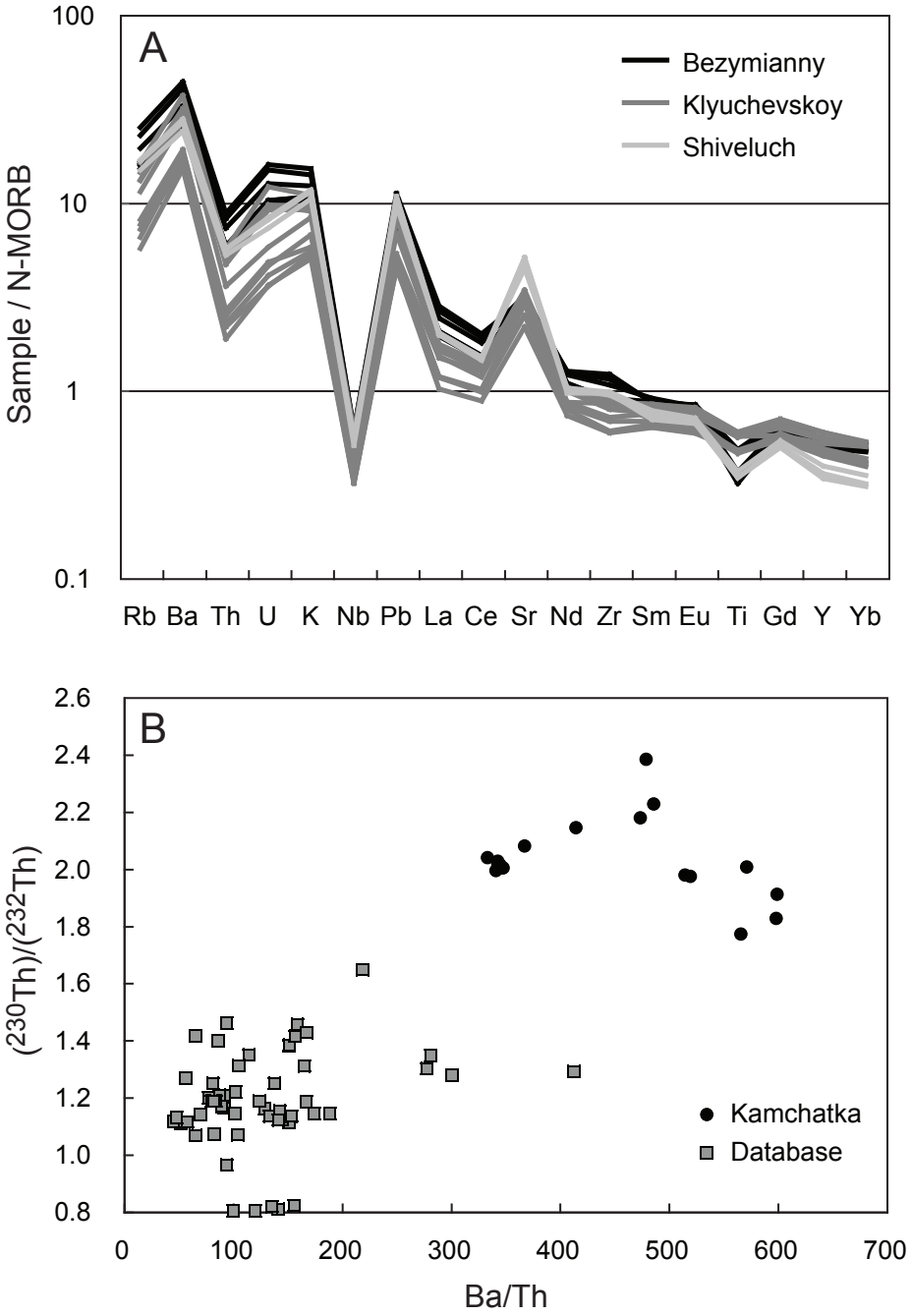

Figure 4. Compositional Evidence for Fluid Transfer Beneath the CKD. **A.** Spider diagram of Bezymianny, Klyuchevskoy and Shiveluch sample compositions normalized to N-MORB (Hofmann 1988). Enrichments in LILE, LREE and fluid mobile elements (U) are characteristic of fluid transfer from the slab to the mantle wedge during subduction. **B.** (^{230}Th)/(^{232}Th) composition of Kamchatka relative to the Th-excess database (**Appendix A**). Samples from Kamchatka (Klyuchevskoy and Bezymianny; black circles) have higher (^{230}Th)/(^{232}Th) than other arcs with Th-excess. (^{230}Th)/(^{232}Th) compositions positively correlate with Ba/Th.

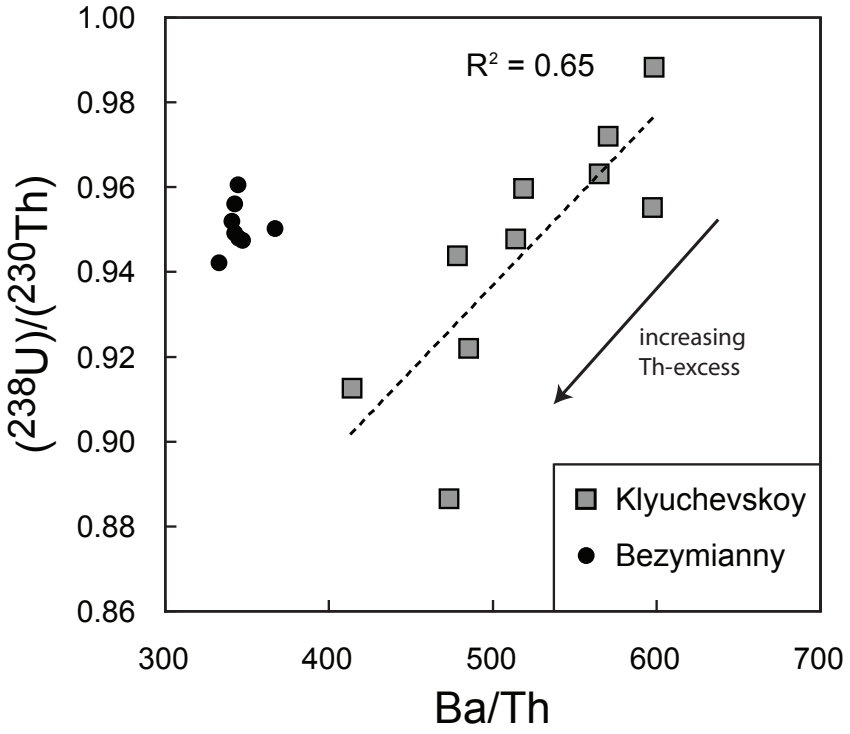

Figure 5. (^{238}U)/(^{230}Th) versus Ba/Th for Bezymianny and Klyuchevskoy Eruptive Products. Th-excess negatively correlates with Ba/Th in Klyuchevskoy tephras (squares). Ba/Th generally increases with fluid transfer from the slab (Ba is more fluid mobile); therefore, Th-excess is not linked to fluid transfer in the mantle wedge beneath Klyuchevskoy. There is no correlation observed between (^{238}U)/(^{230}Th) and Ba/Th at Bezymianny (black circles).

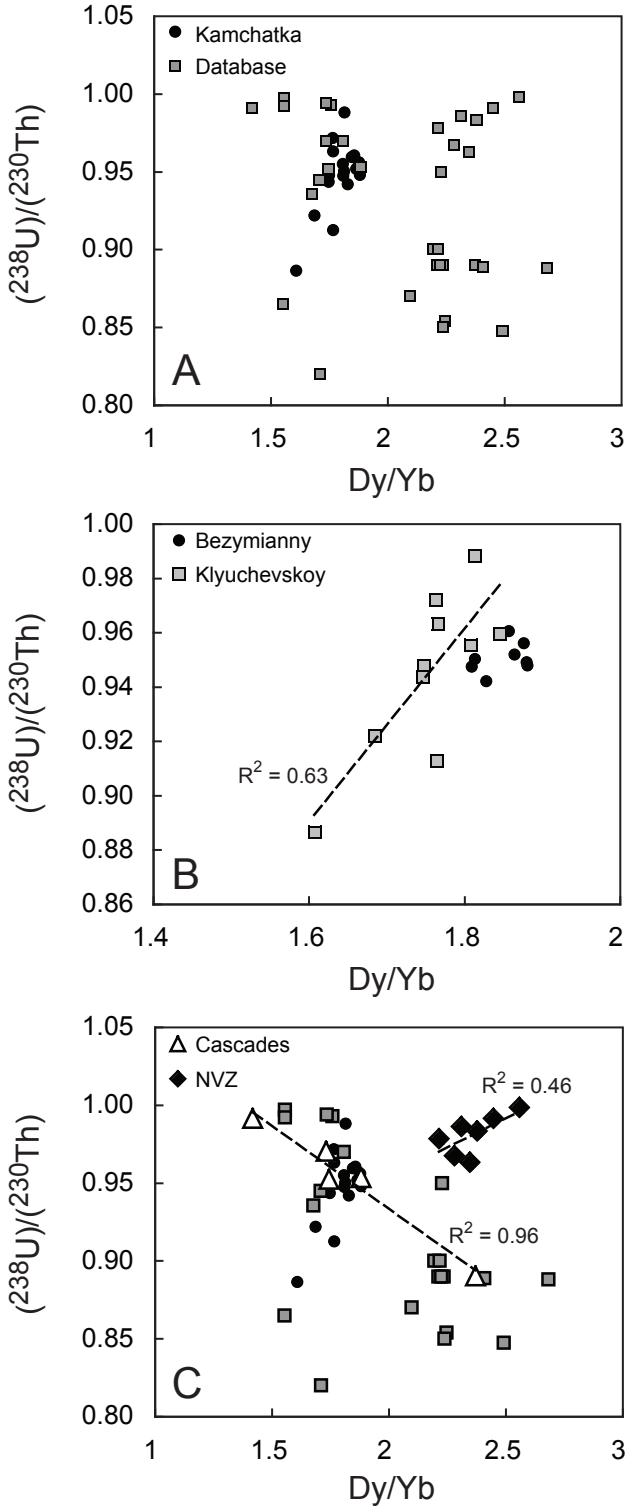

Figure 6. (^{238}U)/(^{230}Th) versus Dy/Yb (garnet indicator). Dy/Yb ratios increase in melts during fractional crystallization of garnet, or when garnet is left as a residual phase during partial melting. **A.** All data from the Th-excess database (**Appendix A**) and Kamchatka (this study). There is no *global* correlation between Th-excess, (^{238}U)/(^{230}Th) < 1, and Dy/Yb. **B.** Kamchatka U-series compositions versus Dy/Yb. Bezymianny samples show no correlation between Th-excess and Dy/Yb. Klyuchevskoy tephra units show a negative correlation between Th-excess and Dy/Yb (dashed line; R^2 = 0.63). If garnet caused Th-excess, there should be a positive correlation between Th-excess and Dy/Yb since Dy/Yb increases with garnet involvement. **C.** All data with samples from the Cascades (Reagan *et al.* 2003) and the Northern Volcanic Zone (NVZ) of the Andes (Garrison *et al.* 2006) highlighted: Cascades = white triangles, NVZ = black diamonds. Samples from the Cascades show the relationship expected if garnet generates Th-excess (positive correlation between Th-excess and Dy/Yb: R^2 = 0.96). Samples from the NVZ, however, record the opposite behavior (negative correlation between Th-excess and Dy/Yb: R^2 = 0.46). NVZ behavior is similar to that observed at Klyuchevskoy (B).

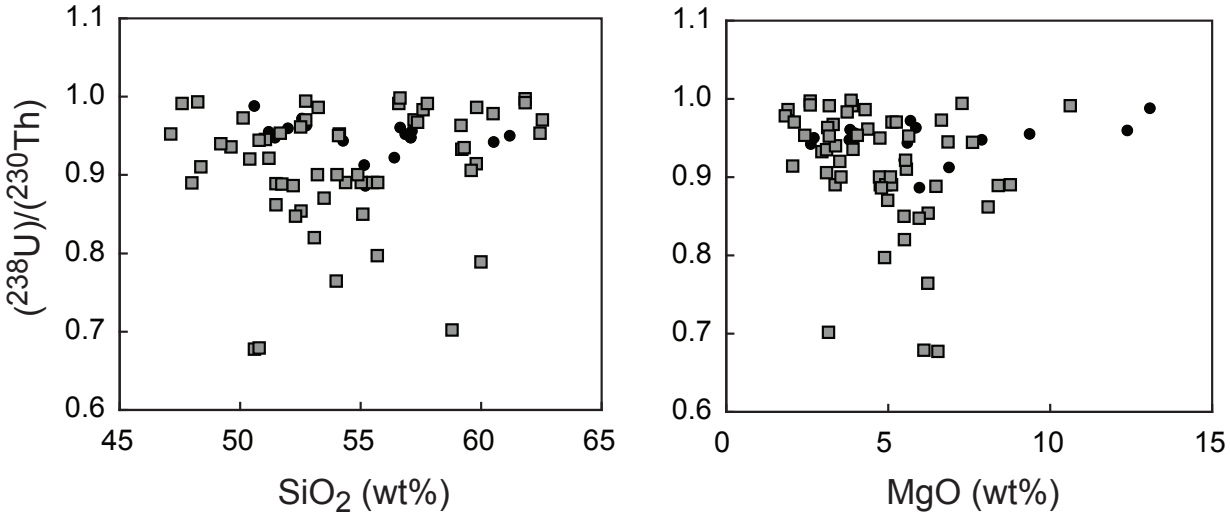

Figure 7. (^{238}U)/(^{230}Th) versus MgO and SiO_2 Compositions. There is no observed correlation between the amount of Th-excess and MgO or SiO_2 abundances in Kamchatka samples (black circles) or in the global Th-excess database (grey squares) (**Appendix A**).

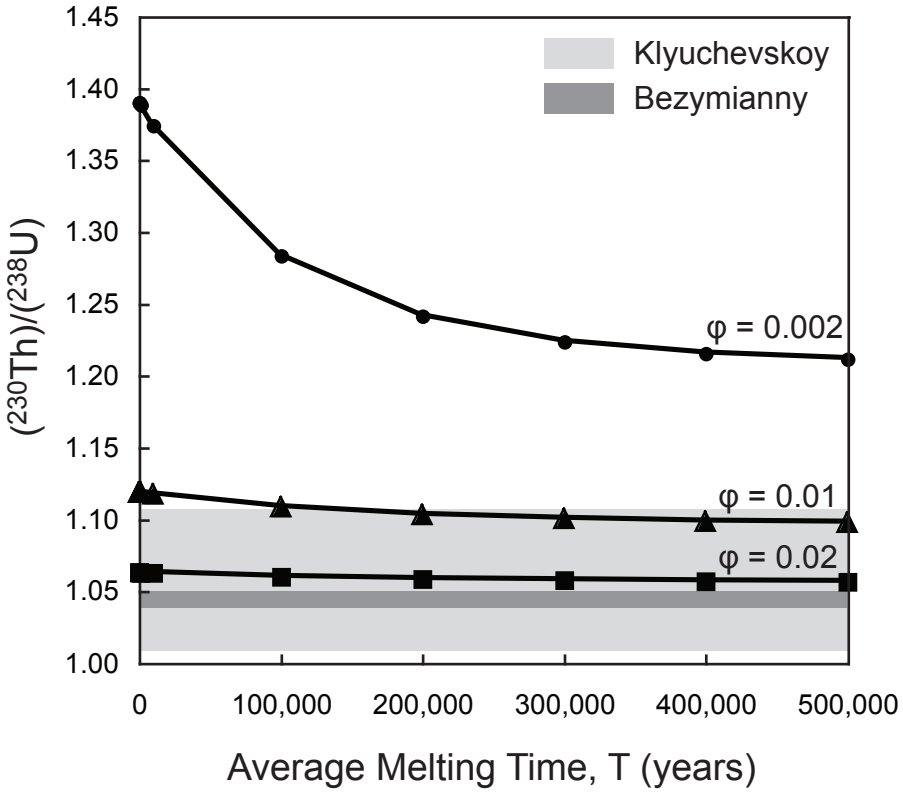

Figure 8. Dynamic Melting Model for the Generation of Th-excess. Dynamic melting was calculated using equations in Zou and Zindler (2000). Assumes mantle modal mineralogy of 66.7% olivine, 22.2% orthopyroxene, and 11.1% clinopyroxene and bulk $D_U = 0.0025$ and $D_{Th} = 0.0013$ (Johnson *et al.* 1998 – mantle modal mineralogy, Landwehr *et al.* 2001 – clinopyroxene; $D_U = 0.0017$, $D_{Th} = 0.0078$, Blundy and Wood 2003 – orthopyroxene; $D_U = 0.0052$, $D_{Th} = 0.002$, olivine; $D_U = 6 \times 10^{-5}$, $D_{Th} = 9.52 \times 10^{-6}$). Melting rate = 0.001 kg/m^3 and porosity is shown by black curves (0.2% - circles, 1% - triangles, and 2% - squares). Degree of Th-excess measured at Klyuchevskoy is shown with a light-grey shaded region, and at Bezymianny with a dark-grey shaded region. Model assumes that initial condition is U-Th equilibrium. Th-excess at Klyuchevskoy and Bezymianny is produced easily with low porosities (<1%). Dynamic melting of a wedge initially in equilibrium is capable of producing between 6% and 38% Th-excess.

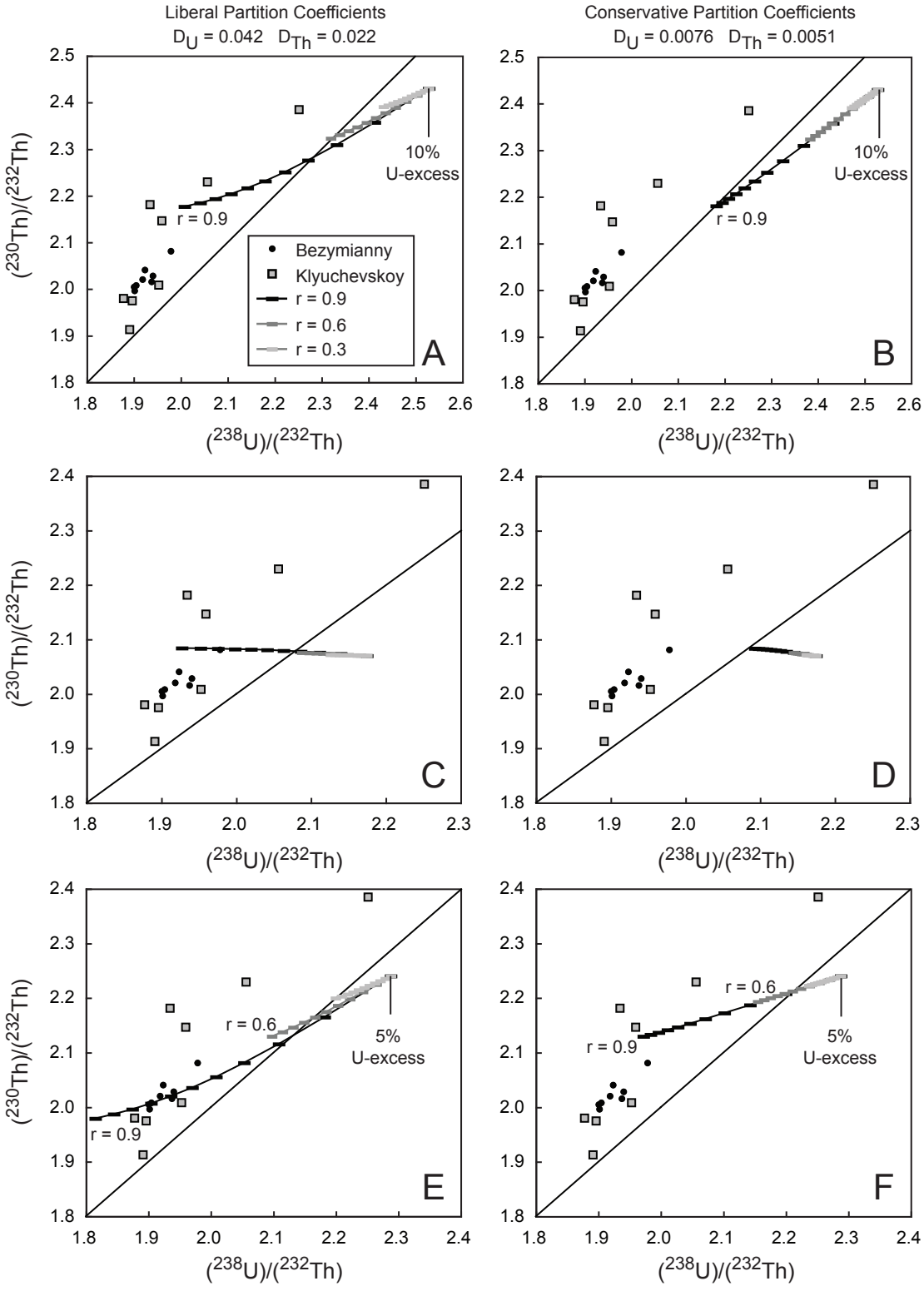

Figure 9. Assimilation and Fractional Crystallization (AFC) Models for the Generation of Th-excess in Kamchatka. (full caption on next page)

Figure 9. Assimilation and Fractional Crystallization (AFC) Models for the Generation of Th-excess in Kamchatka. Calculated U-Th isotope compositions during AFC are shown in panels A-F for varying AFC conditions using equations from DePaolo (1981). Left panels A, C, E assume "liberal" or partition coefficients that strongly fractionate U and Th ($D_U = 0.042$, $D_{Th} = 0.022$) for a fractionating lower crustal assemblage of 40% plagioclase, 20% clinopyroxene, and 40% orthopyroxene taken from Handley *et al.* (2008). Right panels B, D, E assume conservative partition coefficients which minimize U-Th fractionation ($D_U = 0.0076$, $D_{Th} = 0.0051$) calculated based on a fractionating assemblage derived through MELTS (Ghiorso and Sack 1995) runs crystallizing Klyuchevskoy-like basalt between 5 and 7 kbar: 45% clinopyroxene, 17% orthopyroxene, 35% plagioclase, and 3% magnetite. Initial magma compositions are a high-alumina basalt of Klyuchevskoy (panels A, B, E, and F; Kersting and Arculus (1995): sample K-114), and an average composition from Klyuchevskoy tephras (panels C and D). Bulk assimilation is assumed of a lower crust in equilibrium with a composition taken from a lower crustal inclusion in Bezymianny erupted products from 2007 (Kayzar *et al. submitted*, U = 0.2 ppm, Th=0.29 ppm). AFC curves are shown for varying r-values: r = 0.9 (black), r = 0.6 (dark grey), r = 0.3 (light grey). Conditions for the lower crust are expected to be represented by high r-values ~ 0.9 (DePaolo 1981). Ticks on AFC curves represent 5% fractional crystallization and assimilation (5% variations in "F", fraction of remaining liquid). Panels A and B show the U-Th isotopic behavior assuming that the initial magma had 10% U-excess and was a high-alumina basalt. Panels C and D show the same model only assuming that the initial magma has the Klyuchevskoy tephra average composition. Variations in the degree of Th-excess generated are not dependent on initial magma composition, however, the $(^{230}Th)/(^{232}Th)$ composition changes accordingly. In panels E and F, the initial U-excess is reduced to 5% and the starting compositions of the magma and assimilant is adjusted by 5% to represent variation due to ICP-MS measurement error (see text for discussion). It is possible to generate Th-excess by AFC processes under lower-crustal conditions (high r-values) without any crystallization of garnet or magnetite.

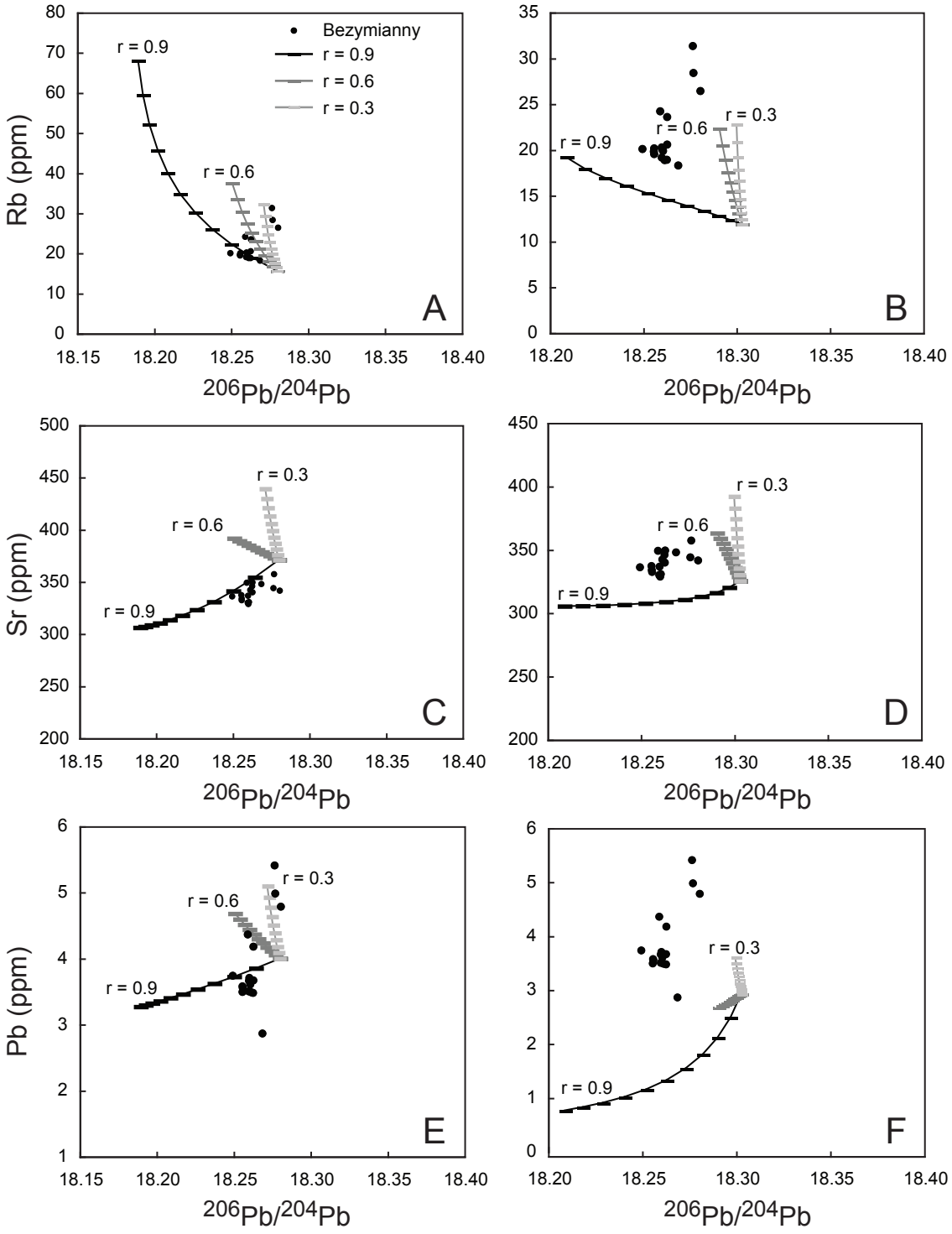

Figure 10. AFC models to Reproduce Bezymianny Trace Element and Pb-Isotope Compositions. (full caption on next page)

Figure 10. AFC models to Reproduce Bezymianny Trace Element and Pb-Isotope Compositions. AFC paths calculated using the equations of DePaolo (1981) for the evolution of Rb, Sr, and Pb in the melt are shown for r-values of 0.9 (black curve), 0.6 (dark grey curve), and 0.3 (light grey curve). **A, C, and E** show the behavior in the melt for an initial magma compositions of a high-alumina basalt (Kersting and Arculus (1995): K-114, Rb = 15.6 ppm, Sr = 371 ppm, Pb = 4 ppm, $^{206}Pb/^{204}Pb$ = 18.280). **B, D, and E** assume an initial magma that is an average of the Klyuchevskoy tephra data (Rb = 11.8 ppm, Sr = 325.3 ppm , Pb = 2.9 ppm, $^{206}Pb/^{204}Pb$ = 18.303). The composition of the assimilant is taken from a lower crustal inclusion from the 2007 eruption of Bezymianny (Rb = 5.85, Sr = 194.74, Pb = 1.49, $^{206}Pb/^{204}Pb$ = 18.183, data from Kayzar *et al. submitted*). The fractionating phase assemblage is the same as that described in **Figure 9** calculated from MELTS (Ghiorso and Sack 1995). Partition coefficients are from the basalt-basaltic andesite compilation of Rollinson *et al.* (1993) for Sr, and Rb, and are from Hauri *et al.* (1994) for Pb in clinopyroxene, Dunn and Sen (1994) for Pb in orthopyroxene and plagioclase, and from Ewart and Griffin (1994) for Pb in magnetite. Tick marks on curves represent 5% intervals of AFC (5% changes in F from 1 to 0.5). Most of the data for Bezymianny eruptive products is best modeled with a high alumina starting magma and lower crustal AFC (r = 0.9) (**A, C and E**). The more evolved domes require lower r-value to fit the data (r between 0.6 and 0.3) (**A and E**) consistent with their evolution in the shallow crust (see text for discussion). Lower crustal AFC also reproduces the Bezymianny compositions using an average Klyuchevskoy tephra composition (**B, D, and E**); however, r-values range between 0.9 and 0.6 and the extent of AFC required to fit the data is much higher (lower F values).

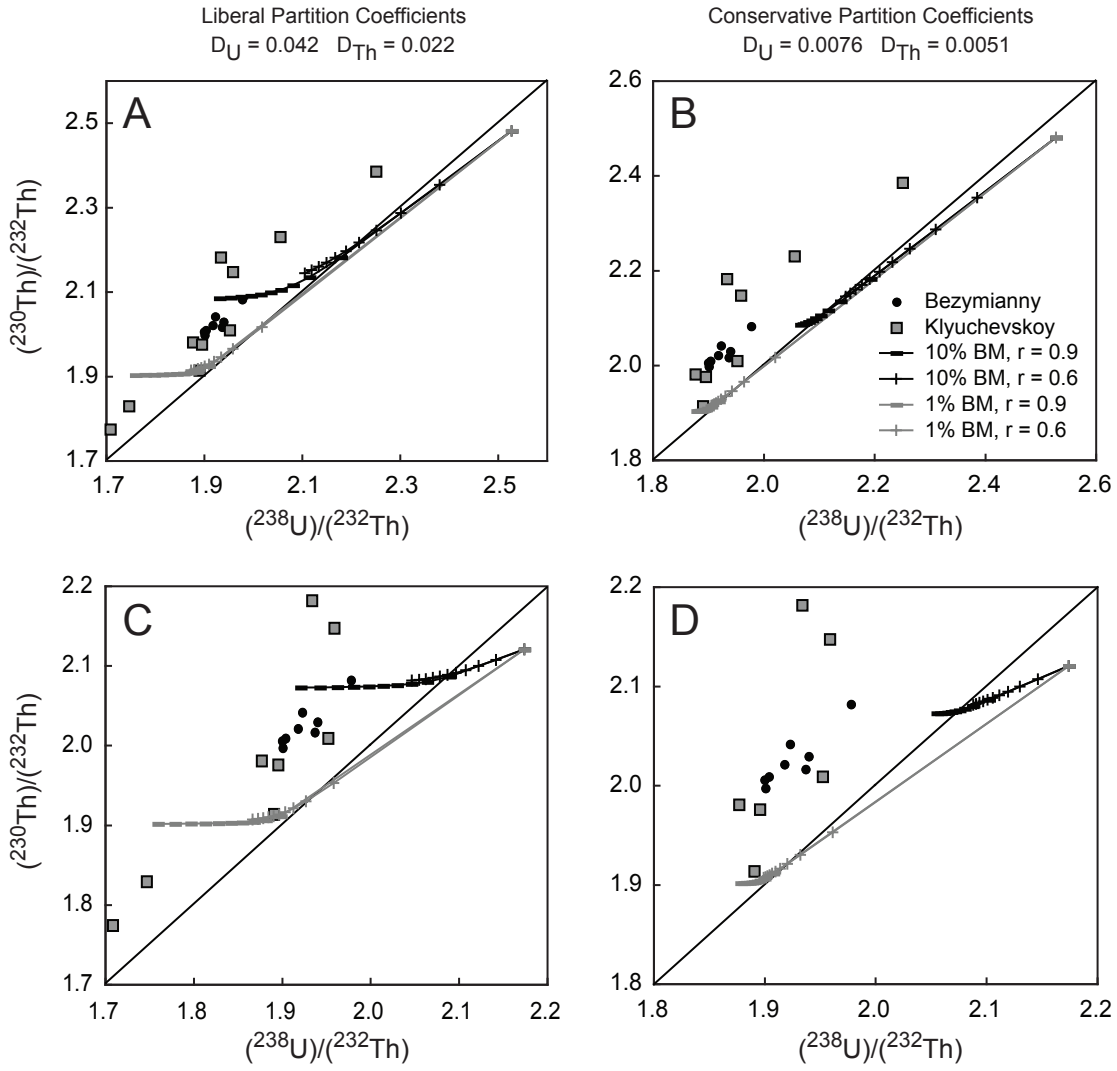

Figure 11. AFC Models of Assimilated Melts to Generate Th-excess in Kamchatka. AFC model parameters and compositions are the same as those described in **Figure 9** with the exception of the composition of the assimilant. The assimilant is assumed to be either a 1% batch melt of the lower crust (grey curves), or a 10% batch melt of the lower crust (black curves). A 5% U-excess is assumed for the initial magmas. **A and B** show the degree of Th-excess generated from an initial high-alumina basalt magma composition. **C and D** show the degree of Th-excess generated from an initial average Klyuchevskoy basalt magma composition. Th-excess is generated most easily with liberal partition coefficients and is reached faster during AFC (higher F-values) in the 1% batch melting case than in the 10% batch melting case. The degree of AFC required to fit the Bezymianny and Klyuchevskoy data for each model is discussed in detail in the text.

TABLES

Table 1. Sample Descriptions, Ages, and Locations

Volcanic Center	Sample Name	Eruption Age[a]	Location GPS(if available)		Description
Shiveluch	SHIV 1993	1993	NA		Dense volcanic material from the 1993 dome
	SHIV 2001PF	2001	NA		Vesicular juvenile material from the 2001 pyroclastic flow
	SHIV 2007	2007	56.5954	161.3233	Vesicular juvenile material from the 2007 pyroclastic flow
Bezymianny	06BZT02a	2006 (May)	55.9502	160.6253	outer rim of juvenile breadcrust bomb, in May 2006 pyroclastic flow
	06BZT02b	2006 (May)	55.9502	160.6253	inner portion of juvenile breadcrust bomb, in May 2006 pyroclastic flow
	06IPE17	2006 (May)	NA		juvenile bomb from May 2006 eruption, large sample from crater
	01BZTK07	2007 (May)	55.9459	160.6290	juvenile breadcrust bomb, in May 2007 pyroclastic flow
	02BZT08	2007 (October)	55.9442	160.6271	juvenile breadcrust bomb, in October 2007 pyroclastic flow
	04BZT08	2007 (October)	55.9426	160.6253	juvenile breadcrust bomb, in October 2007 pyroclastic flow
	06BZT08	Lokmaty (3000-5000 ya)	55.9557	160.5854	Lohkmaty dome, crystalline hornblende-pyroxene andesite
	06BZT04	"youngest" dome (<3000 ya)	NA		crystalline "youngest" dome, highest on Bezymianny edifice
	06BZT05	1956	55.9184	160.6941	crystalline 1956 cryptodome with cooling jointing
Klyuchevskoy[a]	K7-T1-4	212[b]	56.1464	160.8241	Klyuchevskoy tephra in 12m thick tephra section
	K7-T1-14	1054	56.1464	160.8241	Klyuchevskoy tephra in 12m thick tephra section
	K7-T1-31	1590	56.1464	160.8241	Klyuchevskoy tephra in 12m thick tephra section
	K7-T1-51	2823	56.1464	160.8241	Klyuchevskoy tephra in 12m thick tephra section
	K7-T1-70-2	3076	56.1464	160.8241	Klyuchevskoy tephra in 12m thick tephra section
	K7-T1-83	3591	56.1464	160.8241	Klyuchevskoy tephra in 12m thick tephra section
	K7-T1-85-4	3783	56.1464	160.8241	Klyuchevskoy tephra in 12m thick tephra section
	K7-T1-85-1	3911	56.1464	160.8241	Klyuchevskoy tephra in 12m thick tephra section
	K7-T1-88-7	4076	56.1464	160.8241	Klyuchevskoy tephra in 12m thick tephra section
	K7-T1-92-2	4753	56.1464	160.8241	Klyuchevskoy tephra in 12m thick tephra section

[a] Klyuchevskoy tephra layers were dated based on marker tephra layers age dated by C^{14} by Braitseva et al. 1997. Tephra section is described in Portnyagin and Ponomareva 2012.

Table 2. Uranium-Series Concentrations and Isotopic Compositions of Kamchatka Erupted Products

Volcanic Center	Sample Name	Eruption Age[a]	U (ppm)	Th (ppm)	$(^{238}U)/(^{232}Th)$	$(^{230}Th)/(^{232}Th)$	$(^{238}U)/(^{230}Th)$
Shiveluch	SHIV 1993	1993	0.493	0.902	1.658	1.523	1.089
	SHIV 2001PF	2001	0.532	1.008	1.601	1.529	1.047
	SHIV 2007	2007	0.565	1.072	1.600	1.542	1.038
Bezymianny	06BZT02b	2006	0.629	0.986	1.937	2.016	0.961
	06IPE17	2006	0.670	1.061	1.918	2.021	0.949
	02BZT08	2007	0.683	1.068	1.940	2.029	0.956
	06BZT02a	2006	0.654	1.043	1.901	1.997	0.952
	04BZT08	2007	0.674	1.076	1.900	2.005	0.948
	01BZTK07	2007	0.676	1.077	1.904	2.009	0.948
	06BZT08	Lokmaty	1.059	1.472	2.182	2.099	1.040
	06BZT04	"youngest" dome	0.776	1.190	1.978	2.082	0.950
	06BZT05	1956	0.828	1.307	1.923	2.041	0.942
Klyuchevskoy	K7-T1-4	212[b]	0.397	0.705	1.709	1.774	0.963
	K7-T1-14	1054	0.323	0.502	1.952	2.009	0.972
	K7-T1-31	1590	0.279	0.451	1.877	1.981	0.948
	K7-T1-51	2823	0.248	0.398	1.891	1.913	0.988
	K7-T1-70-2	3076	0.333	0.533	1.896	1.976	0.960
	K7-T1-83	3591	0.842	1.135	2.251	2.385	0.944
	K7-T1-85-4	3783	0.680	1.067	1.934	2.182	0.886
	K7-T1-85-1	3911	0.622	0.918	2.056	2.230	0.922
	K7-T1-88-7	4076	0.670	1.038	1.959	2.147	0.913
	K7-T1-92-2	4753	0.250	0.435	1.747	1.829	0.955

[a] Eruption ages for Bezymianny and Shiveluch represent the year of eruption, extrusive domes at Bezymianny have not been formally dated but are older than 1956 and likely Pleistocene in age (Almeev et al. ?).

[b] Klyuchevskoy eruption ages are given here in years before present (BP), measured by KALMAR at IFM-GEOMAR.

[c] Accuracy of measurements is <0.5% for Th and U concentrations, and <1% for $(^{230}Th)/(^{232}Th)$. $(^{234}U)/(^{238}U)$ measured in samples (not shown) is within error of equilibrium (1.000+/-0.004).

APPENDIX A

Appendix A is an electronic database.

APPENDIX B

Appendix B. U-series Analytical Standards

Thorium solution standards, IRMM-035, IRMM-036, and WUN-1, are analyzed repeatedly during sample analysis at the University of Washington. The data for standard analyses are shown here as long-term University of Washington (UW) trends analyzed over the same time period as the data presented in this manuscript. Standard measurements are compared to the accepted inter-laboratory values of Sims *et al.*, (2008) (**Figure B.1**).

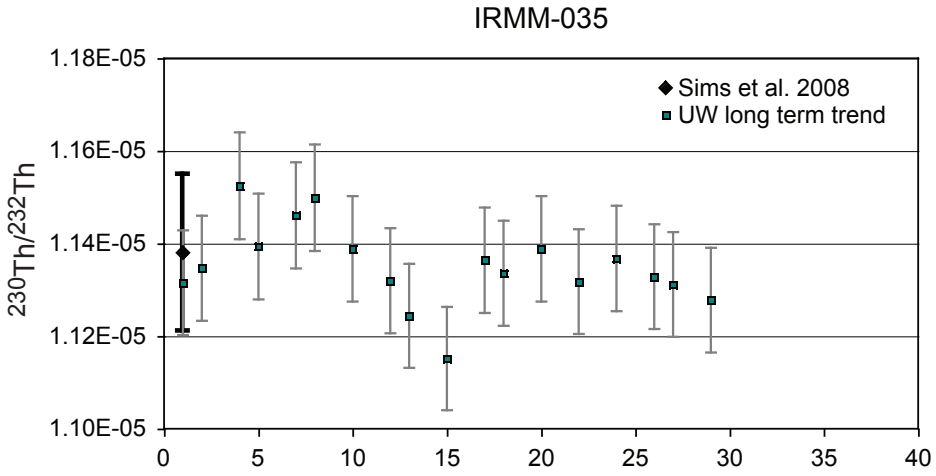
IRMM-035
Sims et al. 2008
UW long term trend
$^{230}Th/^{232}Th$
1.18E-05
1.16E-05
1.14E-05
1.12E-05
1.10E-05
0
5
10
15
20
25
30
35
40

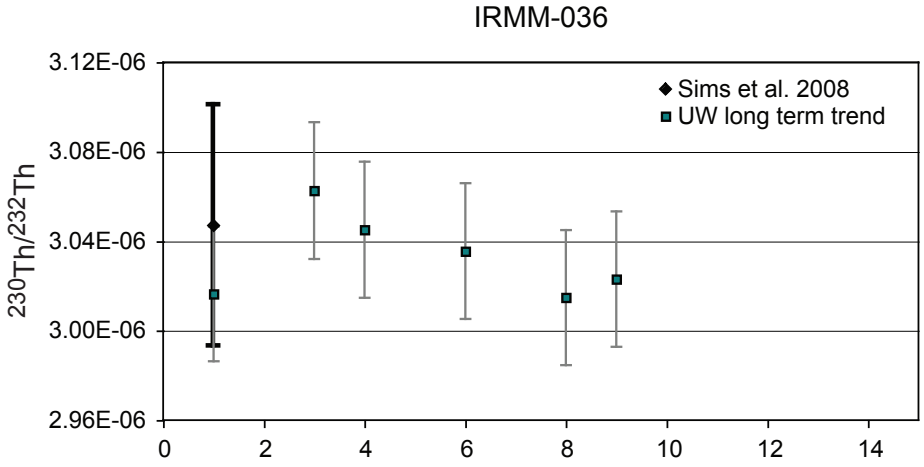
IRMM-036
Sims et al. 2008
UW long term trend
$^{230}Th/^{232}Th$
3.12E-06
3.08E-06
3.04E-06
3.00E-06
2.96E-06
0
2
4
6
8
10
12
14

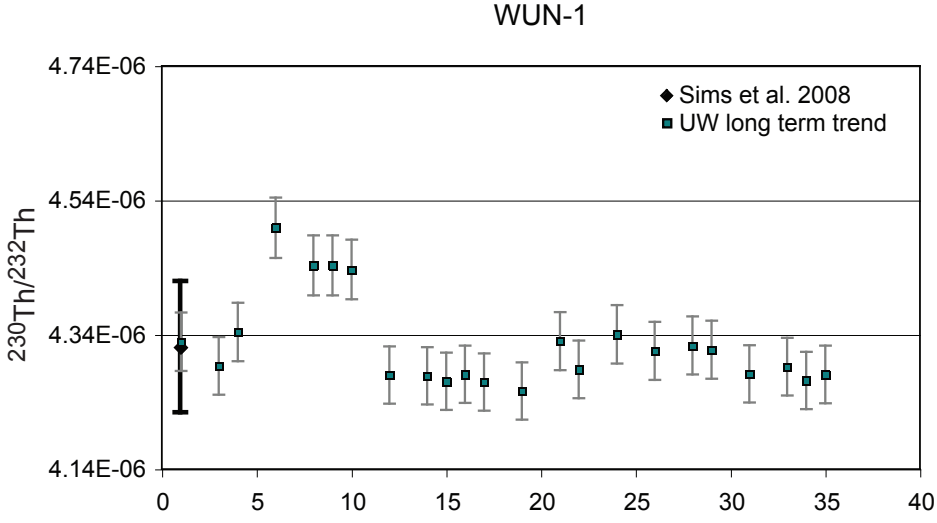
WUN-1
Sims et al. 2008
UW long term trend
$^{230}Th/^{232}Th$
4.74E-06
4.54E-06
4.34E-06
4.14E-06
0
5
10
15
20
25
30
35
40

APPENDIX C

Appendix C. Ambiguity in Existing U-series Measurements from the Central Kamchatka Depression.

Published U-series measurements from the Central Kamchatka Depression (CKD) are contradictory (**Figure C1**). Dosseto *et al.* (2003) report samples with both Th-excesses and U-excesses and interpret their results as mixing between melts caused by metasomatism of the mantle wedge (high-Mg basalts with U-excess) and melts of the subducting oceanic slab (high-Al andesites with Th-excess). Turner *et al.* (2007), however, report no Th-excess in CKD magmas and only observe U-excess caused by fluid-fluxed mantle melting. These data suggest that the subduction zone beneath Kamchatka must simultaneously erupt melts generated by two very different processes.

However, sample locations and ages may not be correctly reported for the samples analyzed in these two studies. Turner *et al.* (2007) cite an eruption of Bezymianny in the year 1950 (sample B000) during which Bezymianny was dormant. Further, there are no flank eruptions of Klyuchevskoy in 1900 and 1910 as reported in Table 1 (samples K0012 and K0032). The only documented eruptions of high-Mg basalts from Klyuchevskoy in the 20th century are the 1932 Tuila vent, and the 1983 Bilyukai vent. Sample compositions also disagree with measured compositions on the same samples by Maxim Portnyagin (pers. comm.). Characteristic compositional features of these two historic high-Mg basalt eruptions of Klyuchevskoy (1932 and 1938) are relatively high K_2O (~1 wt%) and moderately high MgO (7-9 wt%) (see Table 1 in Ozerov 2000). Several independent studies reproduce these same compositional distinctions (Kersting, Arculus 1994; Pineau *et al.* 1999; Dorendorf *et al.* 2000). None of the Turner *et al.* 2007 samples have compositions similar to the previously reported historic high-Mg basalts. In addition, the High Na, Cr, Ni, Sr/Y, low HREE, and Ca of sample B000 strongly suggest that this sample originates from Shiveluch volcano (or broadly speaking from the Shiveluch group of volcanoes) in northern Kamchatka rather than any other volcano in the CKD (Maxim Portnyagin, pers. comm.).

Recently, the data of the Dosseto *et al.* (2003) were re-analyzed (Dosseto and Turner 2011). New measurements on the same samples recorded U-excess rather than Th-excess for all samples.

Due to these discrepancies, we believe we cannot reliably make direct comparisons of our new data to that reported in these two previous studies.

References:

Dosseto, A., Bourdon, B., Joron, J., and Dupre, B. (2003). U-Th-Pa-Ra study of the Kamchatka arc: New constraints on the genesis of arc lavas. *Geochim. Cosmochim. Acta* **67**, 2857-2877.

Dosseto, A., and Turner, S. (2011). Reappraisal of magma genesis under the Kamchatka arc with uranium-series isotopes**.** *AGU Fall Meet. Suppl. Abstracts*, V23C-03.

Ozerov, A.Yu. (2000). The evolution of high-alumina basalts of the Klyuchevskoy volcano, Kamchatka, Russia, based on microprobe analyses of mineral inclusions. *J. Volcanol. Geotherm. Res.* **95**, 65-79.

Turner, S., Sims, K.W.W., Reagan, M., and Cook, C. (2007). A ^{210}Pb-^{226}Ra-^{230}Th-^{238}U study of Klyuchevskoy and Bezymianny volcanoes, Kamchatka. *Geochim. Cosmochim. Acta* **71**, 4771-4785

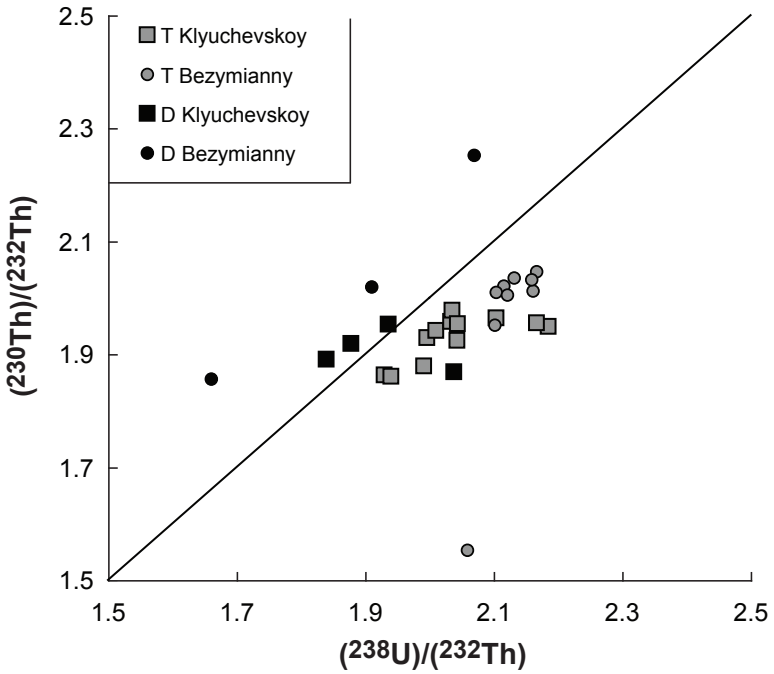

Figure C1. U-series data from Turner *et al.* (2007) – "T Klyuchevskoy" and "T Bezymianny" and Dosseto *et al.* (2003) – "D Klyuchevskoy" and "D Bezymianny". Dosseto *et al.* (2003) primarily record Th-excess, while Turner *et al.* (2007) record U-excess for the Central Kamchatka Depression.

REFERENCES

Aharonov E., Whitehead J.A., Kelemen P.B. and Spiegelman M. (1995) Channeling instability of upwelling melt in the mantle. *J. Geophys. Res.* **100**, 20433-20450.

Albarede F. and Bottinga Y. (1972) Kinetic disequilibrium in trace element partitioning between phenocrysts and host lava. *Geochim. Cosmochim. Ac* **36**, 141-156.

Allegre C.J. and Condomines M. (1982) Basalt genesis and mantle structure studied through Th isotopic geochemistry. *Nature* **299**, 21-24.

Annen C. and Sparks R. S. J. (2002) Effects of repetitive emplacement of basaltic intrusions on thermal evolution and melt generation in the crust. *Earth Planet Sci Lett* **203**, 937–955.

Annen C., Blundy J.D. and Sparks S.J. (2006) The genesis of intermediate and silicic magmas in deep crustal hot zones. *J. Petrol.* **47** 505-539.

Ariskin A.A., Barmina G.S., Ozerov A. Yu. and Nielsen R.L. (1995) Genesis of high-alumina basalts from Klyuchevskoi volcano. *Petrology* **3**, 449-472.

Auer S., Bindeman I., Wallace P., Ponomareva V. and Portnyagin M. (2009) The origin of hydrous, high-δ18O voluminous volcanism: diverse oxygen isotope values and high magmatic water contents within the volcanic record of Klyuchevskoy volcano, Kamchatka, Russia. *Contrib. Mineral. Petrol.* **157**, 209-230.

Ayers J.C., Dittmer S.K. and Layne G.D. (1997) Partitioning of elements between peridotite and H_2O at 2.0-3.0 GPa and 900-1100oC, and application to models of subduction zone processes. *Earth Planet Sci Lett* **150***,* 381-398.

Balesta S.T. (1991). Earth crust structure and magma chambers of the areas of present Kamchatka volcanism. *In: Fedotov, S.A., Masurenkov, Y.P., and Balesta, S.T. eds., Active volcanoes of Kamchatka, Moscow, Nauka.*

Beattie P. (1993a) The generation of uranium series disequilibria by partial melting of spinel peridotite: Constraints from partitioning studies. *Earth Planet Sci Lett* **117**, 379-391.

Beattie P. (1993b) Uranium-thorium disequilibria and partitioning on melting of garnet peridotite. *Nature* **363**, 63-65.

Belousov A. B. (1995) The Shiveluch volcanic eruption of 12 November 1964-explosive eruption provoked by failure of the edifice, *J. Volcanol. Geotherm. Res*. **66**, 357–365.

Belousov A.B., Belousova M.G. and Zhdanova, E.Yu. (1996) Northern group of Kamchatkan volcanoes: Activity in 1990-1992. *J. Volcanol. Seis.* **18**, 161-170.

Belousov A., Belousova M. and Voight B. (1999) Multiple edifice failures, debris avalanches

and associated eruptions in the Holocene history of Shiveluch volcano, Kamchatka, Russia, *Bull. Volcanol*. **61**, 324–342.

Belousov A., Voight B., Belousova M. and Petukhin, A. (2002) Pyroclastic surges and flows from the 8-10 May 1997 explosive eruption of Bezymianny volcano, Kamchatka, Russia. *Bull. Volcanol.* **64**, 455-471.

Berlo K., Turner S., Blundy J. and Hawkesworth C. (2004) The extent of U-series disequilibria produced during partial melting of the lower crust with implications for the formation of the Mount St. Helens dacites. *Contrib. Mineral. Petrol.* **148**, 122-130.

Bindeman I.N., Ponomareva V., Bailey J.C. and Valley J.W. (2004) Volcanic arc of Kamchatka: a province with high-δ18O magma sources and large-scale $^{18}O/^{16}O$ depletion of the upper crust. *Geochim. Cosmochim. Ac* **68** (4), 841-865.

Blundy J. and Wood B.J. (2003) Mineral-melt partitioning of uranium, thorium and their daughters. *In: Uranium-series geochemistry, Reviews in Mineralogy and Geochemistry* **52***,* ed. Bourdon *et al.,* Mineralogical Society of America, 59-123.

Bogoyavlenskaya G. Ye., Braitseva O. A., Melekestsev I.V., Maksimov A. P. and Ivanov B.V. (1991) Bezymianny volcano. In: Fedotov, S.A., and Masurenkob, Y.P. (eds.) *Active volcanoes of Kamchatka, Moscow: Nauka*, 168-197.

Bohrson W. A. and Spera F.J. (2007) Energy-Constrained Recharge, Assimilation, and Fractional Crystallization (EC-RA_XFC): A Visual Basic computer code for calculating trace element and isotope variations of open-system magmatic systems, *Geochem. Geophys. Geosyst., 8, Q11003, doi:10.1029/2007GC001781.*

Bourdon B., Wörner G. and Zellmer A. (2000) U-series evidence for crustal involvement and magma residence times in the petrogenesis of Parinacota volcano, Chile. *Contrib. Mineral. Petrol.* **139**, 458-469.

Bowen, N. L. (1928) *The Evolution of Igneous Rocks. New York: Dover*, pp. 332.

Braitseva O.A., Ponomareva V.V., Sulerzhitsky L.D., Melekestsev I.V. and Bailey J. (1997) Holocene key-marker tephra layers in Kamchatka, Russia. *Quaternary Res* **47**, 125–139.

Brenan J.M., Shaw H.F., Phinney D.L. and Ryerson F.J. (1994) Rutile-aqueous fluid partitioning of Nb, Ta, Hf, Zr, U and Th: implications for high field strength element depletions in island-arc basalts. *Earth Planet. Sci. Lett.* **128**, 327-339.

Churikova T., Dorendorf F. and Wörner G. (2001) Sources and fluids in the mantle wedge below Kamchatka, evidence from across-arc geochemical variation. *J. Petrol.* **42** (8), 1567-1593.

Clark S.K., Reagan M.K. and Plank T. (1998) Trace element and U-series systematics for 1963-1965 tephras from Irazu volcano, Costa Rica: Implications for magma generation processes and transit times. *Geochim. Cosmochim. Ac* **62**, 2689-2699.

Condomines M., Morand P. and Allegre C.J. (1981). ^{230}Th-^{238}U radioactive disequilibria in tholeiites from the FAMOUS zone (Mid-Atlantic Ridge, 36°50'N); Th and Sr isotopic geochemistry. *Earth Planet Sci Lett* **55**, 247-256.

Cooper K.M. and Donnelly C.T. (2009) ^{238}U–^{230}Th–^{226}Ra disequilibria in dacite and plagioclase from the 2004–2005 eruption of Mount St. Helens. In: Sherrod, D.R., Scott, W.E., Stauffer, P.H. (Eds.), *A Volcano Rekindled: the First Year of Renewed Eruption at Mount St. Helens, 2004-2005, U.S. Geological Survey Professional Paper*.

Cunningham H.S., Turner S.P., Dosseto A., Patia H., Eggins S.M. and Arculus R.J. (2009) Temporal variations in U-series disequilibria in an active caldera, Rabaul, Papua New Guinea. *J. Petrol.* **50**, 507-529.

Davaille A. and Lees J.M. (2004) Thermal modeling of subducted plates: tear and hotspot at the Kamchatka corner. *Earth Planet Sci Lett* **226**, 293-304.

Davidson J.P., Hora J.M., Garrison J. M. and Dungan M.A. (2005) Crustal forensics in arc magmas. *J. Volcanol. Geotherm. Res.* **140**, 157-170.

Davidson J., Turner S., Handley H., Macpherson C. and Dosseto A. (2007) Amphibole "sponge" in arc crust? *Geology* **35**, 787-790.

DePaolo D.J. (1981) Trace element and isotopic effects of combined wallrock assimilation and fractional crystallization. *Earth Planet Sci Lett* **53**, 189-202.

Dirksen O., Humphreys M.C.S., Pletchov P., Melnik O., Demyanchuk Y., Sparks R.S.J. and Mahony S. (2006) The 2001-2004 dome-forming eruption of Shiveluch volcano, Kamchatka: Observation, petrological investigation and numerical modeling. *J. Volcanol. Geotherm. Res.* **155**, 201-226.

Dorendorf F., Weichert U. and Wörner G. (2000) Hydrated sub-arc mantle: a source for the Klyuchevskoy volcano, Kamchatka/Russia. *Earth Planet Sci Lett* **175**, 69-86.

Dosseto A., Bourdon B., Joron J. and Dupre B. (2003). U-Th-Pa-Ra study of the Kamchatka arc: New constraints on the genesis of arc lavas. *Geochim. Cosmochim. Ac* **67**, 2857-2877.

Dufek J. and Bergantz G.W. (2005) Lower crustal magma genesis and preservation: a stochastic framework for the evaluation of basalt-crust interaction. *J. Petrol.* **142**, 113-132.

Dufek J. and Cooper K.M. (2005) ^{226}Ra/^{230}Th excess generated in the lower crust: Implications for magma transport and storage times. *Geology* **33**, 833-836.

Dungan M.A. and Davidson J. (2004) Partial assimilative recycling of the mafic plutonic roots of arc volcanoes: An example from the Chilean Andes. *Geology* **32**, 773-776.

Elliott T., Plank T., Zindler A., White W. and Bourdon, B. (1997) Element transport from slab to volcanic front at the Mariana arc. *J. Geophys. Res.* **102**, 14991-15019.

Fedotov, S.A., Masurenkov, Y.P., and Balesta, S.T. eds. (1991) *Active volcanoes of Kamchatka, Moscow, Nauka.*

Fedotov S.A., Zharinov N.A., Gontovaya L.I. (2010) The magmatic system of the Klyuchevskaya Group of volcanoes inferred from data on its eruptions, earthquakes, deformation, and deep structure. *J. Volcanol. Seis.* **4**, 1-33.

Finney B., Turner S., Hawkesworth C., Larsen J., Nye C., George R., Bindeman I., Eichelberger J. (2008) Magmatic differentiation at an island-arc caldera: Okmok volcano, Aleutian Islands, Alaska. *J. Petrol.* **49**, 857-884.

Forsyth D.W. (1975) Fault plane solution and tectonics of the South Atlantic and Scotia Sea. *J. Geophys. Res.* **80,** 1429–1443.

Gao S., Rudnick R.L., Yuan H., Liu X., Liu Y., Xy W., Ling W., Ayers J., Wang X. and Wang, Q. (2004) Recycling lower continental crust in the North China Craton. *Nature* **432**, 892-897.

Garrison J.M. and Davidson, J.P. (2003) Dubious case for slab melting in the Northern volcanic zone of the Andes. *Geology* **31**, 565-568.

Garrison J., Davidson J., Reid M. and Turner, S. (2006) Source versus differential controls on U-series disequilibria: insights from Cotopaxi volcano, Ecuador. *Earth Planet Sci Lett* 244, 548-565.

George R., Turner S., Hawkesworth C., Morris J., Nye C., Ryan J. and Zheng, S. (2003) Melting processes and fluid and sediment transport rates along the Alaska-Aleutian arc from an integrated U-Th-Ra-Be isotope study. *J. Geophys. Res.* **108**, B5, 2252, doi:10.1029/2002JB001916.

George R., Turner S., Hawkesworth C., Bacon C.R., Nye C., Stelling P. and Dreher, S. (2004) Chemical versus temporal controls on the evolution of tholeiitic and calc alkaline magmas at two volcanoes in the Alaska-aleutian arc. *J. Petrol.* **45**, 203-219.

Ghiorso M. S. and Sack R.O. (1995) Chemical Mass Transfer in Magmatic Processes. IV. A Revised and Internally Consistent Thermodynamic Model for the Interpolation and Extrapolation of Liquid-Solid Equilibria in Magmatic Systems at Elevated Temperatures and Pressures. *Contrib. Mineral. Petrol.* **119**, 197-212.

Gill J.B. (1981) *Orogenic andesites and plate tectonics*. Springer.

Gorbach N.V. and Portnyagin, M.V. (2011) Geology and petrology of the lava complex of young Shiveluch volcano, Kamchatka. *Petrology* **19**, 134-166.

Gorbatov A., Kostoglodov V., Suarez G., Gordeev E. (1997) Seismicity and structure of the Kamchatka subduction zone. *J. Geophys. Res.* **102**, 17883-17898.

Handley H.K., Turner S.P., Smith I.E.M., Stewart R.B., Cronin S.J. (2008) Rapid timescales of differentiation and evidence for crustal contamination at intra-oceanic arcs: Geochemical and U-Th-Ra-Sr-Nd isotopic constraints from Lopevi volcano, Vanuatu, SW Pacific. *Earth Planet Sci Lett* **273**, 184-194.

Hauri E.H., Wagner T.P. and Grove T.L. (1994) Experimental and natural partitioning of Th, U, Pb and other trace elements between garnet, clinopyroxene and basaltic melts. *Chem Geol* **117**, 149-166.

Hawkesworth C.J., Turner S.P., McDermott F., Peate D.W. and van Calsteren, P. (1997) U-Th isotopes in arc magmas: Implications for element transfer from the subducted crust. *Science* **276**, 551-555.

Hildreth W. and Moorbath, S. (1988) Crustal contributions to arc magmatism in the Andes of central Chile. *Contrib. Mineral. Petrol.* **98**, 455-489.

Hoogewerff J.A., van Bergen M.J., Vroon P.Z., Hertogen J., Wordel R., Sneyers A., Nastution A., Varekamp J.C., Moens H.L.E. and Mouchel, D. (1997) U-series, Sr-Nd-Pb isotope and trace-element systematics across an active island arc-continent collision zone: Implications for element transfer at the slab-wedge interface. *Geochim. Cosmochim. Ac* **61**, 1057-1072.

Jicha B.R., Singer B.S., Beard B.L., Johnson C.M., Moreno-Roa H., Naranjo J.A. (2007) Rapid magma ascent and generation of ^{230}Th excesses in the lower crust at Puyehue-Cordon Caulle, Southern Volcanic Zone, Chile. *Earth Planet Sci Lett* **255**, 229-242.

Jicha B.R., Johnson C.M., Hildreth W., Beard B.L., Hart G.L., Shirley S.B. and Singer B.S. (2009) Discriminating assimilants and decoupling deep-vs. shallow-level crystal records at Mount Adams using ^{238}U-^{230}Th disequilibria and Os isotopes. *Earth Planet Sci Lett* **277**, 38-49.

Johnson K.T.M. (1998) Experimental determination of partition coefficients for rare earth and high-field-strength elements between clinopyroxene, garnet, and basaltic melt at high pressures. *Contrib. Mineral. Petrol.* **133**, 60-68.

Kayzar T.M., Nelson B.K., Bachmann O., Bauer A.M. and Izbekov, P.E. Pb Isotope Ratios from Time-Series Samples at Bezymianny and Klyuchevskoy Volcanoes Record Lower Crustal Assimilation and Magma Mixing in the Central Kamchatka Depression. *Submitted to J. Petrol.*

Kelemen P.B., Hirth G., Shimizu N., Spiegelmen M., and Hick H.J.B. (1997) A review of melt migration processes in the adiabatically upwelling mantle beneath oceanic spreading ridges. *Phil. Trans. R. Soc. Lond.* **355**, 283-318.

Kepezhinskas P., McDermott F., Defant M.J., Hochstaedter A., Drummond M.S., Hawkesworth C.J., Koloskov A., Maury R.C. and Bellon, H. (1997) Trace element and Sr-Nd-Pb isotopic constraints on a three-component model of Kamchatka Arc petrogenesis. *Geochim. Cosmochim. Ac* **61** (3), 577-600.

Keppler H. (1996) Constraints from partitioning experiments on the composition of subduction-zone fluids. *Nature* **380**, 237-240.

Kersting A.B. and Arculus R.J. (1994) Klyuchevskoy volcano, Kamchatka, Russia: The role of high-flux recharged, tapped, and fractionated magma chamber(s) in the genesis of high-Al_2O_3 from high-MgO basalt. *J. Petrol.* **35**, 1-41.

Kersting A.B. and Arculus R.J. (1995) Pb isotope composition of Klyuchevskoy volcano, Kamchatka and North Pacific sediments: implications for magma genesis and crustal recycling in the Kamchatkan arc. *Earth Planet Sci Lett* **136**, 133-148.

Kessel R., Schmidt M.W., Ulmer P., and Pettke, T. (2005) Trace element signature of subduction-zone fluids, melts and supercritical liquids at 120-180km depth. *Nature* **437**, 724-727.

Konstantinovskaia E.A. (2001) Arc-continent collision and subduction reversal in the Cenozoic evolution of the Northwest pacific: an example from Kamchatka (NE Russia). *Tectonophysics*, **333**, 75-94.

Landwehr D., Blundy J., Chamorro-Perez E.M., Hill E. and Wood B. (2001) U-series disequilibria generated by partial melting of spinel lherzolite. *Earth Planet Sci Lett* **188**, 329-348.

LaTourette T.Z. and Burnett D.S. (1992) Experimental determination of U and Th partitioning between clinopyroxene and natural and synthetic basaltic liquid. *Earth Planet Sci Lett* **110**, 227-244.

LaTourette T., Kennedy A.K. and Wasserburg G.J. (1993) Thorium-Uranium fractionation by garnet: Evidence for a deep source and rapid rise of oceanic basalts. *Science* **261**, 739-742.

Lees J.M. (2007) Seismic tomography of magmatic systems. *J. Volcanol. Geotherm. Res.* **167**, 37-56.

Lundstrom C.C., Gill J., Williams Q. and Perfit, M.R. (1995) Mantle melting and basalt extraction by equilibrium porous flow. *Science* **270**, 1958-1961.

Lundstrom C. C. (2003) Uranium-series disequilibria in mid-ocean ridge basalts: Observations and models of basalt genesis. *In: Uranium-series geochemistry, Reviews in Mineralogy and Geochemistry* **52**, ed. Bourdon *et al.,* Mineralogical Society of America, 175-214.

McKenzie D. (1985) ^{230}Th-^{238}U disequilibrium and the melting processes beneath ridge axes.

Earth Planet Sci Lett **72,** 149- 157.

Macpherson C., Dreher S.T. and Thirlwall, M.F. (2006) Adakites without slab melting: High pressure differentiation of island arc magma, Mindanao, the Philippines. *Earth Planet Sci Lett* **243**, 581-593.

Martin H. (1999) Adakitic magmas: modern analogues of Archaean granitoids, *Lithos* **46**, 411–429.

Melekestsev I.V., Khrenov A.P., Kozhernyaka N.N. (1991) Tectonic position and general description of volcanoes of Northern group and Sredinny Range. *In: Fedotov, S.A., and Masurenkob, Y.P. (eds.) Active volcanoes of Kamchatka, Moscow: Nauka*, 74-81.

Minster J.B. and Jordan T.H. (1978) Present-day plate motions. *J. Geophys. Res.* **83**, 5331-5354.

Mironov N.L., Portnyagin M.V., Pletchov P.Yu. and Khubunaya, S.A. (2001) Kamchatka: Evidence from melt inclusions in minerals of high-alumina basalts. *Petrology* **9** (1), 46-62.

Moyen J. (2009) High Sr/Y and La/Yb ratios: The meaning of the "adakitic signature". *Lithos* **112**, 556-574.

Newman S., Macdougall J.D. and Finkel, R.C. (1984) ^{230}Th-^{238}U disequilibrium in island arcs: Evidence from the Aleutians and the Marianas. *Nature* **308**, 268– 270.

Nicholls I.A. and Harris, K.L. (1980) Experimental rare earth element partition coefficients for garnet, clinopyroxene and amphibole coexisting with andesitic and basaltic liquids. *Geochim. Cosmochim. Ac* **44,** 287-308.

Ozerov A.Yu., Ariskin A.A., Kyle P., Bogoyavlenskaya G.E., Karpenko S.F. (1997) Petrological-geochemical model for genetic relationships between basaltic and andesitic magmatism of Klyuchevskoi and Bezymyannyi volcanoes, Kamchatka. *Petrology* **5**, 550-569.

Ozerov A.Yu. (2000) The evolution of high-alumina basalts of the Klyuchevskoy volcano, Kamchatka, Russia, based on microprobe analyses of mineral inclusions. *J. Volcanol. Geotherm. Res.* **95**, 65-79.

Park J., Levin V., Lees J., Peyton V., Gordeev E. and A. Ozerov (2002) A Dangling Slab, Amplified Arc Volcanism, Mantle Flow and Seismic Anisotropy in the Kamchatka Plate Corner. In: Stein S. and Freymueller J. T. (Eds.) *Plate Boundary Zones*. *Geodynamics Series,* **30,** DOI: 10/1029/030GD18.

Peate D.W. and Hawkesworth, C.J. (2005) U-series disequilibria: insights into mantle melting and the timescales of magma differentiation. AGU, *Rev Geophys* **43**, 1-43.

Ponomareva V. V., Pevzner M. M. and I. V. Melekestsev (1998) Large debris avalanches and associated eruptions in the Holocene eruptive history of Shiveluch Volcano, Kamchatka, Russia,

Bull. of Volcanol. **59,** 490–505.

Portnyagin M., Hoernle K., Avdeiko G., Hauff F., Werner R., Bindeman I., Uspensky V., Garbe-Schoenberg D. (2005) Transition from arc to oceanic magmatism at the Kamchatka-Aleutian junction. *Geology* **33**, 25-28.

Portnyagin M., Hoernle K., Plechov P., Mironov N., Khubunaya S. (2007) Constraints on mantle melting and composition and nature of slab components in volcanic arcs from volatiles (H_2O, S, Cl, F) and trace lements in melt inclusions from the Kamchatka Arc. *Earth Planet Sci Lett* **255**, 53-69.

Portnyagin M., Bindeman I., Hoernle K., Hauff F. (2007) Geochemistry of primitive lavas of the Central Kamchatka Depression: magma generation at the edge of the Pacific Plate. In: *Kamchatka Geophysical Monograph Series*, AGU.

Portnyagin M.V., Mironov N.L., Ponomareva V.V., and Hoernle K. (2008) Millennial Variations of Magma and Volatile Fluxes Inferred From Time-Series Study of Klyuchevskoy Volcano, Kamchatka. *AGU Fall Meeting*, San Fransisco, USA.

Portnyagin M., Mironov N., Ponomareva V., Bindeman I., Hauff F., Sobolev A., and Kayzar T., Garbe-Schonberg D. and Hoernle K. (2011) Arc magmas from slab to eruption: The case of Kliuchevskoy volcano. *Goldschmidt Conference Abstracts* **75**, 1661.

Portnyagin M. and Ponomareva V. (2012) Kliuchevskoi Volcano Diary. *Int J Earth Sci* **101**, 195.

Plechov P.Yu., Tsai A.E., Shcherbakov V.D. and Dirksen, O.V. (2008) Opacitization conditions of hornblende in Bezymyannyi volcano andesites (March 30, 1956 eruption). *Petrology* **16**, 19-35.

Price R.C., Turner S., Cook C., Hobden B., Smith I.E.M., Gamble J.A., Handley H., Maas R., Moebis A. (2010) Crustal and mantle influences and U-Th-Ra disequilibrium in andesitic lavas of Ngauruhoe volcano, New Zealand. *Chem Geol* **277**, 355-373.

Reagan M.K., Morris J.D., Herrstrom E.A. and Murrell M.T. (1994) Uranium series and beryllium isotope evidence for an extended history of subduction modification of the mantle below Nicaragua. *Geochim. Cosmochim. Ac* **58**, 4199-4212.

Reagan M.K., Sims K.W.W., Erich J., Thomas R.B., Cheng H., Edwards R.L., Layne G., Ball L. (2003) Time-scales of differentiation from mafic parents to rhyolite in North American continental arcs. *J. Petrol.* **44**, 1703-1726.

Reubi O., Bourdon B., Dungan M.A., Koornneef J.M., Selles D., Langmuir C.H., and Aciego, S. (2011) Assimilation of the plutonic roots of the Andean arc controls variations in U-series disequilibria at Volcan Llaima, Chile. *Earth Planet Sci Lett* **303**, 37-47.

Rudnick R.L., McDonough W.F., McCullock M.T. and Taylor, S.R. (1986) Lower crustal xenoliths from Queensland, Australia: Evidence for deep crustal assimilation and fractionation of continental basalts. *Geochim. Cosmochim. Ac* **50**, 1099-1115.

Shcherbakov V.D., Plechov P. Yu., Izbekov P.E. and Shipman, J.S. (2011) Plagioclase zoning as an indicator of magma processes at Bezymianny Volcano, Kamchatka. *Contrib. Mineral. Petrol.* **162**, 83-99.

Shimizu N. and Kushiro, I. (1975) The partitioning of rare earth elements between garnet and liquid at high pressures: preliminary experiments. *Geophys Res Lett* **2**, 413-416.

Sigmarsson O., Martin H. and Knowles, J. (1998) Melting of a subducting oceanic crust from U-Th disequilibria in austral Andean lavas. *Nature* **394**, 566-569.

Sigmarsson O., Chmeleff J., Morris J., Lopez-Escobar L. (2002). Origin of 226Ra-230Th in arc lavas from southern Chile and implications for magma transfer time. *Earth Planet Sci Lett* **196**, 189-196.

Sims K.W.W., Gill J.B., Dosseto A., Hoffmann D.L., Lundstrom C.C., Williams R.W., Ball L., Tollstrup D., Turner S., Prytulak J., Glessner J.J.G., Standish J.J. and Elliott, T. (2008) An inter-laboratory assessment of the thorium isotopic composition of synthetic and rock reference materials. *Geostand and Geoanal Res* **32**, 65-91.

Singer B.S., Smith K.E., Jicha B.R., Beard B.L., Johnson C.M. and Rogers, N.W. (2011) Tacking open-system differentiation during growth of Santa Maria Volcano, Guatemala. *J. Petrol.* **52**, 2335-2363.

Sleep N.H. (1988) Tapping of melt by veins and dikes. *J. Geophys. Res.* **93**, 10255-10272.

Sobolev A.V. and Shimizu, N. (1993) Ultra-depleted primary melt included in an olivine from the Mid-Atlantic Ridge. *Nature* **363**, 151-154.

Spera F.J. and Bohrson W.A. (2001) Energy-Constrained Open-System Magmatic Processes I: General Model and Energy-Constrained Assimilation and Fractional Crystallization (EC-AFC) Formulation. *J. Petrol.* **42**: 999-1018.

Spiegelman M. and Elliot, T. (1993) Consequences of melt transport for uranium series disequilibrium in young lavas. *Earth Planet Sci Lett* **118**, 1-20.

Stern C.R. and Kilian, R. (1996) Role of the subducted slab, mantle wedge and continental crust in the generation of adakites from the Andean Austral Volcanic Zone. *Contrib. Mineral. Petrol.* **123**, 263-281.

Taylor H.P. Jr. (1980) The effects of assimilation of country rocks by magmas on $^{18}O/^{16}O$ and $^{87}Sr/^{86}Sr$ in igneous rocks. *Earth Planet Sci Lett* **47**, 243-254.

Thomas R.B., Hirschmann M.M., Cheng H., Reagan M.K. and Edwards L.R. (2002) (^{231}Pa/^{235}U)-(^{230}Th/^{238}U) of young mafic volcanic rocks from Nicaragua and Costa Rica and the influence of flux melting on U-series systematics of arc lavas. *Geochim. Cosmochim. Ac* **66**, 4287-4309.

Turner S., C.J. Hawkesworth, van Calsteren P., Heath E., MacDonald R. and Black S. (1996) U-series isotopes and destructive plate margin magma genesis in the Lesser Antilles. *Earth Planet. Sci. Lett***. 142,** 191-207.

Turner S., McDermott F., Hawkesworth C. and Kepezhinskas P. (1998) A U-series study of lavas from Kamchatka and the Aleutians: constraints on source composition and melting processes. *Contrib. Mineral. Petrol.* **133**, 217-234.

Turner S., Bourdon B., Hawkesworth C. and Evans, P. (2000) ^{226}Ra-^{230}Th evidence for multiple dehydration events, rapid melt ascent and the time scales of differentiation beneath the Tonga-Kermadec island arc. *Earth Planet Sci Lett*, 581-593.

Turner S., Evans P. and Hawkesworth, C. (2001) Ultrafast source-tosurface movement of melt at island arcs from ^{226}Ra-^{230}Th systematics. *Science* **292**, 1363-1366.

Turner S., Bourdon B. and Gill, J. (2003) Insights into magma genesis at convergent margins from U-series isotopes. *In: Uranium-series geochemistry, Reviews in Mineralogy and Geochemistry* **52**, ed. Bourdon *et al.,* Mineralogical Society of America, 255-315.

Turner S., Black S. and Berlo, K. (2004) ^{210}Pb-^{226}Ra and ^{228}Ra-^{230}Th systematics in young arc lavas: implications for magma degassing and ascent rates. *Earth Planet Sci Lett* **227**, 1-16.

Turner S., Sims K.W.W., Reagan M. and Cook, C. (2007) A ^{210}Pb-^{226}Ra-^{230}Th-^{238}U study of Klyuchevskoy and Bezymianny volcanoes, Kamchatka. *Geochim. Cosmochim. Ac* **71**, 4771-4785.

Volpe A.M. and Hammond P.E. (1991) ^{238}U–^{230}Th–^{226}Ra disequilibria in young Mount St. Helens rocks: time constraint for magma fractionation and crystallisation. *Earth Planet Sci Lett* **107**, 475–486.

Volpe A.M. (1992) ^{238}U-^{230}Th-^{226}Ra disequilibrium in young Mt. Shasta andesites and dacites. *J. Volcanol. Geotherm. Res.* **53**, 227-238.

Volynets O.N., Babanskii A.D. and Gol'tsman (2000). Variations in isotopic and trace-element composition of lavas from volcanoes of the Northern Group, Kamchatka, in relation to specific features of subduction. *Geochemistry Int*+ **38**, 974-989.

Walker J.A., Mickelson J.E., Thomas R.B., Patino L.C., Cameron B., Carr M.J., Feigenson M.D. and Edwards, R.L. (2007) U-series disequilibria in Guatemalan lavas, crustal contamination, and implications for magma genesis along the Central American subduction zone. *J. Geophys. Res. Letters* **112**, B06205, doi:10.1029/2006JB004589.

Watson B.F. and Fujita, K. (1985) Tectonic evolution of Kamchatka and the sea of Okhotsk and implications for the Pacific Basin. In *Tectonostratigraphic Terranes* (ed. D.G. Howell), AAPG, 333-348.

Williams, R.W. and Gill, J.B. (1989) Effects of partial melting on the uranium decay series. *Geochim. Cosmochim. Ac* **53**, 1607-1619.

Wood B.J., Blundy, J.D. and Robinson, A.C. (1999) *Geochim. Cosmochim. Ac* **63**, 1613-1620.

Yogodzinski G.M. and Kelemen P.B. (1998) Slab melting in the Aleutians: Implications of an ion probe study of clinopyroxene in primitive adakite and basalt. *Earth Planet Sci Lett,* **158**, 53–65.

Yogodzinski G.M., Lees J.M., Churikova T.G., Dorendorf F., Wörner G. and Volynets O.N. (2001) Geochemical evidence for the melting of subducting oceanic lithosphere at plate edges. *Nature* **409**, 500-503.

Zhang G. and Zeng, Z. (2010) Genesis of ^{230}Th excess in basalts from mid-ocean ridges and ocean islands: Constraints from the global U-series isotope database and major and rare earth element geochemistry. *Sci China* **53**, 1486-1494.

Zou H. and Zindler A. (2000). Theoretical studies of ^{238}U-^{230}Th-^{226}Ra and ^{235}U-^{231}Pa disequilibria in young lavas produced by mantle melting. *Geochim. Cosmochim. Ac* **64**, 1809-1817.

CHAPTER 3

Periodically Erupting Degassed Magma: Inferring Magma Residence Times from the Evolution of Karymsky, Bezymianny, and Shiveluch Volcanoes, Kamchatka, Russia

Co-authors:
Bruce K. Nelson, Mark K. Reagan, Olivier Bachmann

ABSTRACT

Short-lived isotope disequilibria in the ^{226}Ra-^{222}Rn-^{210}Pb decay chain allows for the investigation of shallow magma degassing magnitudes and timescales at three active volcanic systems: Karymsky, Bezymianny, and Shiveluch volcanoes. Fifteen eruptions of Karymsky, Bezymianny, and Shiveluch volcanoes over the past 50 years show chemical evidence for subsurface gas motion. Equilibrium (^{210}Pb)/(^{226}Ra) values of 0.92-1.02 characterize a continued eruption at Karymsky starting in 1996. However, ^{210}Pb disequilibrium follows later quiescent periods of activity. Karymsky eruptive activity decreased in November 2008 while steaming continued. The eruption cycle began again in March and April of 2008. ^{210}Pb excess of 1.10 (10%) in an April 2008 lava bomb suggests gas accumulation prior to explosion. Activity decreased during June, and an explosive phase initiated on July 25, 2008. A ^{210}Pb deficit of 0.97 (3%) is recorded in a lava bomb from this eruption. The chaotic geochemical behavior at Karymsky is evidence that frequently erupting magmatic systems do not establish stable ^{210}Pb-^{226}Ra degassing signals. Bezymianny and Shiveluch volcanoes in northern Kamchatka are similar to Karymsky in that passive degassing occurs at the surface prior to periodic explosive eruptions. Trends towards ^{210}Pb deficits in the past decade are recorded at Bezymianny and Shiveluch with Bezymianny recording deficits of 15% in 2007, and Shiveluch as much as 8% in 2007. In these systems, periodic explosive eruptions may be caused by the loss of gas and formation of a shallow degassed plug of magma sealing a system with continued deep degassing. If we assume that ^{210}Pb deficits at Bezymianny are formed by shallow degassing between eruptions, we record deficits larger than it is physically possible to generate with instantaneous gas loss. This observation suggests that either deep degassing occurs at Bezymianny or that residence times of magmas in shallow chambers are longer than the periodicity between eruptive events.

INTRODUCTION:

Gas overpressure in magmas is a plausible mechanism for initiating explosive volcanic eruptions. Gas is exsolved from magmas by two dominant processes: decompression as magmas rise to the surface, which lowers the confining pressure of the magma, and crystallization, which causes volatile phases to become oversaturated in the melt. Once gas phases are formed in a melt, they are buoyant and can migrate through the melt system. However, the timescales and transport mechanisms associated with volatile motion in the subsurface are difficult to quantify because

volcanic gases are fugitive phases that are difficult to capture and measure (Kazahaya et al. 1994; Barclay et al. 1995; Stevenson and Blake 1998; Wallace 2001; Sparks 2003; Blower et al. 2003; Reagan et al. 2006). Melt inclusions in crystalline phases can provide us with snap shots of volatile concentrations but do not describe an evolution of gas in volcanic systems near the shallow surface.

The U-series decay chain nuclides ^{226}Ra-^{222}Rn-^{210}Pb may be used to quantify gas motion. The intermediate nuclide 222-radon strongly partitions into volcanic gas, potentially fingerprinting gas flux by U-series disequilibria (Sato and Sato 1977; Gill et al. 1985; Gauthier et al. 1999). If gas migrates out of a melt, ^{222}Rn is lost and the ingrowth of ^{210}Pb in the system is no longer supported. This is manifested in (^{210}Pb)/(^{226}Ra) values (parentheses denote activity ratios) < 1, termed ^{210}Pb deficits. However, if gas accumulates in a melt, transport of ^{222}Rn will cause addition of ^{210}Pb and (^{210}Pb)/(^{226}Ra) > 1 or ^{210}Pb excesses. Therefore, if gaseous phases migrate through a melt on short timescales (fast enough to preserve disequilibria before the decay of ^{222}Rn (half-life of 3.8 days) then this system provides a tracer of gas motion that persists in the ^{210}Pb signal even after the gas phase is lost (see review by Berlo and Turner (2010) and references therein). Gauthier and Condomines (1999) were the first to propose a quantitative gas transport model using ^{226}Ra-^{222}Rn-^{210}Pb decay to examine gas loss at Merapi and Stromboli volcanoes. This model has since been applied to multiple studies that examine ^{210}Pb deficits as well as ^{210}Pb excesses (Gauthier et al. 2000; Berlo et al. 2004; Turner et al. 2004; Berlo et al. 2006; Reagan et al. 2006; Cunningham et al. 2009).

^{226}Ra-^{210}Pb studies have brought to light three major concerns for the applied use of this parent-daughter system for interpreting gas motion: 1) gas motion is nearly impossible to quantify without knowing the length of time that the system has been undisturbed. Open system behavior such as melt recharge, magma mixing, etc. all disrupt the decay of ^{226}Ra to ^{210}Pb; therefore, only qualitative models of gas motion can be developed in complex systems with unconstrained degassing histories (Reagan et al. 2006; Kayzar et al. 2009); 2) the physical mechanisms by which gas is transported are controversial. The Gauthier and Condomines (1999) model has been updated by Condomines et al. (2010); however, it remains a box model where gas moves instantaneously from a degassing magma to an accumulating magma. This model may not

capture the actual behavior of ^{222}Rn in magmatic systems (Reagan et al. 2005, Reagan et al. 2006, Kayzar et al. 2009); 3) the volumes of magma needed to supply enough ^{222}Rn to disrupt ^{226}Ra-^{210}Pb equilibria are very large and perhaps unreasonable (Berlo et al. 2006, Reagan et al. 2006, Kayzar et al. 2009). However, new constraints are available from studying ^{226}Ra-^{210}Pb behavior during gas transport in volcanic systems with well-constrained degassing histories.

We report (^{210}Pb)/(^{226}Ra) in products from the active volcanic centers of Karymsky, Bezymianny, and Shiveluch in the Kamchatka volcanic arc. Two of these systems, Bezymianny and Shiveluch, along with Klyuchevskoy produce the highest gas flux in the Kurile-Kamchatka arc (Taran 2009). Because these volcanoes erupt multiple times per year, they are ideal places to examine (^{210}Pb)/(^{226}Ra) disequilibria. Knowing the time elapsed between eruptions places a constraint on possible models describing gas motion mechanisms in subsurface melts between eruptions.

GEOLOGIC BACKGROUND: SUMMARIZED ERUPTIVE HISTORIES

Karymsky volcano, located in the Eastern Volcanic Front of Kamchatka (**Figure 1**) began a continuous eruption in 1996. The eruption was triggered by the emplacement of a basaltic dike that interacted with an andesite magma reservoir beneath the central cone of Karymsky to initiate eruption (Izbekov et al. 2004). Since 2004, Karymsky volcano eruptive behavior is characterized by month long periods of quiescence followed by eruptions occurring on the hour to day timescales. Constant gas jetting, termed “gas chugging” or “puffing” (Johnson et al. 1998, Fischer et al. 2002) occurs between eruptive events.

Bezymianny and Shiveluch volcanoes in northern Kamchatka are similar to Karymsky in that passive degassing occurs at the surface prior to periodic explosive eruptions (Taran 2009). Bezymianny eruptions and Shiveluch eruptions occur on monthly timescales and are well documented by the Kamchatka Volcano Eruptive Response Team (KVERT) at the Institute of Volcanology and Seismology in Petropavlovsk-Kamchatsky, Russia.

TESTING EXISTING $^{210}Pb/^{226}Ra$ DEGASSING MODEL

We collected 15 samples for ($^{210}Pb/^{226}Ra$) from modern eruptions of Karymsky, Bezymianny, and Shiveluch volcanoes (Table 1). These eruptions were targeted as key eruptions because the time elapsed between the studied eruption and the previous eruption is documented. This provides the time constraint of degassing essential to test the applicability of published degassing models.

Laboratory Materials and Methods

Radium analyses were conducted at the University of Washington. Samples were powdered in an agate mortar and pestle, after which large powder splits (5g) were dissolved by microwave acid digestion with a 3:1 solution of concentrated HF:HNO_3. Solutions were dried with added HBO_3 and $HClO_4$ to remove fluorides and were dissolved in 3M HCl + trace HBO_3 to form sample solutions. For accurate (^{210}Pb)/(^{226}Ra) measurements, it is important to analyze both ^{210}Pb and ^{226}Ra from the same solution rather than different powdered splits. Sample solution splits for Ra analysis by isotope dilution were spiked with Ra^{228} and Ra was separated using procedures described in Cooper and Donnelly (2009) and Kayzar et al. (2009). Isotope ratios were measured on Nu Plasma MC-ICP-MS instrument at the University of Washington.

Separate large aliquots of each sample solution (representing ~3g of sample) analyzed by alpha spectrometry at the University of Iowa for ^{210}Po. Analytical techniques for ^{210}Po separation and measurement by alpha spectrometry can be found in Reagan et al. (2005). Briefly, sample stock solutions were dried and re-dissolved in 1 N HCl. A ^{209}Po spike was added to each sample (calibrated using a (^{210}Po) value of 7.95 dpm/g for the standard TML). USGS standard RGM-1 analyzed at about the same time as the Kamchatka samples gave ^{210}Po values of 4.21 ± 0.06 and 4.32 ± 0.07 dpm/g (1σ). Samples were processed through a single anion exchange column charged with 1N HCl and eluted with warm 7.5 N HNO_3. For each sample, collected ^{210}Po was then autoplated on Ag disks for 8h in a mixture of 150 ml of 0.5N HCl and about 20 mg of ascorbic acid. Plated samples were counted on an alpha spectrometer for durations of 6 to 9 days.

Predictions Based on Degassing Models

We use published (^{210}Pb)/(^{226}Ra) models (Gauthier and Condomines 1999, Condomines et al. 2010) to estimate the magnitude of expected disequilibria in the Kamchatka eruptive products. These models calculate the extent of (^{210}Pb)/(^{226}Ra) disequilibrium based on the duration (time) of degassing. Using the time elapsed between eruptive events in Kamchatka in conjunction with measured (^{210}Pb)/(^{226}Ra) from each eruption allows us to compare measured data with model predictions. Given the constant passive degassing behavior at Karymsky, Bezymianny, and Shiveluch volcanoes, we expect to measure ^{210}Pb deficits in erupted lavas and juvenile bombs that are correlated to the time of degassing (or the time between eruptive events). These ^{210}Pb deficits, based on previous models (Gauthier and Condomines 1999, Condomines et al. 2010) should be small due to the short period of time between eruptions. If the measured (^{210}Pb)/(^{226}Ra) disequilibria cannot be reproduced using the existing box model, then either gas transport timescales are longer than assumed and require further study, or ^{226}Ra-^{222}Rn-^{210}Pb disequilibria occurs by processes not currently incorporated in the model (e.g. fractionation by sulfides, crystal growth, etc.).

RESULTS

Karymsky Volcano

Equilibrium (^{210}Pb)/(^{226}Ra) values of 0.92-1.02 characterize a continued eruption at Karymsky starting in 1996. However, we measure disequilibrium following short quiescent periods. Karymsky activity decreased in November 2008 while steaming continued. The eruption cycle began again in March and April of 2008. A ^{210}Pb excess of 1.1 (10%) in an April 2008 lava bomb suggests gas accumulation in the magma prior to explosion. Explosive activity decreased during June and the volcano was in a steady gas-jetting phase prior to another explosive phase initiated on July 25, 2008. We measure a ^{210}Pb deficit of 0.97 (3%) in a lava bomb from this eruption (**Figure 2**). During continuous eruptive activity at Karymsky (1996-1998) there is not enough differential gas motion to create disequilibria between ^{210}Pb and ^{226}Ra. However, when

volcanic activity ceases for months at a time, non-systematic (^{210}Pb)/(^{226}Ra) disequilibria gas signatures are observed – both ^{210}Pb excesses and deficits.

Bezymianny and Shiveluch

At Bezymianny and Shiveluch, we measure a trend towards ^{210}Pb deficits in the past decade. Bezymianny eruptive products have ~ 3% ^{210}Pb deficit in 2006. The ^{210}Pb deficit measured at Bezymianny increases to 15% in the 2007 eruptive unit (**Figure 3**). Shiveluch volcano is less frequently sampled in this study but samples are near equilibrium in 2001 and record an 8% ^{210}Pb deficit in 2007 (**Figure 3**).

MAGMA DEGASSING IMPLICATIONS

Fluctuations in (^{210}Pb)/(^{226}Ra) during continuous activity at Karymsky volcano suggest that the timescales needed to establish systematic gas accumulation or gas loss signals in the (^{210}Pb)/(^{226}Ra) are longer than the time period between eruptions. The equilibrium signal measured during the continuous eruptive episode at Karymsky from 1996-1998 supports this concept (**Figure 2**). Although passive degassing is visually observed between eruptions, the absence of (^{210}Pb)/(^{226}Ra) disequilibria imply that the magnitude of gas lost is not great enough to measurably affect the (^{210}Pb)/(^{226}Ra) composition of the magma. This is not entirely surprising because only a minor shift from equilibrium (6%) was recorded at Mount Pinatubo volcano in the Philippines, which erupted over 17Mt of SO_2 (Gerlach et al. 1996; Kayzar et al. 2009). Also, the number of ^{222}Rn atoms at any time in a magma is minor relative to the number of ^{226}Ra atoms making (^{210}Pb)/(^{226}Ra) disequilibria difficult to establish because rapid and efficient loss of ^{222}Rn is required.

The ^{210}Pb deficits recorded at Bezymianny and Shiveluch support the longer time-period of passive degassing observed at these volcanic centers. Bezymianny and Shiveluch erupt less frequently than Karymsky providing more time to lose ^{222}Rn and increase the magnitude of (^{210}Pb)/(^{226}Ra) disequilibrium. The samples that record ^{210}Pb deficits are volcanic bombs erupted during explosive events. We suggest that in these systems, passive degassing during non-eruptive

periods results in the formation of a shallow degassed plug of magma. This plug likely continues to degas by cracking or adjusting during cooling (Holland et al. 2011) but eventually seals the system. Continued degassing beneath the plug in addition to magma influx to the shallow conduit would then build the pressure to initiate the next eruptive cycle (**Figure 4**). This conceptual model predicts that if rather than sampling dense bombs from the eruption, we were able to sample fine ash from fragmentation, that we may record ^{210}Pb excess rather than ^{210}Pb deficits.

Magma recharge at Bezymianny may also affect the magnitude of ^{210}Pb-^{226}Ra disequilibria. Previously we discuss (^{210}Pb)/(^{226}Ra) assuming that the initial condition is equilibrium in the shallow chamber or conduit. However, if gas is lost at depth, Bezymianny magmas may have ^{210}Pb deficits initially. Conversely, if recharge magmas are not degassed, they may add ^{226}Ra to shallow degassed magma during recharge that would lower the magnitude of ^{210}Pb deficits produced during passive degassing. There is evidence for recharge from plagioclase zoning at Bezymianny (Shcherbakov et al. 2010). Because there is no way to measure the (^{210}Pb)/(^{226}Ra) of recharging magma, we assume it to be in equilibrium for interpretations of ^{210}Pb deficits at Bezymianny.

Examination of Degassing Model

Using the time between eruptive events and the measured (^{210}Pb)/(^{226}Ra) at each volcano, we can compare our data to the (^{210}Pb)/(^{226}Ra) degassing model of Gauthier and Condomines (1999) and Condomines et al. (2010). We identify a "degassed magma paradox" where measured ^{210}Pb deficits are lower than it is physically possible to cause by mechanisms of gas transfer described by the model (**Figure 5**). The box models assumes instantaneous gas loss with no physical transport mechanisms, which is perfectly efficient gas loss; therefore, no (^{210}Pb)/(^{226}Ra) data should ever have values below the curve described by 100% gas loss (red curve, f=1, **Figure 5**). However, data from Bezymianny and Karymsky plot below the theoretical 100% gas loss curve (**Figure 5**). This signal is also seen in data published from other volcanic systems (Turner et al. 2004, Sigmarsson et al. 2005, Cunningham et al. 2009). If the model were adjusted to include bubble drag, timescales of bubble rise or gas channeling transport times (Thomas et al. 1993;

Phillips and Woods 2002; Mueller et al. 2005) this would result in even longer required times to establish (^{210}Pb)/(^{226}Ra) disequilibria. Therefore, our observation of data being inconsistent with the current model would only be exacerbated.

A plausible explanation for this discrepancy is that magma residence times in magmatic systems must be longer than the duration between eruptions. For example, during eruptive episodes, not all magma in the shallow conduit may be evacuated allowing it to continue degassing for periods of time longer than between eruptions (**Figure 4**). At Bezymianny, magmas would need to reside in the plumbing system for ~ 5-13 years longer than the period between eruptions. This hypothesis would predict that stronger eruptions at periodically erupting volcanoes are more likely to erupt these stagnant magmas with ^{210}Pb deficits, which could be tested using detailed sampling of volcanic systems that are geophysically monitored to estimate the strength of eruption. Conversely, magmas may degas over long time periods as they rise to the surface establishing ^{210}Pb deficits prior to shallow magma chamber storage (Rubin et al. 2005; Chakrabarti et al. 2009). If this were true at Bezymianny, the increasing ^{210}Pb deficits recorded from 2005-2007 would suggest that no new magma is added to the system between eruptions. This is inconsistent with petrological observations that suggest reheating prior to every eruptive episode at Bezymianny (Shcherbakov et al. 2010). It is also possible that our understanding of ^{226}Ra, ^{222}Rn and ^{210}Pb partitioning in magmas is not well understood but that is beyond the scope of this study and requires more laboratory experimentation.

CONCLUSIONS

(^{210}Pb)/(^{226}Ra) disequilibria is a geochemical signal that may be used to investigate the behavior of differential gas-melt motion in subsurface magma chambers. However, current models that predict the magnitude of ^{210}Pb deficits as a function of duration of degassing do not predict observations at actively degassing volcanoes. Measured ^{210}Pb deficits are larger than predicted at Bezymianny volcano and Karymsky volcano given the time period of degassing between explosive events. These large ^{210}Pb deficits imply that magma resides in subsurface plumbing systems and degasses for time periods longer than the time between eruptions. In addition, timescales longer than months are required to establish measurable (^{210}Pb)/(^{226}Ra) disequilibria.

Therefore, despite the observation of gas loss at volcanoes with gaseous plumes, if gas loss occurs over short time periods, magmas may not record (^{210}Pb)/(^{226}Ra) disequilibria.

FIGURES

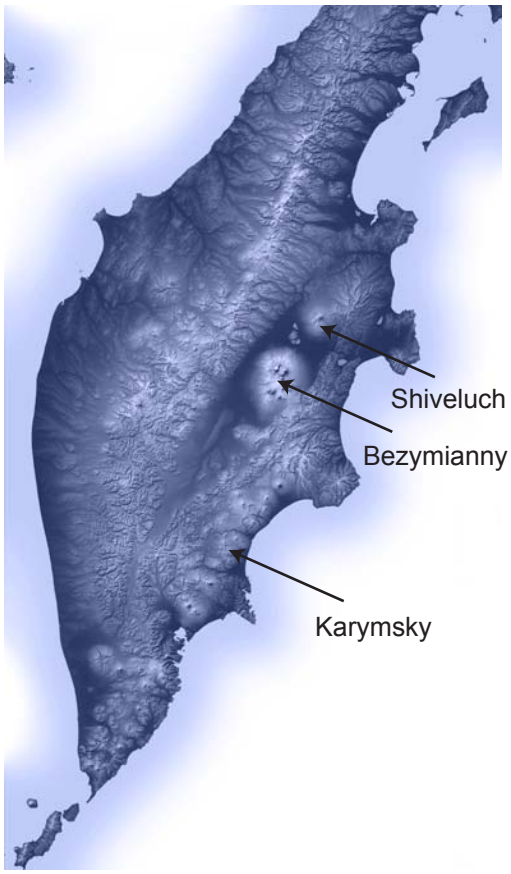

Figure 1. Kamchatka Peninsula with locations of Karymsky (Eastern Volcanic Front), Bezymianny (Central Kamchatka Depression) and Shiveluch (Northern Central Kamchatka Depression) shown. Image modified from NASA.

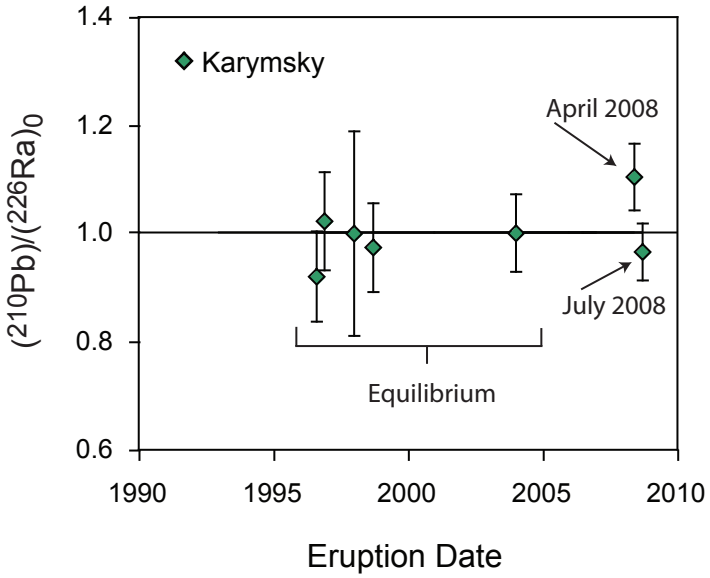

Figure 2. $(^{210}Pb)/(^{226}Ra)$ at Karymsky Volcano. The period of continuous eruptive activity at Karymsky is between 1996 and 2003 where equilibrium $(^{210}Pb)/(^{226}Ra)$ is observed. Prior to April 2008, Karymsky was not continuously erupting but was degassing at the surface of the vent. Disequilibria is measured at Karymsky after longer non-eruptive periods; however, the chemical signal is not stable and records both ^{210}Pb excesses and deficits.

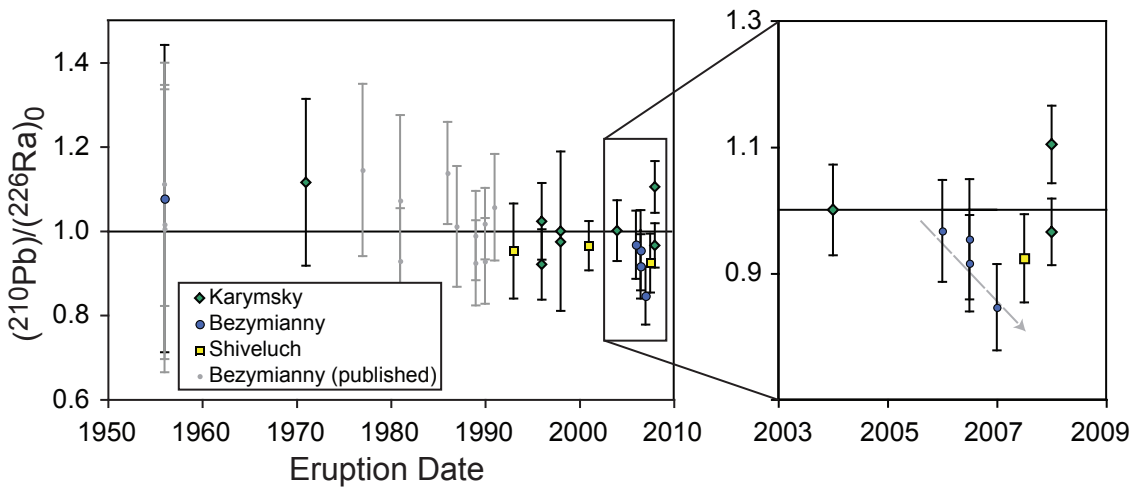

Figure 3. (^{210}Pb)/(^{226}Ra) for all Kamchatka samples: Bezymianny, Shiveluch, and Karymsky. The most recent eruptions at Bezymianny and Shiveluch record ^{210}Pb deficits. The deficit at Bezymianny increases from 2006 to 2007 from 3% to 15% (shown by grey arrow on inset). The 2007 eruptive products from Shiveluch record 8% ^{210}Pb deficits. Published data for older Bezymianny eruptive units (shown in grey) are taken from Turner *et al.* (2007) and all record equilibrium values.

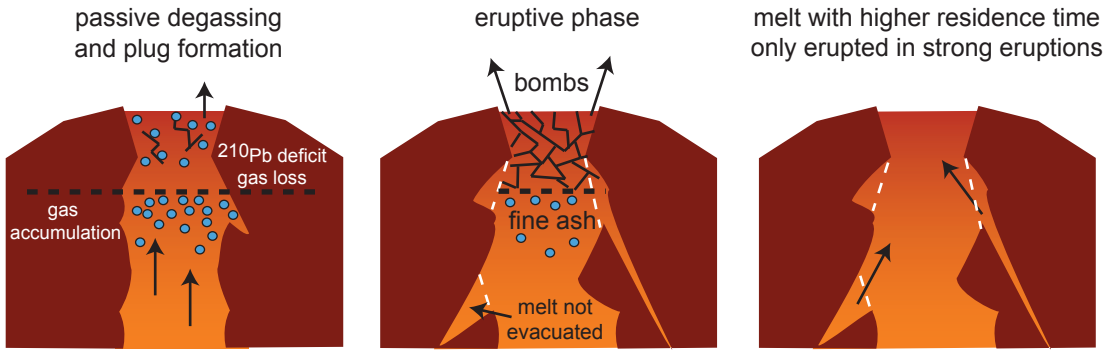

Figure 4. Conceptual model to explain ^{210}Pb deficits at Bezymianny. Between eruptive events at Bezymianny a dense plug is formed in the conduit that degasses creating a ^{210}Pb deficit. This plug seals the conduit and prevents magma and gases from below from leaving the vent. Pressure initiates eruptive events, but during eruption, not all of the magma in the plumbing system is evacuated. These melts that are left can continue to degas for longer durations of time leading to larger ^{210}Pb deficits. Strong eruptions would be more likely to evacuate these magmas.

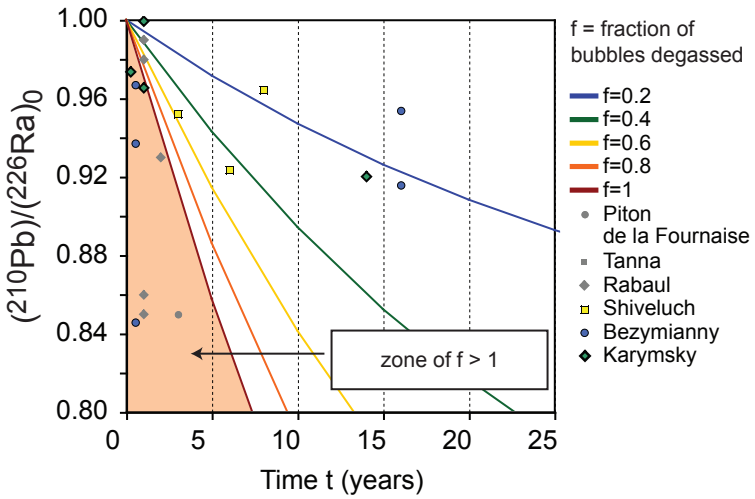

Figure 5. Comparison of Kamchatka data to (^{210}Pb)/(^{226}Ra) model of Gauthier and Condomines (1999); Condomines *et al.* (2010). Model curves represent varying f-values (fraction of bubbles or gas lost from the magma). The red curve, f=1, represents complete gas loss and no data should plot below this line. Samples from Bezymianny and Karymsky as well as data published from Piton de la Fournaise (Sigmarsson *et al.* 2005), Tanna (Turner *et al.* 2004), and Rabaul (Cunningham *et al.* 2009) all plot in a zone on this diagram (zone of f > 1) that is physically impossible to reach if the time of degassing is assumed to be the time between eruptive events. These data suggest that magma resides in plumbing systems longer than the duration between eruptive events, or that magmas lose gas while rising to the surface and are undisturbed (not open-systems with additional magma recharge) after gas loss.

TABLES

Table 1. (^{210}Pb) and (^{226}Ra) measured values and age corrections

Sample Name	Eruption Date	Years (Eruption to Analysis)	^{210}Po[a] (dpm/g)	+/- 1s	(^{210}Pb)o dpm/g	+/- 1s	(^{226}Ra)[b] (dpm/g)	+/- 2s (%)	(^{210}Pb)/(^{226}Ra) (dpm/g)	+/- 1s	(^{210}Pb)/(^{226}Ra)o dpm/g	+/- 2s
Karymsky												
K1971PFMB	1971	39	0.904	0.020	0.974	0.086	0.874	1.02	1.035	0.025	1.115	0.198
97IPE4	1996	14	0.806	0.020	0.782	0.035	0.850	0.99	0.948	0.025	0.920	0.084
98IPE28	1996	14	0.823	0.021	0.829	0.037	0.811	1.19	1.015	0.028	1.023	0.091
98IPE22d	1998	12	0.369	0.023	0.369	0.035	0.369	1.26	1.000	0.063	0.999	0.189
98IPE26	1998	12	0.785	0.020	0.779	0.032	0.800	1.33	0.982	0.027	0.974	0.082
K2004LMB	2004	6	0.752	0.021	0.752	0.027	0.752	1.13	1.001	0.030	1.001	0.072
KTK0508	2008	2	0.867	0.022	0.872	0.024	0.790	1.06	1.098	0.030	1.104	0.062
KYK0908	2008	2	0.773	0.019	0.771	0.021	0.799	1.16	0.968	0.026	0.966	0.053
Bezymianny												
06BZT05	1956	51	0.840	0.025	0.890	0.151	0.827	1.14	1.016	0.032	1.077	0.365
06IPE17	2006	1	0.630	0.025	0.628	0.026	0.686	1.04	0.918	0.038	0.916	0.076
06IPE17*	2006	4	0.658	0.028	0.654	0.033	0.686	1.04	0.959	0.042	0.954	0.095
06BZT02b	2006	1	0.627	0.025	0.626	0.026	0.648	1.24	0.968	0.040	0.967	0.081
02BZT08	2007	1	0.600	0.023	0.597	0.024	0.705	1.78	0.851	0.034	0.846	0.068
Shiveluch												
SHIV1993DMB	1993	15	0.641	0.021	0.629	0.037	0.661	1.15	0.970	0.033	0.952	0.113
SHIV2001PFMB	2001	7	0.592	0.013	0.588	0.018	0.609	1.99	0.971	0.023	0.965	0.058
SHIV72007	2007	1	0.612	0.022	0.610	0.023	0.661	1.42	0.926	0.035	0.924	0.070

a Measured by alpha-spectrometry at the University of Iowa

b Measured by MC-ICP-MS at the University of Washington

c Standard UW-BCR1 (in house, same basalt as USGS BCR-2) measures ^{226}Ra fg/g = 590.87 +/- 1.28 (%, 2 sigma error)

REFERENCES

Barclay, J., Riley, D.S., and Sparks, R.S.J. (1995) Analytical models for bubble growth during decompression of high viscosity magmas. *Bulletin of Volcanology* **57**, 422-431.

Berlo, K., Blundy, J., Turner, S., Cashman, K., Hawkesworth, C., and Black, S., (2004) Geochemical precursors to volcanic activity at Mount St. Helens, USA. *Science* **306**, 1167–1169.

Berlo, K., Turner, S., Blundy, J., Black, S., and Hawkesworth, C., (2006) Tracing pre-eruptive magma degassing using (^{210}Pb/^{226}Ra) disequilibria in the volcanic deposits of the 1980–1986 eruption of Mount St Helens. *Earth and Planetary Science Letters* **249**, 337–349.

Berlo, K. and Turner, S., (2010) ^{210}Pb-^{226}Ra disequilibria in volcanic rocks. Earth and Planetary Science Letters 296, 155-164.

Blower, J.D., Keating, J.P., Mader, H.M., and Phillips, J.C. (2002). The evolution of bubble size distributions in volcanic eruptions. *Journal of Volcanology and Geothermal Research* **120**, 1-23.

Chakrabarti, R., Sims, K.W.W., Basu, A.R., Reagan, M., and Durieux, J. (2009). Timescales of magmatic processes and eruption ages of the Nyiragongo volcanics from ^{238}U-^{230}Th-^{226}Ra-^{210}Pb disequilibria. *Earth and Planetary Science Letters* **288**, 149-157.

Condomines, M., Sigmarsson, O., and Gauthier, P.J. (2010). A simple model of ^{222}Rn accumulation leading to ^{210}Pb excesses in volcanic rocks. *Earth and Planetary Science Letters* **293**, 331-338.

Cooper, K.M., and Donnelly, C.T., (2009) ^{238}U–^{230}Th–^{226}Ra disequilibria in dacite and plagioclase from the 2004–2005 eruption of Mount St. Helens. In: Sherrod, D.R., Scott, W.E., Stauffer, P.H. (Eds.), *A Volcano Rekindled: the First Year of Renewed Eruption at Mount St. Helens, 2004–2005*. U.S. Geological Survey Professional Paper.

Cunningham, H.S., Turner, S.P., Patia, H., Wysoczanski, R., Nichols, A.R.L., Eggins, S., and Dosseto, A. (2009) (^{210}Pb/^{226}Ra) variations during the 1994-2001 intracaldera volcanism at Rabaul Caldera. *Journal of Volcanology and Geothermal Research* **184**, 416-426.

Fischer, T.P., Roggensack, K., Kyle, P.R. (2002) Open and almost shut case for explosive eruptions: vent processes determined by SO_2 emission rates at Karymsky volcano, Kamchatka. *Geology* **30**, 1059-1062.

Gauthier, P.J., and Condomines, M., (1999) ^{210}Pb–^{226}Ra radioactive disequilibria in recent lavas and radon degassing: inferences on the magma chamber dynamics at Stromboli and Merapi volcanoes. *Earth and Planetary Science Letters* **172**, 111–126.

Gauthier, P.J., Condomines, M., and Hammouda, T., (1999) An experimental investigation of radon diffusion in an anhydrous andesitic melt at atmospheric pressure: implications for radon

degassing from eruptive magmas. *Geochimica et Cosmochimica Acta* **63**, 645–656.

Gauthier, P.J., LeCloarec, M.F., and Condomines, M., (2000) Degassing processes at Stromboli volcano inferred from short-lived disequilibria (Pb-210–Bi-210–Po-210) in volcanic gases. *Journal of Volcanology and Geothermal Research* **102**, 1–19.

Gerlach, T.M., Westrich, H.R., and Symonds, R.B., (1996) Pre-eruption vapor in magma of the climactic Mount Pinatubo eruption: source of the giant stratospheric sulfur dioxide cloud. In: Newhall, C.G., Punongbayan, R.S. (Eds.), *Fire and mud: eruptions and lahars of Mount Pinatubo, Philippines*. University of Washington Press, Seattle and London, pp. 415–434.

Gill, J., Williams, K., and Bruland, K., (1985) Eruption of basalt and andesite lava degasses ^{222}Rn and ^{210}Po. *Geophysical Research Letters* **12**, 17–20.

Holland, AS.P., Watson, I.M., Phillips, J.C., Caricchi, L., and Dalton, M.P. (2011). Degassing processes during lava dome growth: Insights from Satiaguito lava dome, Guatemala. *Journal of Volcanology and Geothermal Research* **202**, 153-166.

Izbekov, P.E., Eichelberger, J.C., and Ivanov, B.V., (2004). The 1996 eruption of Karymsky volcano, Kamchatka: Historical record of basaltic replenishment of an andesite reservoir. *Journal of Petrology* **45**, 2325-2345.

Johnson, J.B., Lees, J.M., and Gordeev, E.I., (1998) Degassing explosions at Karymsky volcano, Kamchatka. *Geophysical Research Letters* **25**, 3999–4002.

Kayzar, T.M., Cooper, K.M., Reagan, M.K., and Kent, A.J.R. (2009). Gas transport model for the magmatic system at Mount Pinatubo, Philippines: Insights from (^{210}Pb)/(^{226}Ra). *Journal of Volcanology and Geothermal Research* **181**, 124-140.

Kazahaya, K., Shinohara, H., and Saito, G., (1994) Excessive degassing of Izu-Oshima volcano: magma convection in a conduit. *Bulletin of Volcanology* **56**, 207–216.

Mueller, S., Melnik, O., Spieler, O., Scheu, B., and Dingwell, D.B., (2005) Permeability and degassing of dome lavas undergoing rapid decompression: an experimental determination. *Bulletin of Volcanology* **67**, 526–538.

Phillips, J.C., and Woods, A.W., (2002). Suppression of large-scale magma mixing by melt-volatile separation. *Earth and Planetary Science Letters* **204**, 47-60.

Reagan, M., Tepley III, F.J., Gill, J.B., Wortel, M., and Hartman, B., (2005) Rapid time scales of basalt to andesite differentiation at Anatahan volcano, Mariana Islands. *Journal of Volcanology and Geothermal Research* **146**, 171–183.

Reagan, M.K., Tepley III, F.J., Gill, J.B., Wortel, M., and Garrison, J., (2006) Timescales of degassing and crystallization implied by ^{210}Po–^{210}Pb–^{226}Ra disequilibria for andesitic lavas erupted from Arenal volcano. *Journal of Volcanology and Geothermal Research* **157**, 135–146.

Rubin, K.H., van der Zander, I., Smith, M.C., and Bergmanis, E.C., (2005) Minimum speed limit for ocean ridge magmatism from ^{210}Pb–^{226}Ra–^{230}Th disequilibria. *Nature* **437**, 534–538.

Sato, K., and Sato, J., (1977) Estimation of gas-releasing efficiency of erupting magma from ^{226}Ra–^{222}Rn disequilibrium. *Nature* **266**, 439–440.

Shcherbakov, V.D., Plechov, P. Yu., Izbekov, P.E. and Shipman, J.S. (2011) Plagioclase zoning as an indicator of magma processes at Bezymianny Volcano, Kamchatka. *Contrib. Mineral. Petrol.* **162**, 83-99.

Sigmarsson, O., Condomines, M., and Bachelery, P. (2005) Magma residence time beneath the Piton de la Fournaise volcano, Reunion Island, from U-series disequilibria. *Earth and Planetary Science Letters* **234**, 223-234.

Sparks, R.S.J., (2003) Dynamics of magma degassing. In: Oppenheimer, C., Pyle, D.M., Barclay, J., J. (Eds.), *Volcanic Degassing*. Geological Society, London, Special Publications, vol. 213, pp. 5–22.

Stevenson, D.S., and Blake, S., (1998) Modelling the dynamics and thermodynamics of volcanic degassing. *Bulletin of Volcanology* **60**, 307–317.

Taran, Y.A. (2009) Geochemistry of volcanic and hydrothermal fluids and volatile budget of the Kamchatka-Kurile subduction zone. *Geochimica et Cosmochimica Acta* **73**, 1067-1094.

Thomas, N., Tait, S., and Koyaguchi, T., (1993) Mixing of stratified liquids by the motion of gas bubbles: application to magma mixing. *Earth and Planetary Science Letters* **115**, 161–175.

Turner, S., Black, S., and Berlo, K., (2004) ^{210}Pb–^{226}Ra and ^{228}Ra–^{232}Th systematics in young arc lavas: implications for magma degassing and ascent rates. *Earth and Planetary Science Letters* **227**, 1–16.

Turner, S., Sims, K.W.W., Reagan, M., and Cook, C., (2007) A ^{210}Pb–^{226}Ra–^{230}Th–^{238}U study of Klyuchevskoy and Bezymianny volcanoes, Kamchatka. *Geochemica et Cosmochimica Acta* **71**, 4771–4785.

Wallace, P.J., (2001) Volcanic SO_2 emissions and the abundance and distribution of exsolved gas in magma bodies. *Journal of Volcanology and Geothermal Research* **108**, 85–106.

CHAPTER 4

Investigating Uranium Distribution in Surface Sediments and Waters: A Case Study of Contamination from the Juniper Uranium Mine, Stanislaus National Forest, CA

Co-authors:
Adam C. Villa, Megan L. Lobaugh, Amy M. Gaffney, Ross W. Williams

ABSTRACT

The uranium concentrations and isotopic compositions of waters, sediment leachates and leached sediments from Red Rock Creek in the Stanislaus National Forest of California were measured to investigate the transport of uranium from a point source (the Juniper Uranium Mine) to a natural surface stream environment. The (^{234}U)/(^{238}U) composition of Red Rock Creek is altered downstream of the Juniper Mine. As a result of mine-derived contamination, water (^{234}U)/(^{238}U) ratios are 67% lower than in water upstream of the mine (1.114 -1.127 ± 0.009 in the contaminated waters versus 1.676 in the clean branch of the stream), and leached sediment samples have activity ratios in equilibrium in the clean creek and out of equilibrium in the contaminated creek (1.041-1.102 ± 0.007). Uranium concentrations in water, leached sediment and sediment leachates are highest downstream of the mine, but decrease rapidly after mixing with the clean branch of the stream. Uranium content and compositions of the contaminated creek headwaters relative to the mine tailings of the Juniper Mine suggest that uranium has been weathered from the mine and deposited in the creek. The distribution of uranium between sediment surfaces (leachable fraction) and bulk leached sediment suggests that adsorption is a key element of transfer along the creek. In clean creek samples, uranium is concentrated in the leached sediment residues, whereas in the contaminated creek, uranium is concentrated on the sediment surfaces (~70-80% of uranium in leachable fraction). Contamination only exceeds the EPA maximum contaminant level (MCL) for drinking water in the sample with the closest proximity to the mine. Isotopic characterization of the uranium in this system coupled with concentration measurements suggest that the current state of contamination in Red Rock Creek is best modeled by mixing between the clean creek and contaminated upper branch of Red Rock Creek rather than mixing directly with mine sediment.

1. INTRODUCTION

The transport of uranium through the environment is an issue of concern for many regulatory agencies because uranium is a heavy metal that is both chemically toxic and a radioactive material. Uranium occurs naturally in the environment as three main isotopes: ^{238}U, ^{235}U and ^{234}U. Uranium is nearly ubiquitously present in geologic formations at highly variable concentrations. In most geologic material, uranium concentrations are low and pose no hazard whatsoever to life. However, ore-grade deposits also occur naturally, with significantly higher

uranium concentrations. Prolonged exposure to moderate or high levels of uranium such as exist in ore-grade deposits can be harmful to plants, wildlife, and human populations (Ansoborlo *et al.* 2006; ATSDR 1999; Craft *et al.* 2004). Uranium and its daughter products of decay have been shown to cause genetic mutation and are known carcinogens (ATSDR 1999; Coryell and Stearns 2006; Vahakangas *et al.* 1992). Attempts to limit biological exposure to uranium drive a scientific interest in determining how uranium moves and where it is stored and released in nature.

The isotopic composition of uranium can provide clues to the sources and style of uranium transport especially when anthropogenic activities increase the input of uranium to natural systems. For example, natural surface waters typically have $(^{234}U)/(^{238}U)$ values that are higher than equilibrium (>1) (Ivanovich and Harmon 1992; Kronfeld and Vogel 1991). This is the result of the energetic alpha decay of ^{238}U to ^{234}U, which causes ^{234}U to be more easily leached from sediments into waters either by recoil directly from decay, or by damage to the lattice that holds the daughter nuclide ^{234}U (Cherdyntsev *et al.* 1955; Cowart and Osmond 1977; Fleischer 1988; Kigoshi 1971; Kronfeld 1974; Osmond and Cowart 1976). If an anthropogenic source of uranium to the environment, such as from uranium mining activity, has low $(^{234}U)/(^{238}U)$, addition of this uranium into a stream with high $(^{234}U)/(^{238}U)$ would lower the natural activity ratio of $(^{234}U)/(^{238}U)$. This is one example of how $(^{234}U)/(^{238}U)$ ratios can be used to identify varying sources of uranium in surface waters provided the composition of the different sources is well characterized. Isotopic compositions provide more information than concentration alone and can be used for chemical fingerprinting. Recording a high concentration of uranium in a sediment or water source provides no information about the origin of the uranium.

In this paper, we attempt to chemically fingerprint contamination from a uranium mine in a natural stream system using uranium isotopic compositions of stream water, sediment and sediment leachate. Mining has been found to amplify the levels of naturally occurring metal anomalies in rivers from geologic metal deposits (Helgen and Moore 1996). We propose that mining will increase the influx of uranium from a geologic source to a natural stream system enough to alter the uranium isotopic composition of the stream. Mining in the Sierra Nevada range of California has increased the amount of toxic metals available for transport through the

natural environment (Conaway *et al.* 2004; Goldhaber *et al.* 2009). Our work focuses on a creek emanating from the abandoned Juniper Mine in the Stanislaus National Forest onto recreational forest service land.

Uranium transport is affected by many variables in natural surface water environments including the organic content of the stream and sediment, the grain size and composition of sediment in the stream, the pH of the water in the stream, and the composition of other ions in the water with strong binding affinity for uranium (Cowart and Osmond 1977; Dosseto *et al.* 2006; Hostetler and Garrels 1962; Moliner-Martinez *et al.* 2004; Rodriguez *et al.* 2008; Ryu *et al.* 2009; Vandenhove *et al.* 2009). These variables can be difficult to isolate in large rivers and streams that often have multiple uranium sources such as groundwater aquifers, springs, and geologic units with variable uranium concentrations (Camacho *et al.* 2010; Chabaux *et al.* 2001; Moliner-Martinez *et al.* 2004; Ryu *et al.* 2009).

Red Rock Creek provides an ideal study area with a limited number of factors influencing uranium transport. The Juniper Mine represents a single point source to the natural stream system. The main channel of Red Rock Creek is entirely located in one large geologic formation (Relief Peaks Formation, see study area background for discussion) so we can assume that the natural lithology of the sediments is constant along the length of the creek. In addition, there is an upper branch of the Red Rock Creek that is isolated from contamination by the mine and can be used as a clean creek control sampling area. The goal of our study is to use this ideal environment to study uranium compositions in a natural surface water system versus a contaminated surface water system and to identify the extent and style of uranium transport from the mine onto recreational forest land.

2. MATERIALS AND METHODS

2.1 Study Area Background: Operation of the Juniper Mine and Geology of Red Rock Creek

The Juniper Mine is an abandoned uranium mine located in the Stanislaus River watershed of the Stanislaus National Forest in northern California. Geographically, the Stanislaus National Forest region comprises the western slope of the central crest of the Sierra Nevada range bounded by the Mokelumne River in the north, and Yosemite National Park in the south. The mine itself can be accessed from Forest Road 5N01 (Eagle Meadow Road) off of Highway 108 through Sonora Pass (**Figure 1A**).

Uranium was first discovered in the Sonora Pass region in 1955. The Juniper Mine operated from 1956-1966, producing approximately 45,500 pounds of U_3O_8 from ore that was mined and shipped to Salt Lake City, Utah for processing. This production is equivalent to roughly $1.6 million dollars of uranium, making the Juniper Mine the largest producer of uranium in California (Rapp 1981). Uranium mineralization in the Sonora Pass region is mostly found in the lower section of the Miocene volcanic Relief Peaks Formation, which consists of heterogeneous andesite lahar and conglomerate beds. The open pit of the Juniper Mine is in conglomerate with a friable matrix of medium to coarse-grained lithic sand containing minor amounts of carbonaceous matter (Rapp 1981). Uranium mineralization is thought to source from the Eureka Valley Tuff that overlies the Relief Peaks Formation in much of the Sonora Pass region. The Eureka Valley Tuff has glass compositions of uranium ranging from 10-14 ppm. Details of the geology of the Juniper Mine formations and bedrock can be found in Rapp (1981) and DOE open-file report GJBX-132 by Rapp and Short (1981).

The Juniper Mine was chosen for this study because there is a stream, Red Rock Creek, that emanates directly from the mine onto recreational forest service land. Elevated levels of uranium and gamma radiation have been detected in the vicinity of the mine (which is now closed to the public), raising contamination concerns (Department of Agriculture 2005). Uranium continues to migrate from the mine on sediments transported with spring runoff, frequent summer thunderstorms and windblown dust to areas used by the public, wildlife and grazing cattle (Department of Agriculture 2005). Red Rock Creek has two branches in its upper catchment. The first originates at an elevation of 2682 meters as a clean creek separated from the mine, while the second comes directly from a spring in the open pit of the mine at an elevation of 2590 meters. The two branches meet and mix roughly 30 meters below the mine and continue in a

single streambed for a distance of just over 3.2 kilometers before joining the Middle Fork Stanislaus River (**Figure 2**). The Relief Peaks Formation underlies the 1.9 kilometers of Red Rock Creek sampled for this study, providing consistent bedrock control, and allowing the assumption that stream sediment is compositionally homogeneous along the length of the creek. Thus, the Juniper Mine serves as a point source of uranium into a natural surface water environment where compositional variation of bedrock and source water as the origin of uranium isotope variability is insignificant. An additional creek, Salt Creek, that is separated from Red Rock Creek by a topographic ridge (**Figure 1B**) but is also in the Relief Peaks Formation is used here as a clean creek control site.

2.2 Sampling and Sample Preparation

Samples of sediments and waters were taken from nine sites in the Stanislaus National Forest in addition to one direct sample of the mine tailing sediment below the Juniper Mine open pit (**Table 1**). Three of these sites constitute "clean creek" environments (U-1, SC-8, SC-9) (**Figure 1B)**. The remaining 6 samples (U-2 through U-7) were taken at different distances away from the mine along the contaminated Red Rock Creek (**Figures 1B, 2**). Sediment samples were collected as bulk samples of the upper 5 cm of sediment on the creek bed equidistant (13 cm) from the bank at each sample site. Sampling was focused on areas of the creek with low flow rather than on the turbulent channel to focus on the finest-grained sediment that is preserved in low-flow conditions. Sediment samples were stored in plastic bags in the native creek water on ice for transport from the field to the laboratory where the stream water was poured off and the sediments were dried in an oven overnight at 76°C.

All laboratory procedures and analyses, with the exception of grain size analysis, were completed at Lawrence Livermore National Laboratory. Dried sediments were sieved to remove large grains over 2 mm in diameter and then ~ 100 mg aliquots of each sample were weighed and transferred to a centrifuge tube containing 4 mL of Milli-Q H_2O for leaching. Sieving samples prior to leaching allows us to compare the leachates and sediments between sites without the complication of large differences in grain size. The sediment was leached using 10 mL of 4M HNO_3 (an additional 3.5 mL of Milli-Q H_2O + 2.5 mL concentrated HNO_3). Sediment samples

were shaken for a minute every 30 minutes and leached for 2 hours after which the 4M HNO_3 leachate was transferred to clean 14 mL Teflon vials. The remaining sediment (post-leach) was transferred to 14 mL Teflon vials and digested in a 1:3 solution of concentrated HF:3M HNO_3 on a hotplate at 150°C for 2 days. The samples were then dried and 1 mL of concentrated HNO_3 + 0.5 mL concentrated HF was added. Samples were sonicated, heated overnight, and dried. Finally, 2 mL of Aqua Regia solution (1.5 mL HCl + 0.5 mL HNO_3) were added to break down fluorides and oxides that may have formed during digestion or were not completely digested. Samples were heated in Aqua Regia for 3 hours and then dried and converted to nitrate form for chemical separation using 5 drops of concentrated HNO_3.

Water samples were co-located with sediment sampling sites. Waters were collected in 250 mL polypropylene bottles filled completely to minimize the air volume in the bottle. The pH of each water sample was measured during collection. Waters were chilled for transport and acidified to 2% HNO_3 in the laboratory to prevent organic growth. Water samples were not filtered, so our samples represent a bulk sample of everything in the water column. 150 mL aliquots of each acidified water sample were weighed into Teflon beakers and dried on a hotplate at 125°C. Once dried, 5 mL of Milli-Q H_2O + 5 mL concentrated HNO_3 were added to each sample to decompose precipitates that formed as the water dried. Beakers were then capped, heated, and sonicated, following which the samples were transferred to 14 mL Teflon vials for uranium chemical separation. The water samples remaining after removal of the aliquots for uranium analysis were dried in Teflon vials and then re-constituted in 2% HNO_3 for trace element analysis by ICP-MS.

2.3 Uranium Purification and Analysis Techniques (MC-ICP-MS)

Prior to uranium purification, all samples (waters, sediment leachates, and digested leached sediments) were brought up in ~ 10 mL of 4M HNO_3 and spiked with a ^{233}U tracer. The samples were capped and heated overnight to equilibrate, and then dried. Concentrated HNO_3 was added to the samples, and they were dried again. This step was repeated several times to assure conversion to nitrate form. Samples were brought up in 0.5 mL of 4M HNO_3 for chemical separation of uranium. Uranium was separated using BioRad disposable columns with a 0.6 mL

(with the exception of the mine tailing sample, U-10S/U-Mine which required a 1.2 mL column volume) Eichrom UTEVA® resin bed. Columns were conditioned with Milli-Q H_2O and 4M HNO_3. Samples were loaded onto the columns in 4M HNO_3, washed with 9M HCl and 5M HCl, and U was eluted using 0.1M HCl. After column separation, the U-bearing solutions were dried, converted back to nitrate form, and dissolved in 2 mL of 2% HNO_3 for analysis by MC-ICP-MS.

Samples were analyzed on a Nu Plasma HR multi-collector ICP-MS from Nu Instruments Ltd. at Lawrence Livermore National Laboratory. Sample introduction was done using 2% HNO3 sample solutions and a Cetac Aridus II desolvating nebulizer equipped with a Cetac ASX-112FR Flowing Rinse Micro Autosampler. Certified reference materials used for isotope and concentration measurements were U010 and CRM-129. U010 is used to measure instrument bias and collector gains. CRM-129 is used as a quality control reference sample and was analyzed between every 3-5 samples to monitor instrument stability and accuracy. Expanded 2σ uncertainties are <1% for uranium concentration measurements (with the exception of SC-8 and SC-9 which have 2σ uncertainties of 1.12%). Isotopic composition measurements are reported with expanded 2σ uncertainties of ~0.5% for $^{234}U/^{238}U$ (with the exception of SC-8 and SC-9 with 2σ uncertainties <2%).

2.4 Grain Size Analysis Techniques (Camsizer)

The proportion of each sediment sample that was not used for U analysis was saved as dried sediment for grain size analysis. Aliquots of approximately 10-25 g of sediment from each sample were taken to allow for greater than 20,000 grains per analysis. Samples were sieved with a 32 μm sieve to remove fine material that is below the threshold of analysis. The weight percent of fine material removed from each sample is reported in Table 3. Once fines were removed, each sample was measured individually using a Retsch Technology CAMSIZER® instrument at the University of Washington.

2.5 Water Analysis Techniques (ICP-MS)

Water samples ranging in size from 75 to 125 mL were dried and then brought up in 10 mL of 1M high purity nitric acid. A 10x dilution was made using a 2% high purity nitric acid internal standard spiked solution. Analyses were performed on a Thermo Electron XSeries quadrupole ICP-MS. A fully quantitative analysis using a linear calibration curve based on known standards is performed. The internal standard corrects for instrument drift and suppression from the matrix. K, Fe, As and Se are run in CCT (Collision Cell Technology) mode due to polyatomic interferences. V, Cr and Mn are also run in CCT to confirm values obtained in regular mode that could be affected by high carbon and/or chloride content. Raw data are reported as ng/g (ppb). These results are corrected back through the 10x dilution to the 10 mL volume of the original sample and reported in μg/g. NIST traceable certified reference material 1643e and the National Research Council of Canada's river water reference material, SLRS4, were analyzed for accuracy. The sample SC-9 was prepared in duplicate to assess the level of precision. Duplicate standard error is better than 1% for most elements with the exception of those listed here with their corresponding standard error (Cr 3%; Co 3%; Ga 2%; As 6%; Sb 10%; Nd 2%, Eu 4%; Tb 2%; Hf 2%; Pb 2%).

3. RESULTS

3.1 Uranium Isotopic Compositions

The $(^{234}U)/(^{238}U)$ measured values (parentheses denote activity ratios) for all samples from this study are reported in **Table 2** and shown in **Figures 3A-B**. Variations greater than the analytical uncertainties (Table 2) are measured between clean and contaminated water, sediment, and leachate samples from Red Rock Creek. Water samples from the clean Salt Creek (SC-8 and SC-9) have $(^{234}U)/(^{238}U)$ of 1.247 and 1.256 respectively. The water sample from the clean branch of Red Rock Creek has a slightly higher $(^{234}U)/(^{238}U)$ of 1.676, recording some natural variation in the isotopic composition of uranium between the two different clean creek environments (Salt Creek and Red Rock Creek). To interpret changes at Red Rock Creek, we will, therefore, focus our comparisons mainly to the clean Red Rock Creek control sample. Measured $(^{234}U)/(^{238}U)$ in

water samples from the contaminated branch of Red Rock Creek range from 1.114 to 1.127 ± 0.009. Therefore, the (^{234}U)/(^{238}U) composition of the surface creek water is measurably distinct and on average ~ 67% lower than natural Red Rock Creek water as a result of mine contamination.

Sediment (^{234}U)/(^{238}U) values fall approximately near equilibrium for clean uncontaminated sediments in Salt Creek and Red Rock Creek. The natural range in (^{234}U)/(^{238}U) in clean branches is 1.004 to 1.026 and the clean branch of Red Rock Creek is the sample that records an equilibrium (^{234}U)/(^{238}U) of 1.004 ± 0.007. Contaminated sediments from samples U-2 through U-7 record higher (^{234}U)/(^{238}U) values between 1.041 and 1.513. Sample U-6 has an anomalously high (^{234}U)/(^{238}U) of 1.513 and if this sample is excluded, the range in (^{234}U)/(^{238}U) for the contaminated creek becomes 1.041 to 1.102 ± 0.007. Even with excluding the anomalous U-6 sample site, the sediments in all contaminated samples have (^{234}U)/(^{238}U) values higher than equilibrium. The (^{234}U)/(^{238}U) of contaminated sediment decreases with distance downstream (**Figure 3B**). Sediment from the mine tailing pile within the Juniper Mine has a (^{234}U)/(^{238}U) of 1.145 ± 0.007 consistent with the tailings being the source of the higher (^{234}U)/(^{238}U) of the contaminated sediments. Sediment leachates from clean creek samples have (^{234}U)/(^{238}U) that tend to closely replicate the (^{234}U)/(^{238}U) of their associated surface waters (**Figure 3A**). The (^{234}U)/(^{238}U) of sediment leachates from contaminated creek samples is variable but always lower than what was measured in clean sediment leachates.

3.2 Uranium Concentrations

Measured uranium concentrations for all samples are reported in **Table 2** in μg/g (ppm) for sediments and sediment leachates and ng/g (ppb) for waters. In general, the concentration of uranium measured in all sample types from Red Rock Creek (sediments, leachates, and waters) decreases with distance away from the Juniper Mine open pit (**Figure 4A-C**). Concentrations decrease rapidly in the first 0.3 km and then level off. Clean creek water samples have uranium concentrations between 0.128 ppb and 0.148 ppb in Salt Creek and 0.022 ppb in Red Rock Creek with 2σ errors of ~1%. The contaminated branch water of Red Rock Creek (site U-2) has a uranium concentration of 52.4 ± 0.3 ppb, which is above the EPA maximum contaminant level

(MCL) of 30 ppb for drinking waters. The uranium concentration in the water declines rapidly below the mixing point of the contaminated and clean branches of Red Rock Creek. At a distance of 62 meters the concentration of uranium in the creek is 11.58 ppb and decreases to 3.35 ppb at 750 meters from the mixing point (**Figure 4A**).

Concentrations of uranium in the clean creek sediment leachate samples average to approximately 1 ppm uranium, which is consistent with naturally occurring concentrations of uranium in sediment. The leachate from the contaminated branch of Red Rock Creek contains 22.1 ± 0.2 ppm uranium. Therefore, the concentration of uranium in the contaminated branch is over an order of magnitude higher than concentrations measured in the clean sample locations. Downstream from the mixing point of both upper branches, the concentration of uranium in sediment leachates ranges from 18.9 to 6.64 ppm. Sample U-6 has a uranium concentration lower than the samples both upstream and downstream of this location. Because of this variation, there is no correlation between distance from the mine and the concentration of uranium leached from sediments. The concentration of uranium in the leachate from the mine tailing sediment is 11.35 ± 0.09 ppm. This value is approximately 10 ppm lower than the leachate from sediment in the contaminated creek and will be discussed below in section 4.2.

Sediments from all sample sites were completely digested after leaching to measure the total uranium concentration of the sediment. Uranium concentrations in clean creek sediments ranged from 2.09 - 2.37 ppm at Salt Creek to 2.59 ± 0.02 ppm in the non-contaminated branch of Red Rock Creek. The contaminated creek sediments contain concentrations of uranium that are higher than the clean creek sediments (7.68 – 3.14 ppm) at all sites (**Table 2**). The highest uranium concentration of 7.68 ppm is measured in the contaminated branch of Red Rock Creek above the mixing point (site U-2). This site has more uranium in the sediment than the sediment from the mine tailings (4.29 ppm) similar to what was observed with the concentration in the leachate samples. The elevated uranium concentrations in the leached sediment suggest that contamination of the sediment in the creek is extensive and not entirely removable with a 4M HNO_3 solution.

3.3 Grain Size Measurements

The mean grain size of each creek sediment sample is reported in Table 3. In general, there is variation on the order of <1 mm for all sediment grain size means. However, there is measurable difference in the size of sediments from the more energetic upper branches of Red Rock Creek and the flatter low energy stream channel downstream. Sediment in the upper branches (>1 mm diameter mean) is slightly larger than sediment downstream (range from 0.21 to 0.64 mm diameter means). A mean sphericity of each sediment sample is also reported in Table 3. Sphericity is calculated by the Retsch Technology CAMSIZER® instrument digital image algorithm software which uses Equation 1 below and the measured perimeter of a particle projection, P, as well as the measured area covered by the particle projection, A.

$$SPHT = \frac{4\pi A}{P^2} \quad (1)$$

From the area of the sediment particle projections, the digital image algorithm also calculates the average particle diameters, D, based on the assumption that each sediment particle is a sphere and has an area equivalent circle (Equation 2).

$$D = \sqrt{\frac{4A}{\pi}} \quad (2)$$

Combining the sphericity and diameter equations, it is possible to calculate an average perimeter of each sediment sample (Equation 3). We will use this calculated perimeter as an approximation for the surface area of the sediment below to discuss whether or not adsorbed uranium contamination correlates with measured grain sizes and surface area. Both grain size and calculated perimeters of sediment samples decrease downstream with the exception of sample U-6, which has an anomalously higher grain size and perimeter than the samples both upstream and downstream of this location (Table 3).

$$P = \frac{\pi D}{\sqrt{SPHT}} \quad (3)$$

3.4 Surface Water Compositions

The waters of Red Rock Creek were collected in July of 2010 and recorded pH values (measured in the field during collection) between 4.7 and 5.2 (**Table 1**). Major element and trace element compositions of the surface waters collected at each site are presented in **Table 4**. The major cation concentrations (e.g. Mg, Ca, Na, Fe, etc.) in the contaminated creek are significantly higher than the clean branch of Red Rock Creek and signify a compositional change in the water associated with the mine input. Overall, the concentrations of most measured major and trace elements decrease downstream of the mixing point of the two branches of Red Rock Creek. The concentration of As and Mo is much higher in sites close to the Juniper mine. Sample U-3, taken just below the mixing point of the two branches shows the most compositional variation relative to other waters of Red Rock Creek.

4. DISCUSSION

4.1 Uranium Isotopic Compositions and Mixing

Mobilization of uranium from the Juniper Mine alters the isotopic composition of Red Rock Creek. $(^{234}U)/(^{238}U)$ ratios are lower in contaminated waters and sediment leachates than values measured in the clean creek environment control samples (**Figure 3A**). Kronfeld and Vogel (1991) observed similar behavior in rivers draining uranium mining areas and showed that $(^{234}U)/(^{238}U)$ decreased when uranium concentrations increased. Therefore, we interpret the lowered $(^{234}U)/(^{238}U)$ in the contaminated branch of Red Rock Creek to be the result of the addition of uranium from the mine (likely as both bulk sediment with a high uranium concentration and as dissolved uranium – discussed more below). Sediment leachate samples show a similar trend with lower (but still in excess of equilibrium) $(^{234}U)/(^{238}U)$ observed in the contaminated sample sites. The leachates, however, also reflect the water that is passing by the sediments (**Figure 3A**). In clean creek samples, leachates have high $(^{234}U)/(^{238}U)$ similar to the natural water compositions. In the contaminated creek, the compositions of leachates are slightly more variable but again are similar to the waters from the same site locations. Kronfeld and Vogel (1991) also reported that the isotopic composition of leachable uranium from river

sediment is similar to that in the water, and our data are consistent with this observation. Small variations between uranium compositions in leachates and leached sediments in the contaminated creek can be the result of many stream factors discussed below (organic content, composition of sediments, pH, etc.). The lower (^{234}U)/(^{238}U) in the leachate relative to the leached sediment at site U-2 may imply that this site (which is closest to the mine) has a higher proportion of contamination via particle transfer relative to dissolved uranium contamination. Site U-6 which also shows this pattern is discussed in detail later in this section.

The mine tailing sediment leachate records the lowest (^{234}U)/(^{238}U) with a value well below equilibrium. This suggests that ^{234}U from the tailing has been preferentially removed and transported from the tailing pile to the stream environment leaving a higher relative abundance of ^{238}U, which results in a uranium composition with an activity ratio below equilibrium.

Unlike the water and leachate samples, the (^{234}U)/(^{238}U) in leached contaminated sediment samples is higher than in clean creek samples, which have near equilibrium values (**Figure 3A and B**). The higher (^{234}U)/(^{238}U) in leached contaminated sediments, compared to leached uncontaminated sediments, shows that contamination is not completely removed by our leaching procedure. Therefore, contamination must be distributed in phases that are resistant to 4N HNO_3 or there is contamination in the form of whole sediment grains that have been transported from the mine. Sediment from the mine site has high (^{234}U)/(^{238}U) relative to the clean creek so we hypothesize that some of this sediment has been transported from the mine to the creek and is present in the sediment fraction that was analyzed. This would suggest that contamination moves from the mine to the creek not only as dissolved uranium species but also as suspended sediment. Suspended sediment could be easily transported during large rainstorms and deposited in the creek bed. In addition, the (^{234}U)/(^{238}U) composition of sediment decreases with distance downstream from the contaminated branch of Red Rock Creek (**Figure 3B**) further supporting the hypothesis that the elevated (^{234}U)/(^{238}U) is directly related to mine contamination.

Site U-6 has the most distinct sediment uranium composition (higher (^{234}U)/(^{238}U) than any other sediment including the mine tailings). This composition cannot be explained by any of the stream conditions that we measured as part of this study (grain size, pH, water composition).

However, other variables mentioned earlier, including colloidal transport of uranium, organic content, and composition of the sediment may be the reason for why site U-6 records such a high activity ratio. It was shown by Rapp (1981) that the Sonora Pass region geology contains sporadically distributed zones of uranium enrichment (50-500 ppm) whereas most areas have < 10 ppm U. Therefore, it is possible that there is a minor compositional change in the bedrock or sediment load at site U-6 that may affect the $(^{234}U)/(^{238}U)$. For example, in the Juniper Mine area, carbonaceous matter is distributed as discrete thin beds or streaks (Rapp 1981) and carbonate has a strong affinity for uranium. If there were a thin carbonate bed at the U-6 locality that affects stream sediment composition, then this may preferentially adsorb U from the water column. Also, increases and decreases in discharge or flow can affect $(^{234}U)/(^{238}U)$ ratios (Chabaux *et al.* 2005). This study did not include any flow rate measurements of waters at various sites along Red Rock Creek and cannot confirm whether there is a significantly different flow regime at site U-6.

To test whether or not the variations in uranium isotopic composition of the leached sediments and leachates can be explained completely by mixing between the clean creek sediments and leachates of Red Rock Creek and those of the mine, we calculated mixing models using two end-member sample compositions for mixing: the uranium mine tailings (U-Mine) and the clean Red Rock Creek sample (U-1) located geographically above the mine. Mixing curves for leachates and leached sediments are shown in **Figure 5A and B**. Using these end-member compositions resulted in mixing curves that deviate from contaminated creek sediment and leachate data denoting that the mine sediment is not an appropriate end-member likely resulting from its exposure to surface processes over time. For example, $(^{234}U)/(^{238}U)$ lower than unity in samples, similar to the leachate from the mine tailings, has been shown to result from the mobilization of uranium from materials that have been weathered (Chabaux *et al.* 2001). It is also possible that our sample from the Juniper Mine tailings is not representative of the range of uranium composition within the mine ore given that mines can have multiple zones of mineralization.

Mixing was also modeled using only creek end-members. Rather than the mine sediment representing the contaminant, the sediment and leachate from the contaminated creek branch above the mixing point (site U-2) were selected as the end-members to mix with the clean Red

Rock Creek compositions. These mixing curves fit more measured data for the leachates and sediment samples implying that mixing between the creek branches plays an important role in the isotopic signatures of Red Rock Creek (**Figure 5C and D**). Observed deviations from the mixing lines may, again, be due to changes in lithology of the sediments, stream flow, and organic content discussed above.

4.2 Downstream Spatial Trends

Uranium concentration results for water, leachate, and sediment samples all show elevated concentrations of uranium in the contaminated branch of Red Rock Creek. These concentrations decrease with distance from the mixing point of the contaminated and clean branches systematically (ignoring variation discussed above with site U-6). An interesting observation is that the uranium content of both the leachate and the sediment from site U-2 in the contaminated creek is much higher than the uranium content of the sediment taken directly from the tailings of the Juniper Mine (U-Mine) (**Figures 4B and C**). We interpret this to be the result of uranium transfer from the mine to the contaminated creek where uranium has adsorbed onto the sediment in the contaminated stream branch. The U-Mine sediment sample has very low (^{234}U)/(^{238}U) which is consistent with this interpretation because low activity ratios typically suggest that sediment has been weathered and has lost the more mobile ^{234}U component of the total uranium. It is possible that areas of the mine have a higher U concentration than the mine tailing that we sampled; however, a large detailed study outside of the scope of this work is needed to characterize whether or not U concentration may be higher relative to site U-2.

While the concentration of uranium decreases with distance from the mine in all sampled components of the creek (water, sediment), we did not sample far enough along Red Rock Creek to see the concentration of uranium in water and sediment samples return to background natural levels of less than 0.2 ppb (water) and less than 2.56 ppm (sediment). From these data we can infer that the influence of the mine reaches farther than 1.9 km onto recreational land (distance sampled). However, the uranium concentrations are low and far below EPA levels of concern for biologic exposure. If we fit a linear decreasing trend to leachate data for samples U-4, U-5, and U-7 downstream of the mixing zone, we can extrapolate this trend to estimate where the

downstream influence of the mine would return to background. Using this method suggests that mine contamination would not be measurable ~ 4.5 km downstream of the mixing zone. However, Red Rock Creek joins with the Middle Fork Stanislaus River just over 3.2 km downstream and U concentrations would likely be highly diluted at this convergence.

4.3 Mechanisms of Uranium Transport

Oxidized river waters tend to dissolve the oxidized U(VI) uranyl ion, UO_2^{2+} as complexes with carbonate, phosphate, or sulfate (Sheppard 1980). However, uranium transport can occur by other mechanisms as well including cationic exchange in the water column, binding of uranium to organic molecules and colloids, and the transfer of sediment particles with adsorbed uranium on their surfaces. Here we use sediment grain size data as well as the geochemistry of the Red Rock Creek surface waters to attempt to understand which uranium transport processes may dominate in the system downstream of the Juniper Mine.

Our results demonstrate that uranium isotopic compositions vary systematically in the waters and sediments of Red Rock Creek (**Figure 3**). Large variations in uranium concentration and $(^{234}U)/(^{238}U)$ have been known to occur across redox barriers in nature (Cowart and Osmond 1977); however, we have no reason to believe that the redox conditions of the stream studied here would vary over such short spatial scales (< 3 km). Therefore, changes in the activity ratios from site to site are likely a function of processes aside from redox conditions. Dosseto *et al.* (2006) show that the smallest grain sizes of river sediment correspond to the highest $(^{234}U)/(^{238}U)$ and suggested that variations in $(^{234}U)/(^{238}U)$ correlate with organic content which is concentrated in the smallest grain sizes. We find the opposite correlation between grain size and $(^{234}U)/(^{238}U)$. The largest mean grain size samples have higher $(^{234}U)/(^{238}U)$ (**Figure 6A**). Separating the effect of grain size versus the effect of organics is not possible in our samples, and clay size fractions have the lowest solid-liquid partition coefficients for uranium while organics have the highest partition coefficients (see review, EPA 1999) so these variables have competing effects on uranium mobilization. However, if we assume that the composition of the leachable component is partially a reflection of the water the sediment is in contact with (Kronfeld and Vogel 1991), then our observation that the samples with the largest mean grain sizes have the

highest (^{234}U)/(^{238}U) would suggest that larger grains are more natural in composition. Natural waters tend to have elevated (^{234}U)/(^{238}U). Conversely, the observation that the leachate samples from the sites with the smallest mean grain size have the lowest (^{234}U)/(^{238}U) would mean that these grains have been preferentially contaminated. Therefore, it is possible that smaller size sediment does in fact contain more organics and surface area with which to bind contamination, but in the Red Rock Creek case there is a higher activity of ^{238}U from the contribution of uranium sourcing from the Juniper mine. It is also possible that fine sediments include fine-grained particulate contamination that has been transported downstream from the mine. The degree of correlation between (^{234}U)/(^{238}U) and mean grain size increases if only the sample sites that are contaminated are used (**Figure 6B**). It is important to note that a concentrated 4M HNO_3 leach was used to produce the leachate samples; therefore, the compositions of the leachates do not represent only an exchangeable fraction of the sediment, but also include mineral and organic compositions that can be digested with a 4M acid. There is no correlation between uranium concentrations in sediments and leachates and grain size in the system so while grain size may affect the ability to bind contaminant uranium, the grain size does not control the overall behavior of uranium distribution in the stream. The data show the same patterns if the calculated perimeters of grains used as a proxy for surface area of the sediment rather than grain size.

The major and trace element compositions of surface water allow us to investigate the degree to which uranium transport correlates with chemical parameters of the stream. Weathering and downstream transport of sediment particles and dissolved ions can transfer uranium from a point source downstream. Correlations between cation and uranium concentrations in surface waters have been proposed to be a function of increased weathering in rivers (Moliner-Martinez *et al.* 2004) assuming that uranium is mobilized at the same time as other cationic species. Data from Red Rock Creek show a positive correlation ($R^2 = 0.81$) between total cation content in water (calculated as the sum of Na, Ca and Mg) and the uranium concentration in the water (**Figure 7A**). This can be a function of cation exchange transport of uranium, or of weathering mobilizing both uranium and major cations in the water column.

Particulate uranium has been shown to be associated with high Fe in colloidal fractions, amorphous Fe, and Fe-oxide components (Carvalho *et al.* 2005; Hsi and Langmuir 1985;

Vandenhove *et al.* 2007, 2009). To examine if uranium transport in Red Rock Creek is correlated to Fe-bearing phases, we normalized the U concentration in water samples to the Fe concentration. After normalization between sites, there is still a correlation between total cation content and U/Fe, but the correlation coefficient is lower ($R^2 = 0.63$) showing that sorption onto Fe bearing phases, if present, does not dominate the transport of U through the water column (**Figure 7B**). The change in correlation coefficient potentially signifies that Fe phases help to mobilize uranium that may already be being transported as a result of cation exchange and other mechanisms; however, there is no direct correlation of uranium concentrations with Fe content in the waters of Red Rock Creek. Uranium concentrations do, however, correlate with minor metal trace elements in the waters, notably As and Mo (**Figure 8**). These correlations are likely the response of weathering of mine sediment that has been enriched in metal species during earlier mineralization and formation of the Juniper Mine ore body.

Many studies have suggested that pH and dissolved carbonate complexes are the two most important factors that influence the adsorption of U(VI) in rivers onto sediments since uranium speciation is related to pH (Echevarria *et al.* 2001; EPA 1999; Langmuir 1978; Vandenhove *et al.* 2007). Using Mg/Na and Ca/Na, similar to Ryu *et al.* (2009), we can approximate the carbonate versus silicate component dissolved in the waters of Red Rock Creek (**Figure 9**). Our data for water compositions form a linear trend in Mg/Na vs. Ca/Na space ($R^2 = 0.87$) and the most contaminated sample (U-2) has the highest Mg/Na and Ca/Na, while the clean creek samples have the lowest ratios. While this is an approximation for the carbonate component in the system, it may imply that dissolved carbonate species affect the amount of uranium that is dissolved in the water column. The concentration of uranium in sediment leachate samples also correlates with the pH of the sites and forms a similar trend with the most contaminated sample (U-2) having the highest pH and the clean creek samples having the lowest pH. Data from Red Rock Creek, therefore, support previous observations that pH and carbonate components affect the uranium concentration of waters.

Adsorption of uranium onto charged sediments, colloids, and organic molecules occurs in all stream systems. To quantify the extent of sediment adsorption in the Red Rock Creek system, we compared the concentration of uranium in the 4M HNO_3 leachates at each site to the

concentration of uranium in the complete leached sediment digestion. Doing so, it is possible to calculate the leachable fraction (leachates only) of total uranium (leached sediments + leachates) in the sediments from site to site (**Figure 10**). The results show striking variation between the distributions of uranium in the sediment of a clean creek versus a contaminated creek. The clean system samples (U-1, SC-8, SC-9) have ~ 30% of the total uranium in the leachable component, while the bulk of the uranium is contained in the sediment itself. However, in the contaminated creek, ~ 70-80% of the total uranium content of the sediment is in the leachable component. Therefore, in the contaminated sections of Red Rock Creek, uranium is concentrated onto the surfaces of the sediments. This suggests that adsorption is a dominant process during uranium transport through the creek system.

5. CONCLUSIONS

The natural (^{234}U)/(^{238}U) signature of Red Rock Creek is altered due to contamination from the Juniper Mine. As a result of uranium input, (^{234}U)/(^{238}U) is lowered in waters and sediment leaches and raised in sediments, relative to the clean creek reference compositions. Mixing models using isotopic compositions indicate that the source of uranium contamination is the contaminated creek headwaters and sediments in the branch of Red Rock Creek emanating directly from the mine. The isotopic composition and concentration of the mine tailings suggest that uranium has been transferred from mine tailings to this contaminated creek branch over time. We propose that uranium is transported to the creek likely as both a dissolved uranium fraction and as small particulate matter or suspended solids. The distribution of total uranium in sediment strongly shows that adsorption has a dominant role in controlling uranium distribution in the system. Stream action likely causes the weathering of sediments in the contaminated creek headwaters, mobilizing contamination in the form of dissolved uranium (correlations with cation contents in water) and suspended sediment that is transported downstream. The amount of contamination decreases downstream but does not return to clean levels recorded upstream of the mine denoting that the influence of the mine extends beyond the area sampled by this study and that the dynamic stream is continuing to move mine-associated material. Results from this work demonstrate the need for isotopic investigations of contamination. Concentration alone cannot expose the level of detail that isotopic compositions reveal about environmental systems.

FIGURES

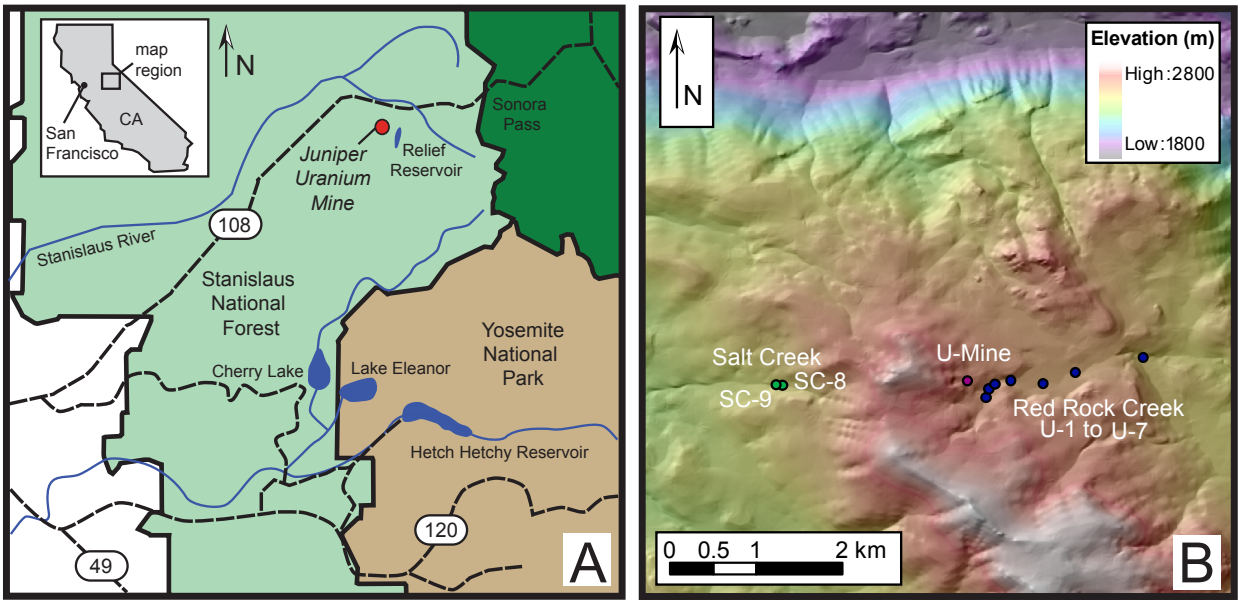

Figure 1. Location of Juniper Uranium Mine. **A.** The mine is located in the Stanislaus National Forest south of Highway 108 and west of Relief Reservoir. **B.** Digital elevation model showing the location of the Juniper Uranium Mine relative to Red Rock Creek and Salt Creek. The clean Salt Creek is separated from the mine by a topographic ridge that runs roughly N-S.

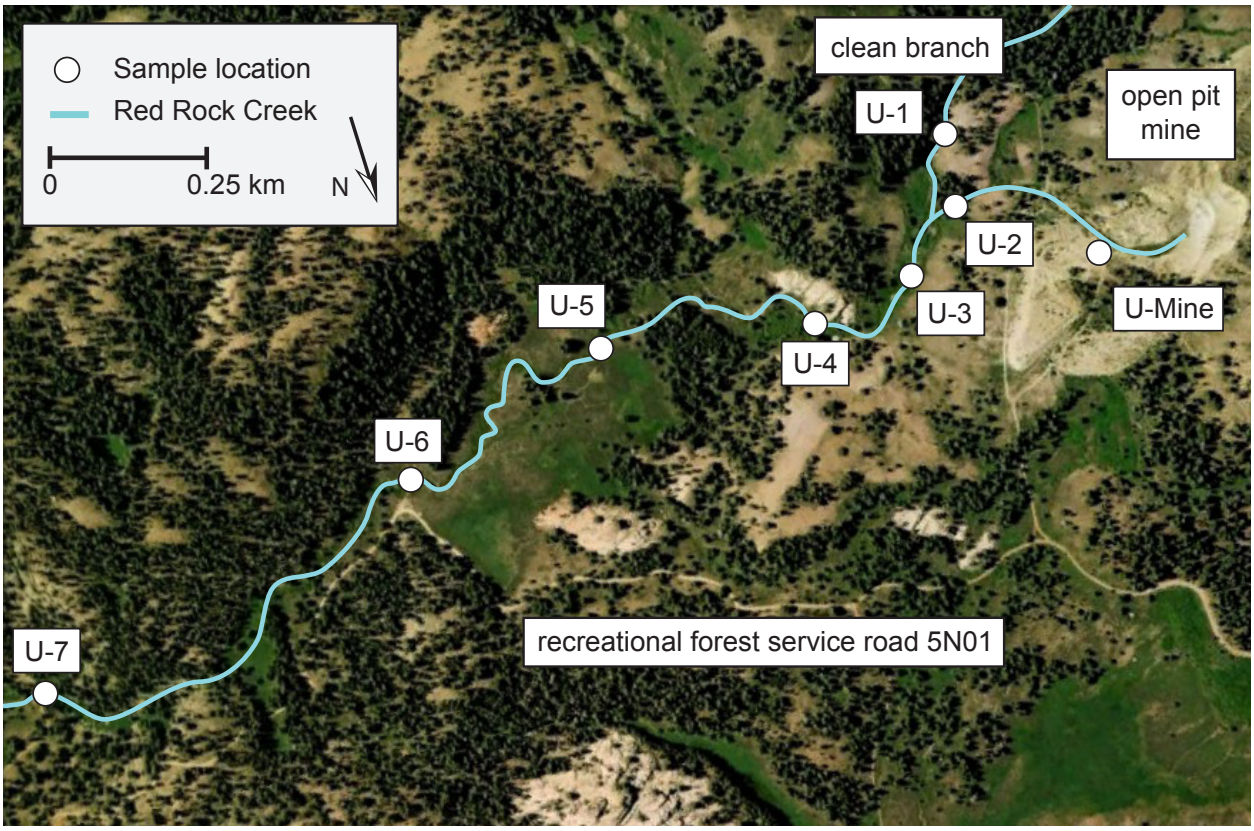

Figure 2. Aerial image of Red Rock Creek and the sampling area. The open pit of the Juniper Uranium Mine is located in the upper right. Red Rock Creek has two upper branches, one of which is separated from the mine and is not contaminated (U-1, clean branch). The branches mix just above sample site U-3 and then continue downstream to sample sites U-4 through U-7. Distances between sampling points are provided in Table 1. Image modified from Google Earth.

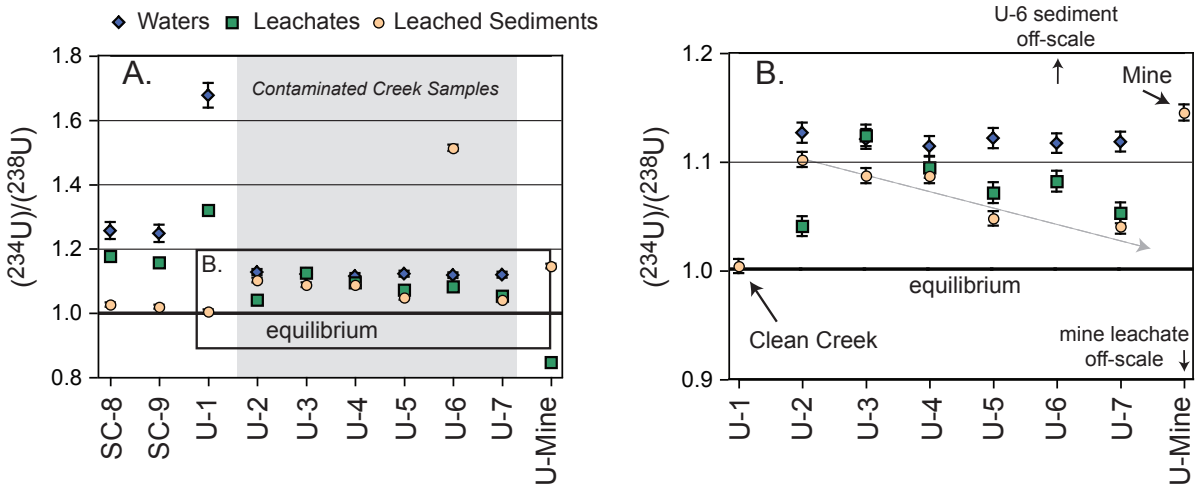

Figure 3. Uranium isotopic compositions of waters, sediment leachates, and sediment. Data are shown as (^{234}U)/(^{238}U) activity ratios (parentheses denote activity). Error bars are shown where larger than symbols. **A.** Red Rock Creek samples downstream of the mine (U-2 to U-7) are denoted as contaminated samples by the gray shaded region. Waters and leachates in the contaminated branch of Red Rock Creek display lower (^{234}U)/(^{238}U) than the clean creek. Leached sediments record higher (^{234}U)/(^{238}U) in the contaminated creek samples relative to the clean creek control samples. The mine tailing has sediment that is out of equilibrium (^{234}U)/(^{238}U)>1 and the leached outer surface records (^{234}U)/(^{238}U) <1. **B.** Closer view of inset from **A.** showing data for the contaminated section of Red Rock Creek. Sediment (^{234}U)/(^{238}U) measurements are elevated above equilibrium in the contaminated creek and the degree of (^{234}U)/(^{238}U) disequilibrium decreases downstream (shown by grey dashed arrow). This trend records the extent of contamination and mixing from the mine into the clean creek (mine and clean creek samples are labeled).

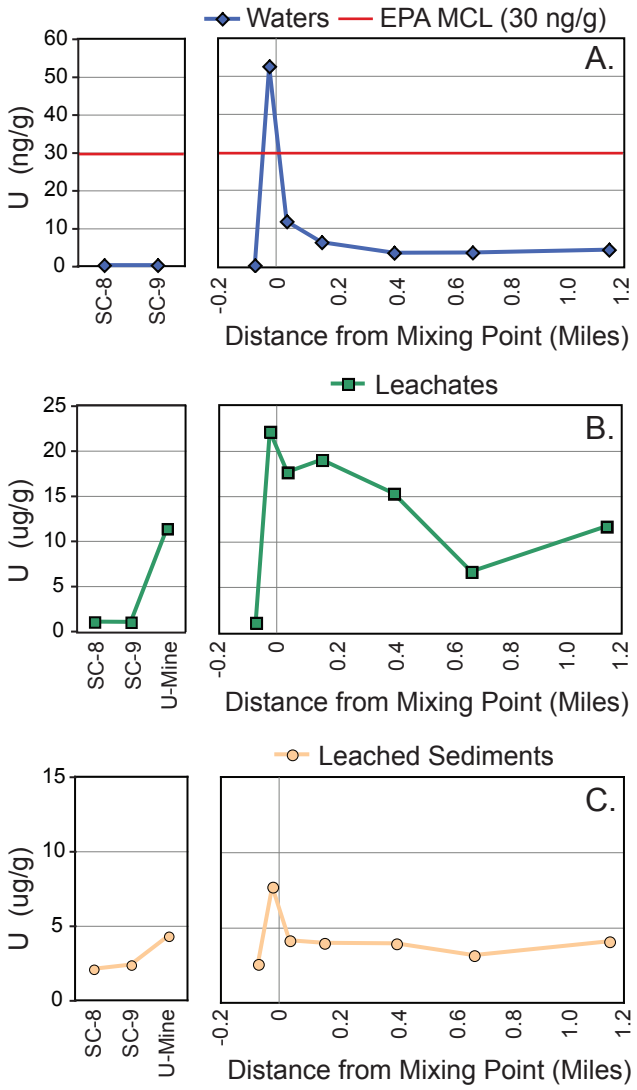

Figure 4. Uranium concentrations in water (**A.**), sediment leachate (**B.**), and leached sediment samples (**C.**). Uncertainties are smaller than symbols. Clean creek control samples from Salt Creek are plotted in the boxes to the left of the diagram with data from the mine tailings at the Juniper Mine. Red Rock Creek samples are plotted according to distance along the creek. The confluence of the clean branch of Red Rock Creek and the contaminated branch emanating from the mine is expressed at the mixing point and given a distance of zero for reference. **A.** Water from site U-2 just upstream of the mixing point has high U concentrations above the EPA Maximum Contaminant Level (MCL) of 30 ng/g (EPA Water). Uranium concentrations decrease rapidly after mixing with the clean creek. **B.** and **C.** Sediment leachates and complete leached sediment digestions record high U concentrations in the contaminated creek branch. These concentrations also decrease downstream following the same behavior as the water samples. The sediment leachates and leached sediments from the contaminated branch of Red Rock Creek have higher U concentrations than the mine tailing from the Juniper Mine.

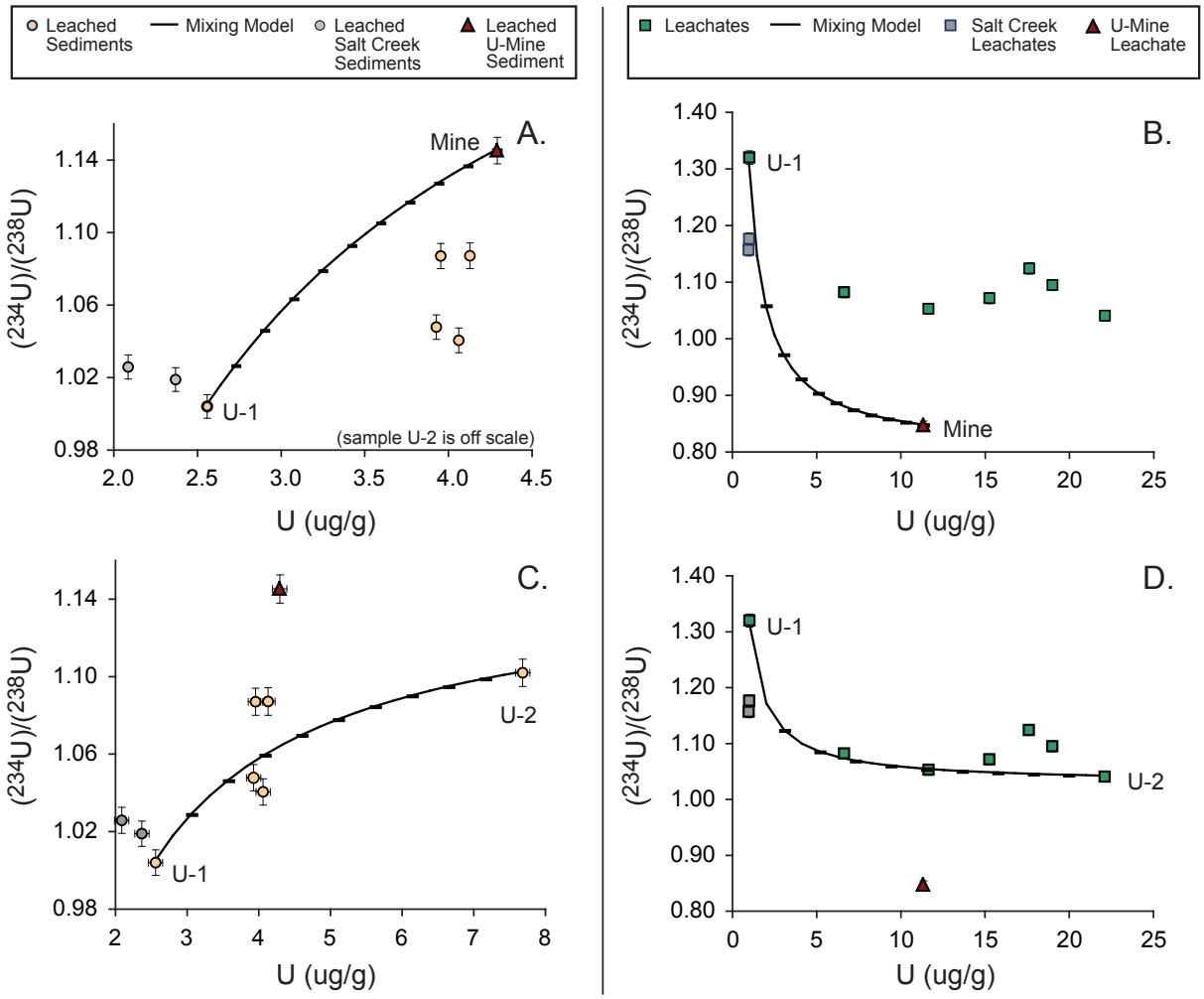

Figure 5. Mixing models to identify source end-members for uranium contamination. Tick marks denote 10% increments of mixing between end-members. **A.** and **B.** Mixing models for leached sediments (**A.**) and leachates (**B.**) using the clean Red Rock Creek sample (U-1) and the mine tailing (U-Mine) as end-members. Data do not fall close to the mixing line. **C.** and **D.** Plots after re-calculating mixing assuming new end-members: the clean Red Rock Creek sample (U-1) is re-modeled but mixed with the contaminated Red Rock Creek upper branch sample (U-2). This model fits the data much better than using the Juniper Mine tailing as an end-member source for contamination. It is likely that the mine tailing isotopic composition has been altered as a result of surface weathering.

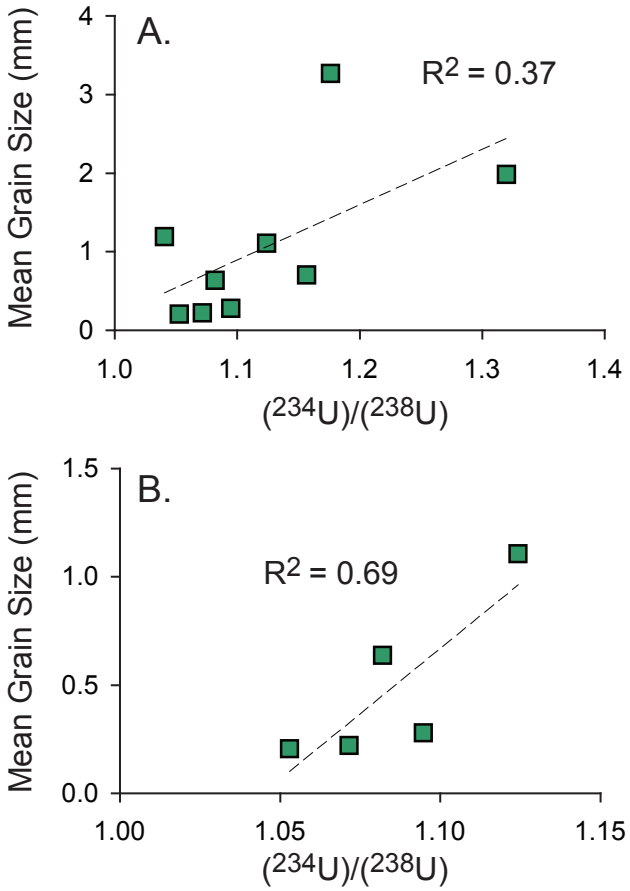

Figure 6. Variation of (^{234}U)/(^{238}U) in leachate samples as a function of grain size. **A.** There is a positive correlation between (^{234}U)/(^{238}U) and grain size with contamination associated with smaller grain sizes (lower (^{234}U)/(^{238}U)). **B.** If only the samples taken downstream of the mine locality are used, the correlation increases from 0.37 to 0.69.

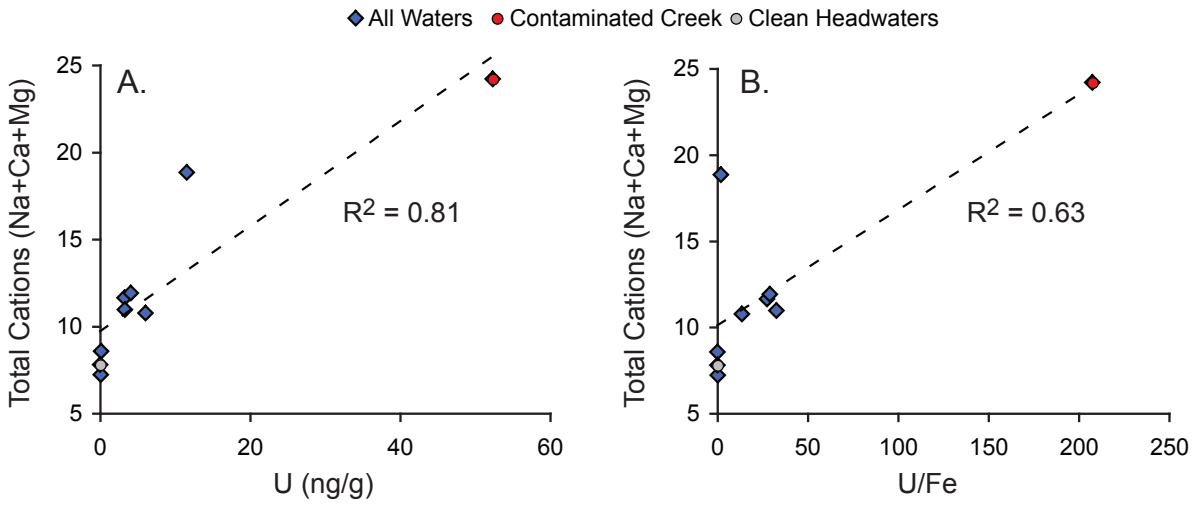

Figure 7. Correlations between total cations and U concentration and Fe-content and U concentration in water samples from Red Rock Creek. **A.** Positive correlation between the cationic concentration (plotted here as Na+Ca+Mg) of Red Rock Creek water and the U concentration of the water. The most contaminated sample (U-2) is plotted as the contaminated creek sample and records the both the highest total cation concentration and U concentration. The clean creek samples comprise the low concentration end of the correlation and the samples from along Red Rock Creek plot between these two end-members. **B.** Normalizing U concentration to Fe concentration in the waters decreases the correlation slightly (0.63 from 0.81). Plots show that both cation exchange transport and Fe-bearing phase mobilization of uranium take place in Red Rock Creek.

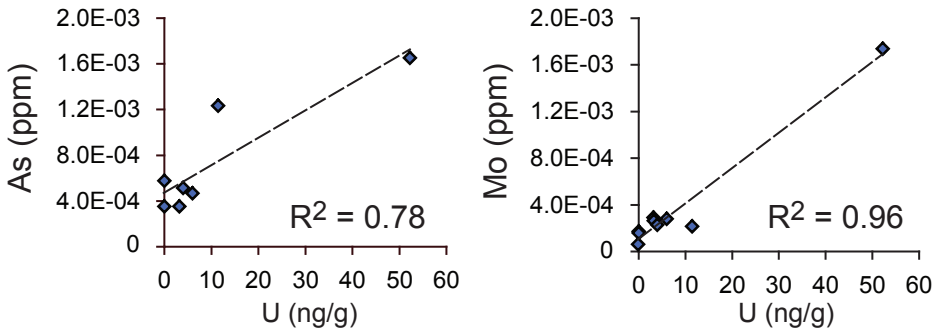

Figure 8. Mobilization of metals in addition to uranium in Red Rock Creek. Uranium concentrations in the waters of the creek increase along with As and Mo. These correlations signify a pollutant source: higher concentrations of As and Mo are likely associated with mineralization that formed the Juniper Mine uranium ore body.

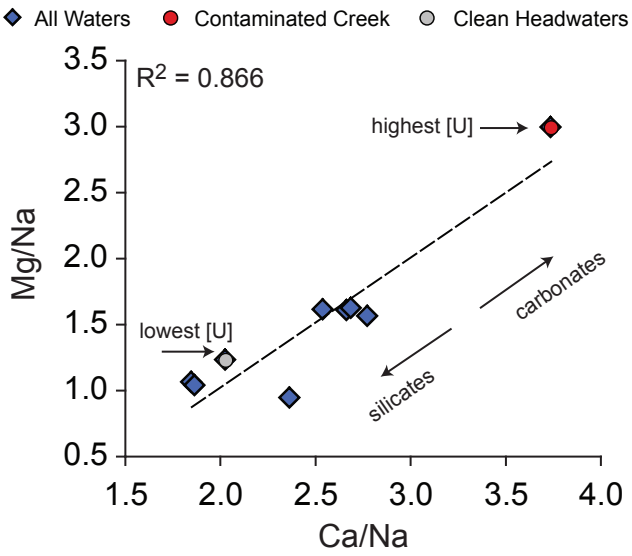

Figure 9. Influence of chemical composition of Red Rock Creek waters on the ability to dissolve and transport uranium. Silicate and carbonate end-member compositions can be separated on a plot of Mg/Na and Ca/Na where carbonates have much higher Mg/Na and Ca/Na ratios. The water compositions in Red Rock Creek form a trend between these two end-member concentrations with the samples with the highest U concentration having higher Mg/Na and Ca/Na (more carbonate-like signal).

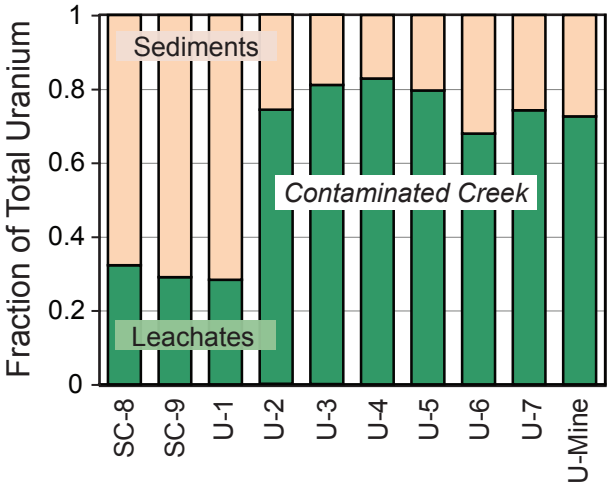

Figure 10. Uranium distribution in sediment samples. Uranium concentrations in the leached outer surface of sediment and the complete digestion of sediment are plotted as fractions of the total uranium content (leachate + sediment) for each sample. Clean creek samples have most of the uranium distributed throughout the grain itself (~70%); however, contaminated creek samples have a concentration of uranium on their outer surfaces (between 70% and 80%). These data show that adsorption occurs during the transport of uranium contamination.

TABLES

Table 1. Sample Descriptions and Locations

Sample Name	Location	Water pH	Distance from Mixing Point along Red Rock Creek (kilometers)	Material Collected
U-1	Red Rock Creek, clean branch	4.7	-0.11[a]	sediment, water
U-2	Red Rock Creek, contaminated branch	5.3	-0.03[b]	sediment, water
U-3	Red Rock Creek, main channel	4.7	0.06	sediment, water
U-4	Red Rock Creek, main channel	5.2	0.26	sediment, water
U-5	Red Rock Creek, main channel	4.9	0.66	sediment, water
U-6	Red Rock Creek, main channel	4.9	1.09	sediment, water
U-7	Red Rock Creek, main channel	5.1	1.85	sediment, water
SC-8	Salt Creek, main channel	4.6	-	sediment, water
SC-9	Salt Creek, main channel	4.5	-	sediment, water
U-10	Juniper Mine tailing sediment	-	-	sediment

[a] distance is negative because sample location is upstream of mixing point, in clean branch of Red Rock Creek

[b] distance is negative because sample location is upstream of mixing point, in contaminated branch originating at mine

Table 2. Measured Uranium Concentrations and Isotopic Compositions

Sediments

Sample Name	Method	U µg/g	2σ error[a]	$^{234}U/^{238}U$	2σ error[a]	$(^{234}U)/(^{238}U)$[b]	2σ error[a]
U-1L	leachate	1.009	0.007	7.252E-05	5.6E-07	1.32	0.01
U-2L	leachate	22.1	0.2	5.718E-05	4.3E-07	1.041	0.009
U-3L	leachate	17.6	0.1	6.177E-05	4.7E-07	1.12	0.01
U-4L	leachate	19.0	0.1	6.015E-05	4.6E-07	1.09	0.01
U-5L	leachate	15.3	0.1	5.887E-05	4.6E-07	1.07	0.01
U-6L	leachate	6.64	0.04	5.945E-05	4.5E-07	1.08	0.01
U-7L	leachate	11.65	0.08	5.785E-05	4.5E-07	1.05	0.01
SC-8L	leachate	0.995	0.006	6.464E-05	5.0E-07	1.18	0.01
SC-9L	leachate	0.968	0.006	6.355E-05	4.9E-07	1.16	0.01
U-10L	leachate	11.35	0.09	4.653E-05	3.6E-07	0.847	0.008
U-1S	bulk digestion	2.56	0.02	5.516E-05	2.6E-07	1.004	0.007
U-2S	bulk digestion	7.68	0.05	6.055E-05	2.7E-07	1.102	0.007
U-3S	bulk digestion	4.13	0.03	5.973E-05	2.8E-07	1.087	0.007
U-4S	bulk digestion	3.95	0.03	5.972E-05	2.7E-07	1.087	0.007
U-5S	bulk digestion	3.93	0.03	5.757E-05	2.6E-07	1.048	0.007
U-6S	bulk digestion	3.14	0.02	8.312E-05	3.8E-07	1.51	0.01
U-7S	bulk digestion	4.06	0.03	5.717E-05	2.7E-07	1.041	0.007
SC-8S	bulk digestion	2.09	0.01	5.636E-05	2.7E-07	1.026	0.007
SC-9S	bulk digestion	2.37	0.02	5.598E-05	2.5E-07	1.019	0.007
U-10S	bulk digestion	4.29	0.03	6.292E-05	2.8E-07	1.145	0.007

Waters

Sample Name	Method	U ng/g	2σ error	$^{234}U/^{238}U$	2σ error	$(^{234}U)/(^{238}U)$[a]	2σ error
U-1	bulk analysis	0.0222	0.0001	9.21E-05	2.1E-06	1.68	0.04
U-2	bulk analysis	52.4	0.3	6.190E-05	4.2E-07	1.127	0.009
U-3	bulk analysis	11.58	0.07	6.158E-05	4.2E-07	1.121	0.009
U-4	bulk analysis	6.10	0.04	6.123E-05	4.2E-07	1.114	0.009
U-5	bulk analysis	3.29	0.02	6.163E-05	4.2E-07	1.122	0.009
U-6	bulk analysis	3.35	0.02	6.137E-05	4.2E-07	1.117	0.009
U-7	bulk analysis	4.12	0.03	6.144E-05	4.2E-07	1.118	0.009
SC-8	bulk analysis	0.148	0.002	6.90E-05	1.4E-06	1.26	0.03
SC-9	bulk analysis	0.128	0.001	6.85E-05	1.5E-06	1.25	0.03

Table 3. Grain Size Measurements

Sample Name	Weight percent <32 μm	Mean grain size (mm)	Mean sphericity	Calculated P[a]
U-1S	0.6	1.98	0.84	6.8
U-2S	1.0	1.19	0.82	4.1
U-3S	1.2	1.11	0.84	3.8
U-4S	4.0	0.28	0.77	1.0
U-5S	2.1	0.22	0.82	0.8
U-6S	0.6	0.64	0.84	2.2
U-7S	3.1	0.21	0.78	0.7
SC-8	0.2	3.27	0.85	11.1
SC-9	0.1	0.71	0.83	2.4

[a]Calculated perimeter of grain from Equation (3). P is an approximation for surface area.

Table 4. Water Uranium Concentrations from ICP-MS

	SC-8	SC-9	U-1	U-2	U-3	U-4	U-5	U-6	U-7
Na	2.19	1.85	1.83	3.13	4.37	2.09	2.21	2.06	2.23
Mg	2.32	1.91	2.24	9.36	4.12	3.36	3.54	3.34	3.48
Al	2.06	0.64	0.15	0.26	14.63	0.70	0.16	0.08	0.09
K	2.19	1.83	1.46	5.72	3.88	2.13	2.10	1.85	1.64
Ca	4.05	3.45	3.71	11.70	10.34	5.30	5.88	5.54	6.19
Ti	0.0188	0.0063	0.0024	0.0032	0.1168	0.0084	0.0022	0.0012	0.0014
V	0.0033	0.0017	0.0014	0.0017	0.0124	0.0021	0.0014	0.0014	0.0013
Cr	0.0006	0.0002	0.0002	0.0003	0.0028	0.0004	-	-	-
Mn	0.0419	0.0067	0.0040	0.0439	0.2438	0.0156	0.0060	0.0162	0.0105
Fe	1.10	0.33	0.10	0.25	5.55	0.44	0.12	0.10	0.14
Co	0.0005	0.0001	0.0001	0.0003	0.0027	0.0002	0.0001	0.0001	0.0001
Ni	0.0007	0.0003	0.0002	0.0007	0.0021	0.0004	0.0003	0.0002	0.0002
Cu	0.0011	0.0004	0.0003	0.0004	0.0031	0.0006	0.0003	0.0003	0.0003
Zn	0.0035	0.0009	0.0008	0.0007	0.0131	0.0013	0.0013	0.0002	0.0003
Ga	0.0005	0.0001	-	0.0001	0.0030	0.0002	-	-	-
As	0.0006	0.0003	-	0.0016	0.0012	0.0005	-	0.0003	0.0005
Rb	0.0057	0.0039	0.0045	0.0107	0.0153	0.0059	0.0053	0.0047	0.0041
Sr	0.0496	0.0405	0.0412	0.1204	0.1698	0.0596	0.0658	0.0632	0.0709
Y	0.0012	0.0004	0.0002	0.0002	0.0022	0.0003	0.0002	0.0001	0.0001
Zr	0.0014	0.0006	0.0002	0.0005	0.0056	0.0007	0.0003	0.0001	0.0001
Mo	0.0002	0.0002	0.0001	0.0017	0.0002	0.0003	0.0003	0.0003	0.0002
Cs	0.0001	-	-	0.0001	0.0005	0.0001	-	-	-
Ba	0.0391	0.0249	0.0258	0.0641	0.1387	0.0362	0.0332	0.0304	0.0273
La	0.0012	0.0003	0.0001	0.0002	0.0045	0.0003	0.0001	0.0001	0.0001
Ce	0.0020	0.0005	0.0003	0.0003	0.0100	0.0006	0.0002	0.0002	0.0001
Pr	0.0003	0.0001	-	-	0.0011	0.0001	-	-	-
Nd	0.0015	0.0004	0.0002	0.0002	0.0043	0.0004	0.0001	0.0001	0.0001
Sm	0.0003	0.0001	-	-	0.0008	0.0001	-	-	-
Eu	0.0001	-	-	-	0.0002	-	-	-	-
Gd	0.0003	0.0001	-	-	0.0007	0.0001	-	-	-
Dy	0.0002	0.0001	-	-	0.0005	0.0001	-	-	-
Er	0.0001	-	-	-	0.0002	-	-	-	-
Tm	-	-	-	-	0.0000	-	-	-	-
Yb	0.0001	-	-	-	0.0002	-	-	-	-
Pb	0.0005	0.0001	-	0.0001	0.0025	0.0001	-	-	-
Th	0.0002	0.0001	-	-	0.0010	0.0001	-	-	-

Concentrations reported in ug/g or ppm. Abundances less than 0.0001 ppm are not reported (Nb, Sb, Tb, Ho, Lu, Tl, Th)

REFERENCES

Ansoborlo, E., Prat, O., Moisy, P., Den Auwer, C., Guilbaud, P., Carriere, M., Gouget, B., Duffield, J., Doizi, D., Vercouter, T., Moulin, C., Moulin, V., 2006. Actinide speciation in relation to biological processes. Biochimie 88, 1605-1618.

Agency for Toxic Substances and Disease Registry (ATSDR), 1999. Toxicological Profile for Uranium (update): Atlanta, GA: Public Health Service.

Bourdon, B., Henderson, G.M., Lundstrom, C.C., Turner, S.P. (*Eds.*), 2003. Uranium-Series Geochemistry. Reviews in Mineralogy and Geochemistry volume 52. The Mineralogical Society of America, Washington DC.

Camacho, A., Devesa, R., Valles, I., Serrano, I., Soler, J., Blazquez, S., Ortega, X., Matia, L., 2010. Distribution of uranium isotopes in surface water of the Llobregat river basin (Northeast Spain). J. Environ. Radioact. 101, 1048-1054.

Carvalho, I.G., Cidu, R., Fanfani, L., Pitsch, H., Beaucaire, C., Zuddas, P., 2005. Environmental impact of uranium mining and ore processing in the Lago Real District, Bahia, Brazil. Environ. Sci. Technol. 39, 8646-8652.

Chabaux, F., Riotte, J., Clauer, N., France-Lanord, C., 2001. Isotopic tracing of the dissolved U fluxes of Himalayan rivers: Implications for present and past U budgets of the Ganges-Brahmaputra system. Geochim. Cosmochim. Acta. 65 (19), 3201-3217.

Chabaux, F., Riotte, J., Schmitt, A., Carignan, J., Herckes, P., Pierret, M., Wortham, H., 2005. Variations of U and Sr isotope ratios in Alsace and Luxembourg rain waters: origin and hydrogeochemical implications. C.R. Geosci. 337, 1447-1456.

Cherdyntsev, V.V., (with Chalov, P.I. *et al.*), 1955. Uranium series disequilibrium dating. In Trans. 3rd Sess. Commission for Determining the Absolute Age of Geol. Formations, Izd. Akad. Nauk SSSR, 175-182.

Conaway, C.H., Watson, E.B., Flanders, J.R., Flegal, A.R., 2004. Mercury deposition in a tidal marsh of south San Francisco Bay downstream of the historic New Almaden mining district, California. Mar. Chem. 90, 175-184.

Coryell, V.H., Stearns, D.M., 2006. Molecular analysis of *hprt* mutations generated in chinese hamster ovary EM9 cells by uranyl acetate, by hydrogen peroxide, and spontaneously. Mol. Carcinog. 45, 60-72.

Cowart, J.B., Osmond, J.K., 1977. Uranium isotopes in groundwater: Their use in prospecting for sandstone-type uranium deposits. J. Geochem. Explor. 8, 365-379.

Craft, E.S., Abu-Qare, A.W., Flaherty, M.M., Garofolo, M.C., Rincavage, H.L., Abou-Donia, M.B., 2004. Depleted and natural uranium: Chemistry and toxicological effects. J. Toxicol. Environ. Health, Part B. 7, 297-317.

Department of Agriculture, 2005. Solicitation Notice RFP-R5-15-05-23. Accessed through http://www.fbodaily.com/archive/2005/07-July/13-Jul-2005/ FBO-00844405.htm

Dosseto, A., Turner, S.P., Douglas, G.B., 2006. Uranium-series isotopes in colloids and suspended sediments: Timescale for sediment production and transport in the Murray-Darling River system. Earth Planet. Sci. Lett. 246, 418-431.

Echevarria, G., Sheppard, M., Morel, J.L., 2001. Effect of pH on the sorption of uranium in soils. J. Environ. Radioact. 53, 257–264.

EPA (Environmental Protection Agency), 1999. Understanding variation in partitioning coefficients, Kd, values: Volume II: Review of geochemistry and available Kd values for cadmium, caesium, chromium, lead, plutonium, radon, strontium, thorium, tritium and uranium. US-EPA, Office of Air and Radiation, Washington, USA. EPA 402-R-99-004B.

EPA Water Maximum Contamination Levels. Accessed October 2011 through http://water.epa.gov/drink/contaminants/.

Fleischer, R.L., 1988. Alpha-recoil damage: relation to isotopic disequilibrium and leaching of radionuclides. Geochim. Cosmochim. Acta. Acta 52, 1459-1466.

Goldhaber, M.B., Morrison, J.M., Holloway, J.M., Wanty, R.B., Helsel, D.R., Smith, D.B., 2009. A regional soil and sediment geochemical study in northern California. Appl. Geochem. 24, 1482-1499.

Helgen. S.O., Moore, J.N., 1996. Natural background determination and impact quantification in trace metal-contaminated river sediments. Environ. Sci. Technol. 30, 129-135.

Hostetler, P.B., R.M. Garrels, 1962. Transportation and precipitation of uranium and vanadium at low temperatures, with special reference to sandstone-type uranium deposits. Econ. Geol. 57, 137.

Hsi, C.K.D., Langmuir, D., 1985. Adsorption of uranyl onto ferric oxy-hydroxides: application of the surface complexation site-binding model. Geochim. Cosmochim. Acta. 49, 1931-1941.

Ivanovich, M., Harmon, R.S., *Eds.* 1992. Uranium-series disequilibrium, Applications to Earth, Marine and Environmental sciences, 2nd edition, Oxford University Press, New York.

Kigoshi, K., 1971. Alpha-recoil thorium-234: Dissolution into water and the uranium-234/uranium-238 disequilibrium in nature. Science. 173, 47-48.

Kronfeld, J., 1974. Uranium deposition and Th-234 alpha-recoil: An explanation for extreme U-234/U-238 fractionation within the trinity aquifer. Earth Planet. Sci. Lett. 21, 327-330.

Kronfeld, J., Vogel, J.C., 1991. Uranium isotopes in surface waters from southern Africa. Earth Planet. Sci. Lett.105, 191-195.

Langmuir, D., 1978. Uranium solution-mineral equilibria at low temperatures with applications to sedimentary ore deposits. Geochim. Cosmochim. Acta. 42, 547–569.

Moliner-Martinez, Y., Campins-Falco, P., Worsfold, P.J., Keith-Roach, M.J., 2004. The impact of a disused mine on uranium transport in the River Fal, South West England. J. Environ. Monit. 6, 907-913.

Osmond, J.K., Cowart, J.B., 1976. The theory and uses of natural uranium isotopic variations in hydrology. Atomic Energy Rev. 14, 621-679.

Rapp, J.S., 1981. Uranium mineralization of the Sonora Pass region, Tuolumne County, California. Calif. Geology 34(3), 43-52.

Rapp, J.S., Short, W.O., 1981. Geology and uranium favorability of the Sonora Pass Region, Alpine and Tuolumne Counties, California: U.S. Department of Energy Report GJBX-132(81), 145p.

Rodriguez, P.B., Tome, F.V., Lozano, J.C., Perez-Fernandez, M.A., 2008. Influence of soil texture on the distribution and availability of ^{238}U, ^{230}Th, and ^{226}Ra in soils. J. Environ. Radioact. 99, 1247-1254.

Ryu, J., Lee, K., Chang, H.,Cheong, C., 2009. Uranium isotopes as a tracer of dissolved solutes in the Han River, South Korea. Chemical Geology 258, 354-361.

Sheppard, M.I., 1980. The environmental behavior of uranium and thorium. Whiteshell Nuclear Research Establishment, Atomic Energy of Canada Limited, Pinawa, Manitoba, 44 pp. (Technical Report AECL-6795).

Vahakangas, K.H., Samet, J.M., Metcalf, R.A., Welsh, J.A., Bennett, W.P., Lane, D.P., Harris, C.C., 1992. Mutations of p53 and *ras* genes in radon-associated lung cancer from uranium miners. Lancet 339, 576-580.

Vandenhove, H., Van Hees, M., Wouters, K., Wannijn, J., 2007. Can we predict uranium bioavailability based on soil parameters? Part 1: Effect of soil parameters on soil solution uranium concentration. Environ. Pollut. 145, 587-595.

Vandenhove, H., Gil-Garcia, C., Rigol, A., Vidal, M., 2009. New best estimates for radionuclide solid-liquid distribution coefficients in soils. Part 2. Naturally occurring radionuclides. J. Environ. Radioact. 100, 697-703.

Curriculum Vitae

Theresa M. Kayzar

Theresa M. Kayzar was born in the desert of Arizona and misses the sun, carved sandstone, and lizards. She obtained a B.Sc. from the University of Arizona in 2005 with a minor in Business Administration. After spending summers working in Mt. Rainier National Park, she decided to pursue a graduate degree at the University of Washington. She moved to Seattle in the fall of 2005, and obtained a M.S. in Geology from the University of Washington in 2007 for her work investigating gas transport in the plumbing system of Mt. Pinatubo volcano in the Philippines. She stayed at the University of Washington and received her PhD in Earth and Space Sciences in 2012 for the work presented in this dissertation on Kamchatkan volcanism and environmental contamination. She has accepted a postdoctoral position at Lawrence Livermore National Laboratory in California.

EDUCATION and HONORS:

2007 - 2012	**Ph.D. in Earth and Space Sciences,** University of Washington, Seattle, WA Dissertation Title: The Complexity of Arc Magmatism: A Geochemical Investigation of Crustal Processes Beneath a Highly Productive Volcanic Center, Kamchatka, Russia
2008 - 2011	**Certificate of Environmental Management**; University of Washington, Program on the Environment Project: Whidbey Island Stormwater Biofiltration Project
2005 - 2007	**M.S. in Geological Sciences,** University of Washington, Seattle, WA Thesis Title: Gas transport model for the magmatic system at Mount Pinatubo, Philippines: Insights from (^{210}Pb)/(^{226}Ra).
2000 - 2005	**B.Sc. in Geosciences, Minor in Business Administration,** University of Arizona, Tucson, AZ Summa Cum Laude with Departmental Honors

---

RESEARCH INTERESTS:

Radioactive isotope geochemistry, environmental geochemistry, volcanology, applications of geochemistry (Uranium-series: U-Th-Ra-(Ba)-Pb-Po, Rb-Sr, Sm-Nd, and Pb radioactive isotope systems), differential gas motion in magmatic systems, generation and transport of melts in volcanic arc settings, transport of toxic metals through the environment.

RESEARCH EXPERIENCE:

2007 – present	**National Science Foundation Graduate Student Fellow; University of Washington, Department of Earth and Space Sciences** Analysis of U-Th-Ra-Rn-Pb systematics in the Kamchatkan Volcanic Arc, Russia. Advisors: Dr. Bruce Nelson, Dr. Olivier Bachmann
2010 – 2011	**Stormwater Biofiltration Project; University of Washington, Program on the Environment** Investigating the potential for compost amended soil to remove N, P, Cu, and fecal coliform from contaminated stormwater. Mentor: Dr. Sally Brown.
2007	**Junior Research Specialist; University of California at Davis, Department of Geology** Assisted in uranium-series clean laboratory set-up at UCDavis. Researching the behavior of uranium-series isotopes in volcanic systems. Advisor: Dr. Kari Cooper.
2006 - 2010	**Field Researcher; Partnerships in International Research and Education (PIRE): National Science Foundation and the University of Alaska Fairbanks** Application of radioactive isotope geochemistry to studies of explosive volcanism in the Kamchatka Volcanic Arc, Russia. Mentors: Dr. John Eichelberger and Dr. Pavel Izbekov

2005 - 2007 **Graduate Research Assistant; University of Washington, Department of Earth and Space Sciences**
Analysis of U-Th-Ra-Rn-Pb systematics at Mount Pinatubo, Philippines and development of gas transport model. Advisors: Dr. Kari Cooper and Dr. Victor Kress

2004 - 2005 **Research Assistant; University of Arizona, Department of Geosciences**
Radiogenic isotopic analysis of granitic rocks, Coast Range Plutonic Complex, British Columbia (NSF funded BATHOLITH project). Advisors: Dr. Jonathan Patchett and Dr. Mihai Ducea

2003 - 2005 **Research Assistant; University of Arizona, Department of Geosciences**
Examined pyroxenite melting in the mantle and the effects on basaltic lava flows in Owens Valley, California. Advisor: Dr. Mihai Ducea

---

ADDITIONAL WORK/RESEARCH EXPERIENCE:

2011 **Lawrence Livermore National Laboratory Summer Teaching Assistant;**
Training in Environmental Sample Analysis for International Atomic Energy Agency (IAEA) Safeguards. Co-taught course in environmental analyses for nuclear safeguards. Mentored 6 summer interns completing group research projects.

Posters from work experience:
Jablonski, J.G., Ko, P., and Wasserman, N., Soil Contamination at LLNL's Site 300: Characterizing Uranium Isotopic Composition, Concentration, and Desorption Properties, Mentors: Ross W. Williams, Theresa M. Kayzar, Adam C. Villa
Hilding-Kronforst, S., Jim, V.Q., and Vazquez, M., An Environmental Analysis of Depleted Uranium Concentration and Composition in Plants, Soils and Surface Waters at Site 300, Mentors: Ross W. Williams, Theresa M. Kayzar, Adam C. Villa

2010 **Lawrence Livermore National Laboratory Summer Intern;**
Training in Environmental Sample Analysis for International Atomic Energy Agency (IAEA) Safeguards. IAEA is an agency that reports to the UN and works with Member States and multiple partners worldwide to promote safe, secure and peaceful nuclear technologies.
Research investigating the transport of uranium downstream from the abandoned Juniper uranium mine.

2009 **Chevron Corporation Earth Science Intern;**
Seismic Amplitude Analysis in the Bay Marchand Oil Field.

FIELD EXPERIENCE:

Lawrence Livermore National Laboratory Site 300, California	Summer 2011
Abandoned Juniper Uranium Mine, Stanislaus National Forest, CA	Summer 2010
Carbonate Reservoirs, ExxonMobil Short Course, Guadalupe Mountains, New Mexico	Mar 2009
Karymsky and Shiveluch Volcanoes, Kamchatka Volcanic Arc, Russia	Summer 2008
Klyuchevskoy Group Volcanoes, Kamchatka Volcanic Arc, Russia	Summer 2006 – 2009
Mount St. Helens Volcano/PIRE workshop, Cascade Volcano Observatory	Summer 2006 - 2007
Mount Pinatubo Volcano, Philippines	Mar 2007
Coast Plutonic Complex Granitic Batholith, British Columbia	Summer 2005
Big Pine Volcanic Field, California	Summer 2004
Field Methods in Volcanology; Kilauea Volcano	
Center for the Study of Active Volcanoes, Hawaii	July 2003 – Aug 2003
USGS Hawaiian Volcano Observatory/University of Hawaii at Hilo	

SKILLS (INSTRUMENTAL AND LABORATORY):

Multi-Collector Inductively Coupled Plasma Mass Spectrometry (MC-ICP-MS) analysis (Pb and U-series isotopes)
Instrument: Nu Plasma, University of Washington, University of California at Davis and Lawrence Livermore National Laboratory
Thermal Ionization Mass Spectrometry (TIMS) analysis (Rb-Sr and Sm-Nd systems)
Instrument: VG Sector, University of Arizona and University of Washington
Laser Ablation (LA-ICP-MS)
Instrument: NewWave DUV 193 ArF Excimer laser system, Oregon State University
Alpha Spectrometry
University of Iowa, collaboration with Dr. Mark Reagan
Electron Microprobe
Instrument: JEOL 733 Superprobe, University of Washington
Isotope clean laboratory geochemistry techniques
Pb isotopes, Rb-Sr isotopes, Sm-Nd isotopes, U-Th-Ra-Ba isotopes, Po isotopes (University of Iowa), Pu Isotopes
UCLA Secondary Ion Mass Spectrometry (SIMS) Workshop Participant 2007

TEACHING EXPERIENCE:

2012, 2010 **Teaching Assistant; Geoclub Hawaii Field Course, University of Washington**
Co-led classroom and field course in volcanology/culture in Hawaii for undergraduate majors

2010 - 2011 **Undergraduate Research Mentor; Student – Annie Bauer, University of Washington**
Advising undergraduate student Annie Bauer on her research investigating the composition the crust in the Kamchatka Volcanic Arc as revealed by Pb-isotopes from xenoliths. Her work was presented at the UW undergraduate research symposium and the GSA Rocky Mountain meeting 2011.

2010 - 2011 **Undergraduate Research Mentor; Student – Jakub Sliwinski, University of Washington**
Advising undergraduate student Jakub Sliwinski on his research investigating U-series isotope systematics in the Canary Islands. Jakub won an award for this work for the Best Undergraduate Oral Presentation at the UW Earth and Space Sciences Research Gala.

2011 **Teaching Assistant; Living with Volcanoes, University of Washington**
Instructor for non-major volcanology course

2011 **Teaching Assistant; Mineralogy and Petrology, University of Washington**
Instructor for lab sessions of ESS212 (mineralogy and petrology for geology majors)

2005 - 2009 **"Rock"ing Out K-12 Educational Science Outreach, University of Washington**
Founder/Coordinator and teacher of Earth and Space Sciences in K-12 classrooms in Washington.

2008 **Guest Lecturer, University of Washington, Bothell Campus**
Instructor for Natural Hazards and Human Disasters.

2006 - 2007 **Teaching Assistant; University of Washington, Department of Earth and Space Sciences**
Instructor for lab sessions and lectures for undergraduate level introductory geology course (ESS101).

2006, 2007 **Guest Lecturer; University of Washington, Department of Earth and Space Sciences**
Instructor for 200-person Living with Volcanoes course (ESS106).

2004 **Guest Lecturer; University of Arizona, Department of Geosciences**
Prepared lab session on volcanic monitoring techniques.

2003- 2004 **Preceptor; University of Arizona, Department of Geosciences**
Teaching assistant for Sedimentology and Stratigraphy course (GEOS302).

AWARDS, FELLOWSHIPS, and SCHOLARSHIPS:

2011	Arizona State University Exploration Postdoctoral Fellowship (declined to accept alternate postdoctoral position)
2011	College of the Environment Graduate Dean's Medalist, University of Washington (top graduate student for service and leadership in the College of the Environment)
2011	Best Graduate Oral Presentation, University of Washington, Earth and Space Sciences Research Gala
2011	Aspect Consulting Award Best Contribution in Geo-Engineering/Environmental Geology, University of Washington, Earth and Space Sciences Research Gala
2011, 2006	Joseph A. Vance Endowed Fellowship, University of Washington Earth and Space Sciences
2010	Best Poster in Chemical Sciences Division, Summer Intern Research Symposium, Lawrence Livermore National Laboratory
2009, 2008	Dorothy G. Stephens Graduate Student Research Award, University of Washington Earth and Space Sciences
2009	Goodspeed Geology Scholarship, University of Washington Earth and Space Sciences
2009, 2008	Chevron Student Scholarship
2008	ExxonMobil Student Research Grant
2007 - 2010	National Science Foundation Graduate Research Fellowship
2006	National Science Foundation Graduate Student Research Fellowship Honorable Mention
2006 - 2010	Earth and Space Sciences Graduate Student Research Award, University of Washington
2005	Misch Fellowship, University of Washington Earth and Space Sciences
2005	University of Washington Graduate Student Fund for Excellence and Innovation Fellowship
2005	University of Washington "Top Scholar" Fellowship
2005	University of Arizona Department of Geosciences Outstanding Senior

---

PROFESSIONAL AFFILIATIONS:
American Geophysical Union (AGU), The Geochemical Society (GS), Geological Society of America (GSA)

SERVICE:

2009 - 2010	Founder and Chair, Earth and Space Science Research Symposium (ESS Gala), University of Washington
2005 - 2010	Workshop Leader, Seattle Expanding Your Horizons Conference, Seattle University
2008 - 2009	Graduate Student Representative to Faculty, University of Washington
2005 - 2008	Founder and Coordinator, "Rock"ing Out K-12 Outreach Program, University of Washington
2004 - 2005	College of Science Ambassador, University of Arizona
2003 - 2005	Junior Education Volunteer, Tucson Gem and Mineral Show

---

PUBLICATIONS AND TALKS:

Papers published/submitted:

Kayzar, T.M., Nelson, B.K., Bachmann, O., Bauer, A.M., and Izbekov, P.I., Pb Isotope Ratios from Time-Series Samples at Bezymianny and Klyuchevskoy Volcanoes Record Source Variations in the Central Kamchatka Depression (*Journal of Petrology, in review*)

Kayzar, T.M., Villa, A.C., Lobaugh, M.L., Gaffney, A.M., and Williams, R.W., Investigating Uranium Distribution in Surface Sediments and Waters: A Case Study of Contamination from the Juniper Mine, Stanislaus National Forest, CA (*Applied Geochemistry, in review*).

Kayzar, T.M., Cooper, K.M., Reagan, M.K., and Kent, A.J.R., Gas transport model for the magmatic system at Mount Pinatubo, Philippines: Insights from (^{210}Pb)/(^{226}Ra), *Journal of Volcanology and Geothermal Research* v.181, 124-140 (2009).

Papers in preparation:

Kayzar, T.M., Nelson, B.K., Bachmann, O., and Portnyagin, M., An Investigation of Th-excess Generation in Volcanic Arcs: (^{238}U)/(^{230}Th) from Erupted Products of the Central Kamchatka Depression (*in prep for Geochemica et Cosmochimica Acta*)

Kayzar, T.M., Nelson, B.K., Reagan, M.K., and Bachmann, O., Periodically Erupting Degassed Magma: Inferring Magma Residence Times from the Evolution of Karymsky, Bezymianny, and Shiveluch Volcanoes, Kamchatka, Russia (*in prep for Geology*)

Abstracts:

Kayzar, T.M.*, Nelson, B.K., Bachmann, O., Portnyagin, M., Ponomareva, V. Examining Canonical Theories of U-series Disequilibria in Volcanic Arcs in Light of a More Comprehensive, Global Database. *AGU Fall. Meet. Suppl. Abstract, 2011*

Kayzar, T.M.*, Nelson, B.K., Bachmann, O., Bauer, A.M. The Formation of U-series Disequilibria in Magmas: Crust or Mantle? *GSA Rocky Mountain Meeting, 2011*

Kayzar, T.M., Nelson, B.K., Bachmann, O., Portnyagin, M., Ponomareva, V. Are U-Series Disequilibria Transparent to Crustal Processing of Magma? A Case Study at Bezymianny and Klyuchevskoy Volcanoes, Kamchatka, Russia, *AGU Fall. Meet. Suppl. Abstract, 2010*

Kayzar, T.M., Lobaugh, M.L., Villa, A.C., Williams, R.W., and Gaffney, A.M., Investigating Uranium Nuclide Fractionation in Sediments and Waters Using MC-ICP-MS: A Case Study of Contamination from the Juniper Mine, Stanislaus National Forest, *Student Poster Symposium, Lawrence Livermore National Laboratory, 2010.*

Kayzar, T.M.*, Nelson, B.K., Reagan, M.K., Izbekov, P.E., Belousova, M., Belousov, A. Periodically Erupting Degassed Magma: The Evolution Of Karymsky, Bezymianny, and Shiveluch Volcanic Systems In The Past Decade, *IAVCEI Cities on Volcanoes International Conference, Tenerife, Spain 2010.*

Kayzar, T.M., Nelson, B.K., Reagan, M.K., Izbekov, P.E., Belousova, M., A Multi-Component Geochemical Study of Short-Term Melt and Volatile Evolution in the Kamchatka Volcanic Arc, *AGU Fall. Meet. Suppl. Abstract, 2009*

Kayzar, T.M.*, Nelson, B.K., Izbekov, P.E., Belousova, M., Belousov, A., and PIRE Research Team, Geochemical Tracing of Volcanic Gases at Bezymianny and Shiveluch Volcano: Implications for Magmatic Plumbing Sources. *JKASP Meeting, Fairbanks, Alaska 2009.*

Kayzar, T.M.*, Nelson, B.K., Izbekov, P.E., Belousova, M., Belousov, A., Volatiles in the Kamchatka Volcanic Arc at Four Volcanic Centers (Bezymianny, Klyuchevskoy, Karymsky, and Shiveluch): Applications for Uranium-Series Isotopic Data. *JKASP Meeting, Fairbanks, Alaska 2009.*

Kayzar, T.M., Nelson, B.K., Izbekov, P.I., and Belousova, M., Fine-Scale Source Variations in Time-Series Samples from Kamchatkan Volcanoes Recorded in High-Precision Pb Isotope Ratios, *AGU Fall. Meet. Suppl. Abstract, 2008.*

Shipman, J.S., **Kayzar, T.M**., Izbekov, P.E., and PIRE Team, Partners in International Research and Education: Student contributions in the collaborative investigation of Bezymianny, Shiveluch, and Karymsky volcanoes, Kamchatka, Russia and Mount St. Helens, WA, USA, *AGU Fall. Meet. Suppl. Abstract, 2008.*

Kayzar, T.M., Cooper, K.M., Reagan, M.K., Kent, A.J.R., and Kress, V.C., Volatile transport and accumulation timescales modeled using (210Pb/226Ra) disequilibrium in tephras from Mount Pinatubo Volcano, Philippines: Moving from the timescales of 222Rn to 210Pb. *AGU Fall. Meet. Suppl. Abstract, 2007*.

Kayzar, T.M., Student response after Russian collaboration and field-work on Bezymianny volcano, *NSF PIRE Participants Meeting Abstract, 2007.*

Wetmore, Paul H., Ducea, M.N., Stair, Kelley N., and **Kayzar, T.**, The geochemical evolution of greater than 100 million years of subduction-related magmatism, Coast Plutonic Complex, west-central British Columbia, *GSA Backbone of the Americas Meeting Abstract, 2006*.

Blondes, M.S., Reiners, P.W., **Kayzar, T.**, Ducea, M.N., Chesley, J., Using temporal-compositional trends in single eruption sequences of primitive basalts to observe systematic time-dependent mantle source variation: an example from the Big Pine Volcanic Field, California, *AGU Fall. Meet. Suppl. Abstract, 2004*.

Wetmore, Paul H,. **Kayzar, T.,** Ducea, M., Patchett, P.J., Gehrels, G., Preliminary results of the petrological-geochemical component to the BATHOLITHS project, *GSA Annual Meeting Abstract, 2004*.

Group Abstracts from Field Collaboration:

Thelen, W., and **PIRE Group**, (2006), Twins across the Pacific: A comparison of Bezymianny Volcano, Russia and Mount St. Helens, USA, *Eos Trans. AGU, 87(52), Fall Meet. Suppl., Abstract V11B-0577*.

Other Publications:

Kayzar, T.*, Preliminary geochemical implications from the collaborative BATHOLITHS study of the Coast Plutonic Complex, British Columbia, *Thirty Third Annual GeoDaze Student Symposium Abstracts, Dept. of Geosciences, University of Arizona*, 2005.

Kayzar, T., Stair, K.N., Ducea, M.N., In-situ clinopyroxene Sr isotopic analyses by LA-ICPMS; A test of mantle melting processes in the Big Pine Volcanic Field, California, *Thirty Third Annual GeoDaze Student Symposium Abstracts, Dept. of Geosciences, University of Arizona*, 2005.

Kayzar, T.*, Ducea, M., Reiners, P., and Blondes, M., Quantifying the role of pyroxenite melting in the mantle beneath the western Unites States: A trace element and isotopic investigation of the Wuacoba basaltic center, Big Pine Volcanic Field, California, *Thirty Second Annual GeoDaze Student Symposium Abstracts, Dept. of Geosciences, University of Arizona*, 2004.

Invited Talks:

Kayzar, T.M.*, Using Isotopes to Fingerprint Metal Contamination, *University of Washington Science and Policy Summit, Graduate Professional Senate, 2011*.

* denotes speaker